CHEMICAL ENGINEERING SCIENCE
GENIE CHIMIQUE

Vol. 16 1961 Nos. 1 and 2

VOL. 16 1962

Nozzle sprays in air streams

MALCOLM A. WEISS and CHARLES H. WORSHAM
Esso Research and Engineering Company, Linden, N.J.

(*Received* 21 *July* 1960)

Abstract—An experimental study was made of the drop size distributions obtained from ten different hydraulic nozzles spraying axially into large steady air streams of high velocity. The drop sizes observed for the nozzles in fast air streams bore little relation to the drop sizes observed for these same nozzles in static tests. As air velocities increased, to 700 ft/sec or more, the nozzle drop sizes closely approached the drop sizes obtained from simple cylindrical tube injectors.

Résumé—Etude expérimentale de distribution de gouttes d'après leurs dimensions. Ces distributions sont obtenues à partir de 10 ajutages hydrauliques différents atomisant axiallement dans des courants d'air à grande vitesse. Les grosseurs des gouttelettes pourdes ajutages en courants d'air rapids sont faiblement liées à celles des gouttelettes observées pour ces mêmes ajutages en essais statiques. Quand la vitesse de l'air augmente, jusqu'à 700 ft/sec et plus, la grosseur des gouttes avec l'ajutage se rapproche énormément de la dimension obtenue avec des injecteurs à simple tube cylindrique.

Zusammenfassung—Es wurden experimentelle Untersuchungen über die Tropfengrössenverteilung zehn verschiedener hydraulischer Düsen, die axial in einen stetigen Luftstrom von hoher Geschwindigkeit sprühten, durchgeführt. Die in schnellen Luftströmungen beobachteten Tropfengrössen zeigten nur wenige Beziehungen zu dem in statischen Versuchen mit den gleichen Düsen erhaltenen Tropfengrössen. Bei zunehmenden Luftgeschwindigkeiten, 700 ft/sec und mehr, näherte sich die Tropfengrösse der Düsen der einfacher zylindrischer Rohrinjektoren.

INTRODUCTION

AN EXPERIMENTAL study was made of the drop sizes resulting from nozzles spraying into large air streams of sustained high velocity. This study was intended to provide data useful in the design of fuel injection systems in jet engines and had two specific objectives. The first was to compare the drop sizes with drop sizes from the same nozzles in still air in order to evaluate the selection of nozzles based on performance in still air. The second objective was to compare the sprays from nozzles in air streams to the sprays from simple tubes, reported previously [1], to determine what advantages resulted from using more costly and complex nozzles rather than tubes.

The experimental programme consisted of injecting a molten synthetic wax through various nozzles mounted on the axis of a 6-in. diameter air duct. Wax was injected at 300°F into the air stream at 300°F and atmospheric pressure. At 300°F the wax had a specific gravity of 0·828, a surface tension of 22·0 dyn/cm and a viscosity of 11·3 cP. About 3 ft downstream of the nozzle a traversing sampling probe collected and froze the wax particles. The particle size distributions were then analysed by sieving and by sedimentation in air. Details of the experimental procedures are given in Ref. [1].

Ten different commercial hydraulic nozzles were tested. They are described in Table 1 along with the mass median drop diameters obtained

Table 1. *Nozzle static tests*

Nozzle	*Manufacturer*	*Type*	*Orifice diam.* (in.)	(Gal/min)	ΔP. (p.s.i.)	*Static* X_{50}, (μ)
Pintle	Eng. Prod. Co.	Var. area*	—	0·33	26	165
			—	1·00	55	146
Piston	Bendix	Var. area†	—	1·00	104	—
H1B	Spraco	Hollow cone	0·047	0·33	(250)	107
1B	Spraco	Full cone	0·047	0·33	73	229
H4B	Spraco	Hollow cone	0·094	0·33	19	524
				1·00	114	225
3C	Spraco	Full cone	0·094	0·33	6	622
				1·00	55	280
4BW	Spraco	Full cone, wide angle	0·094	0·33	5	722
				1·00	37	398
1838	Spraco	Misting	0·073	0·25	80	126
1504	Spraco	Pinjet	0·020	0·12	104	86
16300	Bendix	Hollow cone‡	0·094	0·33	18	367
				1·00	58	252

*Increasing pressure drop moves conical pintle forward to increase annular orifice area.
†Increasing pressure drop moves piston to expose greater length of six rectangular orifice slots.
‡Contains internal minimum-pressure shut-off valve.

by simply spraying the molten wax into still air at room temperature. The nozzles were used as received except that the nozzle bodies were turned down on a lathe to the minimum possible diameter to reduce obstruction of the air stream. Thin struts of flattened $\frac{3}{8}$-in. tubing were used to mount and feed the nozzles in the duct, as shown in Ref. [1].

The drop size distributions observed for each nozzle spray are summarized in Table 2. Each distribution was matched by a best-fitting upper-limit equation proposed by MUGELE and EVANS [2]. This equation expresses the cumulative volume fraction (R) larger than diameter X as a function of three arbitrary constants, the mass median diameter X_{50}, the maximum diameter X_m, and the dimensionless slope S.

$$R = \tfrac{1}{2}\left\{1 + \operatorname{erf}\left[\frac{1}{S\sqrt{2}} \ln \frac{X(X_m - X_{50})}{X_{50}(X_m - X)}\right]\right\} \qquad (1)$$

Each equation was constrained to pass through the observed X_{50}, and X_m and S were then chosen by trial to minimize the standard error between equation and data over the entire drop size range. This error, listed in Table 2, is the R.M.S. difference between observed and computed cumulative volume percentages at drop diameters corresponding to the following observed volume percentages: 2, 5, 10, 20, 30, 40, 60, 70, 80, 90, 95 and 98. For all the runs listed, the average R.M.S. error was 1·5 per cent. Examples of matching the complete distribution data by the upper-limit equation are shown in Fig. 1.

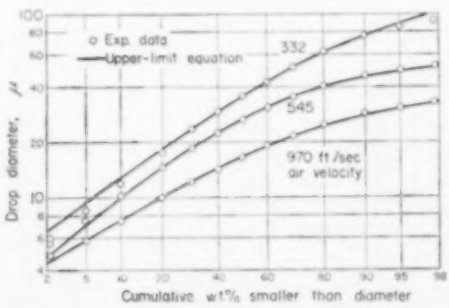

FIG. 1. Fitting experimental data to upper-limit equation. Log-probability co-ordinates. Piston nozzle.

Table 2. Nozzle air stream tests

*Nozzle**	Gal/min	*Air velocity* (ft/sec)	X_{50} (μ)	X_{max} (μ)	UL *equation slope, S*	*Error* RMS (%)
Pintle*	1·00	345	33·1	88	0·97	1·5
Pintle*	0·33	340	42·4	80	1·23	1·7
Pintle*	0·33	770	22·1	37	1·15	1·4
Pintle	1·00	320	66·7	100	1·63	1·0
Pintle	0·33	320	69·9	99	1·88	1·6
16300*	0·34	345	45·2	126	0·99	3·3
16300*	1·00	335	53·7	104	1·23	0·8
3C*	0·34	340	59·2	124	1·01	1·6
3C*	1·00	340	53·0	103	1·03	1·6
4BW*	0·34	335	55·8	96	1·33	1·0
4BW*	1·00	340	52·7	99	1·29	0·8
H4B*	1·00	345	38·0	66	1·18	1·6
1B*	0·33	350	50·3	105	0·98	2·8
1B*	0·33	760	19·2	42	0·96	0·4
1B	0·33	310	94·0	133	1·43	2·7
H1B*	0·33	345	35·5	71	1·26	1·7
H1B*	0·33	750	18·7	33	1·16	1·7
H1B*	0·33	960	14·3	31	0·80	1·1
1504	0·12	560	29·2	49	1·25	1·3
1504	0·12	325	72·2	140	1·12	3·5
1838	0·26	325	55·8	102	1·41	0·8
Piston	1·00	545	26·8	57	1·12	0·6
Piston	1·00	970	16·5	42	0·86	1·3
Piston	1·00	330	35·1	172	0·90	1·2

*Contra-stream injection, others co-stream.

Air Velocity Effects

The effect of injecting into an air stream, as illustrated by Fig. 2, was the expected effect of greatly reducing the average drop size from any given nozzle. For example, the full cone nozzle 1 B had a mass median drop diameter of 19·2 μ in a 760 ft/sec air stream as compared to 229 μ in still air.

There was no correlation between drop sizes from nozzles in the static tests and drop sizes in the air stream tests. At air velocities between 310 and 350 ft/sec the median drop diameters ranged from less than 8 per cent to more than 80 per cent of the drop diameters from static tests of the same nozzles at the same injection rates. Although there were still marked differences between nozzles in the air stream tests these differences were much smaller than the differences in static tests. The maximum

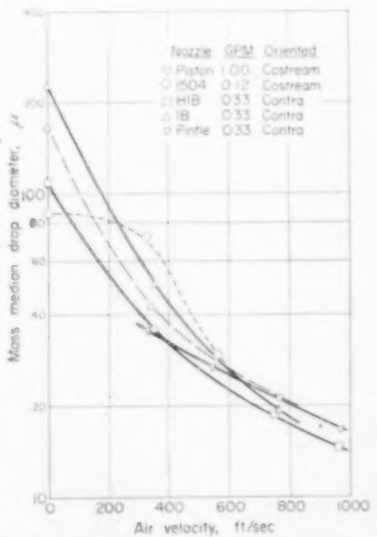

Fig. 2. Effect of air velocity on median drop size.

difference observed in median drop size in static tests was about 8·5-fold; this was reduced to about 2·5-fold at air velocities of about 340 ft/sec and further reduced to less than 1·2-fold at air velocities of 750 ft/sec and higher.

According to Ref. [1] using the liquid and air properties of the nozzle experiments the mass median diameter of sprays from cylindrical tube injectors is given by the following dimensional equation with X_{50} in μ, the injection rate G in gal/min and the relative velocity V in ft/sec:

$$X_{50} = 183{,}000\, G^{1/12}\, V^{-4/3} \qquad (2)$$

Equation (2) predicts that the average drop size from simple tubes varies inversely with relative air velocity to the 4/3 power where relative velocity is defined as air velocity plus initial liquid velocity for contra-stream injection or minus initial liquid velocity for co-stream injection. For the fixed orifice nozzles tested here the average dependence of drop size on air velocity was roughly the same as for tubes. These results, in the 300 + ft/sec velocity range, are quite different from the results of SCHMIDT [3] in the 20–150 ft/sec range. SCHMIDT sprayed water from a very small hollow cone nozzle and observed that average drop size varied inversely with air velocity to only about the $\frac{1}{4}$ power. SCHMIDT's results can be reconciled with these if one concludes that the initial liquid pattern and turbulence are increasingly important relative to air stream action as air velocity decreases. On the other hand at very high air velocities air stream action is dominant in determining spray characteristics, and the exact way in which the liquid is originally introduced into the air stream is relatively unimportant.

These conclusions are also consistent with the data of Fig. 3 which show that at high relative velocities nozzles offer little advantage over simple tubes in terms of spray fineness. In calculating relative velocities average initial liquid velocities along the axis for the nozzles were estimated from the pressure drops across the nozzles and from the observed cone angles. For relative velocities over 600 ft/sec no nozzle gave a median drop size more than 10 per cent smaller than the drop size from tubes predicted by equation (2). For lower velocities, the finest spray produced by any nozzle was about 50 per cent smaller than predicted by equation (2).

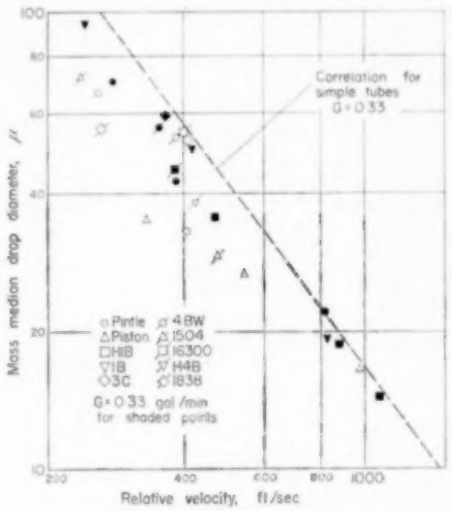

FIG. 3. Comparison of drop sizes from nozzles and tubes in air streams.

NOZZLE VARIABLE EFFECTS

The effect of pressure drop on drop size of four fixed orifice nozzles is shown in Fig. 4. In static tests there is the expected decrease of drop size as pressure drop increases with an average variation of X_{50} as about the $-0{\cdot}36$ power of pressure drop. This value agrees very closely with the results of other investigators of hydraulic swirl nozzles. For example, JOYCE [4] reported $-0{\cdot}35$ and LONGWELL [5] reported $-0{\cdot}375$.

In contrast to these results pressure drop had little effect in a 340 ft/sec air stream. One nozzle (16300) actually showed an increase of drop size with increasing pressure drop at constant air velocity. At constant relative velocity all three nozzles would show a small increase in drop size with increasing pressure drop. Therefore, in an air stream average drop size clearly does not depend on pressure drop as it does in static tests. On the other hand, equation (2) shows that drop sizes from tube injectors do increase very slightly with increasing liquid injection rate at constant relative velocity between liquid and air streams.

The present nozzle data are at least qualitatively consistent with those results. INGEBO's data [6, 7] on impinging jets and on single jets in air streams also showed little effect of liquid injection rate, particularly at high air stream velocities. In the data of MARSHALL [8] and NUKIYAMA and TANASAWA [9] on pneumatic atomizers liquid rate again was unimportant except for its contribution to relative velocity and when the volumetric ratio of liquid to gas became large.

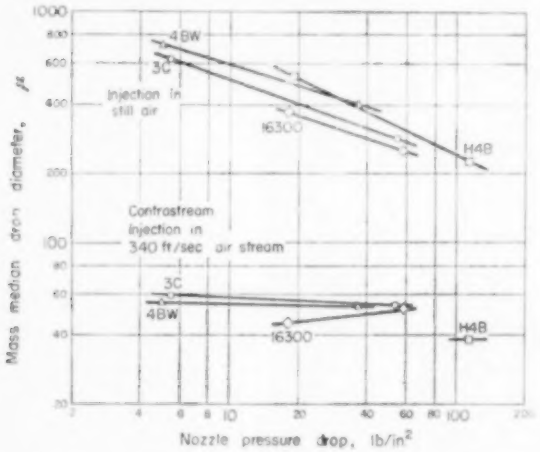

FIG. 4. Effect of nozzle pressure drop in still air and in streams.

The effects of nozzle orifice diameter are not as clear since there were no data allowing direct comparison of geometrically similar nozzles of different sizes at constant pressure drop. However, this comparison can be made by extrapolation of the data of Fig. 4. It shows that increasing orifice diameter has the expected marked effect of increasing drop size in static tests, but has a much smaller effect in air stream tests. Considering both hollow cone and full cone nozzles, doubling orifice diameter from 0·047 to 0·094 in. caused an average increase in X_{50} estimated at 36 per cent during static tests but only 10 per cent during air stream tests. The static test increase of 36 per cent checks well with the 41 per cent predicted by JOYCE [4], while the stream test increase of 10 per cent checks well with the 12 per cent predicted by WEISS and WORSHAM [1] for tubes, e.g. equation (2).

When the direction of injection was changed from co-stream to contra-stream with other conditions constant there was a marked decrease in average drop size. This is the same behaviour observed for simple tubes and presumably results from the change in relative velocity for a given air velocity. For example, the 1 B nozzle injecting 0·33 gal/min co-stream at an air velocity of 310 ft/sec gave an X_{50} of 94 μ compared to 50 μ for contra-stream injection at an air velocity of 350 ft/sec. Similarly, the pintle nozzle injecting into 320–345 ft/sec air streams at 1/3 gal/min gave an X_{50} of 70 μ co-stream compared with 42 μ contra-stream; at an injection rate of 1 gal/min these values were 67 and 33 μ for co-stream and contra-stream injection respectively.

For both variable area nozzles measurements were made of the drop size distributions at several fixed points in the sampling plane about 3 ft downstream of the nozzle. The results showed that local average drop sizes varied by a maximum of 30 per cent from the drop size obtained during the full sampling traverse. This variation from point to point is somewhat larger than the variations observed in sprays from simple tubes [1].

Although atomization is complete 3 ft downstream of the nozzle it is not complete 6 in. downstream. In one set of tests with the pintle nozzle the average drop diameter was 64 μ 6 in. downstream of the nozzle compared with 51 μ 3 ft downstream. Similarly, tests with the piston nozzle gave 51 μ and 36 μ at 6 in. and 3 ft, respectively. Data from [1] and [6] showed that atomization from orifices and tubes was complete at distances of 8–12 in. from the injector.

The over-all magnitudes of the drop sizes observed in this work may be examined in the light of previous studies on the stability of single drops in gas streams. For example, LANE's data [10] showed that a drop should be unstable at a Weber number greater than about 6 in sudden blasts or about 11 in steady streams. (Weber number is defined here as the product of drop diameter, gas density and square of relative velocity, all divided by surface tension). Using relative velocity at the point of injection the

Weber numbers calculated here ranged from about 15 to 60 for the mass median drops, and from about 30 to 150 for the largest drops in the nozzle sprays. This means that the final droplets could not have been exposed to relative velocities as great as those at the point of injection ; in fact, the largest final drops could not have survived velocities higher than 1/4 to 1/5 of the initial ones. The fact that the single drop stability criterion is not the sole determinant of final drop sizes in the sprays is not surprising. Previous studies on sprays in fast air streams, or from pneumatic atomizers, have all shown that relative velocity has a smaller effect than the second power effect resulting from a constant Weber number.

CONCLUSIONS

Evaluation of the drop size distribution of a hydraulic nozzle by conventional static testing is of little or no value even qualitatively for predicting the drop size distribution that will result in a fast air stream. For example, changing orifice size or pressure drop has little effect in a stream despite the large effects in a static atmosphere. With given physical properties of the fluids, drop size is largely controlled by relative velocity at high velocities. Therefore, at high velocities the sprays from even the simplest type of injector will be about as fine as the sprays from a complex hydraulic nozzle. For design purposes, this conclusion can be assumed applicable to velocities of about 700 ft/sec and above. At lower relative velocities nozzle sprays may become finer than tube sprays formed under otherwise similar conditions. However, in the absence of experimental data it would be unsafe to assume the nozzle spray to be more than 20–30 per cent finer even at relative velocities as low as 250 ft/sec.

Nozzles are usually more effective than tubes in distributing the liquid widely throughout the air stream at all velocities. Contra-stream injection rather than co-stream injection will help this wider distribution as well as providing finer sprays for all injectors and air velocities.

VOL
16
196

REFERENCES

[1] WEISS M. A. and WORSHAM C. H. *J. Amer. Rocket Soc.* 1959 **29** 252.
[2] MUGELE R. A. and EVANS H. D. *Industr. Engng. Chem.* 1951 **43** 1317.
[3] SCHMIDT J. M. *Progr. Rep.* 4–101. Jet Propulsion Laboratory, California Institute Technology 1949.
[4] JOYCE J. R. *J. Inst. Fuel* 1949 **22** 150.
[5] LONGWELL J. P. Sc. D. Thesis. Massachusetts Institute Technology 1943.
[6] INGEBO R. D. *Nat. Adv. Comm. Aeronaut.* TN 4222, 1958.
[7] INGEBO R. D. and FOSTER H. H. *Nat. Adv. Comm. Aeronaut.* TN 4087, 1957.
[8] MARSHALL W. R. JR. *Atomization and Spray Drying* pp. 76–77 American Institute Chemical Engineers, New York 1954.
[9] NUKIYAMA S. and TANASAWA Y. *Trans. Soc. Mech. Engrs.* (*Japan*) 1939 **5** S–15.
[10] LANE W. R. *Industr. Engng. Chem.* 1951 **43** 1312.

Chemical Engineering Science, 1961, Vol. 16, pp. 7 to 20. Pergamon Press Ltd., London. Printed in Great Britain.

Thermal decomposition of calcium carbonate

G. NARSIMHAN

Department of Chemical Engineering, National Chemical Laboratory, Poona, India

(*Received* 9 *December* 1959)

Abstract—The process of thermal decomposition of calcium carbonate has been treated as one governed by simultaneous heat and mass transfer, under quasi steady state conditions, to the decomposition interface. It is believed that the surface chemical reaction is very fast and as such does not interfere in the determination of the overall decomposition rate. Rigorous expressions, based on heat transfer rate, have been derived, based on the system properties, for the prediction of decomposition times for definite geometric shapes such as spheres and cylinders. The good agreement observed between the actual and predicted values bears out the soundness of the decomposition scheme assumed for the process. The expression derived are:

Spheres: $\theta_D = \alpha_H (0{\cdot}33 + 0{\cdot}17\, k_H)$

Cylinders: $\theta_D = \alpha_H (0{\cdot}50 + 0{\cdot}25\, k_H)$

Based on an analysis of simultaneous heat and mass transfer rates the following correlation is obtained:

$$\frac{K_g R t\, p_f d}{D_m P} = E' \left(\frac{hd}{k_e}\right)$$

This equation bears very close resemblance to the theoretical expression for the evaporation of small spheres into quiet air. This equation may be rearranged to provide:

$$\left(\frac{h}{k_g}\right) = \frac{C_p}{E'} \left(\frac{\mu/\rho\ D_m}{C_p\ \mu/k_e}\right)$$

which is a modified form of the usual correlation for simultaneous heat and mass transfer based on Chilton–Colburn analogy.

The mathematical treatment has been extended to a two-phase solid system ($Mg\ CO_3$–$Ca\ CO_3$) characterized by finite but different equilibrium decomposition temperatures. The mathematical analysis involves the solution of simultaneous differential equations. This has been done numerically by the modified Runge–Kutta method with the help of an IRM computer. The confirmation of the proposed equation must await future experimental data for the two-phase system.

Résumé—Le processus de décomposition thermique du carbonate de calcium a été considéré comme gouverné par un transfert simultané de masse et de chaleur à l'interface de décomposition, et dans des conditions d'état quasi-stationnaire. On considère que la réaction chimique de surface est très rapide et n'intervient donc pas dans la détermination de la vitesse de décomposition globale. On peut prévoir les temps de décomposition pour des formes géométriques définies telles que sphères et cylindres, au moyen d'expressions définies par la vitesse de transfert de chaleur et les propriétés du système. La concordance entre les valeurs réelles et les valeurs prévues confirme la validité du processus de décomposition supposé. Les expressions dérivées sont:

Sphères $\theta_D = \alpha_H (0{,}33 + 0{,}17\, k_H)$

Cylindres $\theta_D = \alpha_H (0{,}50 + 0{,}25\, k_H)$

Par une analyse des vitesses de transfert massiques et thermiques simultanés on obtient la relation suivante:

$$\frac{K_g R t\, p_f d}{D_m P} = E' \left(\frac{hd}{k_e}\right)$$

Cette équation est très proche de l'expression théorique de l'évaporation de petites sphères dans l'air (au repos). On peut l'écrire :

$$\left(\frac{h}{k_g}\right) = \frac{C_p}{E'}\left(\frac{\mu/\rho\, D_m}{C_p\, \mu/k_e}\right)$$

Cette expression est une forme modifiée de la relation classique fondée sur l'analogie de CHILTON–COLBURN, pour le transfert simultané de masse et de chaleur.

Le raisonnement mathématique a été étendu à un système solide à deux phases ($Mg\,CO_3 - Ca\,CO_3$) caractérisé par des températures d'équilibre définies mais différentes. L'analyse mathématique comprend la solution d'équations différentielles simultanées par la méthode modifiée de RUNGE–KUTTA à l'aide d'un calculateur IBM. L'équation proposée devra attendre les futures données expérimentales pour être confirmée dans les systèmes à deux phases.

Zusammenfassung—Der Vorgang der thermischen Zersetzung von Calciumcarbonat wurde behandelt, als ob er bei quasi stationären Bedingungen vom gleichzeitigen Wärme- und Stofftransport nach der Zersetzungsfläche abhängen würde. Es wurde dabei angenommen, dass die chemische Oberflächenreaktion sehr schnell abläuft und als solche die Bestimmung der Gesamtzersetzungsgeschwindigkeit nicht beeinflusst. Für die Vorausberechnung der Zersetzungszeiten definierter geometrischer Körper wie Kugeln und Zylinder, wurden genaue Ausdrücke abgeleitet, die auf der Wärmetransportgeschwindigkeit und den Systemeigenschaften beruhen. Die beobachtete gute Übereinstimmung zwischen den gemessenen und den vorausberechneten Werten zeigt die Berechtigung des angenommenen Zersetzungsablaufs. Die abgeleiteten Ausdrücke lauten :

Kugeln : $\theta_D = \alpha_H\,(0{,}33 + 0{,}17\,k_H)$

Zylinder : $\theta_D = \alpha_H\,(0{,}50 + 0{,}25\,k_H)$

Aufgrund einer Betrachtung der simultanen Wärme- und Stoffübergangsgeschwindigkeiten wurde folgender Zusammenhang erhalten :

$$\frac{K_g\, Rt\, p_f\, d}{D_m\, P} = E'\left(\frac{hd}{k_e}\right)$$

Diese Gleichung hat eine sehr grosse Aehnlichkeit mit dem theoretischen Ausdruck für die Verdampfung aus kleinen Kugeln in ruhende Luft. Die Gleichung kann umgeform werden zu :

$$\left(\frac{h}{k_g}\right) = \left(\frac{C_p\, \mu/p\, D_m}{E'\, C_p\, \mu/k_e}\right)$$

welche eine modifizierte Form der üblichen Korrelation für gleichzeitigen Stoff- und Wärmetransport nach der Analogie von CHILTON und COLBURN darstellt. Die mathematische Behandlung wurde auf ein zweiphasiges Feststoffsystem ($Mg\,CO_3$–$Ca\,CO_3$) ausgedehnt, das gekennzeichnet ist durch endliche aber unterschiedliche Zersetzungsgleichgewichtstemperaturen. Die mathematische Untersuchung umfasst die Lösung simultaner Differentialgleichungen. Dies wurde numerisch durchgeführt mit der modifizierten RUNGE–KUTTA-Methode mit Hilfe eines IBM-Rechners. Zur Bekräftigung der vorgeschlagenen Gleichung müssen weitere experimentelle Ergebnisse für das Zweiphasensystem abgewartet werden.

PART I—THERMAL DECOMPOSITION OF CALCIUM CARBONATE

THE problem of thermal decomposition of calcium carbonate presents many interesting features that are capable of elaboration and analysis on a mathematical framework. Of the three major rate determining steps, heat transfer, mass transfer and surface chemical reaction, the last one has been defined on the basis of theoretical considerations [1, 11] and plays, probably, a very subordinate role in determining the over-all reaction rate. However, it has been observed that for a reacting mass consisting of particles of approximately 10–15 μ in diameter the chemical reaction effect appears marked in the form of an increased decomposition temperature. For smaller sizes,

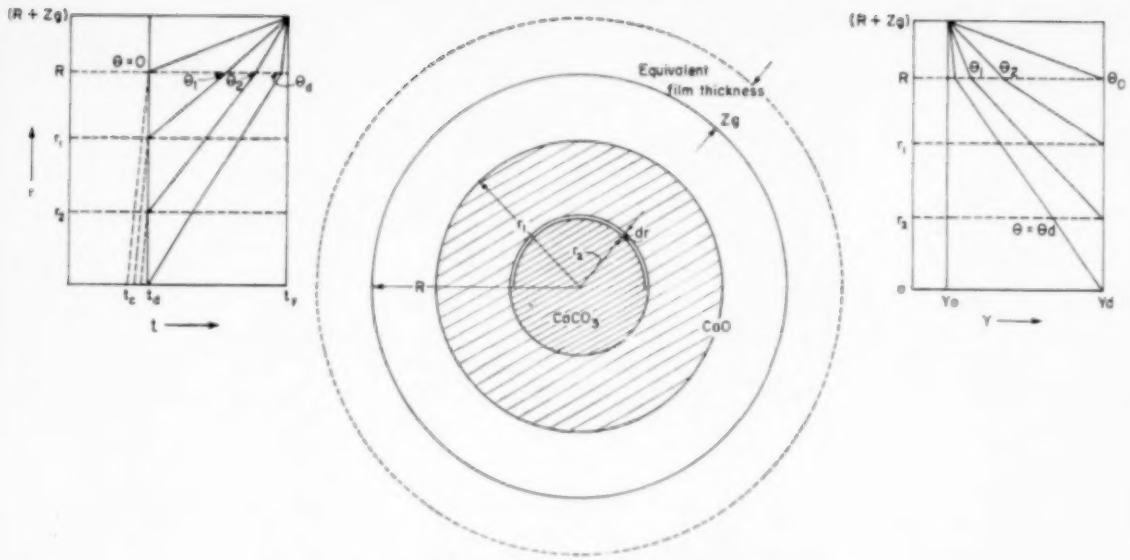

FIG. 1. Decomposition scheme for a sphere of cylinder of $CaCO_3$.
Temperature and concentration gradient during thermal decomposition.

the reaction rate appears to be entirely governed by heat transfer rate to the decomposition plane [2]. It would therefore appear that a mathematical analysis of the general problem of heat transfer to a sample of calcium carbonate undergoing thermal decomposition would provide expressions from which decomposition times may be calculated provided the chemical reaction is fast enough as to cease to influence the over-all decomposition rate. The following analysis will be restricted to a consideration of the decomposition of calcium carbonate in the form of spheres and cylinders, according to the usual form of decomposition scheme. This is represented in Fig. 1.

Case 1. *Sphere*

A. *Heat Transfer.* Consider a sphere of radius R and at an initial temperature t_0, be suspended in a large furnace maintained at a temperature t_f. The surface of the sphere attains the decomposition temperature t_d in a negligible fraction of the total decomposition time θ_d and immediately becomes coated with a growing layer of calcium oxide. The energy interchange between the surface of the sphere and that of the furance depends on their respective emissivities and temperatures. Let the assumption be made that the centre temperature of the sphere levels up with the decomposition temperature within a very short time. This assumption is quite valid considering the large magnitude of the thermal diffusivity of calcium carbonate. On this basis there is no internal temperature gradient and all the heat reaching the decomposition plane is used up for the endothermic reaction.

At any time θ after the surface has attained the temperature t_d, let the decomposition plane be situated at a distance r from the centre of the sphere. In this condition the undecomposed sphere of radius r is covered to a depth of $(R - r)$ by a porous calcium oxide shell of effective thermal conductivity k_e.

The amount of heat that reaches the outer surface of the oxide shell may be given by

$$q_\theta = 4\pi R^2 (h_r + h_c)(t_f - t) \qquad (1)$$

If the contribution due to conduction in the gas phase be considered as small compared to that due to radiation, h_c may be neglected as small compared to h_r. The latter may be given by an equation

VOL.
16
1962

$$h_r = \frac{0{\cdot}173 \times 10^{-8}}{(t_F - t)} \left[\epsilon_1 (t_F + 460)^4 - \epsilon_2 (t + 460)^4\right] \quad (2)$$

The amount of heat that reaches the decomposition interface may be given by the equation

$$q_\theta = \frac{4\,\pi\, r\, R\, k_e (t - t_d)}{(R - r)} \quad (3)$$

Solving equations (1) and (3), for t

$$t = \frac{r\, k_e\, t_d + R\,(R - r)\, h_r\, t_f}{r\, k_e + R\,(R - r)\, h_r} \quad (4)$$

Substituting equation (4) in (3) and rearranging,

$$q_\theta = \frac{4\,\pi\, R^2\, h_r\, (t_F - t_d)\, r'}{r' + \left(\frac{R h_r}{k_e}\right)(1 - r')} \quad (5)$$

where $r' = (r/R)$

$$k_H = (R\, h_r / k_e)$$

Equation (5) reveals that the rate of heat transfer to the decomposition plane may be given by the product of the initial transfer rate q_θ and a variable term which is a function of the dimensionless parameter r' and k_H. The latter may be recognised as a form of Nusselt Number. Fig. 2 represents the dependence of the variable term on the parameters. The instantaneous decomposition rate may be given by

$$dW/d\theta = -\rho\, 4\,\pi\, r^2 \frac{dr}{d\theta} \quad (6)$$

On the basis of a heat balance the following equation may be given:

$$-\frac{dw}{d\theta}\left[\Delta H_d + 0{\cdot}44\, C_p\, (t_F - t_d)\right] = q_\theta \quad (7)$$

Rearranging after substituting equation (5) for q_θ,

$$-\rho\, 4\,\pi\, r^2 \frac{dr}{d\theta}\, \Delta H_T = \frac{4\,\pi\, R^2\, h_r\, (t_F - t_d)\, r'}{r' + k_H\,(1 - r')} \quad (8)$$

Separating the variables and integrating between limits: $r' = 1$, $r' = 0$:

$$\theta_d = \alpha_H\,(0{\cdot}33 + 0{\cdot}17\, k_H) \quad (9)$$

where $\alpha_H = \dfrac{\rho\, R\, \Delta H_T}{h_r\,(t_F - t_d)}$

B. *Mass transfer.* At any time θ the rate of diffusion of CO_2 away from the decomposition interface may be given by

$$N_\theta = \frac{D_e\, 4\,\pi\, r\, R\,(p_d - p)}{R\, t\, p_f} \quad (10)$$

The effective diffusion coefficient D_e may be empirically correlated:

$$D_e = E\, D_m/\beta = E'\, D_m \quad (11)$$

where β may be recognized as a form of tortuosity factor [3]. Equation (10) may be rewritten as

$$N_\theta = \frac{k_g\, 4\,\pi\, r\, R\, E'\, Z_g\,(p_d - p)}{(R - r)} \quad (12)$$

The diffusional rate across the equivalent film on the outside of the porous calcium oxide shell may be given by

$$N_\theta = k_g\, 4\,\pi\, R^2\,(p - p_0) \quad (13)$$

Equations (12) and (13) may be solved for p:

$$p = \frac{Z_g\, E'\, r\, p_d + R\,(R - r)\, p_0}{Z_g\, E' r + R\,(R - r)} \quad (14)$$

Substituting the value of p in equation (13) and rearranging,

$$N_\theta = \frac{k_g\, 4\,\pi\, R^2\,(p_d - p_0)\, r'}{r' + k_M\,(1 - r')} \quad (15)$$

where $k_m = \dfrac{R}{Z_g\, E'}$

The instantaneous decomposition rate and hence the diffusional rate of CO_2 may be given by

$$-0{\cdot}44\,\rho\, 4\,\pi\, r^2 \frac{dr}{d\theta} = N_\theta \quad (16)$$

Substituting equation (15) for N_θ in equation (16), separating the variables and integrating

$$\theta_d = \alpha_M\,(0{\cdot}33 + 0{\cdot}17\, k_M) \quad (17)$$

where $\alpha_M = \dfrac{0{\cdot}44\,\rho\, R}{k_g\,(p_d - p_0)}$

The similarity of expressions given by equations (9) and (17) is not unexpected considering the identical mathematical path followed for the case of mass transfer.

VOL 16 196

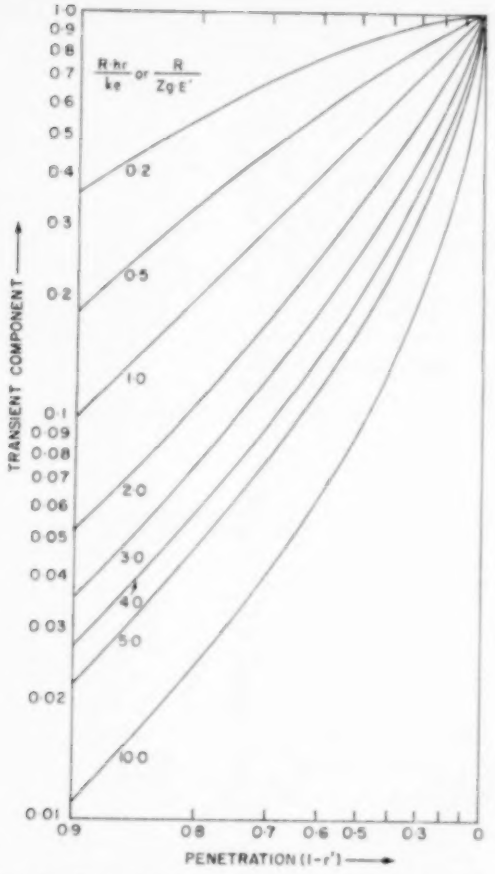

FIG. 2. Dependence of heat/mass transfer rate on depth of penetration and modified Nusselt number for a decomposing sphere.

Case 2. Cylinder

A. *Heat Transfer.* The treatment may now be extended to a cylinder. Consider a cylinder of radius R, length l and at an initial temperature t_0 be suspended in a large furnace maintained at a temperature t_f. Making the same assumptions as in the case of a sphere, at any time θ, the rate of heat transport by radiation to the outer surface of the cylinder may be given by

$$q_\theta = 2\pi R l h_r (t_F - t) \tag{18}$$

The rate of heat transfer by conduction to the decomposition plane at a distance r from the centre of the cylinder may be given by:

$$q_\theta = \frac{2\pi R_m l k_e (t - t_d)}{(R - r)} \tag{19}$$

where $R_m = (R - r)/ln\ R/r$

Solving equations (18) and (19) for t:

$$t = \frac{(R h_r) \ln r' t_F - k_e t_d)}{(R h_r \ln r' - k_e)} \tag{20}$$

Substituting in equation (19) and simplifying,

$$q_\theta = \frac{2\pi R l h_r (t_F - t_d)}{(1 - k_H \ln r')} \tag{21}$$

Equation (21) indicates that the rate of heat transfer to the decomposition plane at any time θ may be given in a manner similar to that of a sphere, by the product of the initial transfer rate and a variable factor which is a function of the same dimensionless parameters which have appeared in the correlation for a sphere. Fig. 3 represents this dependence for a cylinder.

The instantaneous decomposition rate may be given by

$$dW/d\theta = -2\pi\rho l r\, dr/d\theta \tag{22}$$

On the basis of a heat balance the following equation may be obtained:

$$-\Delta H_T \rho l 2\pi r \frac{dr}{d\theta} = \frac{2\pi R l h_r (t_F - t_d)}{(1 - k_H \ln r')} \tag{23}$$

Separating the variables and integrating between limits: $r' = 1$, $r' = 0$:

$$\theta_d = \alpha_H (0{\cdot}5 + 0{\cdot}25\, k_H) \tag{24}$$

B. *Mass transfer.* Without going through the usual mathematical development, the rate of diffusion of CO_2 away from the decomposition interface may be written analogous to the case of heat transfer as

$$N_\theta = \frac{k_g 2\pi R l (p_d - p_0)}{(1 - k_M \ln r')} \tag{25}$$

Equation (22) may be modified to express the instantaneous rate of CO_2 evolution and diffusion as

$$N_\theta = -0{\cdot}44\,\rho\, 2\pi r l \frac{dr}{d\theta} \tag{26}$$

Separating the variables and integrating between the usual limits,

$$\theta_d = \alpha_M (0{\cdot}5 + 0{\cdot}25\, k_m) \tag{27}$$

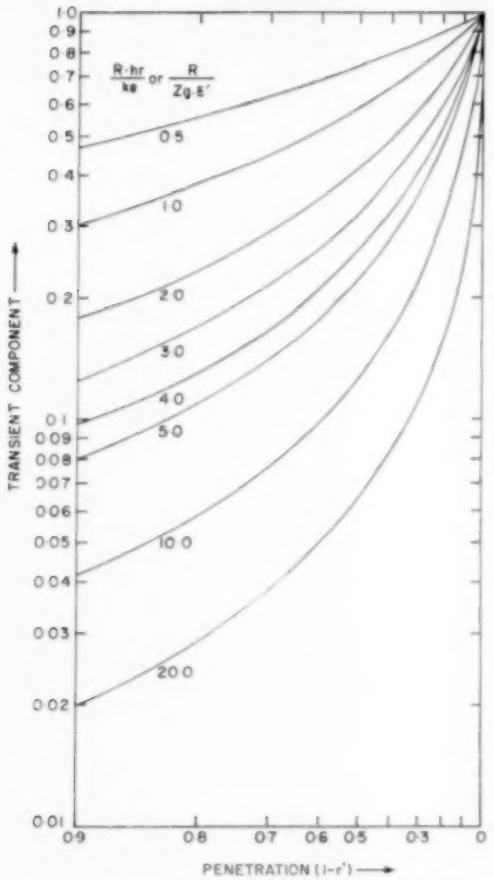

FIG. 3. Dependence of heat/mass transfer rate on depth of penetration and modified Nusselt number for a decomposing cylinder.

Verification

It is usually found that rate equations based on heat transfer are more amenable to experimental verification than those based on mass transfer. This is probably because of the fact that temperatures can be measured with greater accuracy than partial pressures. In order to verify equations (9) and (24) data are taken from published literature [2].

Sphere.

Radius	1·08 cm
Density of $CaCO_3$	1·84 g/ml
Furnace temperature	1835 °F
Decomposition temperature	1650 °F
Effective thermal conductivity of calcium oxide	0·40 B.Th.U/hr ft °F
Heat of decomposition, ΔH_d	710 B.Th.U/lb [4]
Molal heat capacity of CO_2	$6{\cdot}85 + 8{\cdot}53 \times 10^{-3} T - 2{\cdot}48 \times 10^{-6} T^2$ [5]

Estimated values:

Total heat of decomposition, ΔH_T	759 B.Th.U/lb.
Radiation coefficient, h_r	10·13 B.Th.U./hr ft² °F
Dimensionless group, k_H	0·897

On substituting the above values appropriately in equation (9)

$$\theta_d = 0{\cdot}79 \text{ hr}$$
$$= 0{\cdot}75 \text{ hr (experimental)}$$

Cylinder

Radius	1·04 cm
Length	6·84 cm
Furnace temperature	1814 °F
Decomposition temperature	1650 °F

The rest of the data necessary may be taken from the previous example. On substituting the above values in equation (24)

$$\theta_d = 1{\cdot}42 \text{ hr}$$
$$= 1{\cdot}36 \text{ hr (experimental)}$$

It is evident from inspection of decomposition times estimated from the equations developed, that there is fair amount of agreement with the experimental values reported in literature. The calculations are repeated for other cases of cylindrical samples, process conditions and crystal sizes. The results are tabulated in Table 1. These calculations indicate beyond doubt that even in the case of samples made up of large-sized crystals decomposition times may be predicted on the basis of heat transfer rate alone.

Figs. 4 and 5 represent the surface temperature variation as functions of both penetration and percent decomposition. The calculations are based on equations (4) and (20). In the case of cylinder, the agreement is fairly good considering the assumption of lower decomposition temperature.

VOL 16 196

Table 1. *Decomposition time for cylinders and spheres of* $CaCO_3$*

No.	*Shape*	*Radius* (cm)	*Length* (cm)	*Density* (g/ml)	*Furnace temperature* (°F)	*Decomposition temperature* (°F)	*% reacted*	*Decomposition time* (hrs) *Exp.*	*Predicted*
1	cylinder	1·06	6·79	1·86	1782	1652	100	1·84	1·78
2	cylinder	1·04	6·14	1·90	1901	1651	50	0·28	0·26
3	cylinder	1·07	6·69	1·85	1705	1650	100	4·34	4·19
4	cylinder	1·09	6·62	1·87	1751	1651	100	2·02	2·13
5	cylinder	1·04	6·84	1·80	1814	1652	100	1·36	1·42
6	sphere	1·08	—	1·84	1835	1652	100	0·75	0·79

* Data taken from an article by SATTERFIELD and FEAKES [10].

VOL. 16 1962

Simultaneous heat and mass transfer

It is possible to relate equations (5) and (15) on the basis of simultaneous heat and mass transfer. Equating the heat transfer rate to the interface to the heat of reaction multiplied by the mass transfer rate

$$0{\cdot}44\, q_0 = N_g\, \Delta H_T \qquad (28)$$

Or,

$$\frac{0{\cdot}44 \times 4\pi R^2 h_r (t_F - t_d)}{\Delta H_T \{1 + k_H [(1-r)/r']\}} = \frac{k_g 4\pi R^2 (p_d - p_0)}{1 + k_M [(1-r')/r']} \qquad (29)$$

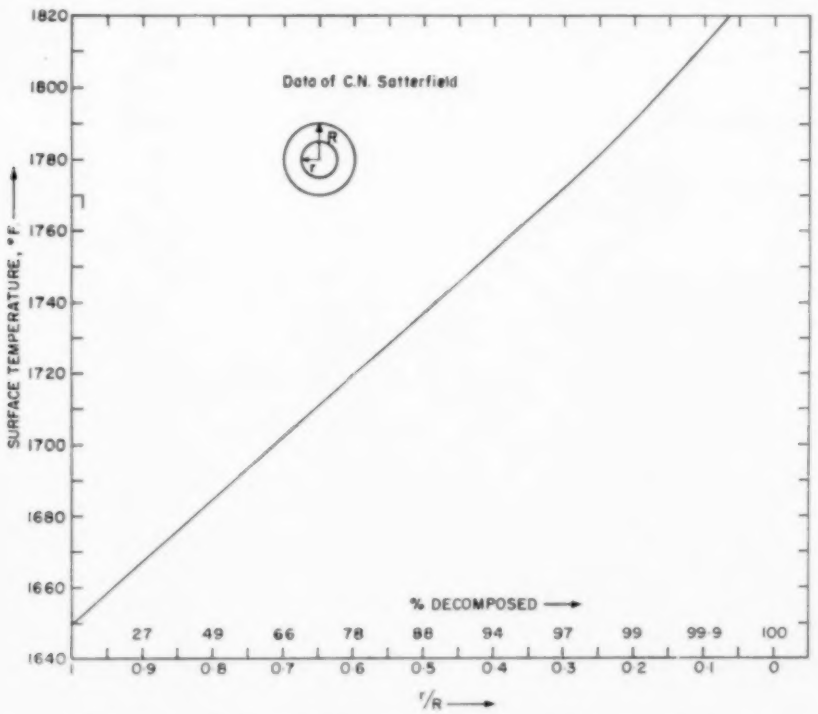

FIG. 4. Prediction of surface temperature during decomposition of $CaCO_3$ in the form of a sphere. $t_f = 1835$ °F, $t_d = 1650$.

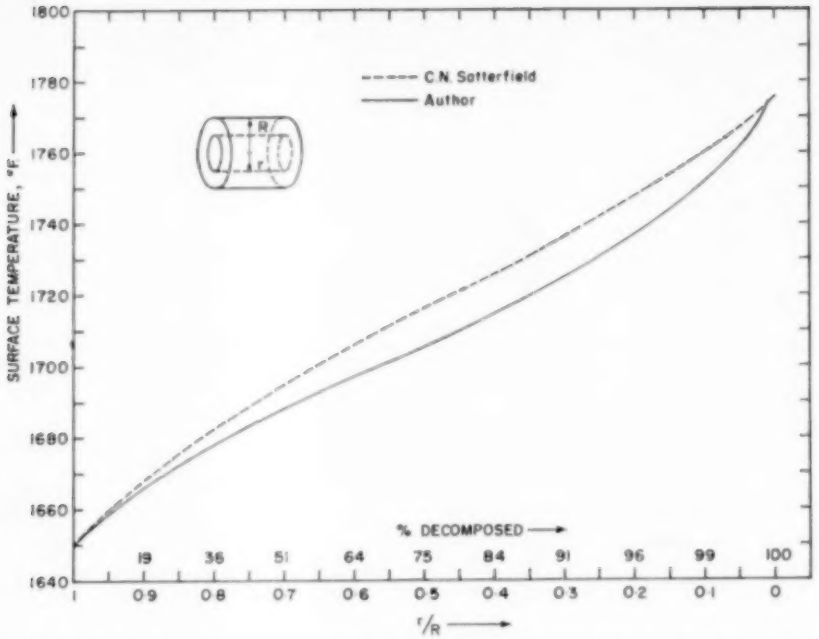

FIG. 5. Prediction of surface temperature during decomposition of $CaCO_3$ in the form of a cylinder. $t_f = 1782$ °F, $t_d = 1650$ °F, $t_d^* = 1675$ °F.

Since at any time the above relationship is valid, at $\theta = 0$, $r' = 1$,

$$\frac{0{\cdot}44}{\Delta H_T} 4\pi R^2 h_r (t_F - t_d) = k_g 4\pi R^2 (p_d - p_0) \quad (30)$$

It is therefore evident that

$$(R h_r/k_e) = (R/Z_g E') \quad (31)$$

Substituting $D_m P/k_g RT p_f$ for Z_g and $d = 2R$, for a general case ($h = h_r$), the following correlation may be obtained

$$\frac{(k_g RT p_f d)}{D_m P} = E' \left(\frac{hd}{k_e}\right) \quad (32)$$

Inspection of equation (32) reveals its close resemblance to the equation for the evaporation of small spheres in quiescent medium [6]. Equation (32) may be rearranged to provide

$$\left(\frac{h}{k_g}\right) = \frac{C_p}{E'} \frac{(\mu/\rho D_m)}{(C_p \mu/k_e)} \quad (33)$$

The above equation is very similar to one which correlates simultaneous heat and mass transfer processes based on CHILTON–COLBURN analogy [7].

Before concluding this part of the investigation it is necessary to offer the following remarks. The mathematical analysis is based on an equilibrium temperature for decomposition and an appropriate partial pressure for CO_2 being operative throughout the decomposition period of the sample. If, for some reason, either the thermal properties of the porous calcium oxide shell take on different values or the bulk partial pressure in the system changes, the assumption of constant t_d and p_d will be violated. A new set of values will be operative which will necessitate recalculation of the decomposition period. It is hoped that this analysis, with its limitations, will be the starting point for a refined treatment of this important process in as much as similar processes like combustion of coal, calcination of limestone, oxidation of metals and even entirely physical process like air drying of moist materials may be analysed on a similar framework now contem-

plated for decomposition of calcium carbonate [8].

The mathematical analysis will now be extended to a two-phase solid system.

Part II—Decomposition of Mixed Carbonates

Case 1: *Sphere*

A. *Heat transfer.* Fig. 6 represents a scheme of decomposition for a mixture of calcium and magnesium carbonates and it does not necessarily apply to 'dolomite' a double salt. Let the two decomposition temperatures be denoted by t_{d1} and t_{d2}, the former pertaining to $MgCO_3$ and the latter to $CaCO_3$. Let the furnace temperature be t_f and the surface temperature t. Let ρ_1 and ρ_2 represent the density of the undecomposed material and the primary decomposition mixture of MgO and $CaCO_3$ respectively. Let $(R\,h_r/k_{e1})$ and $(R\,h_r/k_{e2})$ stand for the modified Nusselt Numbers based on the effective thermal conductivities k_{e1} and k_{e2}. Here k_{e1} is the effective thermal conductivity of the primary decomposition mixture of MgO and $CaCO_3$ and k_{e2} is that of the secondary mixture of MgO and CaO, obtained as a consequence of secondary decomposition.

Let a sphere of radius R be suspended in a large furnace maintained at a temperature t_f. If the assumption is made that the surface of the sphere attains the primary decomposition temperature t_{d1} in a negligible fraction of the total decomposition time and that the surface is immediately coated with a growing layer of MgO, at any time θ subsequent to the initiation of primary decomposition the surface temperature of the composite sphere may be given by an equation analogous to equation (4):

$$t = \frac{t_{d1} + k_{H1}\left[(1 - r')/r'\right]t_F}{1 + k_{H1}\left[(1 - r)/r'\right]} \tag{34}$$

where $k_{H1} = (R\,h_r/k_{e1})$

If substitution of $t = t_{d2}$ is made in the above equation and the equation solved for r', the critical value r_c' will be obtained, representing the depth of penetration of primary decomposition at which secondary decomposition sets in at

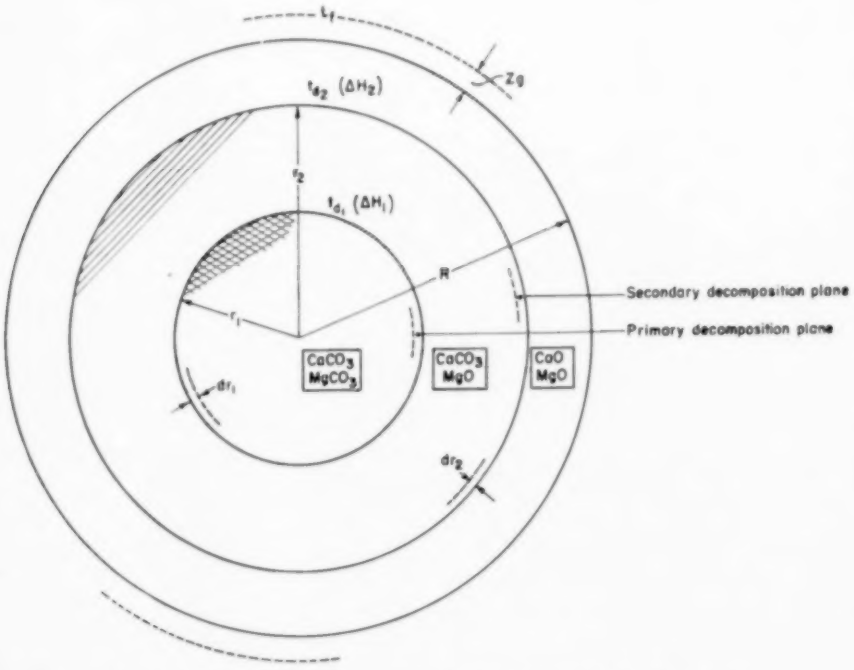

Fig. 6. Decomposition scheme for mixed carbonates ($MgCO_3$–$CaCO_3$).

the surface. r_c' will be given by the following equation:

$$r_c' = \frac{1}{1 + [(t_{d2} - t_{d1})/(t_F - t_{d2})](1/k_{H1})} \quad (35)$$

If the mass fraction of $MgCO_3$ in the mixture is x, the total heat of decomposition $\Delta H_1^{\,t}$, the instantaneous primary decomposition rate may be given by the following equation:

$$\frac{dw}{d\theta} = -\rho_1 4\pi r^2 \frac{dr}{d\theta} \quad (36)$$

The instantaneous heat transfer rate may be given by:

$$q_\theta = \frac{4\pi R^2 h_r (t_F - t_{d1}) r'}{r' + k_{H1}(1 - r')} \quad (37)$$

If the assumption is made that the entire amount of heat reaching the decomposition interface is used up for the endothermic reaction the following heat balance may be given:

$$-\rho_1 x \Delta H_1^{\,T} 4\pi r^2 \frac{dr}{d\theta} = \frac{4\pi R^2 h_r (t_F - t_{d1}) r'}{r' + k_{H1}(1 - r')} \quad (38)$$

Separating the variables and integrating between limits $r' = 1$ and $r' = r_c'$,

$$\theta_c = \alpha_1 \left[\left(\frac{1 - k_H}{3} \right) (1 - r_c'^3) + \frac{k_{H1}}{2} (1 - r_c'^2) \right] \quad (39)$$

θ_c can be easily calculated after substitution of equation (35) for r_c'.

The problem of heat transfer becomes a little complicated when secondary decomposition sets in. Three examples may be visualized.

Example 1.

As per equation (35), if

$$\Delta = \frac{(t_{d2} - t_{d1})}{k_{H1}(t_F - t_{d2})} \text{ and } \Delta > 1 \quad (40)$$

r_c' may be effectually taken as zero and θ_d may be evaluated from equation (39) which simplifies on the substitution of the upper limit of $r_c' = 0$,

$$\theta_d' = \alpha_1 (0{\cdot}33 + 0{\cdot}17\, k_{H1}) \quad (41)$$

Equation (41) defines the duration of primary decomposition, at the end of which $CaCO_3$ begins to decompose and the time of secondary decomposition may be estimated from an equation similar to (41) as under

$$\theta_d^{\,2} = \frac{\rho_2 (1 - x) R \Delta H_2^{\,T}}{h_r (t_F - t_{d2})} [0{\cdot}33 + 0{\cdot}17\, k_{H2}] \quad (42)$$

Example 2.

If $\Delta < 1$

r_c' may be approximated to unity so that it may be assumed that primary decomposition precedes secondary by a very meager time margin. For all practical purposes it may be assumed that both are initiated at once and continue till the entire mass has decomposed. The time of decomposition may be estimated from an equation similar to equation (9) with the physical properties changed appropriately.

Example 3.

If $0 < \Delta < 1$

secondary decomposition sets in for intermediate values of r_c'. A mathematical analysis of heat transfer for this particular case may now be attempted. At a time $\theta = \theta_c$ the primary decomposition plane is situated at a distance $R \cdot r_c'$ from the centre of the decomposing sphere and the surface represents the initiation of secondary decomposition. In order to calculate the rate at which the secondary decomposition plane advances into the sphere it is necessary to calculate the net accumulation of heat at the secondary decomposition interface. At any time θ ($\theta > \theta_c$), let r_1 and r_2 represent the radial positions of the primary and secondary decomposition planes respectively. The rate at which heat flows on to the secondary interface may be given by

$$q_\theta^{\,2} = \frac{4\pi R^2 h_r (t_F - t_{d2}) r_2'}{r_2' + k_{H2})1 - r_2')} \quad (43)$$

where $r_2' = (r_2/R)$

$k_{h2} = (R \cdot h_r/k_{c2})$

The rate at which heat is removed from the same interface will be given by

$$q_\theta^1 = \frac{4\,\pi\,r_1\,r_2\,k_{e1}\,(t_{d2} - t_{d1})}{(r_2 - r_1)} \qquad (44)$$

The net accumulation of heat will therefore be

$$(q_\theta^2 - q_\theta^1) = 4\,\pi\,R^2\,h_r\,(t_F - t_{d2}) \left[f_2(r') - \Delta f_1(r')\right] \qquad (45)$$

where $$f_1(r') = \frac{r_1'\,r_2'}{(r_2' - r_1')}$$

$$f_2(r') = \frac{r^2}{r_2' + k_{H2}\,(1 - r_2')}$$

The rate of secondary decomposition may be given by

$$\left(\frac{dw}{d\theta}\right)_2 = -\,\rho_2\,4\,\pi\,r_2^2\,\frac{dr_2}{d\theta} \qquad (46)$$

Multiplying the above equation by the total heat of reaction term and equating it to equation (45) and simplifying:

$$\frac{-\,\rho_2(1-x)\,\Delta H_2^T\,R}{h_r\,(t_F - t_{d2})}\,\frac{dr_2'}{d\theta} = \left[f_2(r') - \Delta f_1(r')\right] \qquad (47)$$

In a similar manner, equating the heat reaching the primary decomposition interface q_θ^1 to the heat absorbed for the endothermic reaction based on an instantaneous primary decomposition rate, the following equation may be obtained:

$$\frac{-\,\rho_1\,x\,\Delta H_1^T\,R}{h_r\,(t_F - t_{d2})}\,\frac{dr_1'}{d\theta} = f_1(r') \qquad (48)$$

Equations (47) and (48) represent a set of simultaneous ordinary differential equations which could be solved numerically by the modified method of RUNGE–KUTTA [9]. The above equations may be rewritten in convenient forms to facilitate mathematical procedure, as under:

$$-\frac{dx}{d\theta} = k_1\left[\frac{x\,y}{(y - x)}\right] \qquad (47a)$$

$$-\frac{dy}{d\theta} = k_2\left[\frac{y}{y + k_3\,(1 - y)} - k_4\,\frac{xy}{(y - x)}\right] \qquad (48a)$$

The following new symbols may be equated as under

$$X = r_1';\quad Y = r_2';$$

$$k_1 = \frac{h_r\,(t_F - t_{d2})\,\Delta}{\rho_1\,x\,\Delta H_1^T\,R}$$

$$k_2 = \frac{h_r\,(t_F - t_{d2})}{\rho_2\,(1 - x)\,\Delta H_2^T\,R}$$

$$k_3 = k_{H2};\quad k_4 = \Delta.$$

Procedure.

A time increment $\Delta\,\theta$ may be chosen. With the help of the following ten equations and the initial values of X and Y, the increments $\Delta\,X$ and $\Delta\,Y$ are determined. The relevant equations are:

$$\delta_1 = k_1\left(\frac{x_0\,y_0}{y_0 - x_0}\right)\Delta\theta = f(x_0, y_0)\,\Delta\theta$$

$$\partial_1 = k_2\left[\frac{y_0}{y_0 + k_3\,(1 - y_0)} - k_4\,\frac{x_0\,y_0}{(y_0 - x_0)}\right]\Delta\theta = g\,(x_0, y_0)\,\Delta\theta$$

$$\delta_2 = f\left(x_0 + \frac{\delta_1}{2},\ y_0 + \frac{\partial_1}{2}\right)\Delta\theta$$

$$\partial_2 = g\left(x_0 + \frac{\partial_1}{2},\ y_0 + \frac{\partial_1}{2}\right)\Delta\theta$$

$$\delta_3 = f\left(x_0 + \frac{\delta_2}{2},\ y_0 + \frac{\partial_2}{2}\right)\Delta\theta$$

$$\partial_3 = g\left(x_0 + \frac{\delta_2}{2},\ y_0 + \frac{\partial_2}{2}\right)\Delta\theta$$

$$\delta_4 = f(x_0 + \delta_3,\ y_0 + \partial_3)\,\Delta\theta$$

$$\partial_4 = g\,(x_0 + \delta_3, y_0 + \partial_3)\,\Delta\theta$$

$$\Delta x = \tfrac{1}{6}\,(\delta_1 + 2\,\delta_2 + 2\,\delta_3 + \delta_4)$$

$$\Delta y = \tfrac{1}{6}\,(\partial_1 + 2\,\partial_2 + 2\,\partial_3 + \partial_4)$$

Once the space increments are evaluated, the new set of values for the dependent variables X and Y will be the starting point for repetitive procedure outlined above. The numerical analysis will continue till the sum of successive increments in X add up to r_c'. At this stage, it is evident that primary decomposition will be complete. The time taken for this decomposition will be given by the addition of θ_c with the sum of the successive time increments $\Delta\,\theta$ obtained by the numerical procedure. The radial position of the secondary decomposition plane, r_{2c}', will be given by the difference between 1 and the sum of the successive space increments, ΔY. The time taken for the completion of secondary decomposition will be given from a form of equation which may be

obtained by the integration of the rearranged energy balance equation between limits: $r_2' = r_{2c}'$; $r_2' = 0$. The equation may be derived as

$$\theta = \alpha_2 \left[\frac{(1 - k_{H2})}{3} r_{2c}'^3 + \frac{k_{H2}}{2} r_{2c}'^2 \right] \qquad (49)$$

where $$\alpha_2 = \frac{\rho_2 (1 - x) R \Delta H_2^T}{h_r (t_F - t_{d2})}$$

From the above analysis it is evident that in the evaluation of the total time required for the complete decomposition of the mixed carbonates into a mixture of oxides there is partial overlapping of primary and secondary decompositions. Whereas those parts of the decomposition which occur independently may be evaluated from analytical expressions derived in Part I, for those which overlap the decomposition period has to be evaluated by numerical approximations which can be facilitated with the help of an electronic computer.

Case 2. *Cylinder*

Proceeding in a manner similar to that adopted for a sphere, at any time during the free primary decomposition of $MgCO_3$, the surface temperature of the cylinder may be given by an equation similar to (20):

$$t = \frac{(t_F - t_{d1}/k_{H1} \ln r')}{(1 - 1/k_{H1} \ln r')} \qquad (50)$$

The critical radius r_c' will be obtained on substituting $t = t_{d2}$

$$r_c' = \exp(-\Delta) \qquad (51)$$

The duration of the free decomposition may be evaluated through an equation which may be derived as

$$\theta = \alpha_1 \left[(0{\cdot}50 + 0{\cdot}25 k_{H1}) - \right.$$
$$\left. - \frac{r_c'^2}{2} (1 - k_{H1} \ln r_c') + 0{\cdot}25 k_{H1} r_c'^2 \right] \qquad (52)$$

The problem of secondary decomposition will now be examined only for the case when the magnitude of Δ lies between 0 and 1. For this case distinct decomposition boundaries may be visualized for both $MgCO_3$ and $CaCO_3$. Proceeding as for a sphere, the net accumulation of heat at the secondary decomposition plane may be evaluated. On equating this to the instantaneous absorption of heat for the endothermic reaction calculable as the product of instantaneous decomposition rate and heat of reaction, an equation similar to (47) may be obtained as

$$-\frac{dr_2'}{d\theta} = k_2 \left[\frac{1}{r_2' (1 - k_{H1} \ln r_2')} - \frac{\Delta}{(r_2' \ln r_2'/r_1')} \right] \qquad (53)$$

Further, equating the amount of heat reaching the primary decomposition plane to the product of the instantaneous decomposition rate and heat of reaction, another differential equation may be obtained as follows:

$$-\frac{dr_1'}{d\theta} = \frac{k_1}{(r_1' \ln r_2'/r_1')} \qquad (54)$$

The manner of solving the above set of simultaneous ordinary differential equations and the subsequent method of calculation of decomposition times are just similar to those followed for the case of the sphere cited earlier. An illustrative example of the numerical analysis will now be indicated for the case of a sphere.

Data. Most of the data for the system are taken from Handbook or ICT. $MgCO_3$:

Density	3·04 g/ml
Molecular weight	83·43
Heat of decomposition	1186 B.Th.U/lb
Decomposition temperature	1060 °F
Heat capacity of CO_2 (average)	0·298 B.Th.U/lb °F
Furnace temperature	1835 °F
Radius of sphere	1·0 cm
Radiation coefficient	10 B.Th.U/hr ft² °F
Modified Nusselt number	0·9
Weight fraction in mixture	0·5
Effective density of mixture	159 lb/ft³
Critical radius from equation (35)	0·22
Critical time from equation (39)	0·193 hr

The starting values for the space co-ordinates are:

$$X_0 = 0{\cdot}22\,; \quad Y_0 = 1{\cdot}0$$

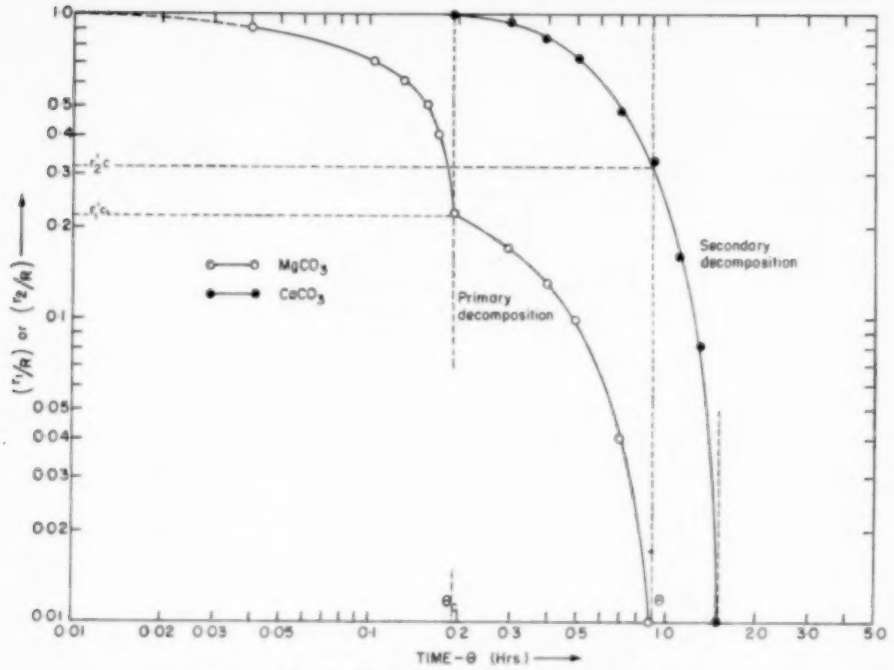

FIG. 7. Thermal decomposition of mixed carbonates.

The numerical values for the constants are

$$k_1 = 1{\cdot}78\,;\ k_2 = 1{\cdot}23\,;\ k_3 = 0{\cdot}9\,;\ k_4 = 3{\cdot}55$$

The time increment may be fixed at 0·01 hr and the numerical computations are performed on an IBM 650 computer. The results are expressed in the form of Fig. 7. From the results it is evident that the primary decomposition is complete within 0·88 hr and the total decomposition, within 1·50 hr.

Conclusions

The mathematical treatment has been based on quasi steady state conditions. It may be possible to develop a more rigorous unsteady state heat and mass transfer analysis for the decomposing sphere or cylinder. This has not been attempted nor an analysis for the case of mass transfer for the two-phase system, based on quasi-steady state conditions, as probably, no new ideas can be visualised. It may appear that the decomposition pattern postulated for the mixed carbonates may be too simple, but such a simplification is a necessity to keep the mathematical complexities within reasonable limits without, however, indulging in over-simplifications. Finally it may be remarked that the verification of the mathematical procedures enumerated in Part II of this contribution must await future reliable experimental data for the physical properties of the system.

NOMENCLATURE

C_p = heat capacity
d = sphere diameter
D = diffusion coefficient
E = porosity
f, g = functions
ΔH = heat of decomposition
h = film coefficient
k_H = Modified Nusselt number
k_g = mass transfer coefficient
k, k_2 = constants
l = length of cylinder
N = mass transfer rate
p = partial pressure
q = heat transfer rate
R = radius of sphere or cylinder, gas constant

r = radial position
r' = dimensionless parameter $= r/R$
r_m = mean radius
t = temperature
W = mass of the substance decomposing
X = mass fraction, dimensionless space co-ordinate
Y = dimensionless space co-ordinate
Z_g = equivalent film thickness
ϵ = emissivity
ρ = density
θ = time
α = constant
β = tortuosity factor
Δ = dimensionless parameter

References

[1] Polanyi M. and Wigner E. *Z. Phys. Chem.* 1928 A **139** 439.
[2] Satterfield C. N. and Feakes F. *Amer. Inst. Chem. Engrs. J.* 1959 **5** 115.
[3] Carmen P. C. *Flow of Gases through Porous Media* p. 79. Butterworth Scientific Publications, London 1956.
[4] Haslam R. T. and Smith V. C. *Industr. Engng. Chem.* 1928 **20** 170.
[5] Bryant W. M. D. *Industr. Engng. Chem.* 1933 **25** 821.
[6] Langmuir I. *Phys. Rev.* 1918 **12** 368.
[7] Chilton T. H. and Colburn A. P. *Industr. Engng. Chem.* 1934 **26** 1183.
[8] Hougen O. A. *Reaction Kinetics in Chemical Engineering* CEP Monograph series, No. 1. Vol. 47 p. 54 1951.
[9] Sherwood T. K. and Reed C. E. *Applied Mathematics in Chemical Engineering* (1st Ed.) p. 132. McGraw Hill, New York 1939.
[10] Satterfield C. N. and Feakes F. *Amer. Inst. Chem. Engrs. J.* 1959 **5** 115.
[11] Britton *Trans. Faraday Soc.* 1952 **48** 63.

VOL. 16 1962

Chemical Engineering Science, 1961, Vol. 16, pp. 21 to 30. Pergamon Press Ltd., London. Printed in Great Britain.

Mass transfer with chemical reaction

J. G. VAN DE VUSSE

Koninklijke/Shell-Laboratorium, Amsterdam
(Shell Internationale Research Maatschappij N.V.)

(*Received* 11 *May* 1960)

Abstract—A description is given of the kinetics of simultaneous mass transfer and chemical reactions as occurring in gas–liquid systems. Expressions have been derived for the over-all reaction rate both for the stationary and the unsteady state. Use has been made of the film theory and of the penetration theory.

The case of a reaction of zero order in the gaseous compound, which has not yet been dealt with in literature, is treated. This case is often encountered in oxidation reactions of hydrocarbons.

It is shown that at high transfer rates the over-all reaction rate will approach the chemical reaction rate.

Résumé—L'auteur donne une description de la cinétique du transfert de matiére et des réactions chimiques se présentant simultanément dans des systèmes gaz–liquide. Il a déduit des équations pour la vitesse réactionnelle totale aussi bien pour l'état stationnaire que pour l'état non-stationnaire, en se servant des théories de la couche mince et de la pénétration.

Le cas d'une réaction d'ordre zéro par rapport au composé gazeux, qui n'a pas encore été mentionné dans la littérature, est traité. Ce cas se présente souvent dans les réactions d'oxydation d'hydrocarbures.

L'auteur démontre qu'à de hautes vitesses de transfert, la vitesse réactionnelle totale s'approchera de la vitesse réactionnelle chimique.

Zusammenfassung—In manchen Gas–Flüssig-Systemen finden Massenübergang und chemische Reaktionen gleichzeitig statt. Die Kinetik dieser gleichzeitig vor sich gehenden Prozesse wird beschrieben. Für die gesamte Reaktionsgeschwindigkeit, sowohl im stationären als im nichtstationären Zustand, wurden mit Hilfe der Film- und der Durchdringungstheorie Formelausdrücke abgeleitet.

Ferner wird der Fall einer Reaktion nullter Ordung (bezogen auf die gasförmige Komponente) behandelt, der bis jetzt in der Literatur unberücksichtigt geblieben ist. Ein solcher Fall tritt häufig in Oxydationsreaktionen von Kohlenwasserstoffen ein.

Es wird gezeigt, dass sich bei hohen Übergangsgeschwindigkeiten die gesamte Reaktionsgeschwindigkeit der chemischen Reaktionsgeschwindigkeit annähert.

1. INTRODUCTION

MASS transfer between phases has become a subject of major importance, particularly in industrial operations involving absorption, extraction, etc. In many of such processes mass transfer and chemical reaction take place simultaneously, as for instance in the chemical absorption of a gas in a liquid.

During recent years the process of simultaneous absorption and chemical reaction has been studied both theoretically and experimentally by many investigators. Most experiments dealt with the absorption of CO_2 and NO_2 in aqueous solutions.

Expressions for the over-all absorption rate, which were derived from the diffusion equation, could be used for evaluation of the experimental results. It might have been expected that in principle identical expressions could be used for evaluation of the over-all reaction rate in gas–liquid reaction systems, e.g. in the oxidation of hydrocarbons by gaseous oxygen. However, an analysis shows that most oxidations belong to a type of reaction to which the existing expressions do not apply.

The existing theories will therefore be revised and extended so as to include this type of reaction.

2. Basic Theory and Equations

Basic theory

Gas–liquid reactions involve physical transport processes and chemical reactions. The over-all reaction rate is controlled by the physical transfer rate and/or by the chemical reaction rate and can in principle be calculated from these two rates. Prior to this calculation a description of the transfer mechanism must be given. Two generally used concepts of this mechanism will be discussed.

Film theory. The theory most frequently applied is based on the two-film concept of Lewis and Whitman [1], [2]. It postulates a stagnant layer or film in the gas and in the liquid phase. At the interface there is equilibrium between the concentrations in the gas and in the liquid. Outside the two films the respective reactant concentrations in liquid and gas are considered to be uniform. On the basis of this theory formulae can be derived for the stationary-state absorption process starting from the diffusion equations for the stationary state.

Penetration theory. More recent theories of Higbie [3] and of Danckwerts [4] assume that after some time the interface is renewed by fresh liquid and fresh gas. The turbulent eddies are supposed to penetrate towards the interface.

The elements of gas and liquid leaving the interface are more or less saturated with the absorbed component. The time of renewal can be the same for all elements of fluid (Higbie) or can be described with a statistical distribution curve (Danckwerts).

On the basis of this theory, formulae for the over-all reaction rate in the stationary state are obtained. First the unsteady-state diffusion equation has to be solved for a semi-infinite space. The ultimate rate equations for the stationary state are then obtained by considering the process as consisting of a sequence of small unsteady-state absorption processes of small elements of volume, which regularly and continuously penetrate to the interface.

In this article therefore three different types of rate equations will be discussed:

(a) The film-theory equation.
(b) The unsteady-state equation.
(c) The penetration-theory equation.

The first and the last equation apply to stationary-state conditions, although the last is derived with the aid of the unsteady-state equation under (b).

Basic equations

In all equations the concentration of the substance to be absorbed by the liquid at the interface A_i is taken as a basis, hence the diffusion in the gas phase may be left out of consideration [5].

After entering the liquid phase the solute starts to diffuse towards the main body of the liquid, but also immediately begins to react with the dissolved substance B. This means that there is also a diffusional transport of B in the opposite direction towards the interface. These processes are expressed by the following differential equations*:

$$\frac{\partial A}{\partial t} = D_1 \frac{\partial^2 A}{\partial x^2} - \xi_1 \dagger, \qquad (1)$$

where ξ_1 is the consumption of molecules A due to the chemical reaction; $D_1 (\partial^2 A / \partial x^2)$ represents the net diffusional transport rate and $\partial A / \partial t$ is the accumulation rate of A. In the same way we get for B

$$\frac{\partial B}{\partial t} = D_2 \frac{\partial^2 B}{\partial x^2} - \xi. \qquad (2)$$

If one molecule of A reacts with Z molecules of B, then $\xi_2 = Z\,\xi_1$. In the following derivations we take $Z = 1$ and also $D_1 = D_2 = D$. In order to solve the differential equations (1) and (2) the initial and boundary equations must be known.

Generally the component B in the liquid is assumed to be non-volatile; the interfacial concentration of A is assumed to be equal to the value in equilibrium with the gas, where the partial pressure of A is constant.

*In these equations a linear co-ordinate system has been applied, although for a dispersed phase a spherical co-ordinate system would have been more logical. However, the mathematical treatment would then become too involved.

†See also Nomenclature.

The initial concentration of B in the liquid before exposure of the liquid to the gas is assumed to be uniform. We now have to distinguish two cases, viz. the unsteady-state absorption process and the stationary-state absorption process.

1. *Transient or unsteady-state diffusion equations.* In this case

$$\frac{\partial A}{\partial t} \neq 0 \text{ and } \frac{\partial B}{\partial t} \neq 0.$$

The body of liquid can be taken as effectively infinite and the concentrations of A and B must remain positive and finite. Then the following boundary conditions apply:

$$t = 0,\ x \geqslant 0: \quad A = A_0, \qquad B = B_0; \tag{3}$$

$$t > 0,\ x = 0: \quad A = A_i, \qquad \frac{\partial B}{\partial x} = 0; \tag{4}$$

$$t > 0,\ x \to \infty: \ A_i \geqslant A \geqslant 0,\ 0 \leqslant B \leqslant B_0. \tag{5}$$

The solutions of equations (1) and (2) subject to these conditions can be used in deriving formulae for the over-all reaction according to the penetration theory.

2. *Stationary-state diffusion equations.* In this case

$$\frac{\partial A}{\partial t} = \frac{\partial B}{\partial t} = 0.$$

Equations (1) and (2) then reduce to:

$$D\frac{d^2A}{dx^2} = \xi \tag{1a}$$

$$D\frac{d^2B}{dx^2} = \xi \tag{2a}$$

The solutions of equations (1a) and (2a) can be applied for the derivation of formulae for the over-all reaction rate based on the film theory.

The boundary condition (4) still applies. However, because of the introduction of a finite film thickness x_L the other boundary condition changes. In the bulk of the liquid ($x > x_L$) the concentrations of A and B are assumed to be uniform: A_L and B_L.

So, the following boundary conditions now apply:

$$x = 0: \qquad A = A_i, \qquad \frac{dB}{dx} = 0; \tag{4a}$$

$$x \geqslant x_L: \qquad A = A_L, \qquad B = B_L. \tag{5a}$$

The chemical reaction, which enters the differential equations by means of the reaction rate ξ, must be expressed in terms of A and B in order to solve the equations.

To obtain from the solutions of these equations the over-all reaction rate we proceed as follows:

The rate of diffusion of A into the liquid is given by

$$N_A = -D\left(\frac{\partial A}{\partial x}\right)_{x=0}. \tag{6}$$

If a/ϕ represents the amount of interface per unit of volume, then the over-all reaction rate R is given by

$$R = N_A\frac{a}{\phi}. \tag{7}$$

Another way of calculating the over-all reaction rate for the film theory is by considering that

$$R = \frac{a}{\phi}(N_A - N_A') + \frac{a}{\phi}N_A' \tag{8}$$

where $a/\phi\,(N_A - N_A')$ gives the number of molecules reacting in the film region and $a/\phi\,N_A'$ gives the number of molecules reacting in the main body of liquid. The latter may be found from

$$\frac{a}{\phi}N_A' = -\frac{a}{\phi}D\left(\frac{dA}{dx}\right)_{x=x_L} = \left(1 - \frac{ax_L}{\phi}\right)\xi_L \tag{9}$$

where ξ_L is the chemical reaction rate per unit volume in the main body of the liquid.

If the stagnant film volume ($a\,x_L$) is small compared with the total volume (ϕ), we may write

$$\frac{a}{\phi}N_A' = \xi_L$$

With regard to the possibility of actually solving the equations the following observations may be made:

If $\xi = k\,AB$ (second-order reaction), a general exact solution appears to be impossible; only for some special cases solutions or approximate solutions have been obtained.

An approximate, but accurate, solution for the stationary state, based on the film theory, has been given by HOFTIJZER and VAN KREVELEN [6].

A theory for a very rapid reaction under unsteady-state absorption conditions has been given by DANCKWERTS [7] and by SHERWOOD and PIGFORD [8].

If $\xi = kA$ (first-order reaction), exact solutions can be obtained. It has been shown by VAN KREVELEN [6], that in case of an excess amount of component B, the solutions for second-order reaction will become equal to the results for a first-order reaction. B is then assumed to be uniform throughout the liquid.

3. First-order Chemical Reactions ($\xi = kA$)

(a) *Stationary-state diffusion process (film theory)*

A solution of the stationary-state diffusion equation for the case of a first-order reaction ($\xi = kA$) and a linear co-ordinate system has been given by HATTA [9]. For the diffusion rate this author finds

$$N_A = A_i \sqrt{kD} \left[\frac{\sinh \alpha + \beta \cosh \alpha}{\cosh \alpha + \beta \sinh \alpha}\right] \qquad (10)$$

where $\alpha = x_L \sqrt{\frac{k}{D}}$ and $\beta = \left(\frac{\phi}{a} - x_L\right) \sqrt{\frac{k}{D}}$

Special cases. (i) $\alpha > 1$.

Then $$N_A = A_i \sqrt{kD} \qquad (11)$$

The reaction takes place within the film. In the bulk of the liquid the concentration of A is zero. The reaction rate ($R = (a/\phi) N_A$) is proportional to the specific surface a/ϕ, hence it will increase with increasing stirring speeds. The value of α, however, will decrease at increasing stirring speeds, till eventually $\alpha \approx 1$ and (11) no longer holds.

In a spherical co-ordinate system with a dispersed phase in the form of spheres there is a radial diffusion into the continuous phase, where the reaction takes place. With the boundary conditions that the concentration at the interface is constant and that the concentration gradient "halfway" between the spheres is zero, HARDEBOL [10] derived for the reaction rate in spherical co-ordinates

$$R = \frac{3 k A_i H}{\psi^2} \left[\frac{(\psi + 1)(1 - p\psi) \exp(p - 1)\psi + (\psi - 1)(1 + p\psi) \exp(1 - p)\psi}{(1 - p\psi) \exp(p - 1)\psi - (1 + p\psi) \exp(1 - p)\psi}\right] \qquad (12)$$

where

H = volume fraction of dispersed phase

$\psi = r \sqrt{\frac{k}{D}}$ (r = radius of sphere)

$p = H^{-1/3}$.

The average "halfway" distance ρ between the spheres follows from

$$n \frac{4}{3} \pi \rho^3 = 1,$$

where

n = number of spheres per unit of volume.

If $\psi \to 0$ (at increasing stirring speeds) or if $H \to 1$ ($r = \rho$), the over-all reaction rate R approaches the chemical reaction rate $k A_i (1 - H)$, hence is independent of specific area and diffusivity, which is in agreement with physical intuition. For $(p - 1)\psi > 2$ and $\psi > 1$, the over-all reaction rate becomes

$$R = \frac{3 H A_i}{r} \sqrt{(kD)} \qquad (13)$$

which is equivalent to equation (11), since $3H/r = a/\phi$.

It may be noted that in the theory of diffusion and reaction in solid particles [11], where also use is made of a spherical co-ordinate system, similar results are obtained. Thus for a particle diameter smaller than $2\sqrt{(D/k)}$, the over-all reaction rate approaches the chemical reaction rate whereas for particle diameters larger than $2\sqrt{(D/k)}$ equation (11) is obtained.

(ii) With the linear co-ordinate system the over-all reaction rate can become equal to the chemical reaction rate only if the quantity α in equation (10) is small compared to 1.

then $$\frac{1}{N_A} = \frac{1}{k_L A_i} + \frac{1}{(\phi/a) k A_i} \qquad (14)$$

and also $N_A = k_L (A_i - A_L)$.

where $k_L = \frac{D}{x_L}$.

In this case the over-all resistance for the mass transfer combined with a chemical reaction may be considered as consisting of the sum of a physical and a chemical resistance.

If $k_L A_i \ll \frac{\phi}{a} k A_i$, then $N_A = k_L A_i$

(physical transfer rate).

If $k_L A_i \gg \frac{\phi}{a} k A_i$, then $N_A = k A_i \frac{\phi}{a}$

(chemical reaction rate).

VOL. 16 1962

(b) *Unsteady-state diffusion process*

A solution of the unsteady-state diffusion equation has been given by Danckwerts [11] and by Sherwood and Pigford [7]. The latter also considers the case of a reversible first-order reaction. For the irreversible reaction the Laplace-transformed concentrations of A and B become

$$\bar{A} = \frac{A_i}{p} \exp\left[-\sqrt{\left(\frac{k+p}{D}\right)} x\right] + \frac{A_0}{(k+p)}\left\{1 - \exp\left[-\sqrt{\left(\frac{k+p}{D}\right)} x\right]\right\}, \text{ and} \quad (15)$$

$$\bar{B} = \frac{B_0}{p} + \left(\frac{A_i}{p} - \frac{A_0}{k+p}\right)\left\{\exp\left[-\sqrt{\left(\frac{k+p}{D}\right)} x\right] - \sqrt{\left(\frac{k+p}{p}\right)} \exp\left[-\sqrt{\left(\frac{p}{D}\right)} x\right]\right\} - \frac{k A_0}{(k+p)\,p} \quad (16)$$

(p = Laplace parameter).

These equations are only valid as long as the concentrations of A and B are positive. However, the concentration of B will after a certain time drop to zero, and since the concentration of A, and hence the rate of reaction, is always the greatest at the interface ($x = 0$) the depletion of B starts at the interface. The concentration of B at the interface amounts to

$$B_{(x=0)} = B_0 + A_i - A_0 - A_i \exp\left(-\frac{kt}{2}\right)\left[(1+kt)\, I_0\left(\tfrac{1}{2}kt\right) + kt\, I_1\left(\tfrac{1}{2}kt\right)\right] + A_0 \exp\left(-\frac{kt}{2}\right) I_0\left(\tfrac{1}{2}kt\right). \quad (17)$$

I_0 and I_1 are the modified Bessel functions of the first kind, of the zero-th and the first order, respectively. It appears from equation (17) that the concentration of B at the interface ($x = 0$) is independent of the diffusivity. This is due to the absence of diffusional transport of B at the interface:

$$D\left(\frac{\partial B}{\partial x}\right)_{x=0} = 0.$$

The "depletion" time t_d, for which $B_{(x=0)} = 0$, follows from equation (17):

$$\exp\left(-\frac{kt_d}{2}\right)\left[(1+kt_d)\, I_0\left(\tfrac{1}{2}kt_d\right) + kt_d\, I_1\left(\tfrac{1}{2}kt_d\right)\right] - \frac{A_0}{A_i}\exp\left(-\frac{kt_d}{2}\right) I_0\left(\tfrac{1}{2}kt_d\right) = \frac{B_0 + A_i - A_0}{A_i}. \quad (17a)$$

This "depletion" time cannot be influenced by diffusivity for the same reason as $B_{(x=0)}$. A graphical representation of relation (17a), which is given in Fig. 1, shows that depletion starts later at higher B_0/A_i ratios and starts sooner if A_0 approaches A_i, as could be expected. For larger values of kt_d equation (17a) simplifies to

$$\frac{B_0 + A_i - A_0}{A_i} = 2\sqrt{\frac{kt_d}{\pi}}.$$

For times greater than the "depletion" time instead of equations (1) and (2), the equations

$$\frac{\partial A}{\partial t} = D\frac{\partial^2 A}{\partial x^2} - k\,A\,H(B) \text{ and} \quad (18)$$

$$\frac{\partial B}{\partial t} = D\frac{\partial^2 B}{\partial x^2} - k\,A\,H(B) \quad (19)$$

must be used,

where the step function $H(B) = 0$ for $B < 0$,

and $H(B) = 1$ for $B \geqslant 0$.

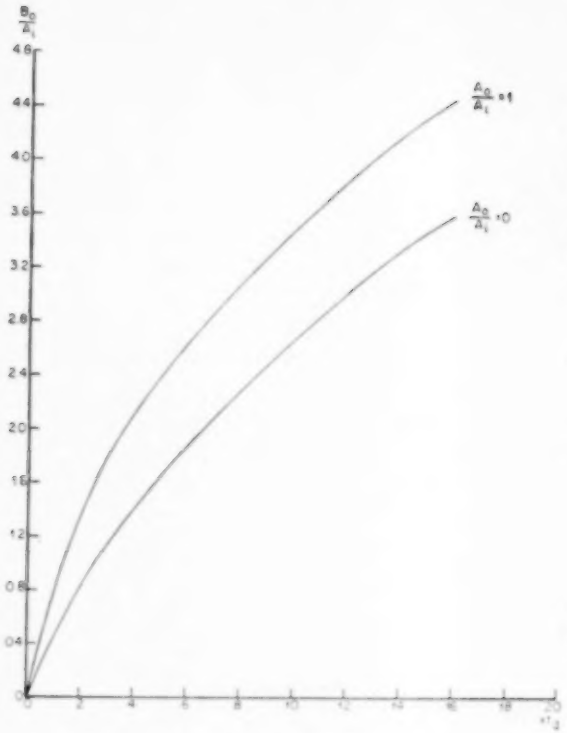

FIG. 1. "Depletion" time as a function of the reactants ratio B_0/A_i for first-order reactions.

The boundary value of x below which B will be zero is a function of t. An analytical solution of this "moving" boundary problem could not be found. At extremely high values of the reaction rate constant k, the problem can be simplified considerably by assuming a thin reaction front at the "moving" boundary, so that the reaction rate ξ can be left out from the diffusion equations. A solution has been given by SHERWOOD and PIGFORD [8] and by DANCKWERTS [7].

For times t smaller than the "depletion" time, the unsteady-state reaction rate follows from

$$N_A = -D\left(\frac{\partial A}{\partial x}\right)_{x=0} =$$

$$= A_i\sqrt{(kD)}\left[\operatorname{erf}\sqrt{(kt)} + \frac{\exp(-kt)}{\sqrt{\pi kt}}\right] - \frac{A_0\sqrt{D}}{\sqrt{\pi t}}. \qquad (20)$$

For large values of kt ($kt \gg 1$), we get

$$N_A = A_i\sqrt{k\,D}. \qquad (21)$$

The rate of diffusion is now independent of t, as could be expected. The expression (21) represents the stationary diffusion rate in the case of a molecular diffusion with simultaneous reaction throughout the liquid. The same expression is obtained in the film theory, if the reaction takes place in the film only (equation 11).

(c) *Stationary-state diffusion process (penetration theory)*

According to the penetration theories the overall reaction rate can be found from

$$R = \frac{a}{\phi}\int_0^\infty N_A f(t)\,dt,$$

where $f(t)$ is a function giving the distribution of residence times of the elements of liquid.

In the HIGBIE concept it is

$$f(t) = \frac{1}{\theta} \text{ for } 0 < t < \theta$$

and $$f(t) = 0 \text{ for } \theta < t < \infty,$$

where θ = residence time on interface.

In the DANCKWERTS concept it is

$$f(t) = s\exp(-st) \text{ for } 0 < t < \infty,$$

where s is reciprocal average residence time of an element of volume at the interface.

Hence, in the DANCKWERTS concept,

$$R = -\frac{a}{\phi}Ds\int_0^\infty \left(\frac{\partial A}{\partial x}\right)_{x=0}\exp(-st)\,dt$$

or

$$R = -\frac{a}{\phi}Ds\left(\frac{\partial \bar{A}}{\partial x}\right)_{x=0}, \qquad (22)$$

where $(\partial\bar{A}/\partial x)_{x=0}$ is the Laplace-transformed gradient of A at $x = 0$, with s as parameter. Since the residence time of the elements of fluid at the interface varies between zero and infinity, strictly speaking equation (15) cannot be applied. However, if the average residence time $1/s$ is

small compared with the "depletion" time, then the contribution in the diffusion rate of the elements of volume with a residence time larger than the "depletion" time will become negligibly small.

Differentiation of equation (15) and substitution in equation (22) gives

$$R = \frac{a}{\phi} A_i \sqrt{[(k+s)\,D]} - \frac{a}{\phi} A_0 s \sqrt{\left(\frac{D}{k+s}\right)}. \quad (23)$$

A_0 is not a specifiable constant in the penetration theory but is rather the average value of A for the elements of fluid that have come to the interface.

The value of the average concentration A_0 of the elements of fluid equals the concentration in the bulk of the liquid and is found from the equivalence of the diffusional transport rate and the bulk reaction rate:

$$R = \frac{a}{\phi} \sqrt{[D\,(k+s)]} \left[A_i - A_0 \frac{s}{k+s}\right] = kA_0.$$

Hence: $R = k\,A_0 =$

$$= \frac{kA_i \sqrt{[D\,(k+s)]}}{[s\,(k+s)] \sqrt{[D\,(k+s)]} + (\phi/a)\,k} \quad (24)$$

It may be assumed that at increasing stirrer speeds both a/ϕ and s will increase.

From equation (24) it follows that

if $$\frac{a}{\phi} \gg \frac{k}{s} \sqrt{\left(\frac{k+s}{D}\right)}$$

the reaction rate R becomes

$$R = k\,A_i \frac{k+s}{s}.$$

If moreover $s \gg k$, then $A_0 = A_i$ and $R = k\,A_i$, as must be expected.

4. Chemical Reactions with Zero-order in A ($\xi = kB$)

No literature has been found on a theory considering this case. This may be due to the fact that a reaction according to this type does not seem to occur frequently in absorption processes. However, it can be shown that a reaction mechanism according to this type frequently occurs in chemical gas–liquid reactions as, for example, in the oxidation of hydrocarbons (see appendix). The equations pertaining to this type of reaction and their solution will be derived below.

(a) *Stationary-state diffusion process (film theory)*

The over-all reaction rate in this theory becomes:

$$R = \frac{a}{\phi} \sqrt{(kD)}\, B_L \tanh x_L \sqrt{\left(\frac{k}{D}\right)} + k\,B_L \left(1 - \frac{ax_L}{\phi}\right). \quad (25)$$

The first term in the right-hand member of equation (25) represents the reaction rate in the film, the second term the reaction rate in the bulk of the liquid.

At low stirrer speeds $x_L \sqrt{(k/D)} > 1$ and equation (25) becomes:

$$R = \frac{a}{\phi} B_L \sqrt{(kD)} + \left(1 - \frac{ax_L}{\phi}\right) kB_L. \quad (26)$$

At high stirrer speeds $x_L \sqrt{(k/D)} < 1$ and then equation (25) becomes:

$$R = kB_L \text{ (chemical reaction rate)}. \quad (27)$$

(b) *Unsteady-state diffusion process*

The solution of the equations (1) and (2) gives for the Laplace-transformed concentrations $\bar{A}$ and $\bar{B}$:

$$\bar{A} = \left[\frac{A_i - A_0}{p} + \frac{k\,B_0}{p\,(k+p)}\right] \exp\left[-\sqrt{\left(\frac{p}{D}\right)} x\right] - \frac{k\,B_0}{p\,(k+p)} + \frac{A_0}{p} \quad (28)$$

and $$\bar{B} = \frac{B_0}{p+k}. \quad (29)$$

The concentration of $B = B_0 \exp(-kt)$ is independent of x as long as A remains positive. However, also here the reactant A will be depleted after a certain time and since the concentration of A will be lowest for $x = \infty$, depletion starts at infinite x. A will be positive for $x = \infty$ only if

$$k\,t \leqslant \ln \frac{B_0}{B_0 - A_0}. \quad (30)$$

VOL. 16 1962

Since in most practical cases A_0 will be small compared with B_0, condition (30) means that the equations (1) and (2) are valid only for small values of kt and even cannot be used at all if $A_0 = 0$. In the same way as with the first-order reactions, the equations

$$\frac{\partial A}{\partial t} = D\frac{\partial^2 A}{\partial x^2} - kB\,H(A) \qquad (31)$$

$$\frac{\partial B}{\partial t} = D\frac{\partial^2 B}{\partial x^2} - k\,B\,H(A) \qquad (32)$$

must be used, instead of equations (1) and (2). Here, $H(A) = 0$, if $A < 0$ and $H(A) = 1$ if $A \geqslant 0$.

An analytical solution of these non-linear differential equations could not be found in this case either.

If condition (30) is fulfilled the rate of diffusion N_A is

$$N_A = -D\frac{\partial A}{\partial x} = \frac{(A_i - A_0)\sqrt{D}}{\sqrt{\pi t}} + 2\,B_0\sqrt{\left(\frac{kD}{\pi}\right)}\int_0^{\sqrt{kt}} \exp(v^2 - kt)\,dv. \qquad (33)$$

The integral $\int_0^{\sqrt{kt}} \exp(v^2 - kt)\,dv$ can only be solved by numerical means [12]. For small values of kt ($kt \ll 1$) the value of the intregal is given by

$$\int_0^{\sqrt{kt}} \exp(v^2 - kt)\,dv = \sqrt{kt}$$

and the number of molecules diffusing into the liquid may then be found from

$$N_A = (A_i - A_0)\sqrt{\left(\frac{D}{\pi t}\right)} + 2\,B_0 k\sqrt{\frac{Dt}{\pi}}. \qquad (34)$$

(c) *Stationary-state diffusion process (penetration theory)*

Here the elements of fluid carry reactant A to the bulk of the liquid ($x \to \infty$), where depletion of A can only be prevented if $1/s$ is small compared with the "depletion" time.

By making use of equations (22) and (28) the reaction rate according to the DANCKWERTS' concept would be

$$R = \frac{a}{\phi}\sqrt{(D\,s)}\left[A_i - A_0 + \frac{kB_0}{k+s}\right]. \qquad (35)$$

The value of A_0 again follows from the equivalence of diffusional transport rate and chemical reaction rate ($R = k\,B$):

$$A_0 = A_i + \frac{kB_0}{k+s} - \frac{kB}{(a/\phi)\sqrt{Ds}}. \qquad (36)$$

The reaction rate ($R = k\,B$) will not be influenced by stirring as long as A is positive throughout the liquid, since B remains independent of x. As soon as A drops to zero (to start with at $x = \infty$), an influence of stirring on reaction rate can be expected.

5. Discussion

In many heterogeneous reaction systems the over-all reaction rate is determined both by the chemical reaction and the transfer of the reactants. In these cases it is of importance to evaluate quantitatively the rate-determining steps, because during scaling-up the individual processes are affected in a different way. In the preceding section the mathematical expressions for the over-all rate, which are necessary for this evaluation, have been derived. These fulfill the condition that at higher transfer rates the over-all rate will approach the chemical reaction rate. The expressions based on the film theory are more explicit than those based on the penetration theory. The quantitative influences of mass transfer and chemical reaction on the overall-rate still await experimental confirmation. Until this has been obtained the equations should be used with some reserve.

Appendix

Kinetic analysis of oxidation reactions

The oxidation of liquid hydrocarbons by oxygen is generally assumed to be a free-radical chain process, where the primary products are hydroperoxides.

The following reaction mechanism is assumed to account for the oxidation of the hydrocarbon (RH) to peroxide [13, 14]:

Initiation: Production of $R^\bullet$ or $RO_2^\bullet$ radicals.

Propagation: $R^\bullet + O_2 \xrightarrow{k_1} RO_2^\bullet$;

$RO_2^\bullet + RH \xrightarrow{k_2} ROOH + R^\bullet$.

Termination: $2R^\bullet \rightarrow$ non-initiating

$R^\bullet + RO_2^\bullet \rightarrow$ or non-propagating

$2\,RO_2^\bullet \rightarrow$ products

It is further assumed that the conditions are such that the mass transfer rate of oxygen is not a limiting factor. This means that when in this autoxidation reaction the concentration of the chain-carrying radicals has reached a stationary state, the oxidation rate (in moles of oxygen consumed per unit time and volume) can be found from [13, 14]:

$$K = \frac{d[O_2]}{dt} = -k_1[R^\bullet][O_2],$$

$$\frac{d[R^\bullet]}{dt} \approx \frac{d[RO_2^\bullet]}{dt} \approx 0 \text{ and}$$

$$\frac{d[RO_2^\bullet]}{dt} = k_1[R^\bullet][O_2] - k_2[RO_2^\bullet][RH].$$

Assuming that $[R^\bullet + RO_2^\bullet]$, which is determined by the intitiation and termination reactions, will be constant, it can easily be shown that

$$\frac{1}{K} = \frac{1}{K_1} + \frac{1}{K_2},$$

where $K_1 = -k_1[O_2][R^\bullet + RO_2^\bullet]$

and $K_2 = -k_2[RH][R^\bullet + RO_2^\bullet]$.

The O_2 absorption rate will not be affected by decomposition of the peroxides, unless O_2 is consumed or formed in the subsequent reactions.

The following two cases can be distinguished:

(1) $\dfrac{k_1[O_2]}{k_2[RH]} > 1.$

Then $K = K_2 = -k_2[RH][R^\bullet + RO_2^\bullet] \approx -k_2[RH][RO_2^\bullet]$.

The reaction is zero-order with respect to oxygen.

(2) $\dfrac{k_1[O_2]}{k_2[RH]} < 1.$

Then $K = K_1 = -k_1[O_2][R^\bullet + RO_2^\bullet] \approx -k_1[O_2][R^\bullet]$.

The reaction is now a first-order with respect to oxygen. This case will occur at low oxygen concentrations in the liquid hence at low oxygen pressures in the gas phase.

The kinetic aspects of the oxidation of hydrocarbons indicated by the mechanism outlined above are in general agreement with experimental evidence [13–17]. At oxygen pressures higher than about 20 cm Hg most oxidation rates are independent of oxygen pressure and proportional to hydrocarbon concentration. This is what is usually encountered in practical applications: most oxidation reactions belong to the type $\xi = kB$ (zero-order chemical reactions).

Nomenclature

A	= concentration of component A	kgmol/m^3
a/ϕ	= interfacial area per unit volume	m^2/m^3
B	= concentration of component B	kgmol/m^3
D	= coefficient of diffusion	m^2/sec
i (subscript)	= interface	
K	= reaction rate	kgmol/sec m^3
k	= reaction constant	sec^{-1}
$k_L (= D/x_L)$	= mass transfer coefficient	m/sec
N_A	= rate of mass transfer per unit area of interface	kgmol/sec m^2
R	= over-all rate of reaction	kgmol/sec m^3
s	= fractional rate of renewal of surface	sec^{-1}
t	= time	sec
x	= dimension perpendicular to interface	m
x_L	= effective film thickness	m
θ	= residence time	sec
ξ	= rate of chemical reaction	kgmol/sec m^3

References

[1] Lewis W. K. and Whitman W. G. *Industr. Engng. Chem.* 1924 **16** 1215.
[2] Whitman W. G. *Chem. Metall. Engng.* 1923 **24** 146.
[3] Higbie R. *Trans. Amer. Inst. Chem. Engng.* 1935 **31** 365.
[4] Danckwerts P. V. *Industr. Engng. Chem.* 1951 **43** 1460.
[5] Hoftijzer P. J. and van Krevelen D. W. *Trans. Inst. Chem. Engng.* 1954 **32** 60.
[6] van Krevelen D. W. and Hoftijzer P. J. *Rec. Trav. Chim.* 1948 **67** 563.
[7] Danckwerts P. V. *Trans. Faraday Soc.* 1950 **46** 300.
[8] Sherwood T. K. and Pigford R. L. *Absorption and Extraction* (2nd Ed.). pp. 328–337, McGraw-Hill, New York 1952.
[9] Hatta S. *Techn. Rep. Tokohû Imp. Univ.* 1932 **10** 119.
[10] Hardebol J. Private communication.
[11] Thiele E. W. *Industr. Engng. Chem.* 1939 **31** 916.

[12] JAHNKE E. and EMDE F. *Funktionentafeln*. Dover Publications, New York 1945.
[13] BATEMAN L. *Quart. Rev.* 1954 **8** 147.
[14] BOLLAND J. L. *Quart. Rev.* 1949 **3** 1.
[15] FORTUIN J. P. Thesis, Delft 1952.
[16] STRANG A. Thesis, Amsterdam 1951.
[17] VAN DE VUSSE J. G. *Chem. Engng. Sci.* 1958 **8** 72.

VOL
16
196

Chemical Engineering Science, 1961, Vol. 16, pp. 31 to 38. Pergamon Press Ltd., London. Printed in Great Britain.

Pore size distribution functions for porous catalysts

J. O. Mingle and J. M. Smith
The Technological Institute, Northwestern University, Evanston, Illinois, U.S.A.

(*Received* 18 *August* 1960; *and in revised form* 25 *November* 1960)

Abstract—A new expression is presented for the thickness of the adsorbed layer of nitrogen on a porous catalyst. Its use requires two commonly derived properties of porous catalysts, the average pore radius, $\bar{r}$ and the heat-of-adsorption constant c obtained from the B–E–T (Brunauer–Emmett–Teller) surface area equation. Using the new expression adsorption isotherms can be developed for analytical pore size distribution functions of any type. These may be compared with experimental adsorption data to ascertain the most suitable pore size distribution. It is advantageous to have an analytical function for the pore size distribution when additional calculations, for example of effectiveness factors, are to be made.

Tables are presented for computed isotherms in terms of values of $\bar{r}$ from 10 to 200Å and c from 50 to 400.

Résumé—Les auteurs présentent une nouvelle expression de l'épaisseur de la couche d'azote adsorbé sur un catalyseur poreux. Son utilisation nécessite la connaissance de deux propriétés inhérentes au catalyseur poreux : le rayon moyen des pores $\bar{r}$, et la constante C, chaleur d'adsorption obtenue à partir de l'équation de B.E.T. (Brunauer–Emmett–Teller). Il est possible à partir de cette pression de déterminer les isothermes d'asorption pour des fonctions analytiques de la distribution des pores suivant leurs dimensions. Ces isothermes peuvent être comparés avec les données expérimentales sur l'adsorption afin d'établir la meilleure distribution des pores. Une telle fonction analytique est intéressante quand on doit calculer par exemple des facteurs d'efficacité.

Des tableaux sont donnés pour des isothermes obtenus par le calcul, avec $10 < \bar{r} < 200$Å et $50 < c < 400$.

Zusammenfassung—Für die Dicke einer adsorbierten Stickstoffschicht auf einem porösen Katalysator wird ein neuer Ausdruck angegeben. Zu seiner Benutzung benötigt man zwei allgemein ableitbare Eigenschaften poröser Katalysatoren, den mittleren Porenradius $\bar{r}$ und die Konstante der Adsorptionswärme c aus der B.E.T. (Brunauer–Emett–Teller) – Oberflächengleichung. Mit Hilfe des neuen Ausdrucks können Adsorptionsisothermen für alle analytischen Porengrössenverteilungsfunktionen entwickelt werden. Sie können dann mit experimentellen Adsorptionsdaten verglichen werden, um die geeignetste Porengrössenverteilung zu ermitteln. Es ist vorteilhaft, eine analytische Funktion für die Porengrössenverteilung zu besitzen, wenn zusätzliche Berechnungen, z.B. von Wirkungsfaktoren, gemacht werden sollen.

Es werden Tabellen angegeben für berechnete Isothermen für Werte von $\bar{r}$ von 10 bis 200Å und für c von 50 bis 400.

For studying temperature and concentration gradients in porous catalysts it is frequently advantageous to have an analytical expression for the pore-size distribution rather than a table of numerical results. The objective of this paper is to be able to predict, from a minimum of data, reliable functions of the Maxwellian or Gaussian type. An important aspect of the prediction procedure is the relationship between the thickness of the adsorbed layer of nitrogen on the pore surface and the relative pressure, P/P_0. It has been found that this thickness depends upon the type of catalyst material, the mean pore radius and the heat of adsorption.

Two general methods have been proposed for evaluating pore size distributions of catalyst materials from low-temperature nitrogen adsorption isotherms. In the first or numerical method the adsorption data are differentiated to obtain a numerical pore size distribution [1, 2]. The second procedure, which yields an analytical distribution function, is to fit proposed functions to the adsorption data. In both methods the volume of the adsorbed nitrogen is divided into

two parts: a physically adsorbed layer and a capillary condensed volume. For the condensed volume the Kelvin [3] equation is applied to a fictitious radius of an assumed cylindrical pore. For the adsorbed layer an empirical equation based upon experimental data is normally employed.

If the Kelvin equation is applied to an isotherm the volume per unit catalyst weight not adsorbed with nitrogen at a relative pressure, P/P_0, is

$$V_g - V = \int_{R_c}^{\infty} \pi (r - t)^2 L Z(r)\, dr \qquad (1)$$

The symbols are defined in the nomenclature. This equation assumes straight, cylindrical pores of varying radius and constant length. The critical pore radius divides the pore size distribution into two parts. At values of pore radius larger than R_c the pores contain only the physically adsorbed layer, while pores smaller than R_c contain capillary condensed nitrogen and are completely filled.

The Kelvin equation applied to nitrogen at − 195·8 °C becomes, in Angstrom units

$$R_c - t = 4{\cdot}1428 \left[\log_{10} \frac{P_0}{P}\right]^{-1} \qquad (2)$$

The second or analytical method, first proposed by Shull [4] and Wheeler [5], is to assume an analytical form for the distribution function, $Z(r)$, and then obtain the adsorption curve by integrating equation (1). These computed adsorption curves are compared with experimental data to ascertain an approximate type of pore size distribution function. In general two types of distribution functions are used, Maxwellian and Gaussian, i.e.

$$Z^M(r) = A^M r \exp(-r/r_0) \qquad (3)$$

$$Z^G(r) = A^G \exp\left[-\beta^2 (r/r_0 - 1)^2\right] \qquad (4)$$

Where β is a width parameter taken as 2 for a moderate distribution spread and as 5 for a narrow distribution spread. A value of infinity would suggest only one size of pore, equal to the most probable radius, r_0. A more convenient parameter to use than r_0 is Wheeler's average pore radius $\bar{r}$ based upon straight cylindrical pores of constant length, i.e.

$$\bar{r} = 2\, V_g\, S_g \qquad (5)$$

To evaluate the relationship between r_0 and $\bar{r}$, equation (5) may be written:

$$\bar{r} = \frac{2 \int_0^{\infty} \pi r^2 L Z(r)\, dr}{\int_0^{\infty} 2 \pi r L Z(r)\, dr} \qquad (6)$$

For a Maxwellian function for $Z(r)$, equation (3), evaluating the integrals in equation (6) leads to

$$\bar{r}/r_0 = 3 \qquad (7)$$

For a Gaussian function the result is

$$\bar{r}/r_0 = \frac{YB + 1}{Y + 1} \qquad (8)$$

where

$$Y = \pi^{1/2} \beta \exp(\beta^2) \left[1 + \operatorname{erf}(\beta)\right] \qquad (9)$$

$$B = 1 + \frac{1}{2\beta^2} \qquad (10)$$

To normalize the functions it is required that the following equation for pore volume be satisfied:

$$V_g = \int_0^{\infty} \pi r^2 L Z(r)\, dr \qquad (11)$$

With this restriction, the normalization constants are

$$A^M = \frac{V_g}{6\pi r_0^4 L} \qquad (12)$$

$$A^G = \frac{2 V_g \rho^2 \exp(\rho^2)}{\pi r_0^3 L} (YB + 1)^{-1} \qquad (13)$$

Evaluation of equation (1) with these functions gives for the Maxwellian case

$$1 - \frac{V}{V_g} = \frac{1}{6} \exp(-\eta) \left[\eta^3 + \tfrac{1}{2} \eta^2 (\Omega - \omega^2) + (\eta + 1)\, \Omega\right] \qquad (14)$$

and for the Gaussian

$$1 - \frac{V}{V_g} = \frac{\beta \exp(\beta^2)}{YB + 1} \left\{ \frac{\exp(-x_c^2)}{\beta} (\eta - 2\omega + 1) + \pi^{1/2} \left[(1 - \omega)^2 + \frac{1}{2\beta^2}\right] \operatorname{erfc}(x_c) \right\} \qquad (15)$$

where :

$$\eta = \frac{R_c}{r_0} \tag{16}$$

$$\omega = t / r_0 \tag{17}$$

$$\Omega = \omega^2 - 4\,\omega + 6 \tag{18}$$

$$x_c = \beta\,(\eta - 1) \tag{19}$$

In utilizing equations (14) and (15) to determine $Z(r)$ it is necessary to have expressions for only $(R_c - t)$ and t in terms of the relative pressure. Equation (2) provides this information for $(R_c - t)$. A relationship for the adsorbed layer thickness is developed in the next section.

Thickness of Adsorbed Layer

The adsorption data made available by Johnson [6] were employed to evaluate the relationship between t and other parameters. These experimental results were obtained in the manner described by Ries [7] and were accurate to appreciably better than 1 per cent. They are similar to earlier data published by Johnson [8]. The data cover a range of catalyst variables whose values are summarized in Table 1. The adsorption information was employed in a trial and error solution of equation (14) to obtain values of t for all the catalyst materials. Data over the same range of relative pressure was used as is required in establishing the B–E–T equation. The results of these calculations were fitted to a Halsey [9] type expression :

$$t = a\,[\log_{10}(P_0/P)]^{-1/n} \tag{20}$$

Here a and n are considered constants for a particular catalyst.

Fig. 1 shows Johnson's data applied to equation (20). Although each particular catalyst fits the equation well, it is apparent that a and n are not universal constants but change from catalyst to catalyst. It is desirable to express a and n in terms of easily obtained parameters. Since the B–E–T equation is widely employed the two constants which can be derived from this equation were used. One such parameter is the average pore radius and the other the thickness of the monolayer. Since the thickness of the monolayer of adsorbed nitrogen can be estimated for an ideal flat surface the deviation from this value was employed. The value of the relative pressure at which one monolayer occurs is evaluated from the B–E–T equation ; i.e.

$$\frac{P}{V(P_0 - P)} = \frac{1}{c\,V_m} + \frac{P\,(c-1)}{V_m\,c\,P_0} \tag{21}$$

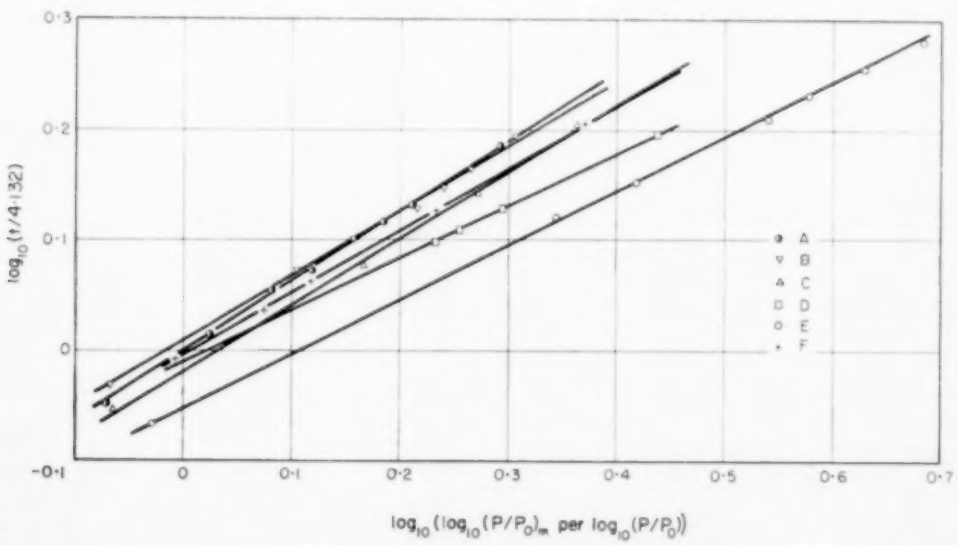

Fig. 1. Adsorbed thickness variance.

Table 1. Catalyst types and computed properties*

Catalyst Code	*Type*	V_g (cm³/g)	S_g (m²/g)	$\bar{r}$ (Å)	c	a'	n
A	Virgin Aerocat, silica–alumina	0·629	588·0	21·4	64·4	0·969	1·58
B	Davison, silica–magnesia, XDA-30	0·520	582·0	17·9	132·0	0·987	1·70
C	Nalco, silica–alumina, HA-60	0·706	430·0	32·9	99·7	0·925	1·66
D	Virgin Filtrol D	0·366	271·0	27·0	230·0	0·942	2·11
E	UOP "J," chromia–alumina	0·265	55·3	96·0	178·0	0·854	2·02
F	γ-Alumina obtained from boehmite	0·475	371·0	25·6	74·0	0·956	1·77

*Data supplied by Johnson [6].

When V is set equal to V_m, the volume adsorbed for a monolayer, the corresponding pressure ratio is

$$(P/P_0)_m = \frac{1 - c^{1/2}}{1 - c} \tag{22}$$

Since a value of c from a B–E–T graph is already needed to determine the surface area, S_g, no additional data are required to evaluate $(P/P_0)_m$.

The thickness of the ideal monolayer can be estimated from the Lennard–Jones force potential function as given by Hirschfelder [10]:

$$\Phi = 4\,\epsilon\left[\left(\frac{\sigma}{\rho}\right)^{12} - \left(\frac{\sigma}{\rho}\right)^{6}\right] \tag{23}$$

If the equilibrium molecule separation ρ_m as given by Φ is assumed to be the molecular separation for the saturated liquid

$$\rho_m = 2^{1/6}\,\sigma = t_m \tag{24}$$

where t_m is the thickness of the adsorbed monolayer. For nitrogen this value is 4·132A. Using this result in equation (20) gives

$$t_m = 4{\cdot}132 = a\left[\log_{10}\left(\frac{P_0}{P}\right)_m\right]^{-1/n} \tag{25}$$

which is an expression for the ideal monolayer thickness corresponding to a flat surface.

Combining equations (20) and (25) results in an equation for the thickness of the adsorbed layer in terms of the monolayer values, i.e.

$$\frac{t}{4{\cdot}132} = a'\left[\frac{\log_{10}(P/P_0)_m}{\log_{10}(P/P_0)}\right]^{1/n} \tag{26}$$

Here a' may deviate from unity because equation (25) is for an ideal monolayer. The t values for the catalysts described in Table 1 were plotted in Fig. 1 so as to evaluate the constants a' and n. It was found that a' varied with the average pore radius, $\bar{r}$, of the material, as shown in Fig. 2. This indicates that the monolayer thickness changes as the average surface becomes more curved, presumably due to changes in the packing arrangement of the molecules. The value of n showed some dependence upon the B–E–T constant c as shown in Fig. 3. This suggests that the heat of adsorption influences the thickness of the adsorbed layer. Utilizing a least squares analysis these results may be written in equation form as follows:

$$a' = 1{\cdot}26\,(\bar{r})^{-0{\cdot}085} \tag{27}$$

$$n = 1{\cdot}42\,(1 + 0{\cdot}00212c) \tag{28}$$

In equation (27) the units of $\bar{r}$ are Å. Utilizing these expressions in equation (26) gives the final equation for predicting the thickness of the adsorbed layer in terms of $\bar{r}$, and c, and P/P_0.

$$t = 5{\cdot}19\,(\bar{r})^{-0{\cdot}085}\left[\frac{\log_{10}\left[(1 - c^{1/2})\,(1 - c)\right]}{\log_{10}(P/P_0)}\right]^{1/1{\cdot}42\,(1\,+\,0{\cdot}00212c)} \tag{29}$$

This expression may be applied to a variety of porous materials, taking into account the specific nature of the catalyst through the values of c and $\bar{r}$. In comparison equation (20) with definite values of a and n will apply for but one material.

VOL.
16
1962

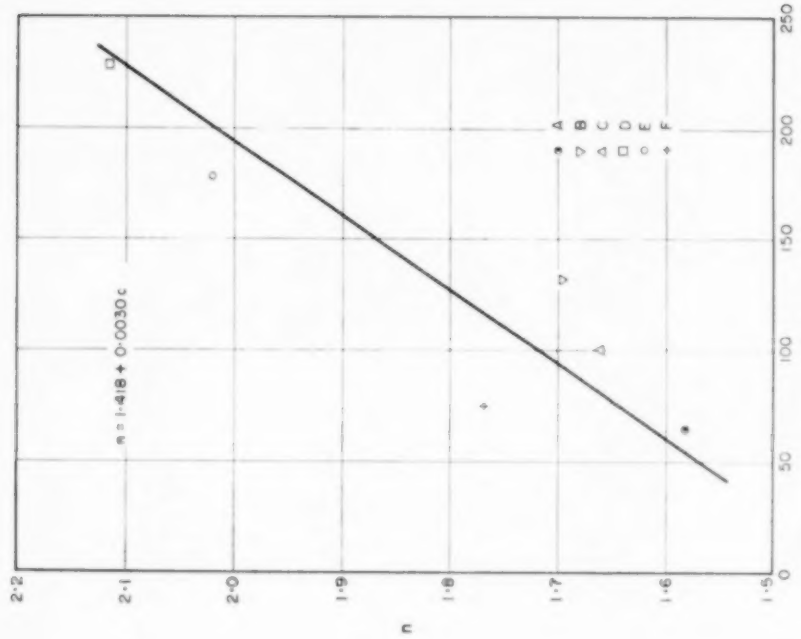

Fig. 2. Monolayer deviation constant.

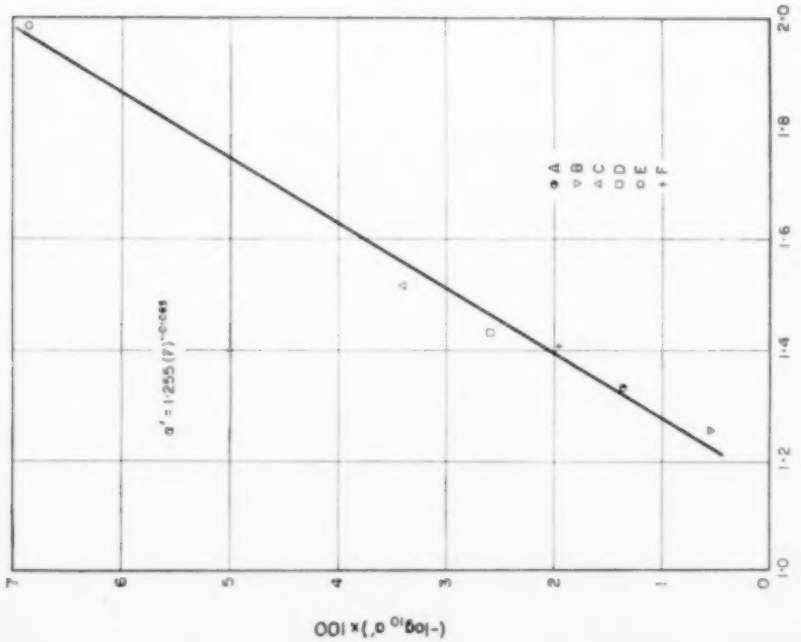

Fig. 3. Exponent "n."

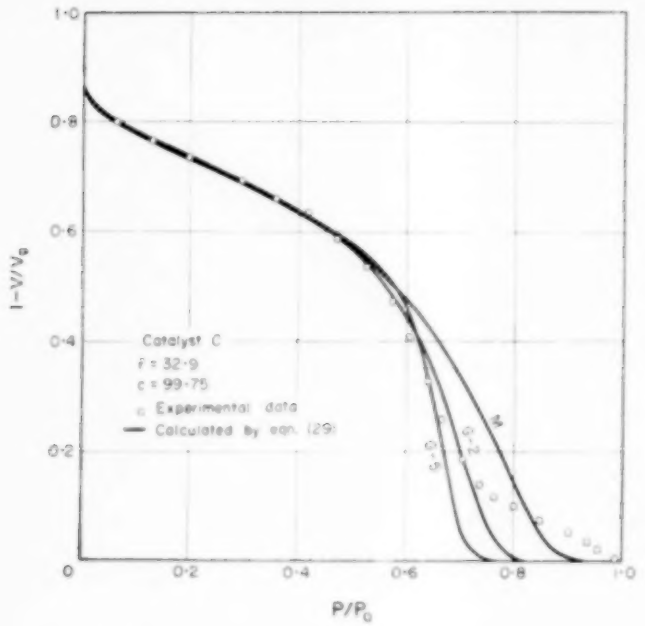

Fig. 4.
Inverted isotherms.

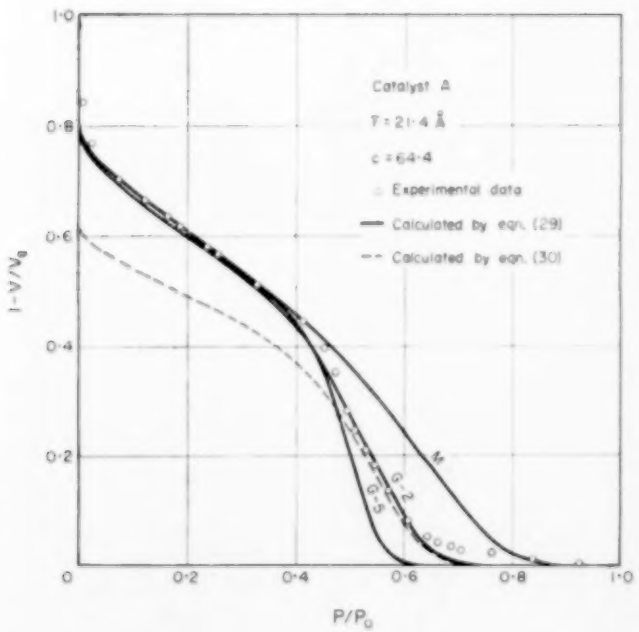

Fig. 5.
Inverted isotherms.

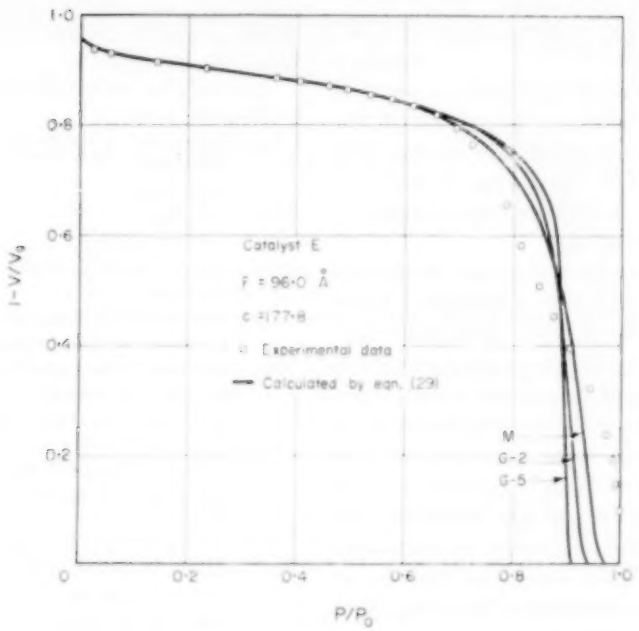

FIG. 6. Inverted isotherms.

RESULTS

Using equation (29) for t and equation (2) for $(R_c - t)$ adsorption curves can be computed for any pore-size distribution function. Figs. 4–6 show the results for three of the catalysts in Table 1. In all cases the calculated distribution fits the experimental data well up to the value of P/P_0 at which the various distribution functions begin to show a marked difference. The calculated curves using the Maxwellian and Gaussian distribution functions cannot be expected to represent the data exactly since the actual pore size distribution may have several peaks in the distribution curve. However the same procedure could be repeated with a more complicated form for the analytical size distribution function. In this way agreement between calculated and experimental results could be obtained up to higher values of P/P_0.

For comparison with the proposed procedure (equation 29), a dotted line in Fig. 4 is shown for the Gaussian distribution using the adsorbed thickness equation recommended by WHEELER [5], i.e.

Table 2. Sample-computed inverse isotherms $\bar{r} = 20$ Å $\quad c = 50$

P/P_0	$1 - V/V_g$		
	Maxwellian	*Gaussian* ($\beta = 2$)	*Gaussian* ($\beta = 5$)
0·050	0·7162	0·7090	0·7067
0·100	0·6699	0·6614	0·6588
0·150	0·6309	0·6215	0·6193
0·200	0·5938	0·5835	0·5829
0·250	0·5565	0·5444	0·5473
0·300	0·5177	0·5017	0·5102
0·350	0·4763	0·4520	0·4661
0·400	0·4315	0·3919	0·3986
0·450	0·3827	0·3179	0·2810
0·500	0·3293	0·2297	0·1243
0·550	0·2715	0·1355	0·0213
0·600	0·2102	0·0559	0·0006
0·650	0·1481	0·0121	
0·675	0·1181	0·0038	
0·700	0·0899	0·0008	
0·725	0·0644		
0·750	0·0425		
0·775	0·0251		
0·800	0·0127		
0·825	0·0052		
0·850	0·0015		

$$t = 4{\cdot}3\left[\frac{5}{\log_e P_0/P}\right]^{1/3} \qquad (30)$$

It is observed that the results using this expression do not agree with the data at low values of the relative pressure. Agreement should be obtained in this pressure range since the change in thickness of the adsorbed layer contributes significantly to the total nitrogen adsorption.

To make the results of this study useful for obtaining analytical, pore size distribution functions, low temperature nitrogen adsorption isotherms have been computed for values of $\bar{r}$ from 10 to 200 and values of c from 50 to 400 [11]. They were obtained by numerical evaluations of equations (14) and (15) using equations (2) and (29) for the thickness of the adsorbed layer. The numerical values for a sample isotherm are given in Table 2. By comparing experimental adsorption data with these Tables one can choose a suitable, analytical distribution function. This procedure has been used to obtain analytical equations subsequently employed for effectiveness factor calculations for porous catalysts [12].

Nomenclature

A = normalization constant for distribution function
a = constant in equation (20) for thickness of adsorbed layer
a' = monolayer multiplication value
$B = 1 + \dfrac{1}{2\beta^2}$
c = B–E–T equation constant
erf = error function
erfc = 1 − erf
L = pore length
n = adsorbed layer thickness equation/constant
P = pressure
P_0 = saturation pressure of nitrogen with infinite curvature
r = pore radius
$\bar{r} = 2V_g/S_g$
R_c = critical radius
r_0 = most probable pore radius for distribution functions
S_g = internal surface area per unit catalyst weight
t = thickness of the adsorbed layer
t_m = thickness of an adsorbed monolayer
V = volume of nitrogen adsorbed and capillary condensed per unit catalyst weight
V_g = total pore volume per unit weight
V_m = volume of liquid nitrogen adsorbed for one monolayer per unit catalyst weight
$x_c = \beta(\eta - 1)$
$Y = \pi^{1/2}\beta \exp(\beta^2)\left[1 + \text{erf}(\beta)\right]$
$Z(r)$ = pore size distribution function
β = width parameter in Gaussian distribution
ϵ = constant in Lennard–Jones potential equation
$\eta = R_c/r_0$
ρ = distance between molecule centres in Lennard–Jones potential
ρ_m = equilibrium separation possible for two like molecules
σ = constant in potential equation
Φ = Lennard–Jones force potential between like molecules
$\Omega = \omega^2 - 4\omega + 6$
$\omega = t/r_0$

Superscripts
M = Maxwellian
G = Gaussian

References

[1] Barrett E. P. *J. Amer. Chem. Soc.* 1951 **73** 373.
[2] Cranston R. W. and Inkley F. A. in *Advances in Catalysis* Vol. IX. Academic Press, New York 1957.
[3] Thomson W. *Phil. Mag.* 1871 **42** 448.
[4] Shull C. G. *J. Amer. Chem. Soc.* 1948 **70** 1405.
[5] Wheeler A. in *Catalysis*, Vol. II Reinhold, New York 1955.
[6] Johnson M. F. L. Sinclair Research Laboratories, Harvey, Ill. Private Communication.
[7] Ries H. in *Advances in Catalysis*, Vol. IV, Academic Press, New York. 1952.
[8] Johnson M. F. L., Kreger W. E. and Erickson H. *Industr. Engng. Chem.* 1957 **49** 283.
[9] Halsey G. D. in *Advances in Catalysis*, Vol. IV. Academic Press, New York. 1952.
[10] Hirschfelder J. O., Curtiss C. F. and Bird, R. B. *Molecular Theory of Gases and Liquids.* John Wiley, New York 1954.
[11] Mingle J. O. Ph.D. Thesis, Northwestern University, Evanston, Illinois 1960.
[12] Mingle J. O. and Smith J. M. *Amer. Inst. Chem. Engrs. J.* 1961 **7** 243.

Chemical Engineering Science, 1961, Vol. 16, pp. 39 to 54. Pergamon Press Ltd., London. Printed in Great Britain.

The continuous phase heat and mass-transfer properties of dispersions

P. H. Calderbank and M. B. Moo-Young

Department of Chemical Technology, University of Edinburgh, Scotland

(*Received* 2 *September* 1960; *in revised form* 22 *December* 1960)

Abstract—Techniques have been developed for measuring the interfacial area in gas–liquid dispersions. It has thus been possible to measure the liquid phase mass transfer coefficients in gas–liquid dispersions such as are produced in aerated mixing vessels, and sieve and sintered plate columns.

The results have been combined with other published data for heat and mass-transfer in liquid–liquid and solid–gas dispersions in which the dispersed phases are free to move under the action of gravity, and also with data on transfer by free convection from spheres.

These data can all be correlated by

$$k_L (N_{Sc})^{2/3} = \frac{h_c}{C_p \rho_c} (N_{Pr})^{2/3} = 0{\cdot}31 \left(\frac{\Delta\rho \, \mu_c \, g}{\rho_c^2} \right)^{1/3}. \quad (1)$$

For large gas bubbles which do not behave like rigid spheres as the smaller ones do

$$k_L (N_{Sc})^{1/2} = 0{\cdot}42 \left(\frac{\Delta\rho \, \mu_c \, g}{\rho_c^2} \right)^{1/3} \quad (2)$$

If the particles of the dispersed phase are not free to move under gravity and transfer is due to turbulence in the surrounding fluid,

$$k_L (N_{Sc})^{2/3} = \frac{h_c}{C_P \rho_c} (N_{Pr})^{2/3} = 0{\cdot}13 \left[\frac{(P/v) \, \mu_c}{\rho_c^2} \right]^{1/4} \quad (3)$$

where P/v is the power dissipation per unit volume. This correlation applies to heat and mass transfer in mixing vessels where the solid phase is in the form of a single fixed submerged body and also predicts the small increase in mass transfer coefficients as the power dissipation level is increased beyond that needed for just completely suspending dispersed solid particles in mixing vessels. The correlation also applies to heat and mass transfer in turbulent fluids flowing through fixed beds of particles and through pipes.

Résumé—Des méthodes ont été développées pour mesurer la surface d'échange dans les dispersions gaz–liquide. C'est ainsi qu'il a été possible de mesurer les coefficients de transfert de masse en phase liquide dans des dispersions gaz–liquide telles que celles qué l'on rencontre dans des mélangeurs à air et dans des colonnes à grilles, et à plateaux frittés.

Les résultats ont été comparés avec d'autres données publiées pour les transferts de masse et de chaleur dans les dispersions liquide–liquide et solide–gaz où les phases dispersées sont libres de se déplacer sous l'action de la pesanteur et également avec les données sur le transfert par convection libre de sphères.

Ces données peuvent toutes être mises sous la forme :

$$k_L (N_{Sc})^{2/3} = \frac{h_c}{C_p \rho_c} (N_{Pr})^{2/3} = 0{,}31 \left(\frac{\Delta\rho \, \mu_c \, g}{\rho_c^2} \right)^{1/3} \quad (1)$$

Pour de grosses bulles gazeuses qui ne se comportent pas comme des sphères rigides contrairement aux petites bulles, on a :

$$k_L (N_{Sc})^{1/2} = 0{,}42 \left(\frac{\Delta\rho \, \mu_c \, g}{\rho_c^2} \right)^{1/3} \quad (2)$$

Si les particules de la phase dispersée ne sont pas libres de se déplacer sous l'action de la pesanteur et si le transfert est dû à la turbulence dans le fluide environnant, on a :

$$k_L (N_{Sc})^{2/3} = \frac{h_c}{C_P \rho_c} (N_{Pr})^{2/3} = 0{,}13 \left[\frac{(P/v)\, \mu_c}{\rho_c^2} \right] \tag{3}$$

ou P/v est la puissance dissipée par unité de volume. Cette relation s'applique au transfert de chaleur et de masse dans les mélangeurs où la phase solide se présente sous forme d'un corps unique fixe et submergé, et prévoit aussi le petit accroissement des coefficients de transfert de masse quand la quantité d'énergie dissipée est augmentée au-delà de ce qui est nécessaire pour disperser complètement les particules solides dans les mélangeurs. La relation s'applique aussi aux transferts de chaleur et de masse dans les fluides turbulents s'écoulant à travers les lits fixes et à travers les tubes.

Zusammenfassung—Es wurden Verfahren entwickelt zur Messung von Phasengrenzflächen in Gas-Flüssigkeits-Dispersionen. Hierdurch war es möglich, die Stofftransportkoeffizienten für die flüssige Phase bei Gas-Flüssigkeits-Dispersionen zu messen, wie sie in begasten Rührkesseln sowie in Kolonnen mit Sieb- und Sinterplatten vorkommen.

Die Ergebnisse wurden kombiniert mit anderen veröffentlichten Daten über den Wärme- und Stoffaustausch in Flüssig-Flüssig- und Gas-Feststoff-Dispersionen, bei denen die verteilten Phasen sich frei unter dem Einfluss der Schwerkraft bewegen, und solchen Daten, bei denen der Transport durch freie Konvektion von Kugeln erfolgt.

Alle Daten können wie folgt korreliert werden :

$$k_L \cdot (N_{Sc})^{2/3} = \frac{h_c}{C_P \rho_c} (N_{Pr})^{2/3} = 0{,}31 \left(\frac{\Delta\rho \cdot \mu_c \cdot g}{\rho_c^2} \right)^{1/3} \tag{1}$$

Für grosse Blasen, die sich nicht wie kleine starre Kugeln verhalten :

$$k_L (N_{Sc})^{1/2} = 0{,}42 \left(\frac{\Delta\rho \cdot \mu_c \cdot g}{\rho_c^2} \right)^{1/3} \tag{2}$$

Wenn die Partikel der verteilten Phase sich nicht frei unter dem Einfluss der Schwerkraft bewegen und der Stofftransport von der Turbulenz des umgebenden Fluidums abhängt, gilt :

$$k_L (N_{Sc})^{2/3} = \frac{h_c}{C_P \cdot \rho_c} (N_{Pr})^{2/3} = 0{,}13 \left[\frac{(P/v) \cdot \mu_c}{\rho_c^2} \right]^{1/4} \tag{3}$$

wobei P/v der Kraftverbrauch pro Volumeneinheit ist. Diese Korrelation kann angewandt werden auf den Wärme- und Stofftransport in Rührkesseln, in denen die feste Phase in Form eines einzelnen festen Körpers vorliegt, und für die Voraussage des leichten Ansteigens der Stofftransportkoeffizienten beim Ansteigen des Kraftverbrauchs bis unterhalb des Wertes, der benötigt wird, um die Feststoffteilchen in völliger Suspension zu halten. Die Korrelation kann auch beim Wärme- und Stofftransport turbulenter Medien in Schüttschichten und Rohren.

Introduction to Previous Work

The present work was undertaken in order to evaluate separately the mass transfer coefficients and interfacial areas in gas–liquid dispersions such as obtain in fermentation vessels and distillation plate columns. Hitherto it has not been possible to arrive at these values because of a lack of means of measuring interfacial areas.

The present authors have described a light transmission method for measuring interfacial areas in not too optically dense dispersions [1] and also a light-reflection technique for dense dispersions of optically transparent phases [2]. In addition, a γ-ray transmission method was described for measuring the gas hold-up in these systems [2], from which the Sauter mean bubble size could be deduced. The latter value was checked in many cases by a statistical analysis of high-speed flash photographs. Details of the photographic techniques and statistical analysis will be described in a subsequent publication.

Experiments were performed in which sparingly

VOL. 16 1962

soluble volatile or gaseous solutes were desorbed from or dissolved in liquid solvents, the gaseous phase being dispersed in the liquid as a bubble cloud. The rate of material transfer and the interfacial area were simultaneously observed, the experimental equipment being such as to ensure that the liquid phase was perfectly mixed. In this way values of the liquid phase mass transfer coefficients were determined in aerated mixing vessels and sintered and sieve plate columns, as has been previously described [2, 3].

This work covered a wide range of bubble sizes and liquid phase diffusion coefficients, extreme variations in the latter being achieved by the use of aqueous glycol and glycerol solutions, and smaller variations by the use of various solutes. Diffusion coefficients of carbon dioxide in aqueous glycol and glycerol were measured by the liquid jet technique [3], and these results have now been confirmed using the Stokes diffusion cell.

The above work showed that the value of the liquid phase diffusion coefficient was the major factor which influenced the value of the mass transfer coefficient. The independent effect of liquid phase viscosity was not, however, revealed. It was clear that agitation intensity, bubble size and bubble free rising velocity had no effect on the mass transfer coefficient, but that large bubbles ($> 2{\cdot}5$ mm diameter) gave greater mass transfer coefficients than small bubbles ($< 2{\cdot}5$ mm diameter) whose mass transfer coefficients correlated well with those observed for solid–liquid dispersions. It was concluded that small "rigid-sphere" bubbles experienced friction drag causing hindered flow in the boundary layer sense, and that under these circumstances the mass transfer coefficient was proportional to the $\frac{2}{3}$ power of the diffusion coefficient, as found by Froessling [4] and others.

For large bubbles ($> 2{\cdot}5$ mm diameter) form drag predominated and the conditions of unhindered flow envisaged by Higbie [5] obtained, and as postulated by Higbie the mass transfer coefficient was proportional to the $\frac{1}{2}$ power of the diffusion coefficient.

It is important to appreciate that the Froessling and Higbie equations have never hitherto been tested with systems of gas bubbles for extreme variations of diffusion coefficients and liquid viscosities. Although the authors' results supported these equations as regards the effect of the diffusion coefficient on the mass transfer coefficient, they also showed that the effects of bubble size and slip velocity were such as to be mutually compensating, so that these variables were replaceable by physical property parameters

Present Work

In the present work the previous mass transfer data for bubble swarms have been extended, firstly by the use of an aqueous thickening agent (Polyacrylamide) which enabled the viscosity to be independently and largely increased without affecting the diffusion coefficient. Solutions having viscosities up to 87 cP were used and found to be Newtonian in rheological behaviour, and to have the same diffusion coefficient for carbon dioxide as pure water (determined with the Stokes diffusion cell).

The data have also been extended to include the high diffusion coefficients obtained using hydrogen as solute. This has been achieved by measuring the rates of catalytic hydrogenation reactions in various solvents containing an excess of catalyst and through which hydrogen bubble swarms were passed. The excess of catalyst ensured that the chemical reaction rate was fast and not rate determining, and the progress of the reaction was determined by the rate of solution of hydrogen, and followed by the infra-red absorption characteristics of the product of reaction.

Finally, published data on continuous phase heat and mass transfer to dispersions of solids and to single bubbles and drops have been combined with the present work to achieve a more comprehensive and convincing correlation.

Results

Fig. 1 shows two correlations for liquid phase mass transfer coefficients for bubble swarms passing through liquids in sieve and sintered plate columns and in aerated mixing vessels. The upper correlation line refers to bubble swarms of average bubble diameter greater than about $2\frac{1}{2}$ mm such as are produced when pure liquids are aerated in

mixing vessels and sieve plate columns, and leads to the result:

$$N_{Sh} = 0{\cdot}42 \quad N_{Sc}^{1/2} N_{Gr}^{1/3} \qquad (2)$$

$$\text{or} \quad k_L (N_{Sc})^{1/2} = 0{\cdot}42 \left(\frac{\Delta\rho \, \mu_c g}{\rho_c^2} \right)^{1/3} \qquad (2)$$

The lower correlation line refers to bubble swarms of average bubble diameter less than about $2\frac{1}{2}$ mm such as are produced when aqueous solutions of hydrophylic solutes are aerated in mixing vessels, or when liquids generally are aerated with sintered plates or plates containing very small perforations. This leads to the result

$$k_L (N_{Sc})^{2/3} = \frac{h_c}{C_P \rho_c} (N_{Pr})^{2/3} = 0{\cdot}31 \left(\frac{\Delta\rho \, \mu_c g}{\rho_c^2} \right)^{1/3} \qquad (1)$$

It will be seen that both correlations show that the liquid phase mass transfer coefficients are independent of bubble size and slip velocity and depend only on the physical properties of the system. In mixing vessels the mass transfer coefficients are independent of the power dissipated by the agitator, and in sieve-plate columns they are independent of the fluid flow rates.

"Small" bubble correlation

The data for "small" bubbles are in agreement with those reported by previous workers for both heat and mass transfer with solid in liquid and liquid in liquid dispersions as shown in Fig. 1.

Fig 2 also shows that the present data are in agreement with those on heat and mass transfer in free turbulent convection from stationary spheres, if the term $\Delta\rho$ is taken as the difference in density between the fluid at the interface, and the bulk in free convection as compared with the difference in density between the dispersed and continuous phases which is employed when the former is free to move under gravity. This result is obviously due to the fact that in both cases the relative rate of flow between the phases is induced, and its magnitude determined, by the appropriate value of the density difference.

Fig. 2 demonstrates the fact that as the density difference between the phases diminishes, the Sherwood and Nusselt numbers approach the value of 2 appropriate to natural convection. Allowing for this, correlation (1) in more precise form becomes

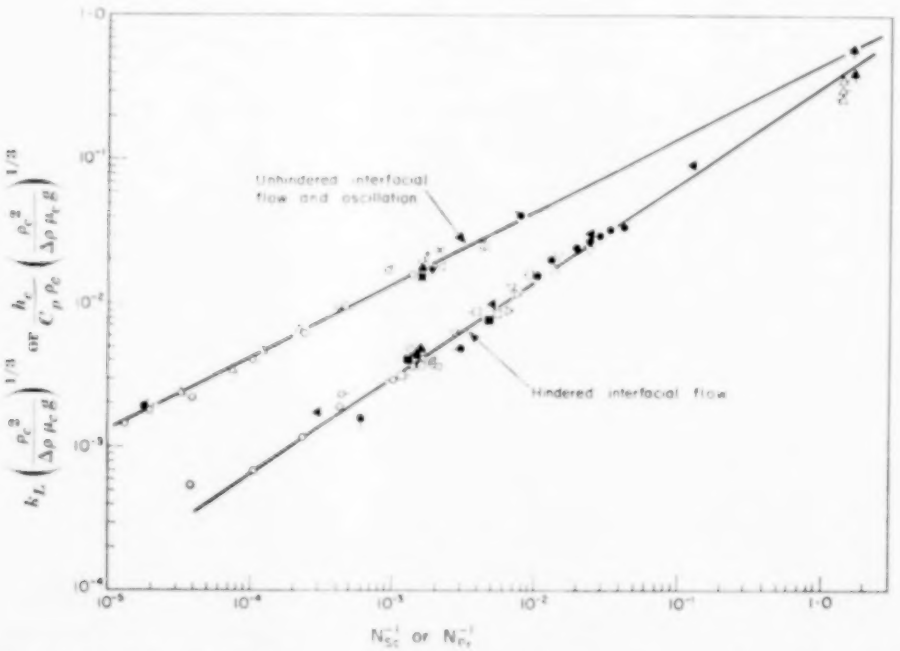

FIG. 1. Correlation of heat and mass transfer coefficients for dispersions of small bubbles and rigid spheres (lower line) and large bubbles (upper line). See "Source of data" and "Range of variables"

Source of data (see Fig. 1).

F.R. Free rise F.F. Free fall S.T. Stirred tank F.B. Fluidized bed

Legend	System	Process	Reference
○	Aq. glycerol solutions – CO_2	Absorption and desorption (F.R., S.T.)	This work
△	Aq. glycol solutions – CO_2	Absorption and desorption (F.R., S.T.)	This work
●	Glycol – CO_2	Absorption and desorption (F.R., S.T.)	This work
×	Water – CO_2	Absorption and desorption (F.R., S.T.)	This work
+	Water – O_2; 15 °C.	Absorption and desorption (F.R., S.T.)	This work
●	Water – O_2; 45 °C.	Absorption and desorption (F.R., S.T.)	This work
◆	Brine – O_2	Absorption and desorption (F.R., S.T.)	This work
♂	Polyacrylamide solutions – CO_2	Absorption and desorption (F.R., S.T.)	This work
▷	Wax – H_2	Absorption (F.R.)	This work
▷	Aq. ethanol solution – C_6H_6	Absorption (F.R.)	This work
◁	Water – Resin beads	Ion exchange (S.T.)	This work
◀	Aq. glycerol solutions – Hg	Heat transfer (F.F.)	[8]
▼	Water – O_2	Absorption (F.R.)	[9]

Legend	System	Process	Reference
▲	Water – O_2	Absorption (F.R.)	[10]
▽	Water – O_2; CO_2	Absorption (F.R.)	[10]
●	Toluene – H_2	Absorption (F.R.)	[11]
◇	Brine – NaCl	Dissolution (S.T.)	[12]
□	Water – KCl	Dissolution (F.B., S.T.)	[13]
■	Water – Urea	Dissolution (F.B., S.T.)	[13]
▷	Brine – NaCl	Crystallization (F.B.)	[14]
◇	Water – sucrose	Dissolution (S.T.)	[15]
○	Solvents – benzoic acid	Dissolution (S.T.)	[16]
●	Water – sodium thiosulphate	Dissolution (S.T.)	[17]
⁻↑	Water – Air	Large rain drops evaporatiug (F.F.)	[18]
↑	Water – air	Small rain drops evaporating (F.F.)	[18]
△	Sand – air	Particles falling through hot air undergoing heat transfer. (F.F.)	[19]
△	Carborundum – air		
△	Aloxite – air		
◻	Air – water	Dissolution in centrifugal apparatus	[20]
◫	H_2 – water	Absorption (F.R.)	[21]
◆	CO_2 – water	Absorption (F.R.)	[22]

Range of Variables (see Fig. 1).

Reference	Legend	k_L (cm/sec)	h_c (cal/cm²sec °C)	D_L (cm²/sec)	λ (cal/cm sec) °C	$\Delta\rho$ (g/cm³)	ρ_c (g/cm³)	μ_c (c P)	d (cm)
This work (large bubbles)	○ ◆ △ ♂ ● × + ■	0·007–0·080	—	$1·9 - 48·1 \times 10^{-6}$	—	1·00–1·178	1·000–1·178	0·6 –87	0·20–0·80
This work (small bubbles and rigid spheres)	○ ◆	0·0024 –0·010	—	$3·4 - 17·8 \times 10^{-4}$	—	1·11 – 1·160	1·11–1·160	1·13 –10·5	0·02– 0·06
This work (small bubbles and rigid spheres)	▷	0·07 – 0·122	—	$2·6 - 9·5 \times 10^{-1}$	—	0·698– 0·772	0·698–0·772	1·99 – 8·9	—
This work (small bubbles and rigid spheres)	◻	0·007	—	$1·13 \times 10^{-5}$	—	1·00	1·00	1·00	0·075
This work (small bubbles and rigid spheres)	◻	0·00122–0·00187	—	$6·5 - 9·3 \times 10^{5}$	—	0·174–0·177	1·0	0·89– 1·52	0·09
[8]	◀	—	0·039–0·459	—	$1·43 - 66·7 \times 10^{-3}$	12·27–12·55	1·0 –1·249	1·08– 3·95	0·225
[11]	●	0·0253 –0·048	—	$4·75 - 14·25 \times 10^{-5}$	—	0·867	0·867	0·28– 0·90	0·14
[12]	◇	0·011	—	$1·35 \times 10^{-5}$	—	0·89	1·178	1·55	0·01–0·065
(13)	□ ■	0·0059 –0·0138	—	$1·06 - 1·84 \times 10^{-5}$	—	1·30 –1·98	1·0	0·4 – 1·0	0·09 –1·2
[10]	▷	0·0127 –0·0215	—	$2·8 - 4·3 \times 10^{-5}$	—	1·165	1·26	0·371– 0·535	0·11
[15]	◇	0·00435	—	$4·5 \times 10^{-6}$	—	0·588	1	1	0·33–0·415
[16]	○	0·0042 –0·00627	—	$11·5 - 17·5 \times 10^{-6}$	—	0·266–0·36	0·79 –1·11	0·55– 1·0	0·45–0·65
[17]	●	0·00291	—	$6·2 \times 10^{-6}$	—	0·69	1·00	1·0	0·14–0·47

$$N_{Sh} = N_{Nu} = 2{\cdot}0 + 0{\cdot}31\, N_{Ra}{}^{1/3}$$

It may be shown that this relationship is formally identical to FROESSLING's equation if the drag coefficient for spheres is inversely proportional to the square root of the Reynolds number.

Figs. 1 and 2 show that a comprehensive correlation for heat and mass transfer in turbulent free convection and for suspended or free falling or rising particles, bubbles and drops is obtained. This correlation holds equally for dispersions and for single particles and shows that "small" bubbles move in liquids as rigid spheres under conditions of hindered flow in the boundary layer sense.

It may be noted that the particle size and velocity are not involved in the correlation, so that heat and mass transfer coefficients in the continuous phase may be predicted from physical properties only.

The correlation is seen to hold accurately for independent and extreme changes in the variables, and has been tested for heat and mass-transfer in turbulent free convection, for mass transfer in mixing vessels where suspended solids and gas bubbles are undergoing dissolution, for mass transfer in liquid fluidised beds of crystallizing solids, for heat transfer when liquid drops fall through other liquids, and for several other similar processes.

The correlation (1) applies to those systems where the particles of the dispersed phase behave as rigid bodies, and where relative movement between the phases is retarded as in boundary layer theory. In the absence of adequate experimental proof FROESSLING's equation has previously been employed in this connexion.

Figs. 1 and 2 show the extent to which a wide variety of previously published data agree with the present observations and the range of variables which the correlation includes. In addition it may be noted that ZDANOVSKII [6] has proposed a correlation for the dissolution of solid suspensions in mixing vessels which is of the same form as correlation (1), while SCHMIDT [7] has proposed a similar equation for turbulent free convective heat transfer.

"*Large*" *bubble correlation*

To produce "large" bubble clouds in aqueous glycerol solutions and thereby effect major changes in the diffusion coefficients of solutes undergoing mass transfer it was necessary to employ the pulsed sieve-plate column described in a previous publication [3]. Without the use of a positive means of producing large bubbles it is extremely difficult to prevent small bubbles forming in aqueous solutions of hydrophilic solvents and impossible to do so in aerated mixing vessels.

The independent effect of liquid viscosity was evaluated using polyacrylamide as a thickening agent for water; it was established that the solutions employed were Newtonian in rheological

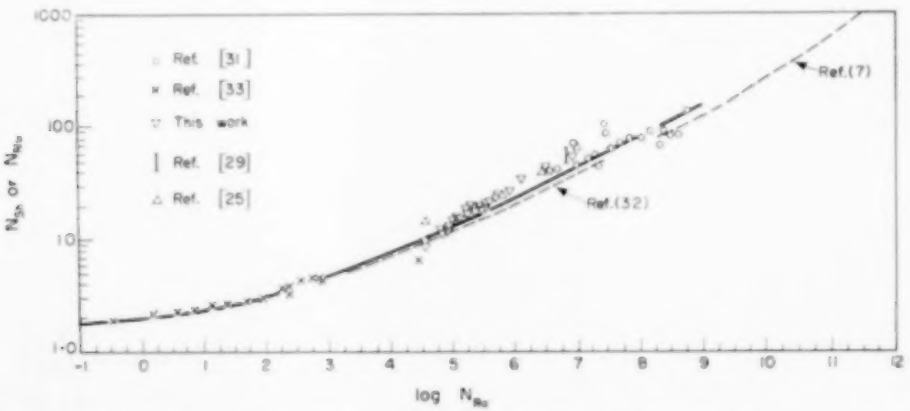

FIG. 2. Correlation of heat and mass transfer coefficients for dispersions of small bubbles and for rigid spheres with natural convection.

behaviour and were without influence on the diffusion coefficient of the solute being transferred.

Mass transfer coefficients for bubbles greater in diameter than about $2\frac{1}{2}$ mm are notably larger than for small "rigid-sphere" bubbles. The mass transfer coefficient is proportional to the square root of the liquid phase diffusivity, implying that the HIGBIE model [5] of unsteady state transfer applies, and that the unhindered flow situation envisaged in this model is responsible for the high transfer coefficients obtained. In this region of bubble size the bubbles are deformed from spherical to elipsoidal shapes.

Transition region between "small" and "large" bubbles

Fig. 3 shows some of the mass transfer data for bubbles of a size intermediate between those previously classified as "large" and "small," exhibiting unhindered and hindered flow respectively. Similar results have been observed by GARNER [23] for gas bubbles, and by GRIFFITH [24] for liquid drops.

It has also been observed by the above workers that surface active agents and trace impurities inhibit the transition from the hindered to the unhindered flow condition. The present observations have not included the effect of surface active agents.

In aerated mixing vessels as the agitator power is increased the gas–liquid interfacial area increases and the bubble size diminishes, while the mass transfer coefficient remains constant until a critical point is reached, at which the transfer coefficient begins to fall rapidly as the bubbles pass through the transition size region. Ultimately the transfer coefficient again becomes constant while the interfacial area continues to increase with increasing power dissipation. The same behaviour is observed with sieve-plate columns as the gass-flow rate is increased.

Fig. 4 shows the results of many new observations carried out on sieve trays operating as previously described [2] under simulated distillation conditions, and for all of which the data have been found to lie in the transition region. Fig. 5 shows that in this region mean values of k_La are almost independent of all variables, except

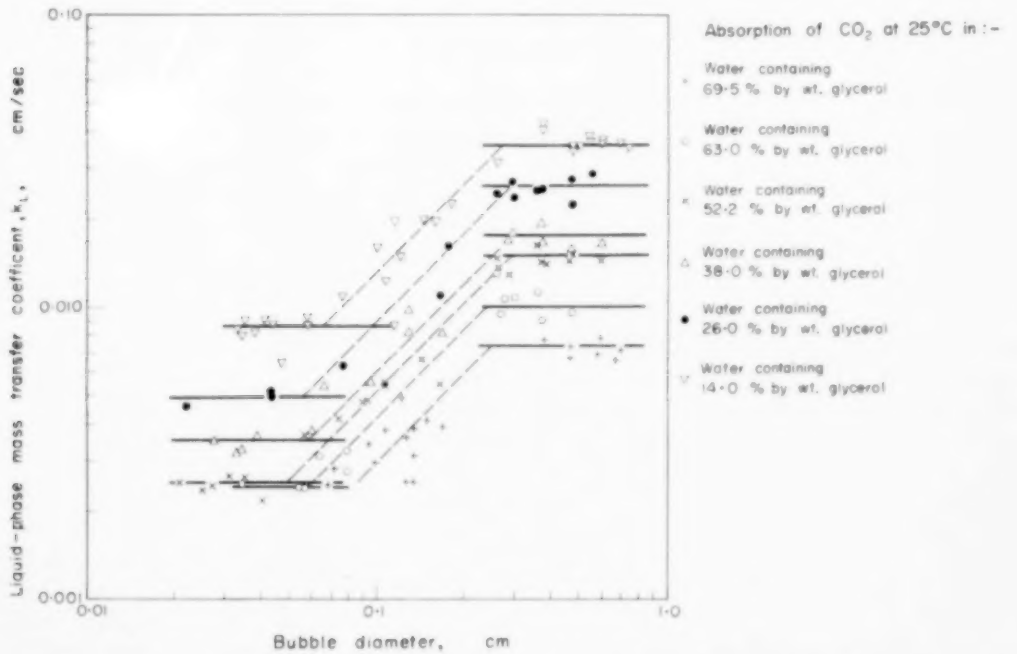
0·10
0·010
0·001
0·01
0·1
1·0
Liquid-phase mass transfer coefficient, k_L, cm/sec
Bubble diameter, cm
Absorption of CO_2 at 25°C in :-
Water containing 69·5 % by wt. glycerol
Water containing 63·0 % by wt. glycerol
Water containing 52·2 % by wt. glycerol
Water containing 38·0 % by wt. glycerol
Water containing 26·0 % by wt. glycerol
Water containing 14·0 % by wt. glycerol

FIG. 3. Typical data for transition from "large" bubble mass transfer coefficients to "small" bubble values.

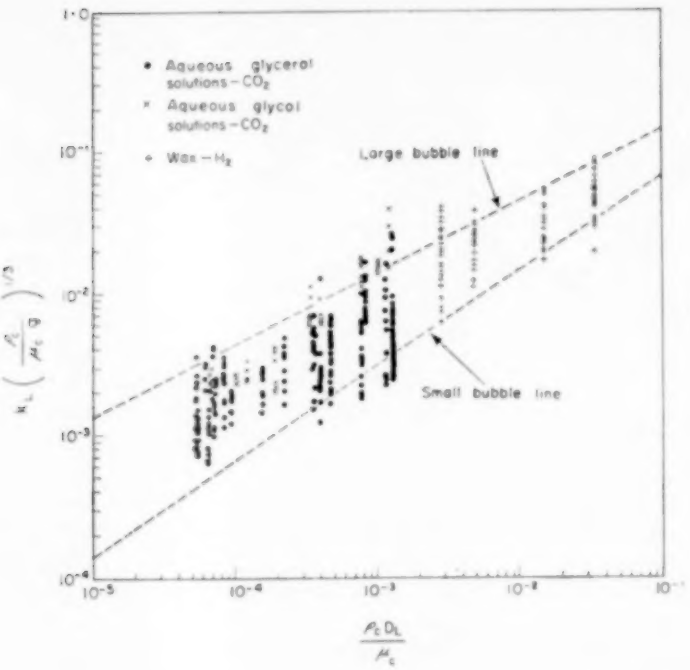

FIG. 4. "Transition" region mass transfer coefficients observed with froths in sieve-plate columns.

the Schmidt group. It was found that under distillation conditions producing a large vapour hold-up in the foam the transition from unhindered to hindered flow occurred with bubbles of greater size than in aerated mixing vessels, where the gas hold-up was comparatively low.

It is evident that further work remains to be done in order to throw light on this interesting region of bubble behaviour, but some relevant observations are worth making at this stage.

(a) The high mass transfer coefficients observed with large bubbles are only obtained in shallow liquid pools. With deep pools a progressive decrease in the point values of the mass transfer coefficient with height or residence time is observed and these values finally decline to those obtained with small rigid-sphere bubbles. These observations have been made by BAIRD [22], GRIFFITHS [24] and DOWNING [25] and the present authors.

(b) Surface active agents cause the high mass transfer coefficients for large bubbles to be reduced to those obtained with rigid spheres [22, 24, 25].

(c) As reported by CALDERBANK [2] high rates of gas flow in sieve-plate columns cause large gas bubbles to rise at rates considerably in excess of their free rising velocities when their mass transfer coefficients approach the rigid-sphere values.

The unhindered flow situation appears to be most readily realised with large bubbles at low rates of liquid flow around them (free rise in viscous liquids or flow round trapped bubbles as studied by HIGBIE [5]). The higher the Reynolds number of the bubble the more rapidly does the mass transfer coefficient decrease with residence time.

These phenomena are probably associated with the properties of the wake behind the bubble as discussed by GARNER and TAYEBAN [26] who observed a similar behaviour in liquid drops.

As shown in Fig. 1, the mass transfer coefficients for large and small bubbles approach each other at low values of the Schmidt group. This fact agrees with the conclusions of TOOR and

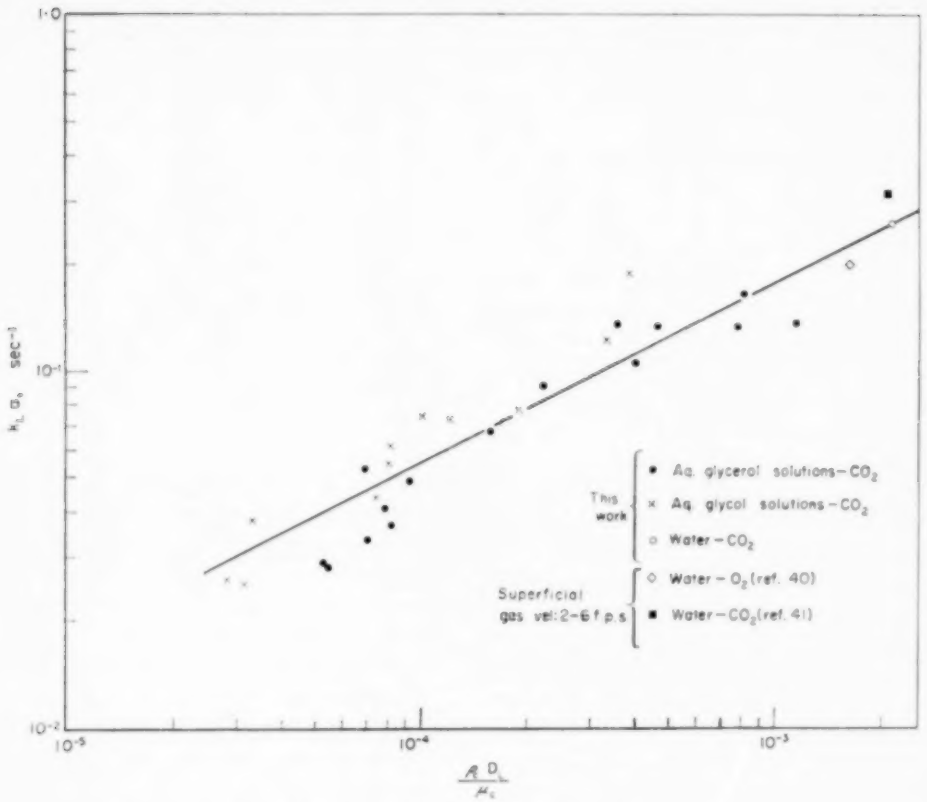

FIG. 5. Average $k_L a$ values observed with froths in sieve plate-columns.

MARSCHELLO [27] who predict that the boundary layer and penetration mechanisms of mass transfer lead to identical results at low values of the Schmidt group.

An important practical conclusion from these observations is that the high mass transfer coefficients for large bubbles in unhindered flow can only be realized in special circumstances and that in industrial situations of high gas flow rates surface active impurities and deep liquid pools the mass transfer coefficients will approach the lower values obtaining for rigid spheres.

DISPERSED PHASE UNDER THE INFLUENCE OF TURBULENCE

The subject matter dealt with in previous parts of this paper refers to dispersions in which the density difference between phases is sufficiently large to cause the force of gravity to determine exclusively the rate of mass transfer. Such dispersions include those in which solid particles are just completely suspended in mixing vessels. It is known that an increase in agitation intensity above the level needed for complete suspension of particles results in a small increase in the mass transfer rate [13, 16].

When the particles in a mixing vessel are just completely suspended, turbulence forces just balance those due to gravity and the mass transfer rates are the same as for particles moving freely under gravity. At higher agitation levels turbulence forces are greater than those due to gravity and can no longer be equated with them so that a separate treatment, described hereunder, has to be applied. This approach which treats tur-

bulent forces as those which determine mass transfer rates has also been applied to fixed bodies submerged in mixing vessels.

In the case of gas–liquid dispersions it is impractical to exceed gravitational forces by mechanically induced turbulence since agitators operate poorly in gas–liquid dispersions.

Local isotropic turbulence

Turbulent flow produces primary eddies which have a wave length or scale of similar magnitude to the dimensions of the main flow stream.

These large primary eddies are unstable and disintegrate into smaller eddies until all their energy is dissipated by viscous flow. When the Reynolds number of the main flow is high, most of the kinetic energy is contained in the large eddies, but nearly all of the dissipation occurs in the smallest eddies. If the scale of the main flow is large compared with that of the energy dissipating eddies, a wide spectrum of intermediate eddies exist which contain and dissipate little of the total energy. In the process the directional nature of the primary eddies is gradually lost.

Kolmogoroff [28] concludes that all eddies which are much smaller than the primary eddies are statistically independent of them, and that the properties of these small eddies are determined solely by the local energy dissipation rate per unit mass of fluid. Thus, if a volume of fluid is considered whose dimensions are small compared with the scale of the main flow the fluctuating components of the velocity are equal, and this so-called local isotropic turbulence exists even though the turbulent motion of the larger eddies may be far from isotropic. In local isotropic turbulence the smallest eddies are responsible for most of the energy dissipation.

The scale of these smallest eddies is given by Kolmogoroff as

$$l = \frac{\mu_c^{3/4}}{\rho_c^{1/2}} \left(\frac{P}{v}\right)^{-1/4}$$

Moreover, the mean square fluctuating velocity over a distance d in a turbulent fluid field where $L > d > l$ (L being the scale of the primary eddies and l that of the smallest eddies) is given by Batchelor [29] as

$$\overline{u_{(d)}}^2 = \text{const.} \left(\frac{P}{v}\right)^{2/3} \left(\frac{d}{\rho_c}\right)^{2/3}$$

The condition for local isotropy where the above equation applies is frequently encountered. For example, in a fluid mixing vessel, operating at an energy input of 10 h.p./1000 gall. of water, l is 25 μ. If the agitator has blades 5 cm wide the scale of the main fluid flow from it is approximately 5 cm. Thus, $L/l = 2000$ which is large enough to allow local isotropy to be assumed.

Turbulence in the immediate vicinity of a particle of a dispersion affects heat and mass transfer rates between the particle and the fluid, and if the particle is itself fluid may lead to its break-up.

The theory of local isotropy gives information on the turbulent intensity in the small volume around the particle. Thus, $\sqrt{[\overline{u_{(d)}}^2]}$ is a statistical parameter describing the variation in the fluctuating velocity over a distance comparable to the particle diameter (d) and may be used in place of the velocity of the particle in correlations of heat and mass transfer rates.

Thus, the Reynolds number for local isotropy is given by

$$\left(\frac{\sqrt{[u_{(d)}^{-2}]}\, d\, \rho_c}{\mu_c}\right) \propto \frac{d^{4/3}\, \rho_c^{2/3}\, (P/v)^{1/3}}{\mu_c}$$

or, alternatively

$$N_{Re}' = \frac{\rho_c^{1/3}\, (P/v)^{1/6}\, d^{2/3}}{\mu_c^{1/2}} \qquad (3)$$

as expressed by Calderbank in a previous publication [2].

The turbulence Reynolds number above was apparently first employed for the correlation of mass transfer rates in turbulent fluids by Oyama [15] and subsequently by Kolar [30] and Calderbank [2].

If we now assume the usual functional relationship between the Sherwood, Schmidt and Reynolds numbers for mass transfer we arrive at the relation

$$\frac{k_L d}{D_L} \propto \left(\frac{\mu_c}{\rho_c D_L}\right) \left[\frac{\rho_c^{1/3}\, (P/v)^{1/6}\, d^{2/3}}{\mu_c^{1/2}}\right]^y$$

Experiments on mass transfer in mixing vessels [12, 16, 31] have led to the conclusion that

$$k_L \propto D_L^{2/3},$$

and k_L does not depend on d.

In order to satisfy these conditions it is necessary that $x = \frac{1}{3}$ and $y = \frac{2}{3}$, whence

$$\frac{k_L d}{D_L} \propto \left[\frac{\rho_c^{1/3}(P/v)^{1/6} d^{2/3}}{\mu_c^{1/2}}\right]^{3/2} \left(\frac{\mu_c}{\rho_c D_L}\right)^{1/3}$$

or
$$k_L \propto \frac{\left\{\left[(P/v)\mu_c\right]/\rho_c^2\right\}^{1/4}}{(\mu_c/\rho_c D_L)^{2/3}} \qquad (3a)$$

the analogous expression for heat transfer being:

$$\frac{h}{C_P \rho_c} \propto \frac{\left\{\left[(P/v)\mu_c\right]/\rho_c^2\right\}^{1/4}}{(C_P \mu_c/\lambda)^{2/3}} \qquad (3b)$$

Following equation (3) heat and mass transfer data observed by many workers in mixing vessels are plotted in Fig. 6. In order to present published data in these forms it was sometimes necessary to reconstruct the agitation equipment and to measure its speed-power characteristics with a

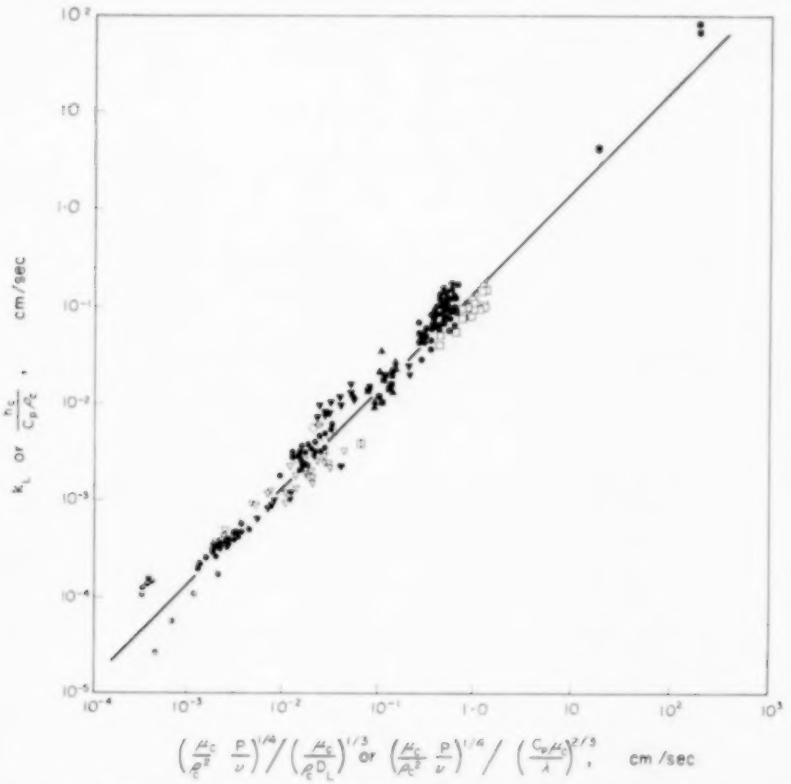

FIG. 6. Continuous phase heat and mass transfer coefficients in mising vessels.

Heat transfer

- ● Water — Ref. [32]
- □ Water
- ■ Glycerol
- ▲ L.M. Oil — Ref [33]
- ▼ A–12 Oil
- ◆ Hot water
- ⊡ Nitrating liquor — Ref. [34]

Mass transfer

Solid dissolution

- ● Sucrose – water — Ref. [15]
- ● Sodium thiosulphate – water — Ref. [17]

Mass transfer

- ◑ Benzoic acid – sperm oil
- ◒ Benzoic acid – cotton seed oil
- ◓ Benzoic acid – rape seed oil — Ref. [16]
- ● Benzoic acid – glycol
- ⧖ Succinic acid – acetone
- ⧗ Succinic acid – *n*-butanol
- ▽ Salycilic acid – benzene — Ref. [35]
- ▼ Salycilic acid – water
- ▽ Benzoic acid – water

Liquid–liquid extraction

- ⊖ Benzoic acid – kerosene – water — Ref. [36]

dynamometer, as only infrequently has this information been reported.

Fig. 6 reveals a correlation which despite a considerable scatter in the data extends for a 10^7-fold change in the variables and therefore merits serious consideration. It may be argued that some of the scatter of the experimental data is due to uncertainties in the values of the interfacial areas for suspended particles as obtained by screen analysis.

The equation of the regression line drawn through the data gives

$$k_L (N_{Sc})^{2/3} = \frac{h_c}{C_P \rho_c} (N_{Pr})^{2/3} = 0{\cdot}13 \left[\frac{(P/v)\mu_c}{\rho_c^2}\right]^{1/4} \quad (4)$$

with a standard deviation of 66 per cent.

It should be noted that equation (4) does not invalidate the use of the impeller Reynolds number for correlating heat and mass transfer rates in mixing vessels. For fully developed turbulence, where $P \propto N^3$, equation (4) may be transformed to give a conventional Reynolds number correlation. However, such a correlation may only be employed with geometrically similar agitation equipment whereas equation (4) is independent of the geometry of the agitation equipment.

It appears probable, however, that the type of agitator used may have a minor influence on the mass transfer coefficients which is not revealed in equation (4). Thus, when the agitator power is increased until the particles just become completely suspended, the mass transfer coefficient is given by equation (1). As the power is further increased, equation (4) is followed, but with the practical limitations of allowable power dissipation, the increase in mass transfer coefficient may not be easily observed. However, it is almost certain that agitators producing high ratios of flow to shear for a given power are most effective for suspending particles, so that particles suspended with these agitators come under the influence of power at a lower value of power dissipation than with agitators producing high shear and low flow rates.

This question is complicated by the fact that small particles are most easily suspended, and if their size is of the order of the scale of the smallest eddies the mass transfer coefficients will remain independent of power dissipation until the latter is raised considerably above that needed for complete suspension. This behaviour has been observed by PIRET *et al.* [12]. As a result of these considerations some scatter of the results shown in Fig. 6 is to be expected due to variations in agitator characteristics in the several experiments reported.

It should be made clear that the range of variables in Fig. 6 is largely made up of variations in the Schmidt group and that variations in the power dissipation factor for a given system are comparatively small, so that the figure confirms the two-thirds exponent of the Schmidt group but does not provide precise evidence for the form of the power factor used.

VOL 16 196

MASS TRANSFER IN PACKED BEDS

It is perhaps surprising to find that equation (4) also holds for mass transfer from packed beds to fluids flowing through them in turbulent flow.

This conclusion is reached from the mass transfer correlation for packed beds recently proposed by FALLAT [37] at a result of some careful determinations.

We may compute the power dissipated per unit volume of fluid in a packed bed as the flow work.

$$\frac{P}{v} = \frac{\Delta p}{L} \frac{G}{\rho_c \Sigma} \quad (5)$$

The pressure drop in packed beds has been correlated by CHU [38] as

$$\frac{\Delta p}{L} = 35{\cdot}4 \left(\frac{\mu_c (1-\Sigma)}{dG}\right)^{0{\cdot}44} \frac{G^2 (1-\Sigma)}{d \rho_c \Sigma^3}$$

whence, from equation (5)

$$\frac{P}{v} = 35{\cdot}4 \frac{\mu_c^{0{\cdot}44} (1-\Sigma)^{1{\cdot}44} G^{2{\cdot}56}}{d^{1{\cdot}44} \rho_c^2 \Sigma^4}$$

Inserting this equation for P/v into equation (4) and using 0·13 as the value of the dimensionless constant we find

$$\frac{k_L d}{D_L} = 0{\cdot}13 \left(\frac{\mu_c}{\rho_c D_L}\right)^{1/3} \left(\frac{\rho_c^{1/3} (P/v)^{1/6} d^{2/3}}{\mu_c^{1/2}}\right)^{3/2}$$

$$= 0{\cdot}318 \left(\frac{\mu_c}{\rho_c D_L}\right)^{1/3} \left(\frac{d G}{\mu_c}\right)^{2/3} \left(\frac{1-\Sigma}{\Sigma}\right)^{1/3} \quad (6)$$

Since the work of FALLAT [37] covered a range of values of Σ of 0·40 to 0·42, taking $\Sigma = 0{\cdot}41$, we find

$$N_{Sh} = 0{\cdot}69\, N_{Re}^{2/3}\, N_{Sc}^{1/3}$$

or

$$j_d = 0{\cdot}69\, N_{Re}^{-1/3} \tag{7}$$

This result may be compared with that given by FALLAT [37] as

$$j_d = 0{\cdot}626\, N_{Re}^{-0{\cdot}322}$$

which, for the range of experimental data reported by him can be almost as well represented by

$$j_d = 0{\cdot}67\, N_{Re}^{-1/3} \tag{8}$$

The agreement between equations (7) and (8) is substantially complete.

VOL. 16 1962

Heat and mass transfer in pipe flow

For turbulent flow in pipes the Blasius equation

$$\frac{\Delta p \cdot d_p \cdot \rho_c}{LG^2} = 0{\cdot}0396\,(N_{Re})^{-1/4}$$

may be used to predict the pressure drop and hence the power dissipation per unit volume of fluid. If this result is then combined with equation (4) in the same fashion as in the previous Section we find

$$j_{d,h} = 0{\cdot}058\, N_{Re}^{-0{\cdot}31} \tag{9}$$

which may be compared with the correlation of CHILTON and COLBURN [39] which gives

$$j_{d,h} = 0{\cdot}023\, N_{Re}^{-0{\cdot}20}$$

This equation agrees with equation (9) at a value of $N_{Re} = 10{,}000$ and results in a maximum deviation from it of only $\pm$ 12 per cent over the Reynolds number range 2000–20,000, which is the range over which most experimental data have been reported. The significance of the present findings is the realization that power dissipation per unit volume of fluid is the factor which allows a comprehensive correlation of heat and mass transfer coefficients for turbulent fluids to include fluids where the turbulence is induced by mechanical agitation.

It should be noted that equation (4) was derived by combining the theory of local isotropic turbulence with a conventional mass transfer correlation and by using some experimental findings with mixing vessels to evaluate the constants in this correlation. The result has been found to apply reasonably well to turbulent flow in packed beds and pipes where the theory of local isotropic turbulence could not be supposed to apply.

It would appear that a more general law operates to interrelate energy dissipation and the specific rates of turbulent transport phenomena.

POWER REQUIRED TO SUSPEND SOLIDS IN MIXING VESSELS

As previously discussed the rate of solution of particles just completely suspended in a mixing vessel is dependent on factors which do not include the agitator power, although as the power dissipation is further increased a comparatively small increase in solution rate may be realized.

At the point of compete suspension of solids the mass transfer coefficient is given by either correlations (1) or (4), so that on equating these relationships so as to eliminate the mass transfer coefficient, we arrive at an expression for the power required to just suspend the particles, which takes the form

$$\frac{P}{v} = \text{const.}\, \frac{(g\,\Delta\rho)^{4/3}\,\mu_c^{1/3}}{\rho_c^{2/3}} \tag{10}$$

This result may be compared with that proposed by KNEULE [13] who finds

$$\frac{P}{v} = \text{const.}\, \frac{(g\,\Delta\rho)^{1{\cdot}5}\, d^{1/2}\, H^{1/2}}{\rho\, D^{1/2}}$$

and with that proposed by ZWIETERING [40] who finds

$$\frac{P}{v} = \text{const.}\, \frac{(g\,\Delta\rho)^{1{\cdot}35}\,\mu_c^{0{\cdot}3}\, d^{1/2}\, H^{0{\cdot}39}}{\rho_c^{0{\cdot}35}}$$

while OYAMA and ENDOH [41] report

$$\frac{P}{v} = \text{const.}\, \frac{(g\,\Delta\rho)^{3/2}\, d^{1/2}}{\rho_c^{1/2}}$$

The most obvious discrepancy between the present result and the formulae previously proposed is that equation (10) does not contain the particle size as a variable, and it would seem reasonable to suppose that it ought.

However, if the square root of the particle diameter is included in equation (10) as suggested by the experimental correlations above, this might imply that correlation (4) should include a factor of $d^{1.8}$. It is unlikely, with the present precision of experimental mass transfer data obtainable with solid dispersions, that this factor could be identified with certainty.

The same argument suggests that it is only slightly more likely that an effect of solids hold-up on the mass transfer coefficient could be easily identified, although in this connexion both Piret *et al.* [12] and Wilhelm *et al.* [42] report a small influence.

Conclusions of practical interest from the foregoing

One clear conclusion is that when a dispersed phase is suspended, or in free rise or fall and under the influence of gravity, the heat and mass transfer coefficients are almost completely unaffected by mechanical power dissipated in the system. Thus, for example, in dissolving solid particles in liquids, little advantage can be gained by increasing the agitation intensity above the point at which the particles are freely suspended. Clearly, mixing impellers should be designed to secure suspension of particles with a minimum power consumption which should not greatly exceed this level.

For gas–liquid dispersion power dissipation increases the gas–liquid interfacial area and increases the mass transfer rate for this reason although, as before, little effect on the mass transfer coefficient can be realized.

Correlation (1) shows the important influence of the difference in density between the suspended dispersed and the continuous phases on the transfer coefficients. This means that where this difference in density is small transfer rates are extremely low. This situation is most likely to be realized in some liquid–liquid extraction processes and can be countered by increasing the gravitational field strength as in centrifugal extractors. The problem is also met with in dissolving polymers in solvents, where the density difference between polymer solution and solid polymer can be quite small, and the rate of solution is further impeded by the high viscosity of the solution as would be expected from correlation (1).

An important further example is found in aerobic fermentation processes, where the over-all rate process can be determined by the rate of supply of oxygen to the growing organism, whose density may not differ greatly from that of the surrounding nutrient fluid. Thus, although the rate of supply of oxygen from aerating gas bubbles to liquid may be increased by agitation (by increasing the gas–liquid interfacial area), the rate of assimilation of dissolved oxygen by the organism is unaffected by agitation, and is seriously restricted by the small solid–liquid density difference, and frequently also by the high viscosity of the liquid medium. In this case the very high interfacial area between the organisms and the oxygenated fluid surrounding them assists the rate of oxygen consumption. It may be found, however, that the product of the high organism–liquid interfacial area and low mass transfer coefficient may be less than the product of the comparatively low gas–liquid interfacial area and high mass transfer coefficient, in which case the rate of oxygen supply is no longer under the control of the plant operator or designer, but is determined by the physical properties of the system.

When diffusion-controlled crystallization processes are carried out in suspended beds of crystals the maximum rate of crystallization is achieved, and where the density difference between crystal and liquor is small, as in some organic preparations, rather low rates will have to be tolerated because the mass transfer coefficients are almost unaffected by agitation.

Note added in proof: It may be shown that correlation (1) can be derived from the Froessling equation when this is combined with the equation proposed by Allen [49] for the free rising or falling velocities of small particles.

$$\text{i.e.} \quad V = \tfrac{1}{4}\left(\frac{\Delta\rho^2 g^2}{\rho_c u_c}\right) d$$

A constant of 0·28 instead of 0·31, as proposed, is thereby obtained.

Again correlation (1) may also be derived by

combining with Stokes' Law the equation for mass transfer from spheres moving in the Stokes' region, as deduced theoretically by FRIEDLANDER [50], [$N_{SL} = 0{\cdot}89\ (dV/D_L)^{1/3}$] when a constant of 0·34 is obtained.

Recent correspondence has revealed that correlation (2) represents the data of BAIRD [22] obtained with spherical cap bubbles of equivalent diameters up to 5 cm as well as the theoretical equation proposed by this worker.

$$\text{i.e.} \quad K_L = 0{\cdot}975\ D_L^{1/2} \left(\frac{g}{d}\right)^{1/4}$$

Acknowledgements—It has recently come to the authors' notice that the general principle employed in this and previous work of measuring gas–liquid interfacial areas by light transmission is similar to that described by SAUTER [43] for measuring these properties in sprays.

Dr. R. EDGE and Mr. F. EVANS were responsible for the mass transfer data obtained in sieve-plate columns.

This paper is published by permission of the Director, Warren Spring Laboratory, Stevenage, Herts. and the work was carried out while the authors were employed by the Department of Scientific and Industrial Research.

NOTATIONS

C_p = Specific heat at constant pressure of continuous phase fluid
d = particle diameter of dispersed phase
d_p = pipe diameter
D_L = diffusion coefficient in continuous phase
G = mass superficial fluid flow rate
g = acceleration due to gravity
h_c = heat transfer coefficient in continuous phase
H = mass fraction of solids in dispersion
$J_{d,h}$ = mass or heat transfer factor dimensionless

$$J_d = \frac{k_L}{V_s} (N_{Sc})^{2/3} \qquad J_h = \frac{h_c}{C_p \rho_c V_s} (N_{Pr})^{2/3}$$

k_L = continuous-phase mass transfer coefficient
l = scale of smallest eddies in turbulent fluid
L = scale of primary eddies in turbulent fluid

N_{Re} = Reynolds number $= \left(\frac{dV\rho_c}{\mu_c}\right)$ dimensionless

$N_{Re'}$ = Reynolds Number $\left(\frac{\rho_c^{1/3} (P/v)^{1/6} d^{2/3}}{\mu_c^{1/2}}\right)$ dimensionless

N_{Nu} = Nusselt Number $\left(\frac{h_c d}{\lambda}\right)$ dimensionless

N_{Sh} = Sherwood Number $\left(\frac{k_L d}{D_L}\right)$ dimensionless

N_{Ra} = Raleigh Number $\left(\frac{d^3 \Delta\rho g}{\mu_c D_L}\right)$ dimensionless

N_{Sc} = Schmidt Number $\left(\frac{\mu_c}{\rho_c D_L}\right)$ dimensionless

N_{Pr} = Prandtl Number $\left(\frac{C_p \mu_c}{\lambda}\right)$ dimensionless

N_{Gr} = Grashof Number $\left(\frac{d^3 \rho_c \Delta\rho g}{\mu_c^2}\right)$ dimensionless

(P/v) = power dissipated by agitator per unit volume of continuous phase
$\Delta p/L$ = pressure drop per unit length of pipe
V_s = superficial fluid velocity in packed bed
V = velocity of particles of disperse phase
$\sqrt{[u^2_{(d)}]}$ = root mean square fluctuating velocity over distance d
ρ_D = dispersed phase density
ρ_c = continuous phase density
μ_c = continuous phase viscosity
$\Delta\rho$ = difference in density between dispersed and continuous phases
Σ = volume fraction voids in packed bed
λ = thermal conductivity of continuous phase fluid
x, y = dimensionless constants

REFERENCES

[1] CALDERBANK P. H. *Trans. Inst. Chem. Engrs.* 1958 **36** 443.
[2] CALDERBANK P. H. *Int. Symposium on Distillation, European Federation of Chemical Engineering, England*, 1960.
[3] CALDERBANK P. H. *Trans. Inst. Chem. Engrs.* 1959 **37** 173.
[4] FROESSLING N. *Beitr. Geophys.* 1938 **32** 170.
[5] HIGBIE R. *Trans. Amer. Inst. Chem. Engrs.* 1935 **31** 365.
[6] ZDANOVSKII P. and KARAZHANOV N. A. *J. Appl. Chem.* (U.S.S.R.) 1959 **32** 1291.
[7] SCHMIDT E. *Chem.-Ing.-Tech.* 1956 **28** 175.
[8] CALDERBANK P. H. and KORCHINSKI I. J. O. *Chem. Engng. Sci.* 1956 **6** 65.
[9] COPPOCK P. D. and MEIKLEJOHN G. T. *Trans. Inst. Chem. Engrs.* 1951 **29** 75.
[10] SHENG-LI-PANG Ph.D. Thesis, University of Washington 1953.
[11] MCGREA D. Ph.D. Thesis, University of Edinburgh 1956.
[12] PIRET E. L., MATTERN R. U. and BILOUS O. *Amer. Inst. Chem. Engrs.* 1957 **3** 497.
[13] KNEULE F. *Chem.-Ing.-Tech.* 1956 **28** 221.
[14] RUMFORD F. and BAIN J. *Trans. Inst. Chem. Engrs.* 1960 **38** 11.

[15] Oyama Y. *Chem. Engng.* (*Japan*) 1956 **20** 575.
[16] Hixson A. W. and Baum S. J. *Industr. Engng. Chem.* 1944 **36** 528.
[17] Humphrey D. W. and van Ness H. C. *Amer. Inst. Chem. Engrs. J.* 1957 **3** 283.
[18] Kinzer G. D. and Gunn R. J. *Meteorology* 1951 **8** 71.
[19] Johnstone H. F., Pigford R. L. and Chapin J. H. *Trans. Inst. Amer. Chem. Engrs.* 1941 **37** 95.
[20] Williams E. E. National Physical Laboratory, Ship Division Report No. 7 1959.
[21] Hammerton D. Ph.D. Thesis, University of Birmingham 1953.
[22] Baird M. H. I. Ph.D. Thesis, University of Cambridge 1960.
[23] Garner F. H. and Hammerton D. Symposium on Gas Absorption. *Trans. Inst. Chem. Engrs.* 1954 **32** Supplement No. 1, S.18.
[24] Griffith R. M. *Chem. Engng. Sci.* 1960 **12** 198.
[25] Downing A. L. *Inst. Chem. Engrs.* Biochemical Engineering Symposium, London, 1961 (in press).
[26] Garner F. H. and Tayeban M. *An. Soc. Esp. Fis. Quim.* 1960 **56** B 491.
[27] Toor H. L. and Marchello J. M. *Amer. Inst. Chem. Engrs. J.* 1958 **4** 97.
[28] Kolmogoroff A. N. (*C. R. Acad. Sci. U.S.S.R.* 1941 **30** 301 ; *C. R. Acad. Sci. U.S.S.R.* **31** 538 1941 ; *C. R. Acad. Sci. U.S.S.R.* 1941 **32** 16 1941 ; *Dokl. Akad. Nauk. S.S.S.R.* 1949 **66** 825.
[29] Batchelor G. K. *Proc. Camb. Phil. Soc.* 1951 **47** 359.
[30] Kolar V. *Coll. Czech. Chem. Commun.* 1959 **24** 3309.
[31] Barker J. J. and Treybal R. E. *Amer. Inst. Chem. Engrs. J.* 1960 **6** 289.
[32] Rushton J. H., Lichtmann R. S. and Mahony L. H. *Industr. Engng. Chem.* 1948 **40** 1082.
[33] Chilton T. H., Drew T. B. and Jebens R. H. *Industr. Engng. Chem.* 1944 **36** 510.
[34] Brown R. W., Scott R. and Toyne C. *Trans. Instn. Chem. Engrs.* 1947 **25** 181.
[35] Johnson A. I. and Chen-Jung Huang *Amer. Inst. Chem. Engrs. J.* 1956 **2** 412.
[36] Treybal R. E. *Amer. Inst. Chem. Engrs. J.* 1958 **4** 202.
[37] Fallat R. J. Master's Thesis, University of California 1959.
[38] Chu J. C. *Chem. Engng. Progr.* 1953 **49** 141.
[39] Chilton T. H. and Colburn A. P. *Industr. Engng. Chem.* 1934 **26** 1183.
[40] Zwietering Th. N. *Chem. Engng. Sci.* 1958 **8** 244.
[41] Oyama Y. and Endoh K. *Chem. Engng.* (*Japan*) 1956 **20** 666.
[42] Wilhelm R. H., Conklin L. H. and Sauer T. C. *Industr. Engng. Chem.* 1941 **33** 453.
[43] Sauter J. *Forscharb. Ingwes.* 1928 **2**–**8** 312.
[44] Garner F. H. and Keey R. B. *Chem. Engng. Sci.* 1959 **9** 218.
[45] Meyer P. *Trans. Inst. Chem. Engrs.* 1937 **15** 127.
[46] Mathers W. G., Madden A. J. and Piret E. L. *Industr. Engng. Chem.* 1957 **49** 961.
[47] Foss A. S. and Gerster J. A. *Chem. Engng. Progr.* 1956 **52** 28–J.
[48] West C. B., Gilbert W. D. and Shimitzu T. *Industr. Engng. Chem.* 1952 **44** 2470.
[49] Allen H. S. *Phil. Mag.* 1900 **50** 323.
[50] Friedlander S. K. *Amer. Inst. Chem. Engrs. J.* 1957 **3** 43.

Chemical Engineering Science, 1961, Vol. 16, pp. 55 to 66. Pergamon Press Ltd., London. Printed in Great Britain.

The effect of interfacial films on mass transfer rates in liquid–liquid extraction

J. T. Davies and G. R. A. Mayers*

Department of Chemical Engineering, University of Cambridge

(*Received* 19 *July* 1960)

VOL. 16 1962

Abstract—An investigation of " interfacial resistances " has shown that the liquid–liquid mass transfer rate in a stirred cell is reduced in the presence of both soluble and insoluble surface-active agents. For 200 r.p.m. stirring in each liquid phase the over-all coefficient, calculated on the basis of the water film, for the transfer of *iso*propyl alcohol from water to benzene was decreased from 6×10^{-4} to $1{\cdot}3 \times 10^{-4}$ cm/sec by the presence of a plasma albumin protein film of surface concentration 1·3 mg/m^2. This was the maximum reduction obtainable for all protein film concentrations and signifies the presence of an interfacial film strong enough to prevent " surface renewal." A " surface clearing model " is used to explain the effect of film strength (as measured by the surface modulus of compressibility) on surface renewal, and therefore on the mass transfer rate.

Both film strength and rate of transfer were dependent on the type of aqueous substrate on which the protein film was spread. Substrates used with the benzene–water–*iso*propyl alcohol system were redistilled water, tap water, 0·01 N sodium hydroxide and 0·01 N hydrochloric acid. Similar results were obtained with the ethyl acetate–water system for the effect of plasma albumin films on the rate of solution of ethyl acetate in the water, using both redistilled water and tap water as substrates. For both of these systems measurements of the interfacial viscosity of the surface film indicated that this property had no direct effect on the transfer process.

The effect of surface-active films on mass transfer rates has been further studied through a smaller number of experiments, including the spreading of an acid resistant protein (porcine mucosa pepsin) for acetic acid transferring from water to benzene, and also the spreading of films of cetyltrimethylammonium bromide and of octadecyltrimethylammonium chloride for the benzene–water–*iso*propyl alcohol system.

Résumé—Une étude de " résistances interfaciales " a montré que la vitesse de transfert de masse liquide-liquide dans une cuve agitée est diminuée en présence de deux agents de surface solubles et insolubles. Pour une agitation de 200 r.p.m. dans chaque phase liquide, le coefficient global, calculé avec les bases du coefficient de l'eau, pour le transfert de l'eau vers le benzène d'alcool isopropylique diminuait de 6×10^{-4} à $1{,}3 \times 10^{-4}$ cm/sec en présence d'un film de protéines (albumine plasmatique) d'une concentration superficielle de 1,3 mg/m^2. C'est la diminution maximum que l'on peut obtenir pour toutes les concentrations en protéines du film et ceci indique la présence d'un film interfacial suffisamment puissant pour éviter un renouvellement de la surface. Un " modèle de la surface nette " est utilisé pour expliquer l'effet de la concentration du film (mesurée par le module de compressibilité de la surface) sur le renouvellement de la surface et par conséquent sur la vitesse de transfert massique.

Concentration de film et vitesse de transfert dépendant toutes deux du substrat aqueux dans lequel le film de protéines diffuse. Les substrats utilisés avec le système benzène – eau – alcool isopropylique était l'eau redistillée, l'eau du robinet la soude 0,01 N et l'acide chlorhydrique 0,01. Des résultats similaires ont été obtenus avec le système acétate d'éthyle – eau pour l'effet des films d'albumine plasmatique sur la vitesse, de la solution d'acétate d'éthyle en utilisant l'eau redistillée et l'eau du robinet comme substrats.

Pour ces systèmes, les mesures de la viscosité interfaciale de la surface du film montrent qu'elle n'a pas d'influence sur le transfert.

*Present address: c/o B.I.C.M., 23 Carel van Bylandtlaan, The Hague, Holland.

L'effet de films à surface active sur la vitesse de transfert de masse a été étudiée ultérieurement par les expériences suivantes : I) Diffusion d'une protéine résistant aux acides, (pepsine de muqueuse porcine) pour le transfert d'acide acétique de l'eau dans le benzène.

(II) – Diffusion de films de bromure de cétyl – méthyl-ammonium et de chlorure d'octadécyl – triméthylammonium pour le système benzène – eau – alcool isopropylique.

Zusammenfassung—Eine Untersuchung der "Zwischenflächenwiderstände" zeigte, dass die Stofftransportgeschwindigkeit bei Flüssig-Flüssig-Systemen in einem Rührgefäss in Gegenwart von sowohl löslichen als auch unlöslichen oberflächenaktiven Substanzen herabgesetzt wird. Bei einer Rührgeschwindigkeit von 200 Upm vermindert sich der Gesamtkoeffizient (bezogen auf den Wasserfilm) für den Transport von Isopropylalkohol aus Wasser in Benzol von 6×10^{-4} auf $1{,}3 \times 10^{-4}$ cm/sec durch die Anwesenheit eines Bluteiweissfilmes mit der Oberflächenkonzentration 1,3 mg/m². Dies war die maximal erreichbare Erniedrigung bei allen Proteinfilmkonzentrationen und bedeutet die Anwesenheit eines Zwischenflächenfilms, welcher stark genug ist, um eine "Oberflächenerneuerung" zu verhindern. Ein "surface clearing model" wird benutzt, um den Einfluss der Filmstärke (gemessen durch den Oberflächenmodul der Kompressibilität) auf die Oberflächenerneuerung und damit auf die Stoffübergangsgeschwindigkeit zu erklären.

Sowohl die Filmstärke als auch die Übergangsgeschwindigkeit waren vom Typ des wässrigen Substrates abhängig, auf dem sich der Proteinfilm befand. Benutzte Substrate im System Benzol-Wasser-Isopropylalkohol waren redestilliertes Wasser, Leitungswasser, 0,01 N NaOH und 0,01 N HCl. Aehnliche Ergebnisse wurden mit dem System Aethylacetat-Wasser erhalten in bezug auf den Einfluss der Eiweissfilme auf die Lösungsgeschwindigkeit des Aethylacetats im Wasser, wobei redestilliertes Wasser und Leitungswasser als Substrate benutzt wurden. Für beide Systeme haben Messungen der Zwischenflächenviskosität des Filmes gezeigt, dass diese Eigenschaft keinen direkten Einfluss auf den Übergangsprozess hat. Der Einfluss von oberflächenaktiven Filmen auf die Stofftransportgeschwindigkeit wurde weiterhin in einer kleineren Zahl von Experimenten studiert, einschliesslich der Verwendung eines säurebeständigen Proteins für den Übergang von Essigsäure aus Wasser in Benzol, und ebenso der Verwendung eines Filmes aus Cetyltrimethylammoniumbromid und von Oktadecyltrimethylammoniumchlorid im System Benzol-Wasser-Isopropylalkohol.

Introduction

In recent years considerable attention has been given to the phenomenon of "interfacial resistance" both in liquid–liquid extraction and in gas absorption. In his two-film theory Whitman [1] assumes continued equilibrium across the interface between the two phases, but one of the explanations of Kennedy [2] for an apparent interfacial resistance during the absorption of carbon dioxide was a suggested departure from interfacial equilibrium. However, Lynn, *et al.* [3] observed low rates of absorption of sulphur dioxide into stagnant films on short wetted-wall columns, and in the presence of Teepol the height of the stagnant zone depended inversely on the concentration of surface-active agent. Cullen and Davidson [4] reported similar effects for absorption into jets. In this case some correlation was obtained between the surface tension difference across the jet and the product of the height of the stagnant layer and the estimated mean shear stress between the jet and the film.

The above observations suggest that "interfacial resistance" may be due to the mechanical effects of interfacial films through interference with fluid motion, rather than to any lack of interfacial equilibrium, particularly so since Kennedy [2] also reported the presence of a stagnant layer. Moreover, several workers [5, 6, 7] have studied diffusion in unstirred cells, and there appears to be no evidence for a large interfacial resistance in this type of system, provided that chemical reaction and the damping of spontaneous interfacial turbulence are excluded. This absence of a measurable resistance in static liquid–liquid systems again suggests that interfacial films cause an apparent resistance to mass transfer due to a hydrodynamical effect, but not due to any blocking of the interface by the large surface-active agent molecules, nor to any lack of interfacial equilibrium.

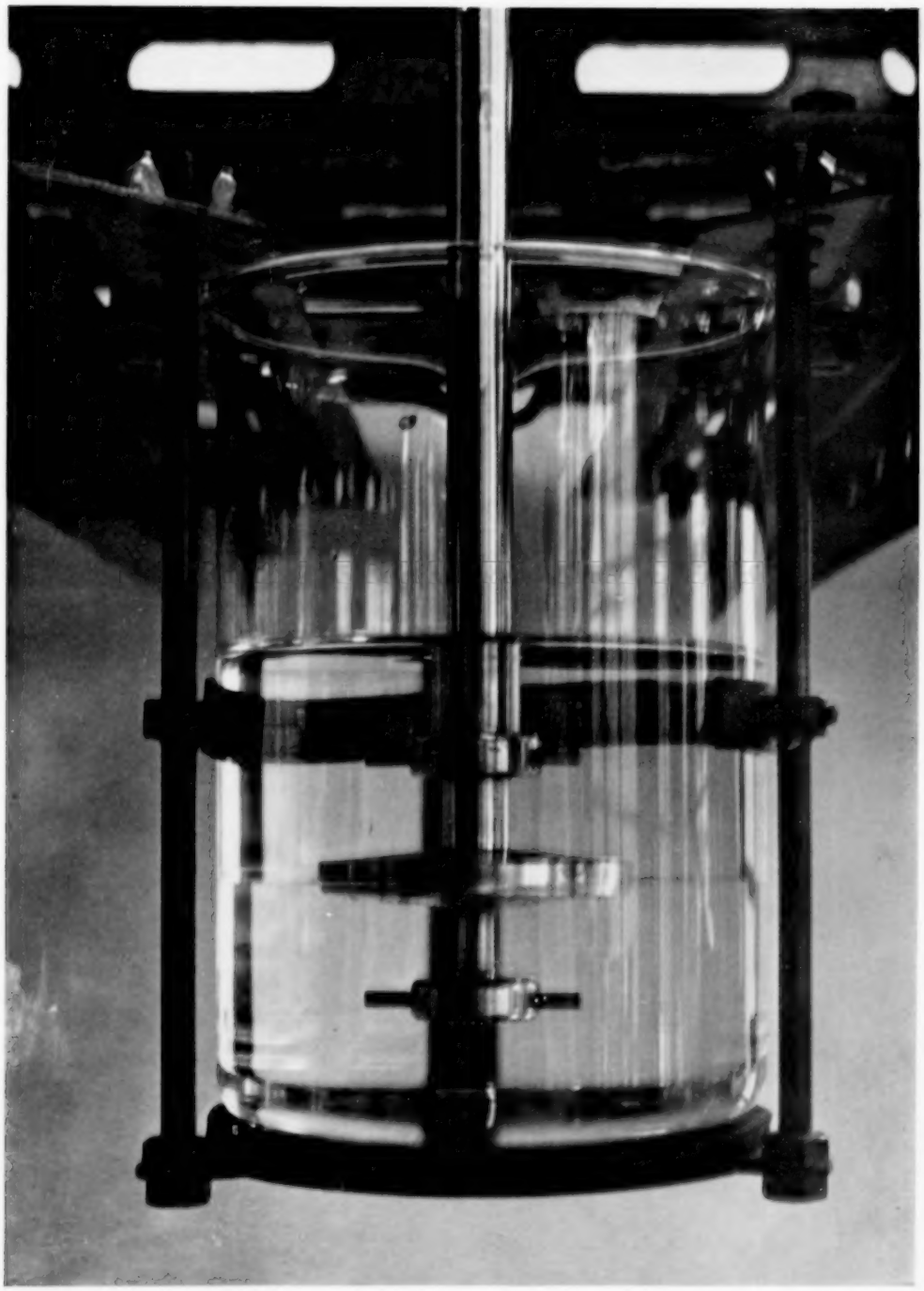

FIG. 1. Photograph of the mass transfer cell showing the stirrer assembly and the sharpened interface between benzene and water.

VOL
16
196

VOL. 16 1962

Experiments reported by LEWIS [8] on the rates of mass transfer in the mutual saturation of two liquid phases in a stirred cell, showed that rigid films of protein at the liquid–liquid interface reduced the transfer rate by interfering with the transfer of turbulence from one phase to the other. On the other hand "mobile" films of octadecyltrimethylammonium chloride spread at the interface seemed to have no effect. A suggestion was made that the interfacial viscosity of the protein films probably controlled the transfer of turbulence between the phases.

The present work examines in detail the physical properties of interfacial monomolecular layers and their effects on rates of transfer in a stirred cell. The development of a new type of surface viscometer for use at liquid–liquid interfaces [9] has enabled measurements to be made of the interfacial viscosity of two-dimensional protein films as a function of surface concentration.

A second important physical property of films is the surface modulus of compressibility, which is analogous to the surface modulus of elasticity in three-dimensional systems. This property measures the strength of a film to resist compression in its own plane by the action of surface pressure (or tension) differences. The importance of surface tension gradients and surface concentration gradients as controlling factors in the rate of mass transfer from liquid drops has been mentioned by LINTON and SUTHERLAND [10]. LEVICH [11] has also attributed the damping of ripples by surface-active films to this property, which he refers to as "a coefficient of elasticity in compression of the film."

THE DIFFUSION CELL

A stirred cell of the type described by LEWIS [8] was employed since this was the only type of apparatus which would give a large degree of liquid movement near the interface to emphasize the hydrodynamical effects. It also gave a well-defined and reproducible mass transfer area, to which accurately controlled additions of insoluble surface-active agents could be applied.

However, the present cell differed from the LEWIS cell in two important aspects. Firstly, it was a plain vessel (one litre Pyrex-glass beaker of internal diameter 4·05 in.) with no upper and lower parts separated by gaskets which would introduce unwanted surface-active impurities. Secondly, the outer baffle was found to be unnecessary as it decreased the total transfer area (present area 67·8 cm²) and made the actual area uncertain due to the unknown contact angle of the phases at the baffle. The interface in the present cell could be made very flat by ensuring that the contact angle was approximately 90°: this was achieved by pre-coating the cell with traces of an organo-silicon compound (M441 silicone from I.C.I. Ltd.). Fig. 1 gives an indication of the sharpness of the interface obtainable by this method. (The Perspex constant-temperature jacket has been removed in this photograph).

Fig. 1 shows the stirrer assembly, which consisted of two contra-rotating stirrer blades (each 1·25 in. long) and shafts, separated by the stationary interfacial baffle and its supporting shaft. The shafts fitted one inside the other to make a compact unit. The stirrers were driven through 3:1 reduction mitre-bevel gearing by 2000 rev/min, 24 V, 0·1 h.p., d.c. shunt motors with rheostat controlled battery-charger d.c. supply for speed control. The speed could be maintained within 3 rev/min of the desired value by manipulation of the rheostats, and was continuously indicated by direct-coupled tachometers.

MATERIALS

Ordinary laboratory-distilled water was found to be unsuitable for surface film experiments since it contained traces of surface active impurities (probably from plastic tubing conveying the water from the still) and of heavy metal ions. This water was therefore redistilled from weak alkaline potassium permanganate solution in all-glass equipment and collected in a specially prepared glass receiver. If this became contaminated at any time with stray surface-active impurities the whole stock was discarded.

The benzene, *iso*propyl alcohol and acetic acid were of A.R. purity. At first these were also redistilled, but later this was found to be unnecessary. The ethyl acetate used was of ordinary

commercial purity as supplied in bulk. Higher purity material hydrolysed to acid, which interfered with the properties of one of the types of protein used at the liquid–liquid interface.

The proteins used were obtained from Armour and Company and were as follows: (i) crystallized bovine plasma albumin, batch 23351 and (ii) crystallized pepsin, porcine mucosa, batch BL 1390. Other spread films of surface-active agents used were of cetyltrimethylammonium bromide (CTAB) kindly supplied in a highly pure, crystalline form by I.C.I. Ltd., and of octadecyltrimethylammonium chloride (ODTAC) from the same sample as that used by Davies [12] and by Lewis [8].

Experimental

Most of the experimental work was concerned with the effects of interfacial monomolecular films of bovine plasma albumin on the rate of transfer of *iso*propyl alcohol from water to benzene. A series of experiments was performed using water phases of slightly different compositions (viz. redistilled water, tap water, 0·01 N hydrochloric acid and 0·01 N sodium hydroxide) as this affected both the physical properties of the albumin film and the rate of mass transfer. A very slight amount of spontaneous interfacial turbulence was observed in this system in the absence of protein films. For this reason a similar series of experiments was performed in the absence of even such a slight trace of turbulence, using the two-component ethyl acetate–water system. The rate of transfer of the ethyl acetate into the water was measured for plasma albumin films of various strengths. Both tap water and redistilled water were used as the aqueous phase.

The experimental procedure will not be described in detail here as it is quite similar to that of Lewis [8]. However, it is important to mention the spreading technique for the formation of interfacial monomolecular layers of the plasma albumin protein [13]. These were spread from a 60 to 40 *iso*propyl alcohol–water solution made 0·5 M with respect to sodium acetate and containing 1 mg of protein per ml of total solution. This solution was applied to the interface in minute amounts at numerous, widely-scattered points to ensure an evenly distributed film: the application was made from a very fine hypodermic needle fed from an Agla microsyringe, the plunger of which was actuated by a micrometer screw gauge. One mm advance of the screw corresponded to 0·0198 ml of solution or to 19·8 μg, of protein and each application was only a few hundredths of a ml.

The formation of a very condensed layer of protein at the interface required only 0·04 ml of spreading solution. This was the maximum amount ever used for a single interface, and most of the experiments were performed with less than 0·01 ml on the 67·8 cm^2 interface. The effect of this amount of solution on the bulk properties of the phases was negligible.

In a few experiments spread films of the long-chain quaternary ammonium compounds CTAB and ODTAC were used. These were spread from solutions containing 0·5 mg of substance per ml of *iso*propyl alcohol solution.

During an experimental run the rate of transfer of the diffusing component was followed at various time intervals by analysing refractometrically. Small samples of only 2 or 3 drops were withdrawn from the bulk phase concerned by means of a long hypodermic needle and a microsyringe and analysed immediately by means of an Abbe refractometer of $\pm$ 0·0001 units accuracy. The calibration data are reported in detail elsewhere [14].

Mass Transfer Results

The individual and over-all film coefficients have been defined in the usual way and calculated from the experimental data after the methods summarized by Lewis [8]. For the benzene–water–*iso*propyl alcohol system the initial concentrations of the alcohol in the benzene and water phases were respectively 0 g/l. and 126 g/l. For the purpose of comparing all runs in this one system in terms of the different levels of protein addition the over-all coefficients, K_{ow}, have been calculated between concentrations in the benzene phase of 5 g/l. and 10 g/l. Over this range the distribution coefficient, H, varied from 0·122 to 0·135.

Fig. 2 shows some of the initial experimental

VOL 16 196

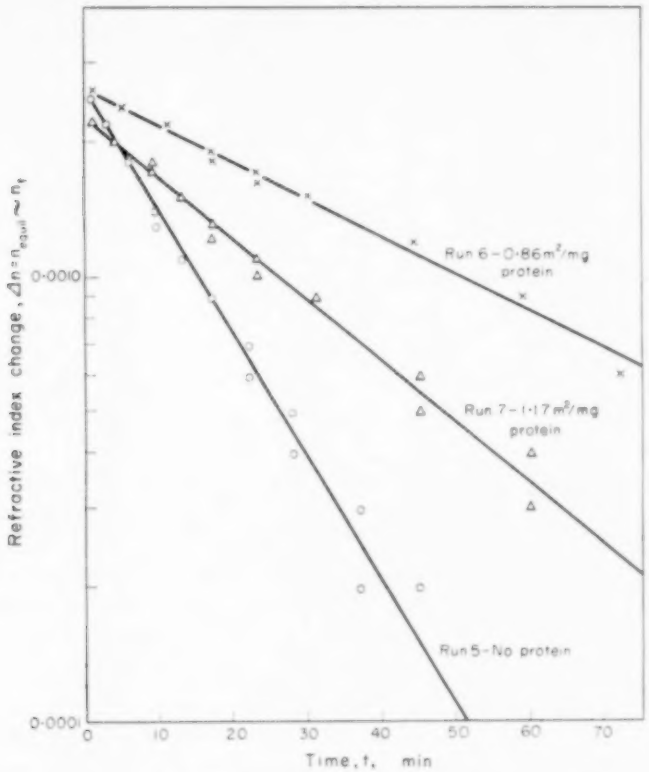

FIG. 2. Typical experimental runs showing the effect of monomolecular films of bovine plasma albumin on the transfer of *iso*propyl alcohol from water to benzene in terms of the approach to the equilibrium refractive index of the benzene phase.

data plotted with semi-logarithmic co-ordinates in terms of the approach to the final equilibrium refractive index of the benzene phase. For these three runs each liquid phase was stirred at a speed of 200 rev/min and redistilled water was used as the aqueous phase. Run 5 proceeded at the fastest rate since no surface-active agent was present at the interface. The rate of transfer was reduced by the addition of a plasma albumin film spread to a coverage of 1·17 m²/mg of the protein, and further protein addition to a coverage of 0·86 m²/mg in Run 6 caused a greater reduction. The respective over-all coefficients for Runs 5, 7 and 6 were $5{\cdot}72 \times 10^{-4}$, $2{\cdot}82 \times 10^{-4}$ and $1{\cdot}71 \times 10^{-4}$ cm/sec.

The influence of the type of aqueous substrate on the rate of transfer is shown in Fig. 3 where the over-all coefficients for 200 rev/min stirring in each phase are plotted as a function of the protein interfacial concentration for the four aqueous substrates. The results for the tap water and the 0·01 N sodium hydroxide substrates were not easily separable in the present experiments, but were intermediate between those for redistilled water and 0·01 N hydrochloric acid. An important feature of this graph is that for each curve there is a protein concentration beyond which further protein additions have no effect on the mass transfer rate. Similar results were obtained at higher stirring speeds, as shown in Fig. 4 for the redistilled water and 0·01 N hydrochloric acid substrates.

LEWIS [8] reported that spread films of ODTAC appeared to have no effect on the rate of mass transfer. However, changes in contact angle (with consequent increases in the mass transfer

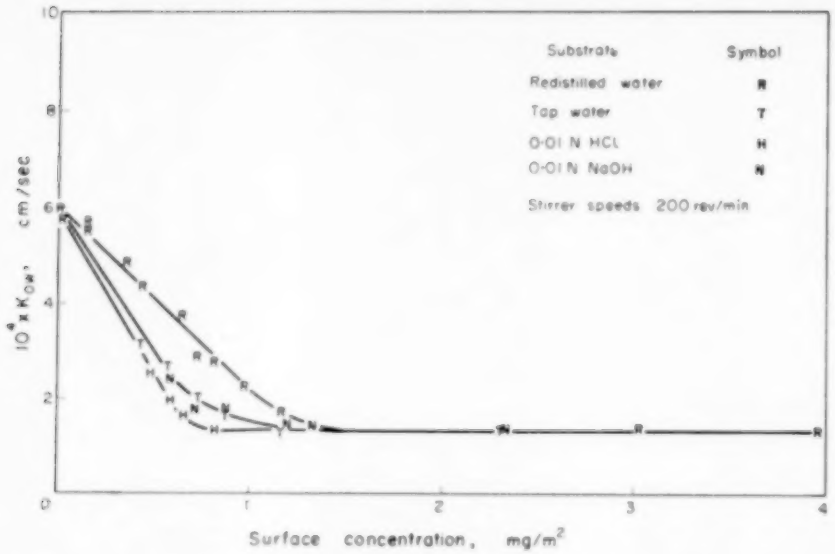

Fig. 3. The reduction of K_{ost} by bovine plasma albumin films for the benzene–water–*iso*propyl alcohol system at 20 ± 0·1°C with four different types of aqueous substrates.

area) were noted. Such changes and their effects were minimized in the present apparatus so the experiment of Lewis was repeated. As reported in Fig. 5 the over-all rate of mass transfer was reduced to almost 70 per cent of the value for a clean interface. For a surface coverage of 37·5 Å² per molecule the monolayer would be in a very compressed state, so that a larger reduction in the transfer rate might be expected on the basis of the previous protein film experiments. However,

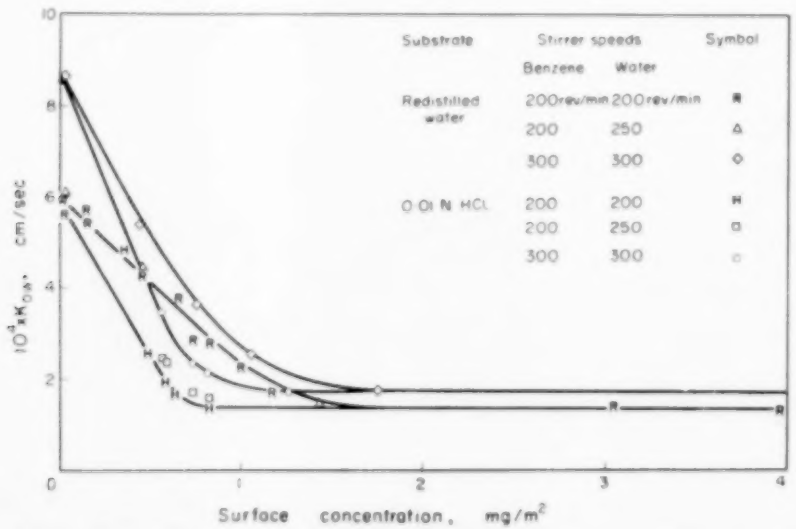

Fig. 4. The effect on K_{ost} of increasing the stirrer speeds in the benzene and aqueous phase (redistilled water and 0·01 N hydrochloric acid) in the presence of bovine plasma albumin films of given concentration at 20 ± 0·1°C.

VOL.
16
1962

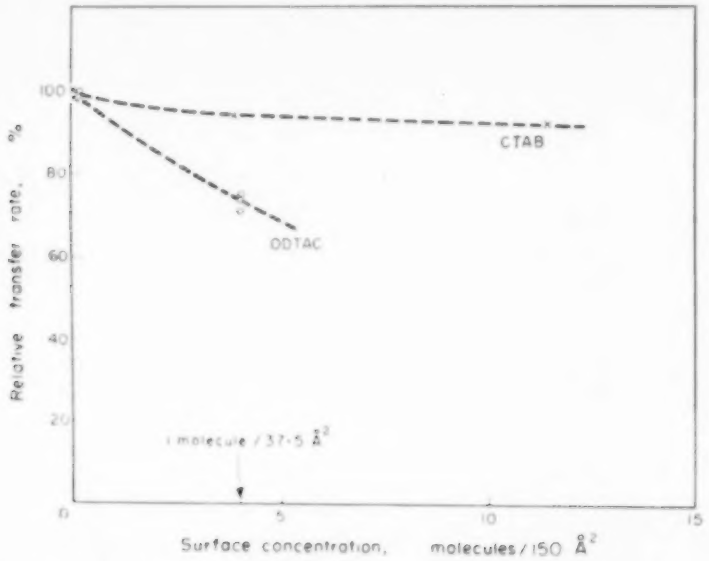

FIG. 5. Reduction in the relative rate of transfer of *iso*propyl alcohol from water to benzene at 20 ± 0·1°C caused by spread films of CTAB and ODTAC. The stirrer speed was 200 rev/min in each phase.

the ODTAC compound is quite soluble and is very quickly taken into solution in a stirred cell, though in a static cell the diffusion away from the interface is slow [12]. For spread films (or, more correctly, very weak solutions) of CTAB, very slight reductions in the mass transfer rates were detected.

In order to demonstrate that the above effects

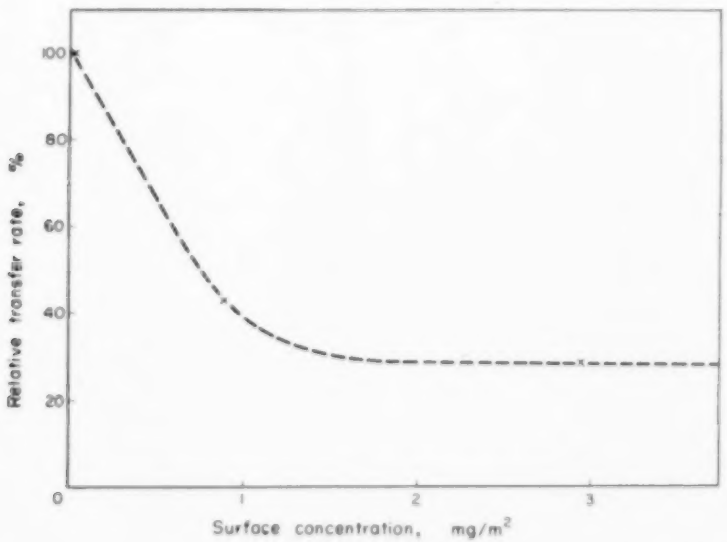

FIG. 6. Reduction in relative rate of transfer of acetic acid from water to benzene at 25 ± 0·2°C caused by porcine mucosa pepsin films. Stirrer speeds, 200 rev/min ; initial concentration of acetic acid in water, 126 g/l.

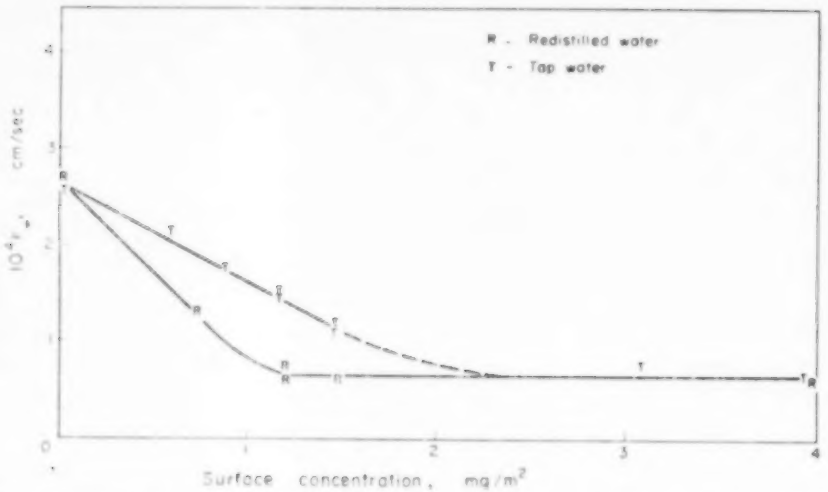

Fig. 7. Reduction of k_w caused by bovine plasma albumin films spread on two different substrates. Two-component ethyl acetate–water system with ethyl acetate transferring at 20 ± 0·1°C.

were not peculiar to the benezene–water–*iso*propyl alcohol system or to the plasma albumin films two other short series of experiments were undertaken. In the first of these, acetic acid was transferred from water to benzene in the presence of films of acid resistant protein, viz. porcine mucosa pepsin. Fig. 6 indicates that the same general form of curve was obtained as before. The second series confirmed that bovine plasma albumin produces a reduction in the observed single film coefficient in the two-component ethyl acetate–water system just as it had reduced the over-all transfer coefficient in the three component system. In Fig. 7 it is also observed that the type of aqueous phase (redistilled water or tap water for the present system) affects the reduction achieved by a given amount of protein.

The Interfacial Properties of the Protein Films

In accordance with the suggestion [8] that the surface viscosity of two-dimensional films may have some influence on the hydrodynamics of the interfacial mass transfer process a new method was developed for the measurement of this property of films at the liquid–liquid interface. In this method the surface viscosity (measured in surface poise, s.p.) is obtained from the rate of flow of the film in a two-dimensional circular canal. Two stationary concentric wire rings form the canal at the liquid–liquid interface while liquid motion is provided by the rotation of the bulk phases in a pan on a turntable. The method relies on the calibration of the rate of rotation of talc particles at the centre of the canal with films of known viscosity at the air–liquid surface.

The viscosities determined in this way have been plotted in terms of surface concentration in Figs. 8 and 9 for the benzene–water system and for the ethyl acetate–water system respectively. From these Figs. it is evident that the interfacial viscosity is very dependent on the protein concentration and on the type of aqueous substrate used.

Consideration was given to differential surface tension forces in the interface, as well as to the stresses resulting from surface viscosity. Such differential surface tension forces are related to differences in surface concentration that may arise between adjacent parts of the film due to exterior mechanical effects. This relationship defines the surface compressibility, C, of the film, viz.

$$C = -\frac{1}{A}\frac{dA}{d\Pi} = \frac{Ad(A^{-1})}{d\Pi} \qquad (1)$$

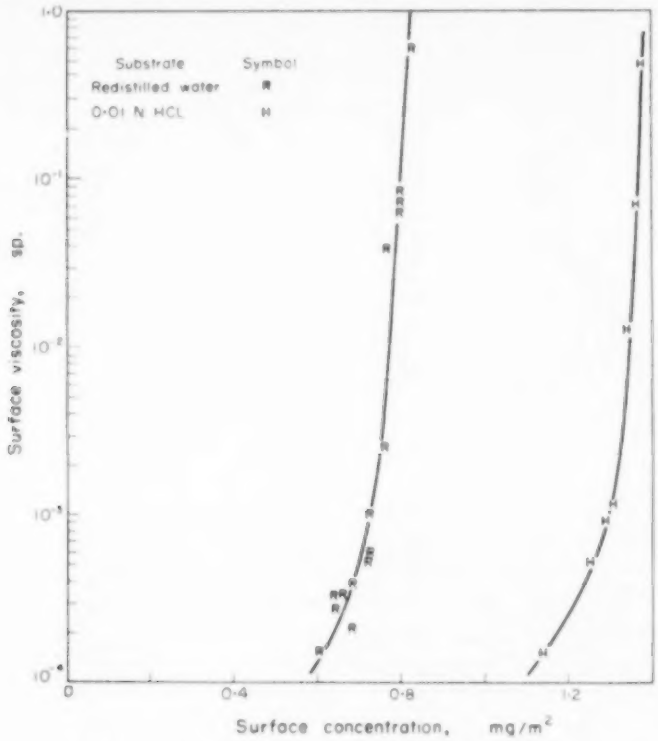

FIG. 8. The interfacial viscosity of bovine plasma films for the benzene–water system at 20 ± 1°C.

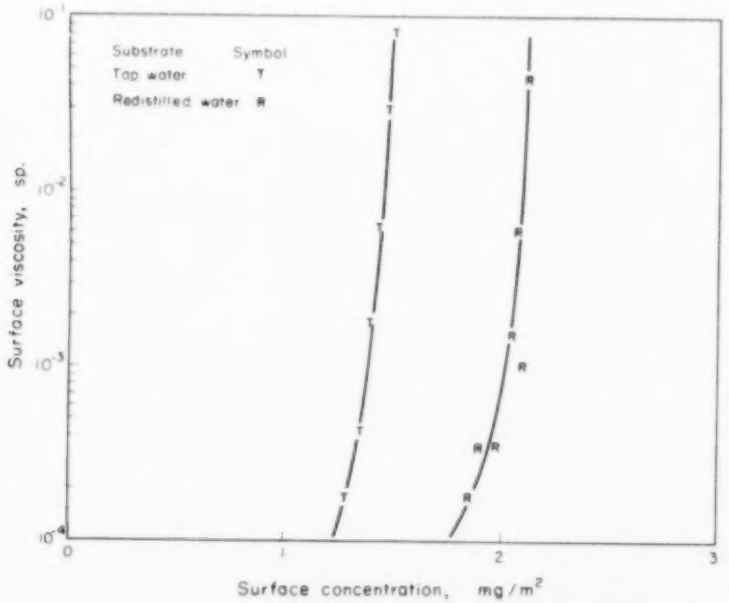

FIG. 9. The interfacial viscosity of bovine plasma films for the ethyl acetate–water system at 20 ± 1°C.

where A is the surface coverage in m^2/mg, A^{-1} is the surface concentration in mg/m^2, and Π is the corresponding surface pressure in dyn/cm. The first part of equation (1) is the normal definition used in surface chemistry literature [15], but the second form was found to be more convenient for the calculation of C.

The surface or film pressure is defined as the difference,

$$\Pi = \gamma_0 - \gamma_f,$$

where γ_0 is the surface tension of the clean surface, and γ_f is the surface tension in the presence of the surface-active film. The more surface-active material there is present the smaller will be γ_f and the greater the surface pressure.

The two-dimensional film is analogous in certain respects to the three-dimensional gaseous, liquid and solid systems. The Π vs. A diagram resembles the pressure vs. volume diagram, and both lead to the calculation of a compressibility or of a modulus of compressional elasticity. In two-dimensional systems C^{-1} is the surface compressional modulus: it expresses the strength of the film (force per unit strain) at a given surface concentration.

In the present work the interfacial tension was determined by the du Noüy ring method [16]. The standard laboratory apparatus was modified by the fitting of suitable mirrors to give a light path of total length approximately 6 m. This so increased the sensitivity that a 1 mm scale reading corresponded to a force of $7{\cdot}16 \times 10^{-4}$ g weight and to a surface tension of approximately 0·057 dyn/cm, the exact value depending on the ring correction factor [15].

The surface pressure obtainable at the ethyl acetate–water interface with bovine plasma albumin proved to be only 1 dyn/cm even at high surface concentrations, (in view of the low initial interfacial tension) so that the measurement of changes in surface compressibility of the film at the very low concentrations required would not be sufficiently accurate. The surface pressure at the benzene–water interface for low protein concentrations (e.g. 0·02 mg/m²) was, however, high enough to be measured accurately. Small differences in the film pressures were observed in

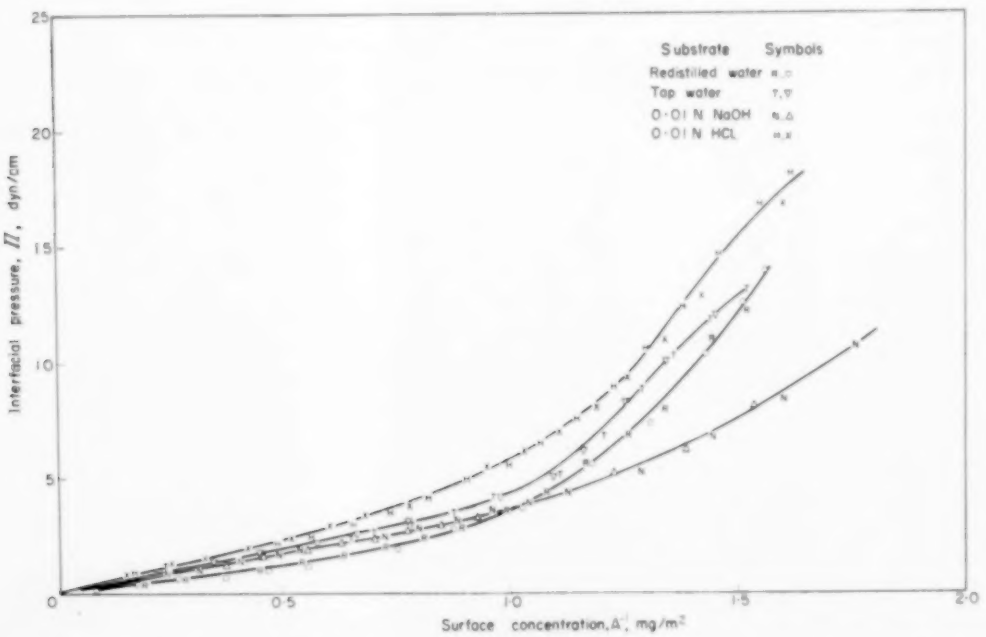

Fig. 10. The interfacial pressures of bovine plasma albumin films at the benzene–water interface at 20 ± 1°C.

VOL. 16 1962

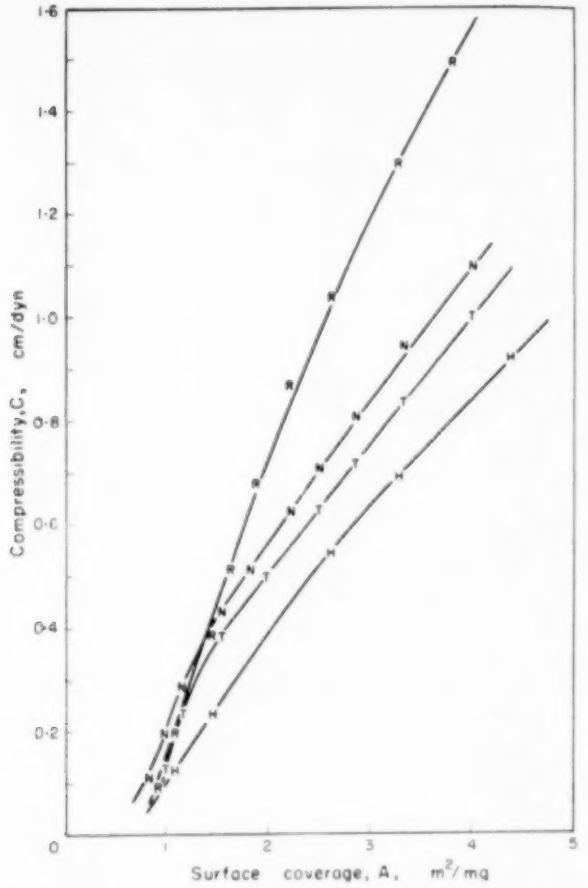

FIG. 11. Surface compressibility data for bovine plasma albumin films at 20 ± 1°C at the benzene–water interface for the four aqueous substrates shown in Fig. 10.

the presence of different aqueous substrates as shown in Fig. 10. From the slopes of these curves, which are linear near the origin, can be calculated the surface compressibility, C, by means of the second form of equation (1).

Fig. 11 shows that for high available surface areas, A, i.e. at low surface concentrations, the compressibilities on the various substrates are high, whereas for small values of A the films are not very compressible, i.e. they show a greater strength and modulus C^{-1}. For large values of A it can be seen that the redistilled water substrate produces the most easily compressible films, and that the strongest films are formed on the dilute hydrochloric acid substrate. The tap water and dilute sodium hydroxide substrates give intermediate compressibilities.

Discussion

(a) *The effect of surface viscosity*

One important feature of the mass transfer results is that a very small amount of surface-active material can cause a large reduction in the mass-transfer rate. Thus for the benzene–water–*iso*propyl alcohol system only 0·7 mg of bovine plasma per m² of interfacial area reduced the over-all coefficient from 6×10^{-4} to $1{\cdot}3 \times 10^{-4}$ cm/sec (Fig. 3) in the presence of 0·01 N hydrochloric acid. (This amount of substance is less than 5 μg on the 67·8 cm² interfacial area in the

transfer cell). However, the data in Fig. 8 show that more protein, viz. 1·2 mg/m², was required on the same substrate before the interfacial viscosity become detectable. By comparison of Figs. 3 and 8 it is seen that the protein was more effective in producing an apparent resistance to mass-transfer when spread on dilute hydrochloric acid rather than on redistilled water, but less effective in forming a viscous interfacial film. Thus the protein films do not reduce the transfer rate because of increased interfacial viscosity.

A similar conclusion can be drawn from Figs. 7 and 9 in regard to the two-component ethyl acetate–water system. The maximum resistance was reached at a protein concentration of 1·4 mg/m² on redistilled water, but more than 1·8 mg/m² was required before the interfacial viscosity had become appreciable. Furthermore, the protein was more efficient in causing an interfacial viscosity when spread on the tap water substrate, but the rate of transfer is reduced further when the protein was spread on redistilled water.

The combined evidence suggests that interfacial viscosity is not the property of surface-active films responsible for the "interfacial resistance" caused by such films. The results of Lewis [8] had implied the importance of interfacial viscosity since a large resistance was obtained with rigid or extremely viscous protein films but not with the negligibly viscous "mobile" films of octadecyltrimethyl-ammonium chloride. However, Fig. 5 shows that a resistance was obtained in the present work with dilute solutions of this substance applied initially as a spread film.

(b) *The effect of the surface modulus*

Figs. 3 and 4 demonstrate respectively the results of using different aqueous substrates and different stirring speeds. Within the experimental range of stirring speeds, viz. 100–300 rev/min, the film coefficients may be correlated by the group $(Re_1\ Re_2)^{1/2}$ for a given liquid–liquid system. The results obtained in the benzene–water–*iso*propyl alcohol system for the various substrates and protein concentrations may be further correlated by plotting $K_{ow}(Re_1\ Re_2)^{-1/2}$ as a function of the surface modulus, C^{-1}, as shown in Fig. 12. This is justified by the initial observations that at a given protein surface concentration

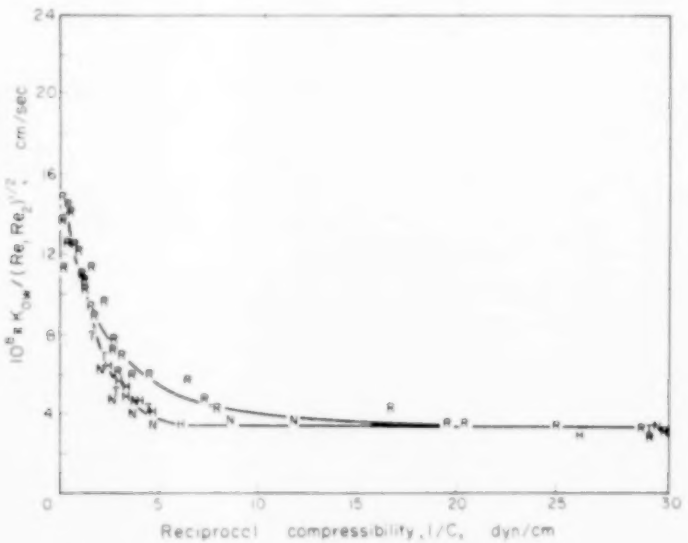

Fig. 12. Correlation of K_{ow} for various rates of stirring, with the surface modulus or reciprocal compressibility, C^{-1}, for the four substrates.

the hydrochloric acid substrate gave the strongest films together with the greatest reduction in mass transfer rate ; the redistilled water substrate gave the weakest films and lowest reduction ; the tap water and sodium hydroxide substrates gave intermediate values. In this way the maximum deviation of ± 40 per cent from an average curve in Fig. 3 is reduced to ± 25 per cent in Fig. 12.

The departure of the data for the redistilled water substrate from those of the other three substrates in the vicinity of surface modulus 5 dyn/cm has not been investigated further here. It may result from the appreciable interfacial viscosity of the film in this region, though the effect on the mass transfer rate is of secondary importance since a reduction of more than 50 per cent has already occurred at a modulus of 2 dyn/cm.

(e) *The surface-clearing model*

The influence of surface films on the mass transfer process can be explained in terms of a simple model based on what can be called "surface-clearing." This may be observed at both liquid–liquid and gas–liquid interfaces – at the latter by directing a weak air jet on to the surface after it has been sprinkled with clean talc particles. A large *circular* area of the surface will be cleared of particles when the jet is directed *vertically* on to the surface. If an easily compressible protein film is applied to the surface and the talc redistributed evenly, the size of the cleared area will be decreased for the same jet strength ; also the area closes up again on removal of the jet. Less compressible protein films cause the size of the cleared area to decrease until the films are too strong to be cleared. At this point a slight increase in the jet strength again causes a small area to be cleared.

It will be obvious that the compressibility of the surface film in such a process will determine for a given disturbance the size of cleared area and the rate of recovery on removal of the disturbance. It is proposed that the disturbances in the mass transfer process, i.e. the eddies of various magnitudes, are controlled in a similar way. Thus there will be a control on the rate of renewal of interfacial area with fresh solution from the bulk, and therefore in the light of the surface renewal theories [17, 18] a control on the mass transfer process.

The results expressed in Fig. 12 are a demonstration of the Toor–Marchello [18] model which states that the rate of transfer is high for short surface ages and decreases with increasing age until for long contact times the rate reaches a steady value corresponding to the steady state diffusion through a Whitman film. For zero film modulus the surface renewal takes place in the normal way, but with increasing modulus the renewal by some eddies is prevented, the average surface age increases and the transfer rate decreases. For a modulus C^{-1} of 10 dyn/cm surface renewal is apparently negligible in the present system ; consequently increases in the modulus above this value do not further reduce the transfer rate.

It must be noted here that Levich [11] has deduced theoretically that surface films act on ripples through a similar mechanism. The damping of ripples is attributed to the surface forces which result from local surface concentration differences caused by wave motion. A surface modulus is defined and it is found that for very large values of the modulus the surface behaves as "an incompressible solid lamina." Beyond this condition no further damping is possible.

Both surface rippling and surface renewal can be controlled by differential surface tension forces without any *direct* relation between the two phenomena being implied. For very large ripples such as those that may build up in a falling film there may be some direct contribution to the mass transfer rate through increased turbulence.

Conclusions

The present experiments with the stirred cell have shown that :

(i) Minute amounts of surface-active material, viz. of the order of 1 mg/m^2 for the types of protein investigated, cause the maximum reduction in mass-transfer rate, and therefore that slight contamination in liquid–liquid extraction systems can seriously affect the transfer rate.

(ii) "Interfacial resistance" is not directly related to the surface viscosity of interfacial films.

(iii) The nature of "interfacial resistance" can be explained in terms of a surface-clearing model on the basis of the hydrodynamics of the mass-transfer process and the strength of the interfacial film as defined by the surface compressional modulus, C^{-1}.

(iv) The presence of an incompressible monolayer on an interface reduces the rate of mass-transfer by changing the control from surface renewal to diffusion through a stagnant film.

Acknowledgement—One of us (G.R.A.M.) gratefully acknowledges the award of a scholarship by the Shell Company of Australasia Limited. The authors wish to thank Mr. J. B. Lewis of A.E.R.E., Harwell, for helpful discussions.

Notation

A = surface coverage, i.e. available area per mg or per molecule — m^2/mg or Å^2/molecule
C = surface compressibility — cm/dyn
C^{-1} = surface modulus — dyn/cm
H = equilibrium distribution ratio, solvent to aqueous phase, for diffusing component
k_B = individual film coefficient for benzene phase — cm/sec
k_w = individual film coefficient for water phase — cm/sec
K_{ow} = over-all mass transfer coefficient based on aqueous phase concentrations — cm/sec
$= Hk_B$ for the benzene–water–*iso*propyl alcohol system
L = length of stirrer blade — cm
n_{equil} = refractive index at $t = \infty$
n_t = refractive index at time t
N = stirrer speed — rev/sec
Re = liquid phase Reynolds number $= (L^2 N \rho/\mu)$
Re_1 = liquid phase Reynolds number, based on first phase properties
Re_2 = liquid phase Reynolds number, based on second phase properties
t = time — min
γ_0 = surface tension at an uncontaminated interface — dyn/cm
γ_f = surface tension in the presence of a surface-active film — dyn/cm
Π = surface pressure, $\gamma_0 - \gamma_f$ — dyn/cm
ρ = density — g/cm^3
μ = bulk viscosity — p

References

[1] Whitman W. G. *Industr. Engng. Chem.* 1923 **29** 146.
[2] Kennedy A. M. *The Kinetics of Liquid Film Processes in Gas Absorption.* Camb. Univ. Ph.D. Thesis, Cambridge University, 1954.
[3] Lynn S., Straatemeier J. R. and Kramers H. *Chem. Engng. Sci.* 1955 **4** 58.
[4] Cullen J. and Davidson J. F. *Trans. Faraday Soc.* 1957 **53** 113.
[5] Hahn H. T., U.S.A.E.C. Report HW-32626, 1954.
[6] Ward A. F. H. and Brooks L. H. *Trans. Faraday Soc.* 1952 **48** 1124.
[7] Wiggill J. B. *Some Studies of Diffusion.* Ph.D. Thesis, Cambridge University, 1958.
[8] Lewis J. B. *Chem. Engng. Sci.* 1954 **3** 248, 260.
[9] Davies J. T. and Mayers G. R. A. *Trans. Faraday Soc.* 1960 **56** 691.
[10] Linton M. and Sutherland K. L. *Proc. 2nd Int. Congr. Surf. Act.* Vol. I, p. 503. Butterworths, London 1957.
[11] Levich V. G. *Physico-Chemical Hydrodynamics.* Akad. Nauk SSSR 1952.
[12] Davies J. T. *Proc. Roy. Soc.* 1951 **208** A 224.
[13] Alexander A. E. and Teorell T. *Trans. Faraday Soc.* 1939 **35** 727.
[14] Mayers G. R. A. *Mass Transfer in Liquid–Liquid Systems.* Ph.D. Thesis, Cambridge University, March 1959.
[15] Alexander A. E. and Johnson P. *Colloid Science*, Clarendon Press, Oxford (1949).
[16] Weissberger A. *Physical Methods in Organic Chemistry*, p. 176. Interscience, New York 1945.
[17] Danckwerts P. V., *Industr. Engng. Chem.* 1951 **43** 1460.
[18] Toor H. L. and Marchello J. M. *J. Amer. Inst. Chem. Engrs.* 1958 **4** 97.

Chemical Engineering Science, 1961, Vol. 16, pp. 69 to 75. Pergamon Press Ltd., London. Printed in Great Britain.

The correlation of individual film coefficients of mass transfer in a stirred cell

G. R. A. MAYERS*

Department of Chemical Engineering, University of Cambridge

(*Received* 29 *July*, 1960)

Abstract—To assist in the interpretation of over-all mass transfer coefficients in liquid–liquid extraction in stirred cell experiments the following improved correlation has been derived on the basis of the data of LEWIS:

$$(k_1 L/D_1) = 0{\cdot}00316\,(\mathrm{Re}_1\,\mathrm{Re}_2)^{1/2}\,(\mu_2/\mu_1)^{1{\cdot}9}\,(0{\cdot}6 + \mu_2/\mu_1)^{-2{\cdot}4}\,(\mathrm{Sch}_1)^{5/6}$$

This relation has been confirmed by new experimental data obtained using a cell of slightly modified construction. Systems studied were:

(1) The benzene–water–*iso*propyl alcohol system.
(2) The benzene–water–amyl alcohol system.
(3) The ethyl acetate–water system.
(4) Systems (1) and (2) in the presence of polyethylene oxide in the aqueous phase to increase the viscosity.

During the development of the correlation it is shown that the individual film coefficients, k_1, are not entirely independent of the diffusion coefficients, D_1, of the respective phases, so that the transfer is not completely controlled by eddy diffusivity. It was found that k_1 is proportional to D_1 with an exponent of $\frac{1}{6}$, which is less than the exponent of $\frac{1}{2}$ required if the transfer takes place only by unsteady-state diffusion into stagnant surface elements, but which is nearer the exponent of zero required if the transfer takes place by a turbulent mixing process.

Résumé—Pour faciliter l'interprétation des coefficients de transfert de masse globaux dans l'extraction liquide-liquide en cuves agitées on a utilisé la relation suivante dérivée des données de LEWIS.

$$(k_1 L/D_1) = 0{,}00316\,(\mathrm{Re}_1\,\mathrm{Re}_2)^{1/2}\,(\mu_2/\mu_1)^{1{\cdot}9}\,(0{,}6 + \mu_2/\mu_1)^{-2{\cdot}4}\,(\mathrm{Sch}_1)^{5/6}$$

Cette relation a été vérifiée par de nouvelles données expérimentales obtenues avec une cuve légèrement modifiée.

Les systèmes suivants ont été étudiés:

(1) – Benzène – eau – alcool isopropylique
(2) – Benzène – eau – alcool amylique
(3) – Acétate d'éthyle – eau
(4) – Systèmes (1) et (2) en présence d'oxyde de polyéthylene en phase aqueuse pour accroître la viscosité.

Pour établir la relation on montre que les coefficients de film individuels, k_1, ne sont pas entièrement indépendants des coefficients de diffusion, D_1, des phases respectives de même que le transfert n'est pas entièrement controlé par la diffusibilité tourbillonnaire. On montre que k_1 est proportionnel à $(D_1)^{1/6}$.

L'exposant 1/6 est plus faible que l'exposant 1/2 requis si le transfert se fait uniquement par diffusion entre la surface non turbulente séparant les deux éléments, alors qu'il se rapproche du zéro requis lorsque le transfert se fait avec turbulence.

Zusammenfassung—Zur besseren Deutung von Gesamt-Stoffübergangskoeffizienten bei der Flüssig-Flüssig-Extraktion in Rührzellen wurde die folgende Beziehung aufgrund der Daten von LEWIS abgeleitet:

*B.I.C.M., 23 Carel van Bylandtlaan, The Hague, Holland.

$$(k_1 L/D_1) = 0{,}00316\,\mathrm{Re}_1\,\mathrm{Re}_2)^{1/2}\,(\mu_1/\mu_2)^{1.9}\,(0{,}6 + \mu_2/\mu_1)^{-2.4}\,(\mathrm{Sch}_1)^{5/6}$$

Diese Beziehung wurde durch neue experimentelle Daten bestatigt, die in einer etwas modifizierten Apparatur erhalten wurden. Die folgenden Systeme wurden untersucht:

1. Systeme Benzol – Wasser – Isopropylalkohol
2. System Benzol – Wasser – Amylalkohol
3. System Aethylacetat – Wasser.
4. Die Systeme (1) + (2) in Anwesenheit von Polyäthylenoxyd in der wässrigen Phase zur Viskosittäserhöhung.

Bei der Ableitung der Beziehung wird gezeigt, dass der individuelle Filmkoeffizient k_1 nicht gänzlich unabhängig vom Diffusionskoeffizient D_1 der entsprechenden Phasen ist, so dass der Transport nicht allein durch die Wirbeldiffusion bestimmt wird. Es wurde gefunden, dass k_1 proportional D_1 ist mit dem Exponenten $\frac{1}{3}$, welcher kleiner ist als der Exponent $\frac{1}{2}$, der notwendig ist, wenn der Transport nur durch unstetige Diffusion in die ruhenden Oberflachenelemente geschieht. Er ist aber näher dem Exponenten 0, der autritt, wenn der Transport durch turbulente Mischvorgänge stattfindet.

Introduction

Methods of data correlation have been well-developed in the field of heat transfer since the design of much industrial heat transfer equipment relies on correlations of suitable pilot plant data. The application of dimensional analysis and the selection of the relevant dimensionless groups have been extensively discussed in the literature, so reference is made here only to the work of Colburn [1] who pointed out the inadequacies of the earlier methods of plotting data. Colburn recommended the use of a j-factor defined as

$$j_H = (\mathrm{Nu})\,(\mathrm{Pr})^{-1/3}\,(\mathrm{Re})^{-1}.$$

It was shown that previous methods were equivalent to plotting a function of (Re) vs. (Re) itself, and that the inclusion of $(\mathrm{Re})^{-1}$ in the j-factor removed the effect of the rate of fluid flow implicit in the Nusselt number. This gave a more correct estimate of the degree of true correlation.

Chilton and Colburn [2] later drew attention to the analogy between heat and mass transfer and applied a similarly defined j-factor to the correlation of mass transfer data. However, the previously established correlation for film coefficients of mass transfer in a stirred cell [3] does not follow the j-factor approach but has the non-dimensionless form

$$60\,\rho_1 k_1/\mu_1 = 6{\cdot}76 \times 10^{-6}\,(\mathrm{Re}_1 + \mathrm{Re}_2\,\mu_2/\mu_1)^{1.65} + 1, \qquad (1)$$

where the subscripts refer to the first and second liquid phases. In equation (1) the film coefficient, k_1, is independent of the viscosity of the other phase, μ_2, since this cancels in the term $(\mathrm{Re}_2\,\mu_2)$; and for high values of μ_1 is approaching direct proportionality to μ_1, since the second term on the right is controlling. The latter means that higher rates of transfer can be predicted for high viscosity phases. For these reasons an improved correlation of the data employed in [3] and as given in [4] has been sought along the lines suggested by the Colburn j-factor.

Development of the Correlation

The j-factor is defined for the present purposes as

$$j = (k_1 L/D_1)\,(\mathrm{Sch}_1)^{-1/3}\,(\mathrm{Re}_1)^{-1}, \qquad (2)$$

where the characteristic dimension, L, is taken as the tip-to-tip length of the equal stirrer blades.

Previously the assumption was made that the liquid phase diffusion coefficient, D_1, did not influence the film coefficient, k_1, in the present type of highly turbulent system for the reason that the transfer would be by eddy diffusion entirely and not by molecular diffusion. Certainly a very small exponent of D_1 may apply since, for example, the work of Pasquill [5] on turbulent diffusion in evaporation in a wind-tunnel resulted in an exponent of approximately 2/9 instead of zero, as for eddy diffusion.

The definition of j above contains D_1 to the exponent of 2/3, but this can be tested by plotting the j-factors for otherwise identical conditions as a function of the Schmidt number. If it is found

that the resultant line has a slope of 2/3 then k_1 is independent of D_1.

The data of LEWIS [4] for the rates of transfer between mutually-saturating liquid phases, were recalculated to give j-factors, and a number of preliminary plots of these indicated that for a given liquid phase the j-factor was inversely proportional to the square root of (Re_1) and directly proportional to the square root of (Re_2). This is shown in Fig. 1, where j has been plotted vs. the ratio of the Reynolds numbers, and whence for a given liquid phase we have

$$j = \alpha\,(Re_1/Re_2)^{-1/2}. \qquad (3)$$

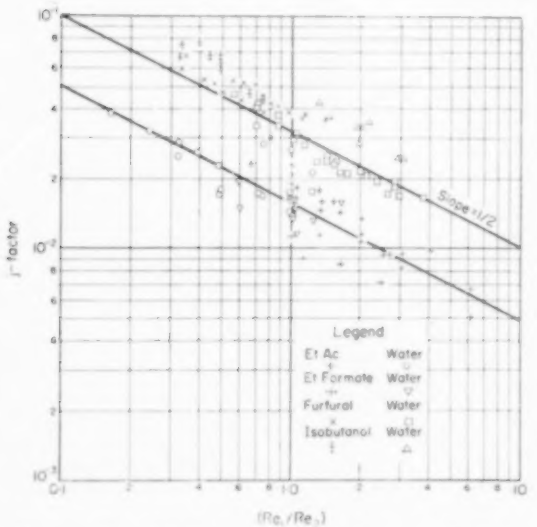

FIG. 1. The j-factor vs. (Re_1/Re_2) for the Lewis data.

In this equation α is a function of the properties of the liquid phase or phases.

Before the form of the function α was determined it was necessary to check the dependence of k_1 on D_1. This was done by plotting α vs. the Schmidt number as shown in Fig. 2. The points plotted in this Fig. are representative of the spread of the data for each liquid phase in that they define the best straight lines through the points on Fig. 1 and the maximum variations above and below this. The data are distributed according to the parameter μ_2/μ_1, with the exception of the furfural phase ($\mu_2/\mu_1 = 0{\cdot}59$), which LEWIS also found to be irregular [3]. Two lines have been drawn through equal values of the parameter, viz. 2·3 and 0·3, and these have a slope of $\frac{1}{2}$. A line of slope $\frac{2}{3}$ is also drawn since this is the necessary slope for k_1 to be independent of D_1. However, the data correlate more closely to the lines of slope $\frac{1}{2}$, so the effect

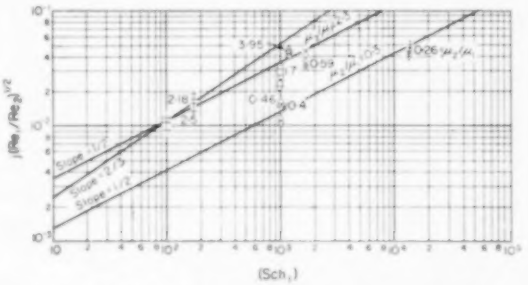

FIG. 2. Effect of the Schmidt Group and of the viscosity ratio.

of D_1 is not entirely absent. The correlation is then of the form

$$j\,(Re_1/Re_2)^{1/2} = \beta\,(Sch_1)^{1/2}, \qquad (4)$$

$$\text{i.e.} \quad k_1 L/D_1 = \beta\,(Re_1\,Re_2)^{1/2}\,(Sch_1)^{5/6}, \qquad (5)$$

where β is a function of the parameter (μ_2/μ_1).

The quantity β could be a function of a number of the physical properties considered by LEWIS [3]. POTTER [6] has pointed out the importance of both viscosity and density of the liquid phases in the laminar flow system. However, the range of densities is quite small, viz. 0·8–1·2 g/cm³, compared with the range of viscosities, viz. 0·4–4 cP, so the influence of viscosity alone has been considered. A series of plots has given the form of the function β to be

$$\beta = \delta\,(\mu_2/\mu_1)^{1{\cdot}9}\,(0{\cdot}6 + \mu_2/\mu_1)^{-2{\cdot}4},$$

where δ is a numerical factor in the present work. The data are shown correlated by this and the other dimensionless groups in Fig. 3. There still remains some degree of stratification of the data into levels corresponding to different liquid phases, but this is no greater than the scatter due to experimental error. Certainly the data for the water phase of the ethyl acetate–water system scatter across the whole band of data as the result of experimental variations. For this reason no

further investigation of the dependence of β and δ on the phase properties is possible.

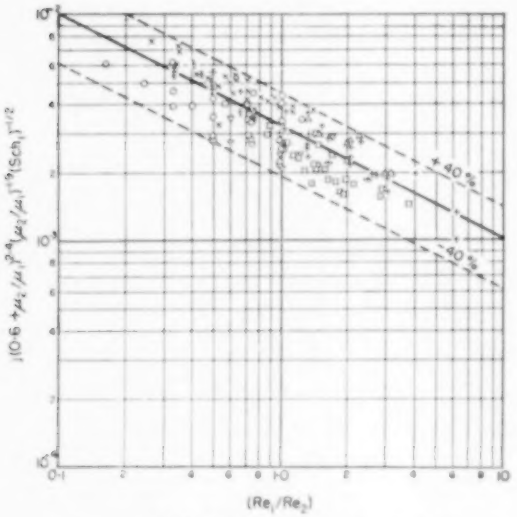

Fig. 3. Correlation plot of the Lewis data.

The correlation in its final form can be expressed more conveniently without the j-factor as follows:

$$(k_1 L/D_1) = 0{\cdot}00316\,(\mathrm{Re}_1\,\mathrm{Re}_2)^{1/2}\,(\mu_2/\mu_1)^{1{\cdot}9}\,(0{\cdot}6 + \mu_2/\mu_1)^{-2{\cdot}4}\,(\mathrm{Sch}_1)^{0{\cdot}5/6}. \qquad (6)$$

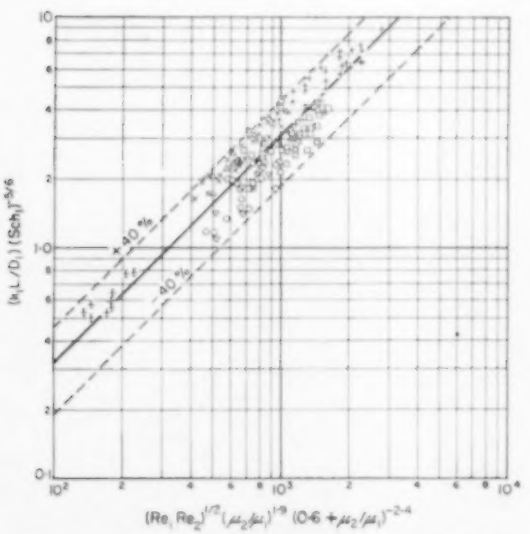

Fig. 4. Alternative form of the correlation plot.

This equation determines the line of positive slope shown in Fig. 4, which is the form of presentation used by Lewis (4).

Experimental Details

New experimental data have been obtained in the course of the work as described in the previous joint paper. These were the data for the pure systems (i.e. in the absence of surface-active agent) benzene–water–*iso*propyl alcohol and ethyl acetate–water. The range of Reynolds numbers represented is from 1120 in the aqueous phase to 6820 in the solvent phase [7].

At the suggestion of Dr. J. T. Davies other experiments were performed using an aqueous phase of 20·4 g amyl alcohol per l. and determining the rate of transfer of the amyl alcohol up to a concentration of 9 g/l. in the benzene phase. This was investigated in the presence of 1 per cent polyethylene oxide in the aqueous phase to increase the viscosity artificially. (The oxide was kindly supplied in the form of a light-amber coloured powder of type WSR–205 by the Union Carbide Chemicals Co.). The viscosity of the 1 per cent solution depended on the mode of preparation, but was measured on each occasion by means of a Ferranti Portable Viscometer over a shear rate range of 68 to 950 sec^{-1} and found to be Newtonian within the experimental error of $\pm$ 0·2 cP. Further, this solution was surface-active and deposited interfacial impurities over a period of time. The runs were therefore conducted with a heavy protein monolayer at the interface so that the interfacial condition would be reproducible. Similar runs were performed using the benzene–water–*iso*propyl alcohol system.

Experimental Results

(a) *The benzene–water–*isopropyl *alcohol system*

The rate of transfer is controlled by the benzene phase film coefficient since the distribution coefficient, H, has the low average value of 0·128 over the range of benzene concentrations from 5 to 10 g/l at 20°C [7]. Now the standard equation for the total resistance is

$$\frac{1}{K_{ow}} = \frac{1}{k_w} + \frac{1}{Hk_b} \qquad (7)$$

which, as far as the present system is concerned, can be written

$$\frac{1}{K_{ow}} \doteq \frac{1}{Hk_b} \tag{8}$$

whence k_b can be calculated from the experimentally determined values of K_{ow}.

The magnitude of the error involved in the approximation can be demonstrated for a typical run, say for 200 rev/min stirring in each phase. The diffusion coefficients for *iso*propyl alcohol in benzene and in water can be calculated by the methods of ARNOLD and WILKE [8] to be, respectively, 2×10^{-5} and 1×10^{-5} cm²/sec. The calculation on the basis of Equations (6) and (7) gives:

$$\frac{1}{K_{ow}} = \frac{1}{0{\cdot}00316} + \frac{1}{0{\cdot}0039 \times 0{\cdot}128}$$
$$= 316 + 2000$$
$$= 2316 \text{ sec/cm}$$

Hence the benzene phase constitutes 2000 2316, i.e. 0·86, of the total resistance. However, the plot of the experimental data in Fig. 5 shows that the resulting deviation of approximately 15 per cent is negligible in terms of the relative position of the data and the ± 40 per cent limits.

The above calculation in terms of the correlation equation (6) gives K_{ow} for this particular run as $1/2316 = 4{\cdot}32 \times 10^{-4}$ cm/sec, which compares with the experimental value of $5{\cdot}72 \times 10^{-4}$ cm/sec. The LEWIS correlation predicts $3{\cdot}6 \times 10^{-4}$ cm/sec.

(b) *Benzene–water–amyl alcohol system*

The over-all coefficient for 200 rev/min stirring in each phase was determined over the amyl alcohol concentration range of zero to 9 g/l. in the benzene phase, and for an initial aqueous phase concentration of 20·4 g/l. The result was $7{\cdot}1 \times 10^{-4}$ cm/sec in the presence of a protein film of very high compressional modulus. In the previous joint paper it was shown that for the benzene–water–*iso*propyl alcohol system such a film reduced the over-all coefficient by a factor of 4·5 under the same stirring conditions. Hence the K_{ow} for a clean interface in the present system would be $4{\cdot}5 \times 7{\cdot}1 \times 10^{-4} = 3{\cdot}2 \times 10^{-3}$ cm/sec.

The above result can be compared with that predicted by the correlation. The calculated diffusion coefficients of amyl alcohol in water and in benzene are $8{\cdot}35 \times 10^{-6}$ and $1{\cdot}65 \times 10^{-6}$ cm²/sec respectively [8]. Whence by equation (6) the film coefficients are $k_w = 3{\cdot}08 \times 10^{-3}$ and $k_b = 3{\cdot}81 \times 10^{-3}$ cm/sec. By equation (7) and for the experimentally determined distribution coefficient of $H = 4$ at 20°C, it follows that $K_{ow} = 2{\cdot}6 \times 10^{-3}$ cm/sec, which is in agreement with the experimental value of $3{\cdot}2 \times 10^{-3}$ cm/sec.

(c) *Addition of polyethylene oxide*

For two runs at 200 rev/min stirring in each phase of system (a) with an aqueous phase viscosity of 15 cP, the experimental values of the over-all coefficients were $7{\cdot}0 \times 10^{-5}$ and $6{\cdot}6 \times 10^{-5}$ cm/sec. If equation (6) is applicable at this high viscosity the predicted value is $5{\cdot}5 \times 10^{-5}$ cm/sec, which is approximately 80 per cent of the experimental values. If this extrapolation to 15 cP is approximately correct (the correlation is based on systems with viscosities only up to 4 cP) then the protein film evidently has little effect in reducing the transfer rate.

The value of K_{ow} predicted by the Lewis correlation for system (a) and the aqueous phase viscosity of 15 cP is $3{\cdot}8 \times 10^{-4}$ cm/sec, which is higher than the above experimental values for the reason that a large film coefficient is predicted for the viscous phase due to the approximate proportionality of k_1 to μ_1 in that correlation.

For two runs at 200 rev/min stirring in each phase of system (b) with an aqueous phase viscosity of 10 cP the experimental values of K_{ow} were $2{\cdot}7 \times 10^{-4}$ and $2{\cdot}8 \times 10^{-4}$ cm/sec, while equation (6) predicts $3{\cdot}4 \times 10^{-4}$ cm/sec. (The Lewis correlation predicts $1{\cdot}8 \times 10^{-3}$ cm/sec). Thus again the effect of the protein film at the interface would appear to be small as far as the rate of transfer in the presence of a highly viscous phase is concerned.

(d) *Ethyl acetate–water system*

The diffusivity of ethyl acetate in water has been experimentally determined by LEWIS [9] to be $1{\cdot}0 \times 10^{-5}$ cm²/sec. This, together with the other physical properties [3] of the system, has

been used to express the experimentally determined [7] film coefficients in the water phase, k_w, in dimensionless form in Fig. 5. The agreement with the correlation is well within the limits of error. For 200 rev/min stirring in each phase the experimental k_w was $2{\cdot}67 \times 10^{-3}$ cm/sec, while the correlation, equation (6), predicts $2{\cdot}9 \times 10^{-3}$ cm/sec. The value predicted by the Lewis correlation is $2{\cdot}3 \times 10^{-3}$ cm/sec, which is also in agreement with the experimental result.

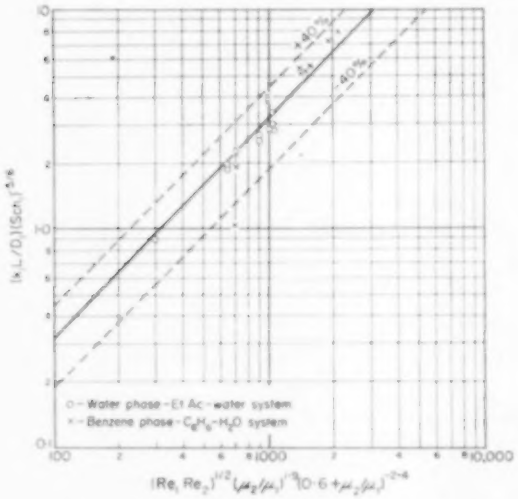

Fig. 5. Comparison of the new data (for the ethyl acetate–water system and for the benzene–water–*iso*propyl alcohol system) with the correlation.

Discussion

The correlation, equation (6), has been based on the data for the major liquid–liquid systems used by Lewis [4] in the mutual saturation runs including those for the furfural phase of the furfural–water system. In this system the furfural phase film coefficients exceeded by approximately 100 per cent the values calculated from the Lewis correlation. The present correlation represents a satisfactory improvement in this respect. The experiments of the present work were performed in a cell of identical size to the Lewis cell but with the outer annular baffle omitted in order to give a larger interfacial area. However, as Fig. 5 shows, the present data fall within the same limits as the data of Lewis. The conclusion is that the baffle does not interfere with the eddies promoting the renewal of interfacial elements; or, alternatively, that in the presence of the baffle there is a compensating increase in the interfacial area as the result of the contact angle not being a right angle.

For the highly viscous systems studied the modified correlation predicts over-all coefficients that are within $\pm$ 25 per cent of the experimental values in the presence of interfacial protein films. Thus, evidently, in such systems interfacial monomolecular films have little effect on the transfer rate by interfering with the renewal of interfacial elements since such renewal has already been greatly reduced by the resistance offered by the highly viscous phase.

The exponent of one-sixth obtained for the dependence of the film coefficient upon the diffusion coefficient is an approximation based on the data available at present. Such data represent a range of diffusion coefficients from $3{\cdot}6 \times 10^{-6}$ cm^2/sec for *iso*butyl alcohol in water to $43{\cdot}5 \times 10^{-6}$ cm^2/sec for ethyl formate in water, and of viscosities from 3·95 cP to 0·4 cP respectively. In normal systems the variation of diffusion coefficient from one system to another is closely related to the variation of viscosity. Some degree of separation of these two variables has been obtained by satisfying firstly the dependence of the film coefficient on the Schmidt number (Fig. 2), and secondly the dependence on the relative viscosity of the phases (Fig. 3). The correlation derived in this way predicts the rate of transfer in the two systems for which polyethylene oxide was used to increase artificially the aqueous phase viscosity by a factor of 10 to 15 without affecting the diffusion coefficient.

Sherwood [10] has mentioned that for highly turbulent mixing in the bulk phase the rate of transfer should be independent of the diffusion coefficient, i.e. the exponent should be zero; and that near the interface the exponent should approach unity. However the theory of Toor and Marchello [11] indicates that this latter assumption applies only to those surface elements of sufficiently great age for an approximate steady-state to be established, and that

for very new surface elements the DANCKWERTS model [12] may apply with an exponent of 0·5 for the diffusion coefficient. On this basis alone, therefore, values of the exponent should lie between 0·5 and unity. It should be stated in this connexion that the value of 0·5 is derived from the initial assumption that the transfer takes place by a penetration or unsteady-state process. For such a process Fick's law of diffusion can be applied which then leads by the solution of the differential equation to the statement that the rate of transfer is proportional to the square root of the diffusion coefficient. The assumption of other models for the interfacial mass transfer process leads to different values for the exponent. In practice, for well-stirred conditions and in the presence of clean liquid–liquid interfaces the exponent will lie between 0·5 and zero since the physical process involves both penetration and turbulent mixing at the interface.

VOL. 16 1962

CONCLUSIONS

(i) A correlation of the form of equation (6) is applicable to both the data of LEWIS [4] and the data obtained in the present work in which a cell of slightly modified construction was used.

(ii) The effect of the coefficient of diffusion, D, on the film coefficient of mass transfer is not entirely negligible for the stirred cell system. As near as can be determined with the present data available, the exponent of D is one-sixth.

(iii) Equation (6) predicts the film coefficients in the presence of highly viscous phases, and is in that respect more acceptable than the Lewis correlation.

(iv) Monolayers of protein and other impurities at a liquid–liquid interface where one of the liquids concerned is highly viscous have very little effect on the rate of transfer in a stirred cell. The liquid motion is sufficiently damped by the viscous effect alone so that a monolayer contributes no additional effect.

Acknowledgement—The experimental work was carried out at the Shell Department of Chemical Engineering, University of Cambridge under the direction of Dr. J. T. DAVIES. The author gratefully acknowledges the award of a Shell Postgraduate Scholarship in Applied Science.

NOTATIONS

C_b = solute concentration in benzene phase g/l.
C_w^* = equilibrium solute concentration in water phase g/l.
D = diffusion coefficient cm^2/sec
H = distribution coefficient $= C_b/C_w^*$
K_{ow} = overall mass transfer coefficient based on water phase concentrations cm/sec
k = individual film coefficient of mass transfer cm/sec
L = tip-to-tip length of stirrer blade = 3·18 cm
N = stirrer speed rev/sec
ρ = density g/cm^3
μ = viscosity P

Dimensionless groups

j_H = Colburn j-factor for heat transfer $= (\mathrm{Nu})\,(\mathrm{Pr})^{-1/3}\,(\mathrm{Re})^{-1}$
j = j-factor for mass transfer $= (k_1 L/D_1)\,(\mathrm{Sch}_1)^{-1/3}\,(\mathrm{Re}_1)^{-1}$
(Nu) = Nusselt number for heat transfer
(Pr) = Prandtl number for heat transfer
(Re) = Reynolds number $= (L^2 N\rho/\mu)$
(Sch) = Schmidt number $= (\mu/\rho D)$
α, β, γ, δ = dimensionless factors as defined in the text

Subscripts

1 = phase under consideration
2 = adjacent phase
b = benzene phase
w = water phase

REFERENCES

[1] COLBURN A. P. *Trans. Amer. Inst. Chem. Engrs.* 1933 **29** 174.
[2] CHILTON T. H. and COLBURN A. P. *Industr. Engng. Chem.* 1934 **26** 1183.
[3] LEWIS J. B. *Chem. Engng. Sci.* 1954 **3** 248.
[4] LEWIS J. B. A.E.R.E. Report CE/R 1118, 1954.
[5] PASQUILL F. *Proc. Roy. Soc.* 1943 **A 182** 75.
[6] POTTER O. E. *Chem. Engng. Sci.* 1957 **6** 170.
[7] MAYERS G. R. A. *Mass Transfer in Liquid–Liquid Systems.* Ph.D. Thesis, Cambridge University 1959.
[8] TREYBAL R. E. *Liquid Extraction.* pp. 102–8. McGraw-Hill, New York 1951.
[9] LEWIS J. B. *J. Appl. Chem.* 1955 **5** 228.
[10] SHERWOOD T. K. *Chem. Engng. Sci.* 1955 **4** 290.
[11] TOOR H. L. and MARCHELLO J. M. *J. Amer. Inst. Chem. Engrs.* 1958 **4** 97.
[12] DANCKWERTS P. V. *Industr. Engng. Chem.* 1951 **43** 1460.

Chemical Engineering Science, 1961, Vol. 16, pp. 76 to 81. Pergamon Press Ltd., London. Printed in Great Britain.

Relationships between the transport coefficients of fluids

E. McLAUGHLIN
Department of Chemical Engineering, Imperial College, London S.W.7

(*Received* 11 *January* 1960)

Abstract—Dimensionless numbers used to characterize the transport properties of fluids are derived starting with the phenomenological laws of Fick, Newton, Fourier and Ohm which define the transport coefficients. Explicit values for these numbers, where possible, are discussed in terms of various assumed models.

Résumé—Des nombres sans dimension utilisés pour caractériser les propriétés de transport des fluides sont obtenus à partir des lois de Fick, Newton, Fourier et Ohm relatives à ce phénomène qui définit les coefficients de transport. Des valeurs déterminées de ces nombres, quand cela est possible, sont discutées en fonction des divers modèles considérés.

Zusammenfassung—Zur Charakterisierung der Transporteigenschaften strömender Medien wurden dimensionslose Grössen benutzt, wobei von den phänomenologischen Gesetzen von Fick, Newton, Fourier und Ohm, welche die Transportkoeffizienten definieren, ausgegangen wurde.

Explizite Werte dieser Grössen wurden, wo möglich, in Ausdrücken verschiedener angenommener Modelle diskutiert.

IN THE practical applications of chemical engineering use is made of certain dimensionless quantities e.g. the Schmidt and Prandtl numbers which are characteristic properties of a fluid. The present paper illustrates a method by which such dimensionless numbers and other general relationships between transport coefficients can be derived. Where possible explicit values of these numbers are given in terms of the properties of the constituents of the fluid.

In a system perturbed from equilibrium by the effects of concentration, velocity, temperature or electric potential gradients the perturbing influence of the gradient tends to be eliminated by an irreversible flux of molecular or electrical quantities down the gradient.

The flux of mass down a concentration gradient gives rise to the phenomenon of diffusion, the flux of momentum down a velocity gradient to viscosity, the flux of heat down a temperature gradient to thermal conductivity and the flux of charge down a potential gradient to electrical conductivity. Empirical relationships between the fluxes and forces were proposed by Fick, Newton, Fourier and Ohm with the proportionality constants between the fluxes and forces defining the transport coefficients.

These laws and the dimensions of the transport coefficients derived from them are given by equation (1)

Fick's Law

$$\frac{J}{A} = -D\frac{\partial c}{\partial x} \qquad D = l^2 t^{-1}$$

Newton's Law

$$\frac{F}{A} = -\eta\frac{\partial v}{\partial z} \qquad \eta = m\, l^{-1} t^{-1}$$

Fourier's Law

$$\frac{q}{A} = -\lambda\frac{\partial T}{\partial x} \qquad \lambda = m\, l\, t^{-3}\, T^{-1}$$

Ohm's Law

$$\frac{Q}{A} = -\sigma_e\frac{\partial V}{\partial x} \qquad \sigma_e = Q^2\, t\, l^{-3}\, m^{-1}$$

where the fundamental quantities that have been chosen are length, time, mass, charge and temperature.

The dimensional equations in (1) are not in a useful form because of the time dimension which may be eliminated by the definition of absolute temperature [1] to give

$$t = m^{1/2}\, l\, \mathbf{k}^{-1/2}\, T^{-1/2}$$

and the transport coefficients rewritten

$$D = m^{-1/2}\, l\, \mathbf{k}^{1/2}\, T^{1/2} \qquad \eta = m^{1/2}\, l^{-2}\, \mathbf{k}^{1/2}\, T^{1/2}$$
$$\lambda = m^{-1/2}\, l^{-2}\, \mathbf{k}^{3/2}\, T^{1/2}$$
$$\sigma_e = Q^2\, m^{-1/2}\, l^{-2}\, \mathbf{k}^{-1/2}\, T^{-1/2} \qquad (2)$$

Various combinations of the transport coefficients can now be chosen depending on whether or not the system contains charged particles.

1. Systems containing uncharged particles

Three ratios can be chosen in this case from D, η and λ which from equation (2) may be written

$$\frac{\lambda}{\eta} = \frac{\mathbf{k}}{m}\alpha\,; \quad \frac{D}{\lambda} = \frac{V}{\mathbf{N}\mathbf{k}}\beta\,; \quad \frac{D}{\eta} = \frac{V}{\mathbf{N}m}\gamma \qquad (3)$$

where l^3 has been replaced by $V/\mathbf{N}$ and α, β and γ are dimensionless quantities. While for spherical molecules it is possible to show [2] from purely dimensional arguments that α, β and γ depend only on the dimensionless quantities $\mathbf{k}T/\epsilon$ and $V/\mathbf{N}\sigma^3$ where $\epsilon/\mathbf{k}$ is the intermolecular force constant and σ the molecular diameter, explicit values cannot be obtained without recourse to detailed statistical theories.

Boltzmann's constant $\mathbf{k}$ may now be expressed in terms of the specific heat. Using the equipartition value for the molar specific heat of a monatomic gas, viz. $C_p = 5\mathbf{N}\mathbf{k}/2$, equation (3) may be rewritten in the more familiar form

$$\frac{C_p\,\eta}{\mathbf{N}m\,\lambda} = \frac{5}{2\alpha}\,; \quad \frac{C_p\,\rho\,D}{\mathbf{N}m\,\lambda} = \frac{5\gamma}{2\alpha}\,; \quad \frac{\eta}{\rho\,D} = \frac{1}{\gamma} \qquad (4)$$

The first ratio is the Prandtl number, the third the Schmidt number and the second their ratio.

Further relationships between the coefficients may now be obtained from taking the products of the coefficients. Of these the commonest relationship is

$$\frac{\mathbf{k}\,T}{D\,\eta\,l} = \delta \qquad (5)$$

which is the Stokes–Einstein equation if l is replaced by the radius of the diffusing particle.

As numerical values for the coefficients α, β, γ and δ can only be obtained from the detailed statistical theories these will now be considered for special cases.

(a) *Dilute gases*

Only in this case has a satisfactory statistical theory of transport processes been obtained. In terms of this theory [3] developed principally by Chapman and Enskog, the transport coefficients are in the first approximation

$$D_0 = \frac{3}{8n\,\sigma^2}\sqrt{\left(\frac{\mathbf{k}\,T}{\pi\,m}\right)}\,\frac{1}{\Omega^{(1,1)*}(T)^*}\,;$$

$$\eta_0 = \frac{5}{16\,\sigma^2}\sqrt{\left(\frac{m\,\mathbf{k}\,T}{\pi}\right)}\,\frac{1}{\Omega^{(2,2)*}(T^*)}\,;$$

$$\lambda_0 = \frac{75}{64\,\sigma^2}\sqrt{\left(\frac{\mathbf{k}^3\,T}{\pi\,m}\right)}\,\frac{1}{\Omega^{(2,2)*}(T^*)} \qquad (6)$$

where $\Omega^{(1,1)*}(T^*)$ and $\Omega^{(2,2)*}(T^*)$ are correcting factors to the rigid sphere model of molecules to allow for an intermolecular potential of the Lennard–Jones 12 : 6 form

$$\phi(r) = 4\,\epsilon\left[\left(\frac{\sigma}{r}\right)^{12} - \left(\frac{\sigma}{r}\right)^{6}\right] \qquad (7)$$

In this equation σ is the molecular diameter at $\phi(r) = 0$ and ϵ is the depth of the potential energy minimum. If the molecules can be treated as rigid spheres these correcting factors become unity. Other forms of the intermolecular potential and corresponding correcting factors have also been proposed [3].

Substituting equations (6) in (3) gives

$$\frac{\lambda_0}{\eta_0} = \frac{15}{4}\,\frac{\mathbf{k}}{m}\,; \quad \frac{D_0}{\lambda_0} = \frac{8\,V}{25\,\mathbf{N}\mathbf{k}}\,\frac{\Omega^{(2,2)*}(T^*)}{\Omega^{(1,1)*}(T^*)}\,;$$

$$\frac{D_0}{\eta_0} = \frac{6\,V}{5\,\mathbf{N}\,m}\,\frac{\Omega^{(2,2)*}(T^*)}{\Omega^{(1,1)*}(T^*)} \qquad (8)$$

which are exact expressions for the transport coefficient ratios for gases interacting according to equation (7). If C_p is assumed independent of temperature and assigned its equipartition value $5\,\mathbf{N}\mathbf{k}/2$ then equation (8) can be rewritten :

$$\frac{C_p\,\eta}{\mathbf{N}\,m\,\lambda} = \frac{2}{3}\,; \quad \frac{\rho\,D\,C_p}{\mathbf{N}\,m\,\lambda} = \frac{4}{5}\,\frac{\Omega^{(2,2)*}(T^*)}{\Omega^{(1,1)*}(T^*)}\,;$$

$$\frac{\eta}{\rho\,D} = \frac{5}{6}\,\frac{\Omega^{(1,1)*}(T^*)}{\Omega^{(2,2)*}(T^*)} \qquad (9)$$

which gives the values of the unknowns in equation (4).

Fig. (1) shows the variation of the Schmidt and Prandtl numbers and $\rho\,DC_p/\mathbf{N}\,m\,\lambda$ as a function of reduced temperature $\mathbf{k}\,T/\epsilon$ for monotamic gases assuming they interact as rigid spheres and as Lennard–Jones 12 : 6 molecules. This shows

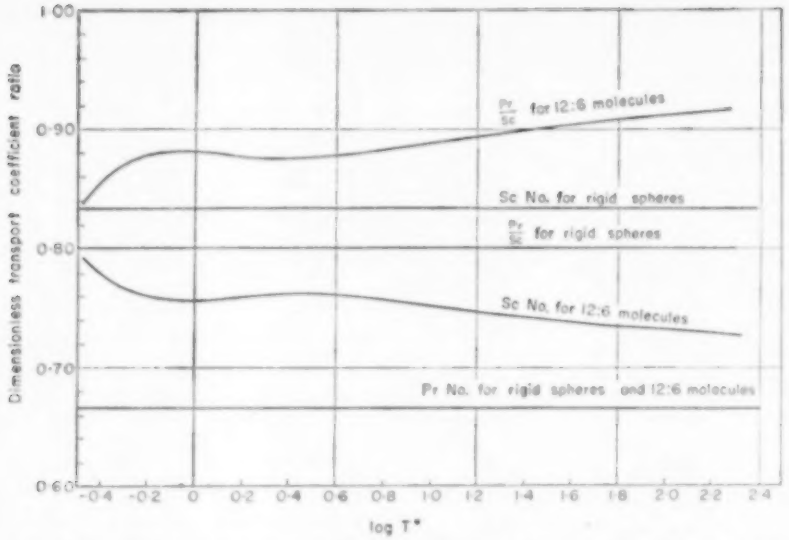
1·00
0·90
0·80
0·70
0·60
Dimensionless transport coefficient ratio
Pr/Sc for 12:6 molecules
Sc No. for rigid spheres
Pr/Sc for rigid spheres
Sc No. for 12:6 molecules
Pr No. for rigid spheres and 12:6 molecules
-0·4 -0·2 0 0·2 0·4 0·6 0·8 1·0 1·2 1·4 1·6 1·8 2·0 2·2 2·4
log T*

FIG. 1. Variation of Schmidt and Prandtl Numbers and the Ratio for a Gas of rigid sphere molecules and spherically symmetric molecules interacting with a Lennard-Jones 12 : 6 Potential.

that the Prandtl number unlike the other two is in the first approximation independent of the assumed law of force between the molecules and has the value 2/3.

On the other hand, for a polyatomic gas with internal degrees of freedom it can be seen that by going from equation (8), which is exact, to equation (9) the Prandtl number does not give exactly the relative magnitudes of η_0 and λ_0 as C_p may not have the value $5\,\mathbf{Nk}/2$ and in addition is temperature dependent. Likewise the thermal conductivity of polyatomic molecules itself is influenced by the internal degrees of freedom and must be corrected to account for the lag in the transmission of energy between the translational and internal degrees of freedom of the molecule [3]. However, in reality some compensation between C_p and λ variations with temperature occurs to keep the Prandtl number for polyatomic molecules, as determined from experiment, approximately constant.

The form of the Stokes–Einstein equation can also be obtained considering D in equation (5) as a self-diffusion coefficient and using equation (6). This gives

$$\frac{\mathbf{k}\,T}{D_0\,\pi\,r'\,\eta_0} = \frac{256}{15}\frac{\mathbf{N}\,\sigma^3}{V}\,\Omega^{(1,1)*}(T^*)\,\Omega^{(2,2)*}(T^*) \quad (10)$$

where r', the radius of the diffusing particle, is $\sigma/2$.

(*b*) *Dense gases*

For this case attention will be restricted to the variation with pressure of the transport coefficient ratios. However as the theory here is less well developed only the rigid sphere model can be used.

While in a dilute gas the transport of mass, momentum and energy takes place mainly over a "mean free path" between collisions by a convective mechanism, in a liquid or dense gas the largest transfer of momentum and energy is by the collisional mechanism. This simply means that because in a liquid or dense gas the distance between molecular centres at contact is greater than the average distance between the peripheries of molecules the largest fraction of the transport is over the distance between centres at collision as compared with that between peripheries. This additional transfer does not affect the diffusion coefficient.

On the basis of this mechanism ENSKOG [3] derived the equations for the transport coefficients in terms of the corresponding dilute gas coefficients η_0, λ_0 and D_0 as

$$\left.\begin{aligned}\frac{\eta V}{\eta_0 b_0} &= \frac{1}{y} + 0{\cdot}8 + 0{\cdot}7614\, y \\ \frac{\lambda V}{\lambda_0 b_0} &= \frac{1}{y} + 1{\cdot}2 + 0{\cdot}7574\, y \\ \frac{DV}{D_0 b_0} &= \frac{1}{y}\end{aligned}\right\} \qquad (11)$$

where $y = (pV/RT) - 1$ and $b_0 = 2/3\,\pi N\sigma^3$. At low densities y may be written in the virial form

$$y = \frac{b_0}{V} + 0{\cdot}6250\left(\frac{b_0}{V}\right)^2 + \text{- - - - - - -} \qquad (12)$$

from which it can be evaluated, but at higher densities is best evaluated from the radial distribution function [4]. It can therefore be seen that the dense gas coefficients reduce to the dilute gas expressions in the low density limit when y is replaced by its virial expansion.

From equation (11) expressions corresponding to (8) can be obtained which may be written

$$\left.\begin{aligned}\frac{\mathbf{k}\,\eta}{m\,\lambda} &= \frac{4}{15}\left(\frac{1 + 0{\cdot}8\,y + 0{\cdot}7614\,y^2}{1 + 1{\cdot}2\,y + 0{\cdot}7574\,y^2}\right) \\ \frac{\mathbf{k}\,D\,\rho}{m\,\lambda} &= \frac{8}{25}\left(\frac{1}{1 + 1{\cdot}2\,y + 0{\cdot}7574\,y^2}\right) \\ \frac{\eta}{\rho\,D} &= \frac{5}{6}\,(1 + 0{\cdot}8\,y + 0{\cdot}7614\,y^2)\end{aligned}\right\} \qquad (13)$$

Numerical values of these ratios are given in Table 1 as a function of y. In the case of the first ratio the reciprocal is given for convenience in the comparison of these results with corresponding ratios for liquids.

Table 1. Transport Coefficient Ratios of a Dense Gas of Rigid Spheres as a Function of Compressibility

y	$m\,\lambda/\mathbf{k}\,\eta$	$\mathbf{k}\,D\,\rho/m\,\lambda$	$\eta/\rho\,D$
0	3·7495	0·3200	0·8333
0·2	4·0000	0·2519	0·9916
0·4	4·1632	0·1999	1·2010
0·6	4·2571	0·1607	1·4611
0·8	4·3066	0·1310	1·7718
1·0	4·3271	0·1083	2·1333
1·2	4·3290	0·0907	2·5455
1·4	4·3240	0·0769	3·0085
1·6	4·3048	0·0659	3·5221
1·8	4·2845	0·0571	4·0864
2·0	4·2644	0·0499	4·7015
3·0	4·1684	0·0308	8·5374
4·0	4·0933	0·0179	13·6412
5·0	4·0388	0·0124	20·0128
6·0	3·9968	0·0091	27·6523

These results indicate the expected behaviour with pressure. As η and λ as a function of density pass through minima due to the changing mechanism of transport so therefore does $\mathbf{k}\,\eta/m\,\lambda$. Likewise as the diffusion coefficient is unaffected by collisional transport and continually decreases with increasing density $\mathbf{k}\,D\,\rho/m\,\lambda$ and $\eta/\rho\,D$ respectively decrease and increase with increasing pressure.

(c) *Liquids*

At present no completely rigorous theory of transport process in liquids exists to enable

Table 2. Ratio of $m\,\lambda/\mathbf{k}\,\eta$ for liquids

Liquid	*Temperature* (°K)	$m\,\lambda/\mathbf{k}\,\eta$	*Liquid*	*Temperature* (°K)	$m\,\lambda/\mathbf{k}\eta$
Benzene	288·2	2·02	Nitrogen	69·1	2·20
	298·2	2·28		71·4	2·39
	308·2	2·55		77·3	2·98
	318·2	2·83	Carbon monoxide	72·0	2·19
Carbon tetrachloride	298·2	2·19		77·7	2·64
	308·2	2·42		80·8	2·80
	318·2	2·78	Methane	93·2	2·21
Argon	84·2	2·16		103·2	2·75
	87·3	2·31		108·2	2·98

VOL. 16 1962

Table 3. D,η for non-polar organic liquids

Liquid	*Temperature* (°K)	$D\,\eta \times 10^8$	*Liquid*	*Temperature* (°K)	$D\,\eta \times 10^8$
n-Pentane [6]	194·7	10·42	*Cyclo*hexane [7]	298·2	12·47
	250·3	10·54	*Iso*pentane [7]	298·2	11·61
	273·2	11·47	Neopentane [7]	298·2	11·08
	298·2	12·08	2-Methylpentane [7]	298·2	11·74
	308·7	12·27	3-Methylpentane [7]	298·2	10·97
n-Hexane [7]	298·2	12·21	2 : 2 Dimethylbutane [7]	298·2	11·87
n-Heptane [6]	194·7	10·42	2 : 3 Dimethylbutane [7]	298·2	12·60
	250·3	10·67	Acetone [7]	298·2	14·64
	273·2	10·92	Nitromethane [7]	298·2	13·10
	305·7	11·60	Benzene [5]	288·2	13·12
	329·7	11·87		298·2	12·91
	353·4	13·19		308·2	12·56
	369·0	13·25		318·2	12·33
n-Octane [7]	298·2	10·20	Carbon tetrachloride [5]	298·2	12·67
n-Nonane [7]	298·2	11·39		308·2	14·05
n-Decane [7]	298·2	11·14		318·2	13·71
n-Octadecane [7]	298·2	10·76			

prediction of numerical values of transport coefficient ratios. However examination of some of the available data may provide a rough guide to help in the prediction of these quantities.

Table 2 gives experimental values [5] of the ratio $m\,\lambda/\mathbf{k}\,\eta$ for some simple molecules.

It can be seen that this ratio is within ± 11 per cent of 2·48.

While the Stokes–Einstein ratio for liquids is known to be temperature dependent [5] Table 3 shows that for a variety of non-polar organic liquids the product $D\,\eta \times 10^8$ can be taken as 12 within about ± 10 per cent.

2. Systems containing Charged Particles

With the introduction of charged particles the possibility of further relationships arises from Ohm's law. Of the possible combinations only those which produce commonly known relationships are discussed.

From equation (1) we obtain the following:

$$\left.\begin{aligned} \frac{\lambda}{\sigma_e} &= \frac{\mathbf{k}^2\,T}{Q^2}\,\xi \\ \frac{D}{\sigma_e} &= \frac{P^2\,\mathbf{k}\,T}{Q^2}\,\zeta \\ \eta\,\sigma_e &= Q^2\,l^{-4}\,\psi \end{aligned}\right\} \qquad (14)$$

where ξ, ζ and ψ are dimensionless quantities. Interpretation of these equations will now be considered where applicable for the case of electrons and ions respectively.

The electron gas

Unlike the self-diffusion and viscosity coefficients of molten metals which are normal, it is known that the thermal conductivity is anomalously large [5]. In addition the change of thermal conductivity of metals on melting is small. This problem was largely solved by LORENTZ [3] who attributed it to the conduction due to free electrons. He derived expression for the thermal and electrical conductivities of a degenerate electron gas which although they could not be evaluated explicitly give a simple ratio

$$\frac{\lambda}{\sigma_e\,T} = \frac{\pi^2\,\mathbf{k}^2}{3\,\mathbf{e}^2} \qquad (15)$$

ξ therefore in equation (14) is $\pi^2/3$ when the unit charge Q is taken as the charge on the electron in e.s.u. units. Equation (15) is known as the Wiedemann–Franz law and can be used to obtain values of the thermal conductivities of molten metals from measurements of the electrical resistance and temperature alone.

VOL 16 196

Ions

In this case the second equation in (14) may be transformed to

$$\frac{\sigma_e}{D} = \frac{\mathbf{F}^2}{\mathbf{N}\,l^2\,\mathbf{N}\mathbf{k}\,T}\,\frac{1}{\zeta} \tag{16}$$

where the unit charge in e.s.u. is converted to e.m.u. and replaced by the Faraday $\mathbf{F} = \mathbf{Ne}/\mathbf{c}$. It is obvious then that $\sigma_e\,\mathbf{N}\,l^3$ is the equivalent conductance Λ if $\mathbf{N}\,l^3$ is the volume of solution containing 1 g-equiv. of conductors. Equation (16) may therefore be transformed to

$$\Lambda = \frac{\mathbf{F}^2}{\mathbf{N}\mathbf{k}\,T}\,D\,\frac{1}{\zeta} \tag{17}$$

which is the Nernst–Einstein equation for an electrolyte solution.

Likewise the third equation in (14) may be written

$$\eta\,\Lambda = \frac{\mathbf{F}^2}{\mathbf{N}\,l}\,\psi \tag{18}$$

where l^3 has been replaced by $V/\mathbf{N}$. This is a form of Walden's rule which states that the equivalent conductivity multiplied by the viscosity is a constant. The rule holds only in very dilute solution and the product varies somewhat for different solvents [8]. This can be explained if the remaining l in equation (18) is replaced by the ion radius which can vary from solvent to solvent due to solvation.

Acknowledgement—I wish to thank Professor K. G. Denbigh for helpful comments on this work.

Notation

J/A = flux of mass per unit area
F/A = flux of momentum per unit area
q/A = flux of heat per unit area
Q/A = flux of charge per unit area
D = coefficient of diffusion
η = coefficient of viscosity
λ = coefficient of thermal conductivity
σ_e = coefficient of electrical conductivity
c = concentration
v = velocity
$\mathscr{V}$ = electrical potential
l = length
m = molecular mass
t = time
Q = unit charge
T = absolute temperature
$\mathbf{k}$ = Boltzmann's constant
V = total or molar volume
ϵ = potential energy minimum
σ = molecular diameter
$\mathbf{N}$ = Avogadro's number
C_p = molar specific heat
ρ = density
n = number density
$\Omega^{(1,1)*}\,\Omega^{(2,2)*}$ = kinetic theory collision integrals
T^* = reduced temperature
$D_0,\ \eta_0,\ \lambda_0$ = coefficients of self-diffusion, viscosity and thermal conductivity for an infinitely dilute gas
$\phi(r)$ = intermolecular potential energy function
r = intermolecular separation
r' = molecular radius
y = compressibility factor minus one for a rigid sphere gas
$pV/\mathbf{R}T$ = compressibility factor
b_0 = second verial coefficient for rigid spheres
$\mathbf{e}$ = electronic charge e.s.u.
$\mathbf{F}$ = the Faraday
$\mathbf{c}$ = velocity of light
Λ = equivalent conductance
$\alpha, \beta, \gamma, \delta, \xi, \zeta, \psi$ = dimensionless quantities

References

[1] Focken C. M. *Dimensional Methods and their Applications.* Edward Arnold, London 1953.
[2] McLaughlin E. *Physica, 'sGrav.* 1960 **26** 650.
[3] Chapman S. and Cowling T. G. *The Mathematical Theory of Non-Uniform Gases,* Cambridge University Press 1939. Hirschfelder J. O., Curtiss C. F. and Bird R.
[4] Kirkwood J. G., Maun E. K. and Alder B. J. *J. Chem. Phys.* 1950 **18** 1040; McLellan A. G. *Proc. Roy. Soc.* 1952 **210** A 509.
[5] McLaughlin E. *Quart. Rev. Chem. Soc.* 1960 **14** 236.
[6] Fishman E. *J. Phys. Chem.* 1955 **59** 469.
[7] Douglas D. C. and McCall D. *J. Phys. Chem.* 1958 **62** 1102. *Phys. Fluids* 1959 **2** 1.
[8] Stokes R. H. and Robinson R. A. *Electrolyte Solutions,* Butterworths, London 1955.

Chemical Engineering Science, 1961, Vol. 16, pp. 82 to 86. Pergamon Press Ltd., London. Printed in Great Britain.

Liquid–vapour equilibria and Azeotropic data for acetic acid and toluene

C. O. Haughton

Courtaulds Limited, Research Laboratories, Coventry

(*First received* 22 *October* 1960; *in revised form* 2 *January* 1961)

Abstract—Liquid–vapour equilibria have been determined for acetic acid toluene mixtures, from which the composition and boiling point of the azeotrope were found. The results differ from figures published in standard reference books.

Résumé—L'auteur détermine l'équilibre liquide-vapeur des mélanges acide acétique-toluène, et trouve la composition et le point d'ébullition de l'azéotrope. Les résultats diffèrent de ceux publiés par les ouvrages de références classiques.

Zusammenfassung—Für Gemische von Essigsäure-Toluol wurden Dampf-Flüssigkeits-Gleichgewichte bestimmt, aus denen die Zusammensetzung und der Siedepunkt des Azeotrops ermittelt wurden. Die Ergebnisse weichen von den in Handbüchern veröffentlichten Darstellungen ab.

VOL
16
196

Introduction

The data published for the azeotrope of acetic acid and toluene are conflicting (see Table 1). The only published liquid–vapour equilibria for the two components at atmospheric pressure appear to be those of Othmer (Table 1, Ref. 8). The author, however, carried out some determinations in 1931, which differed from Othmer's results, but were never published. In view of the above-mentioned confusion, the equilibria have been redetermined more accurately. Both reagents used were analytically pure ("Analar" grade ex British Drug Houses Limited).

Apparatus and Method

The apparatus used was of the Hands–Norman type of equilibrium still (*Trans. Inst. Chem. Engng.* 1945 **23** 80) Fig. 4. It consisted of a 1 litre flask fitted with a jacketed vapour take-off leading to a condenser, at the base of which was a two-way tap to return condensate to the boiler or take off a sample when required. The whole apparatus was enclosed in an asbestos screen with only the thermometer and condensers projecting.

About 700 ml of a mixture of toluene and acetic acid of the approximate composition required was added to the boiler and boiled gently with the tap set to recycle the condensate. After 15 min the temperature was read and a sample of about 10 ml of condensed vapour was collected by reversing the tap. The heat was then turned off and after cooling, a sample of the boiler liquid was withdrawn. Each sample was analysed by weighing a suitable quantity into water and titrating with standard alkali using phenolphthalein. The weight and mol per cent acetic acid were calculated from the titres.

Results

The results are shown in Table 2 and the values plotted in Figs. 1 and 2 together with the values published by Othmer and also those obtained by the author in 1931. The points in Fig. 1 fall slightly further from the diagonal than the 1931 values, but the curves cross the diagonal at the same point 44·7 mol per cent acetic acid (34·5 wt. per cent). Othmer's curve agrees with the results from the Hands–Norman still at the lower end but diverges when the liquid contains over 25 mol per cent toluene and crosses the diagonal at 37·5 mole per cent acetic acid. Othmer's boiling point curve as seen in Fig. 2 again diverges as the toluene increases in concentration and gives a minimum of 100·6° compared with 104·4° obtained

Table 1. *Published data for the azeotrope of acetic acid and toluene*

Ref.	*Observer*	*Source of Reference*	*Wt. % Acid*	*Mol % Acid*	*b.p.* (°C)
1	Zawidzki	*Z. Phys. Chem.* 1900 **35** 129	(30)	—	(80)
2	G. Ryland	*Amer. Chem. J.* 1899 **22** 384 ; *Chem. News (Lond.)* 1908 **15** 42, 50.	30	[39·5]	104 at 761 mm
3	Golodetz	*Chem. Z.* 1913 **36** 273, 297, 302.	32	[41·8]	—
4	M. Lecat	*Azeotropisme.* Lamertin, Brussels 1918.	28	37·3	105·4
5	M. Lecat	*Ann. Soc. Sci. Brux.* 1928 **48** BII 113.	34	[44]	104·95
6	C. O. Haughton	Unpublished data (1931).	34·5	44·7	105·4
7	D. F. Othmer	*U.S. Pat.* 2395010 (17.2.41).	38	[48]	107
8	D. F. Othmer	*Industr. Engng. Chem.* 1943 **35** 614.	[28·1]	[37·5]	100·6
9	C. O. Haughton	Present publication	34·5	44·7	104·4
10	C. O. Haughton	Present publication	34·9	45·1	104·6

N.B. Figures in brackets are not given in the original references but are inserted for comparison.

Remarks :

Ref. 1 : Full liquid–vapour equilibrium data are given but at constant temperature of 80°C. (Zawidski's apparatus is illustrated in *Distillation Principles and Processes* by S. Young, 1922).

Ref. 2 : Ryland's values are quoted by S. Young (Ref. [1]), and also in C. S. Robinson, *Elements of Fractional Distillation.* 1922).

Ref. 4 : Compositions are erroneously listed by Lecat (Ref. No. 132) as 72% and 62·7 mol % acetic acid instead of toluene. This error is repeated in *International Critical Tables* Vol. III, 319, and also in W. H. Perry's *Chemical Engineers' Handbook* 1953. But the corrected figure " 28% acetic acid at 105·4 °C " is quoted (presumably from this source) by Doolittle in *The Technology of Solvents and Plasticizers* 1954.

Ref. 5 : This value for the azeotrope composition published later by Lecat is very different from the previous value. It is quoted in Horsley's " original table of azeotropes," *Analyt. Chem.* 1947, and also in Marsden's *Solvents Manual,* 1954.

Ref. 6 : Full liquid–vapour equilibria were determined by Zawidski's method, but at atmospheric pressure. (See Figs. 1 and 2).

Ref. 7 : The source of this data is not mentioned in Othmer's patent.

Ref. 8 : The figures inserted in this reference are obtained by plotting Othmer's values for liquid–vapour equilibria (see Fig. 1) and reading off the point of intersection with the diagonal. The boiling point is given by the minimum on the curve (Fig. 2). The value 28·1% acetic acid at 100·6°C is given in Horsley's revised tables of *Azeotropic Data* published by the American Chemical Society 1952.
G. Glaxton on the other hand in his recent book *Physical and Azeotropic Data,* published by the National Benzole and Allied Products Association 1958, gives 72·5% toluene (i.e. 37·5% acetic acid as the azeotrope composition). His reference is to Horsley's tables but he erroneously transposes mole % to wt. %.

Ref. 9 : From revised liquid-equilibrium values. (See Figs. 1 and 2).

Ref. 10 : Azeotropic data by fractional distillation.

with the Hands–Norman still. The curve obtained in 1931 gives values about 1 °C higher than the latter but there was probably some super-heating in the apparatus used.

The results have been tested for thermodynamic consistency by the method of Redlich and Kister (*Industr. Engng. Chem.* **40** 341 (1948). The slope factor S was calculated on the assumption that $P_1 = p_1^\circ$ and $P_2 = p_2^\circ$, the relationship $\log pt/$ being constant over the range used, i.e. 0·0124

VOL. 16 1962

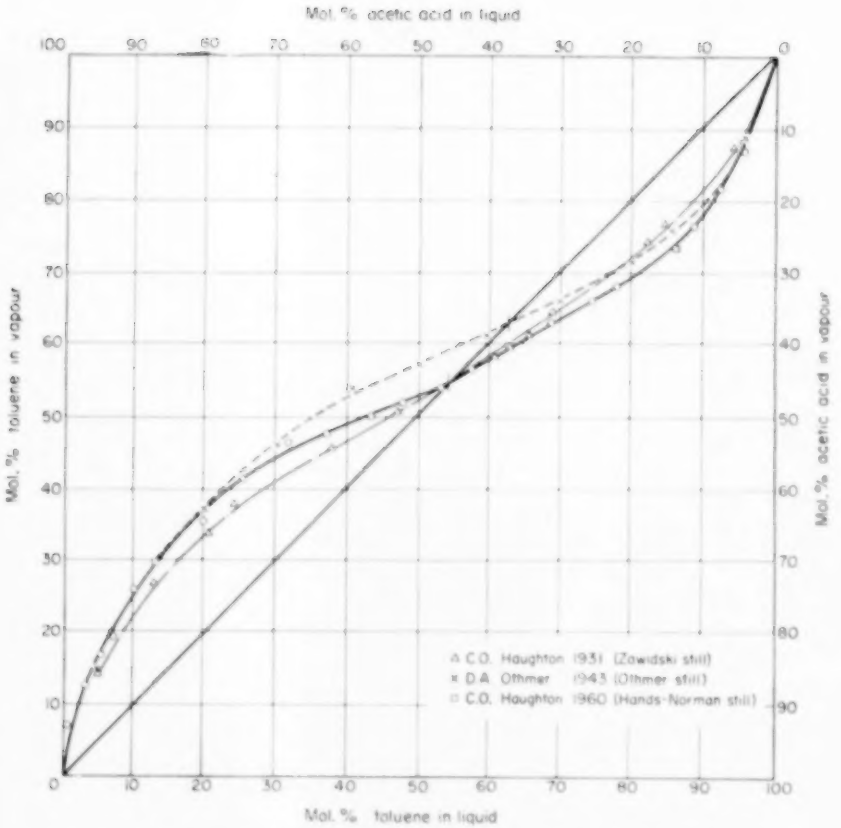

Fig. 1. Liquid–vapour equilibrium of acetic acid and toluene.

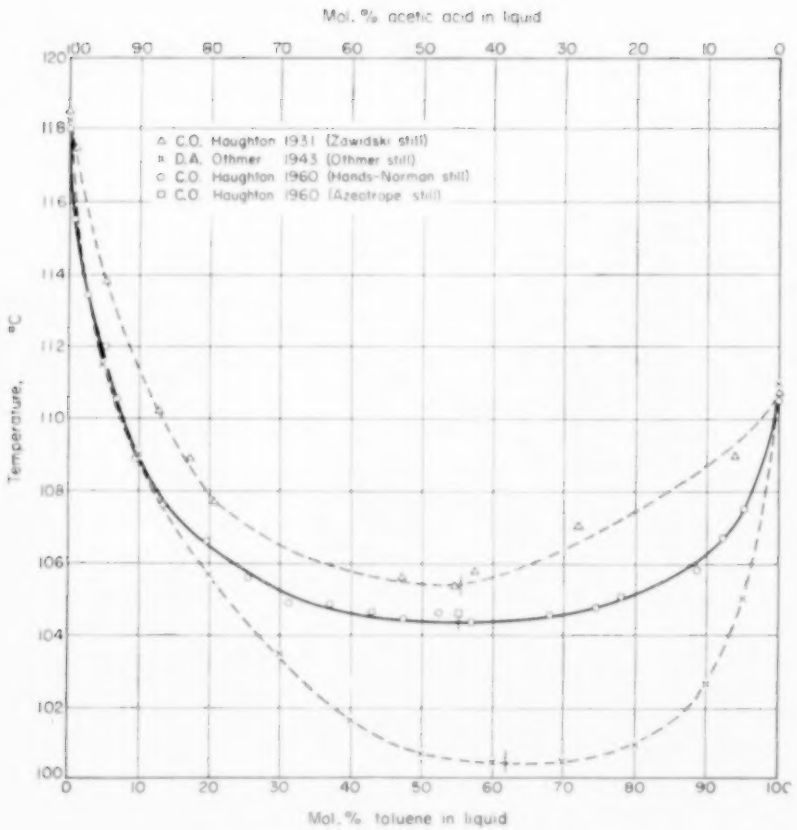
Mol. % acetic acid in liquid
100 90 80 70 60 50 40 30 20 10 0
120 118 116 114 112 110 108 106 104 102 100
Temperature, °C
△ C.O. Haughton 1931 (Zawidski still)
x D.A. Othmer 1943 (Othmer still)
○ C.O. Haughton 1960 (Hands-Norman still)
□ C.O. Haughton 1960 (Azeotrope still)
0 10 20 30 40 50 60 70 80 90 100
Mol. % toluene in liquid

FIG. 2. Boiling point of acetic acid and toluene.

Table 2. Liquid–vapour equilibria of acetic acid and toluene

Pressure (mm Hg)	*Temperature* (°C*)	*Wt % acetic acid*		*Mol fraction toluene*		*dy/dt*		α
		Liquid	*Vapour*	*x*	*y*	*Obs.*	*Calc.*	
755	118·0	99·8	99·8	0	0	− 35	—	—
c. 750	115·5	98·8	89·5	0·008	0·071	− 35	− 28	10·5
c. 750	113·4	95·1	81·2	0·030	0·129	− 35	− 26	4·8
c. 750	112·0	92·2	77·6	0·053	0·163	− 35	− 24	3·48
c. 750	110·5	89·6	72·8	0·070	0·195	− 34	− 24	3·23
c. 750	108·8	85·4	65·8	0·098	0·253	− 28	− 24	3·12
c. 750	107·6	80·7	61·1	0·134	0·295	− 25	− 23	2·70
742	106·6	72·8	52·4	0·194	0·360	− 18	− 22	2·34
742	105·6	65·8	47·7	0·253	0·418	− 16	− 21	2·13
743	104·9	58·9	43·6	0·313	0·467	− 12	− 19	1·93
743	104·9	52·5	41·9	0·371	0·477	− 11	− 13	1·545
747	104·7	46·1	39·3	0·428	0·502	− 7	− 9	1·345
746	104·5	42·1	37·7	0·473	0·519	− 4	− 6	1·200
742	104·7	37·1	35·3	0·525	0·545	− 1	− 2·6	1·082
742	104·4	32·8	33·6	0·571	0·565	0	0·8	0·975
750	104·6	22·7	27·6	0·687	0·631	7	8	0·780
750	104·8	18·3	25·2	0·745	0·650	8	14	0·655
749	105·1	14·7	23·4	0·781	0·681	10	15	0·600
750	105·8	7·8	16·8	0·885	0·764	13	23	0·420
753	106·7	5·05	12·6	0·922	0·819	18	24	0·384
755	107·5	3·21	9·13	0·952	0·867	21	25	0·332
755	110·5	Nil	Nil	1·000	1·000	—	—	—

*Corrected to 760 mm

for toluene and 0·0149 for acetic acid. The value of S thus found ranged from 29 at $x = 0$ to 35 at $x = 1$. The calculated values for the slope of the vapour curve dy/dt are given in Table 2 alongside of the observed slopes obtained by drawing a smooth curve through the experimental points. It is seen that the experimental slopes are steeper than the calculated ones for low values of y, but are less than the calculated ones for high values of y. The relative volatilities (α) are also given in Table 2.

Azeotrope Data

The composition and boiling point of the azeotrope was checked by distilling through a small fractionating column a series of mixtures of acetic acid and toluene of compositions close to that of the azeotrope, and analysing the boiler liquid and distillate. The differences between the boiler and distillate compositions when plotted graphically against the boiler composition indicated that the azeotrope contained 34·9 per cent acetic acid (45·1 mol per cent). It boiled at 104·6 °C.

It is believed that these values are more accurate than those obtained from Figs. 1 and 2. They are in fair agreement with Lecat's revised figures. (Table 1, Ref. 5). The wide discrepancy in Othmer's data suggests that one of the components used in his laboratory (probably toluene) was an impure sample which, as he states "no attempt was made to purify."

Acknowledgements—Thanks are due to the Directors of Courtaulds Limited for permission to publish this paper.

Chemical Engineering Science, 1961, Vol. 16, pp. 87 to 96. Pergamon Press Ltd., London. Printed in Great Britain.

The concept of available energy

RICHARD A. GAGGIOLI

Department of Mechanical Engineering, University of Wisconsin, U.S.A.

(*Received* 24 *August* 1960)

Abstract—The primary objectives of this paper are:

(i) To present an available energy balance reflecting the Second Law of Thermodynamics to complement the macroscopic balances of BIRD which are dictated by conservation of mass, the laws of motion and the First Law of Thermodynamics.

(ii) To develop an equation which relates the loss of available energy to the entropy production.

(iii) To point out that the dead state (the state of zero available energy) is a variable for the open system.

The equations are valid, in general, for chemically reacting or non-reacting systems, with or without diffusion. Although the potential energy term implies like conservative body forces on each constituent the equations can be extended to include unlike and/or time-dependent body forces; this is accomplished with the generalized definition of potential energy presented earlier ([7], first footnote).

Résumé—Le but de cet article est:

(i) De présenter un bilan énergétique valable rendant compte du 2ème principe de la thermodynamique pour compléter les bilans macroscopiques de BIRD qui sont imposés par la loi de conservation de la masse, les lois dela cinétique et le premier principe de la thermodynamique.

(ii) De développer une équation qui relie les pertes d'énergie utilisables à la variation d'entropie.

(iii) De mettre en évidence que l'état de référence (état zéro de l'énergie utilisable) est une variable pour un système ouvert.

Les équations sont valables, en général, pour ces systèmes de réactions chimiques ou pour des systèmes non réagissant, avec ou sans diffusion. Bien que le terme d'énergie potentielle implique la conservation des liaisons internes de chaque constituant les équations peuvent être étendues au cas de liaisons internes variables et fonctions du temps; ceci peut être réalisé en considérant que les variations dans l'énergie des champs de force résultant de variations intérieures au système, sont provoquées par le travail fourni par le système plutôt que par des variations de son énergie potentielle. Les développements sont en outre limités aux cas où la concentration de masse est une hypothèse valable. Ainsi les équations ne sont généralement pas valables pour des systèmes comportant des réactions nucléaires; mais pratiquement, les écarts vis à vis de la conservation de la masse peuvent être suffisamment faibles pour que l'énergie apportée par de telles réactions puisse être considéré comme une source de chaleur $\rho\hat{Q}_n(x, y, z, t)$ et cette contribution peut être incluse dans les équations développées ici (il suffira d'ajouter un terme).

Zusammenfassung—Die wichtigsten Gegenstände dieser Arbeit sind:

(i) Die Angabe einer verfügbaren Energiebilanz bezüglich des zweiten Satzes der Thermodynamik zur Ergänzung der makroskopischen Bilanzen von BIRD, welche auf der Erhaltung der Masse, den Gesetzen der Bewegung und dem ersten Satz der Thermodynamik beruhen.

(ii) Die Entwicklung einer Gleichung, welche den Verlust an verfügbarer Energie zur Entropieproduktion in Beziehung setzt.

(iii) Die Betonung, dass der "Nullzustand" (der Zustand, bei dem die verfügbare Energie gleich Null ist) eine Variable für das offene System ist.

Die Gleichungen sind allgemein gültig für chemisch reagierende und nicht reagierende Systeme mit und ohne Diffusion. Obwohl die Potential-energie-Terme die Massenerhaltungskräfte jeder Komponenten einschliessen, können die Gleichungen erweitert werden, so dass sie ungleiche und/oder zeitabhängige Massenkräfte einschliessen; das ist erfüllt durch die Betrachtung, dass eine Veränderung der Kraftfelder, die aus Aenderungen innerhalb des Systems herrührt, mehr durch Arbeit verursacht wird, die das System leistet, als durch Aenderung seiner potentiellen Energie. Die Ableitungen sind beschränkt auf die Fälle, bei denen die Massenerhaltung (Kontinuitätsgleichung) eine gültige Annahme darstellt. Damit sind die Gleichungen nicht allgemein gültig für Systeme mit Kernreaktionen; praktisch sind die Abweichungen von der Massenerhaltung aber so klein, dass die zusätliche Energie durch solche Reaktionen als Wärmequelle $\rho\hat{Q}_n(x, y, z, t)$ betrachtet werden kann und dieser Beitrag in die hier entwickelten Gleichungen (durch einfache Addition eines Termes) eingeschlossen werden kann.

1. Introduction

Available energy has been a subject somewhat neglected by the chemical engineer with but scant references to be found in his textbooks, although it was Weber and York [1] who pointed out years ago the utility of the concept for establishing a rational efficiency for the heat exchanger. General expressions for the macroscopic mass, momentum and energy balances have been developed by Bird [2], as well as Bernoulli equations for the viscous friction of a process. But since friction is a *degradation* and not a complete *loss of available energy* a macroscopic available energy balance is also required to complete the study of the engineering problem; this balance allows the engineer to analyse rationally the *effectiveness* of the process in yielding the desired result.

2. The Available Energy

The available energy of a system is defined [3] as *the maximum useful (net) work which could be obtained by bringing the system (which is enclosed and allowed to communicate only with the surrounding atmosphere) to its dead state – its equilibrium state at the temperature and pressure of the atmosphere.* For fixed p_0 and T_0, the available energy is a *property*: Consider *all* reversible processes from the state ($\mathcal{V}$, S) to the dead state, and such that all heat exchanges are ideally made by a reversible cycle operating between the temperature of the process and the ambient temperature. The available energy at state ($\mathcal{V}$, S) – the maximum useful work obtainable solely as a result of bringing the system to the dead state – is equal to the useful work of any such reversible process plus that of the cycle, and this work can have but one value. Otherwise, it would be possible, in a complete cycle, to produce no effect except the production of work and the extraction of heat from the atmosphere.

To evaluate the available energy select the following reversible processes (which require no auxiliary cycle for heat exchange with the atmosphere): (i) an isentropic to T_0, and (ii) an isothermal from S to S_0. Then the total useful work is

$$\begin{aligned} a = -\Delta W_u &= \Delta Q - \Delta U - \Delta K - \Delta \Phi \\ &\quad - p_0 \, \Delta \mathcal{V} \\ &= U + p_0 \mathcal{V} - T_0 S + K + \Phi \\ &\quad - (U_0 + p_0 \mathcal{V}_0 - T_0 S_0) \end{aligned} \tag{1}$$

The reader might wish to verify, say by considering areas on a $p - \mathcal{V}$ diagram, that this quantity is never negative: $a = 0$ only at the dead state, at all other states $a > 0$ (whether or not $T < T_0$ and/or $p < p_0$).

3. The Dead State

The dead state is defined as the equilibrium state at p_0 and T_0 for the contents of the system.

Let A represent any extensive property. For a specified closed system the value of the property at the dead state, A_0, is constant (unless variations in the temperature and pressure of the atmosphere are considered). For an open system, however, A_0 is not necessarily constant since the components within the system may change with time. For example (with say, $p_0 = 14.7$ p.s.i.a., $T_0 = 520\ ^\circ R$) an open system at time t_1 may contain stoicheiometric quantities of H_2 and O_2; the dead state at this instant would be that corresponding essentially to pure water. The same system at time t_2 may contain H_2 with an excess of O_2; the dead state at this instant would be essentially that with the excess oxygen gas over the water. Thus, the value of A_0 may vary with time if the composition of the system varies:

$$A_0 = A_0 (M_1 (t), M_2 (t), \ldots .) = A_0 (t) \tag{2}$$

The partial specific values of A_0 are defined in the usual manner:

$$\overline{A_{0j}} \equiv \frac{\partial A_0 (M_1, M_2, \ldots .)}{\partial M_j} = \overline{A_{0j}} (t) \tag{3}$$

4. Availability

The availability of work is defined as the net decrease in available energy of a reversible system solely as the result of work exchange. From the definition it follows immediately that the availability of work is equal to the work itself, less that required to push aside the atmosphere:

$$a_w (t) = W (t) - p_0 \left[\mathcal{V} (t) - \mathcal{V} (0) \right] \tag{4}$$

VOL 16 196

Differentiating,

$$\dot{a}_w = \dot{W} - p_0 \dot{\mathscr{V}} \tag{5a}$$

The work can be divided into two parts: that done on the boundary (i) by pressure,

$$W_p \equiv \int_{\mathscr{S}} [p\, \boldsymbol{v}_{\mathscr{S}} \cdot \boldsymbol{n}]\, d\mathscr{S}$$

and (ii) by shear stresses,

$$W_v \equiv \int_{\mathscr{S}} [(\boldsymbol{\tau} \cdot \boldsymbol{v}_{\mathscr{S}}) \cdot \boldsymbol{n}]\, d\mathscr{S}$$

So,

$$\dot{a}_w = \dot{W}_p + \dot{W}_v - p_0 \dot{\mathscr{V}} = \int_{\mathscr{S}} [(p - p_0)\, \boldsymbol{v}_{\mathscr{S}} \cdot \boldsymbol{n} + (\boldsymbol{\tau} \cdot \boldsymbol{v}_{\mathscr{S}}) \cdot \boldsymbol{n}]\, d\mathscr{S} \tag{5b}$$

Paralleling the foregoing definition, *the availability of heat is equal to the net change in available energy of a reversible system solely as the result of heat exchange*. To evaluate the availability of heat consider a reversible closed system with heat exchange but without work exchange; then the change in available energy of the system equals the availability of heat transfer, or

$$\dot{a}_Q = \dot{\hat{a}} = \dot{U} + \dot{K} + \dot{\Phi} + p_0 \dot{\mathscr{V}} - T_0 \dot{S}$$

With the First Law

$$\dot{a}_Q = \dot{Q} - T_0 \dot{S}]_{\text{rev}} = \dot{Q}\,[1 - (T_0/T)] \tag{6}$$

Equation (6) shows that the availability of heat is dependent solely upon the quantity of heat and its temperature of exchange. And also, it shows that a_Q corresponds to the maximum work of a cycle between T and T_0 (and this conclusion is the usual *definition* of the availability of heat; see Dodge [4], for example).

The availability of heat flux is equal to

$$\boldsymbol{a}_\epsilon = \boldsymbol{\epsilon}\,[1 - (T_0/T)] \tag{7}$$

The availability of flow energy is defined as the change in available energy of a reversible system because of bulk mass flow across the boundary, because of the mass-average velocity [5] relative to the boundary. This quantity could be directly derived, but since it evolves nicely in Section 6, it is evaluated there (equation 19).

The availability of diffusional energy transfer is defined as the net change in available energy of a reversible system because of diffusional mass transfer across its boundary (diffusion relative to the mass-average motion at the boundary). This quantity can be evaluated by considering the reversible change in available energy of a workless adiabatic system with diffusion (but no net mass transport) across its boundary. Hirschfelder *et al.* [6] show that the energy flux coincident with diffusion is equal to

$$\boldsymbol{e}_d = \Sigma\, \rho_j H_j \boldsymbol{v}_j \tag{8}$$

and, also, that the entropy flux with diffusion is

$$\boldsymbol{s}_d = \Sigma\, \rho_j S_j \boldsymbol{v}_j \tag{9}$$

where $\boldsymbol{v}_j \equiv \boldsymbol{u}_j - \boldsymbol{v}$ is the velocity of constituent j relative to the mass-average velocity $\boldsymbol{v}$: the diffusion velocity [5].

Hence

$$\dot{E} = -\int_{\mathscr{S}} \Sigma\, \rho_j H_j\, (\boldsymbol{v}_j \cdot \boldsymbol{n})\, d\mathscr{S} \tag{a}$$

and

$$T_0 \dot{S} = -T_0 \int_{\mathscr{S}} \Sigma\, \rho_j S_j\, (\boldsymbol{v}_j \cdot \boldsymbol{n})\, d\mathscr{S} \tag{b}$$

Since the system is workless its volume must remain constant lest there be work done by pressure and shear stresses on the boundary:

$$p_0 \dot{\mathscr{V}} = 0 \tag{c}$$

Also, with equation (3)

$$\dot{H}_0 - T_0 \dot{S}_0 = -\Sigma\,(\overline{H_{0j}} - T_0 \overline{S_{0j}}) \int_{\mathscr{S}} \rho_j\, (\boldsymbol{v}_j \cdot \boldsymbol{n})\, d\mathscr{S} \tag{d}$$

Combination of (a) through (d) yields the rate of change of available energy of this reversible workless adiabatic system, because of diffusion across its boundary:

$$-\int_{\mathscr{S}} [\Sigma\, \rho_j (H_j - T_0 S_j - \overline{H_{0j}} + T_0 \overline{S_{0j}})\, (\boldsymbol{v}_j \cdot \boldsymbol{n})]\, d\mathscr{S} \equiv -\int_{\mathscr{S}} (\boldsymbol{a}_d \cdot \boldsymbol{n})\, d\mathscr{S} \tag{10}$$

Thus, the availability of diffusional energy flux is given by

$$a_d \equiv \Sigma (H_j - T_0 S_j - \bar{H}_{0j} + T_0 \bar{S}_{0j}) \rho_j \mathbf{v}_j \quad (11)$$

The various availabilities defined above account for the change in available energy of a reversible system because of transports across the system boundary – because of work, heat, and mass transfer.

5. The Differential Available Energy Balance

The loss of available energy within a system can be defined by the *available energy balance*:

$$\left\{\begin{matrix}\text{Rate of available energy}\\ \text{loss within the system}\end{matrix}\right\} \equiv$$

$$\left\{\begin{matrix}\text{Rate of increase of available energy}\\ \text{in the system if it were reversible}\end{matrix}\right\}$$

$$- \left\{\begin{matrix}\text{Actual rate of increase of}\\ \text{available energy within the system}\end{matrix}\right\} \quad (12)$$

First, consider any system coincident with the volume $\mathscr{V}$, whose surface $\mathscr{S}$ moves with the local mass-average velocity $\mathbf{v}(x, y, z, t)$. Were the system reversible the change in available energy would equal the sum of the availabilities of the heat, work and the diffusional energy transfer:

$$\left\{\begin{matrix}\text{Net rate of increase for}\\ \text{hypothetical reversible system}\end{matrix}\right\}$$

$$= -W + p_0 \dot{\mathscr{V}} - \int_{\mathscr{S}} \left[1 - (T_0/T)\right] (\boldsymbol{\epsilon} \cdot \mathbf{n})\, d\mathscr{S}$$

$$- \Sigma \int_{\mathscr{S}} \left[(H_j - T_0 \bar{S}_j - \bar{H}_{0j} + T_0 \bar{S}_{0j}) (\rho_j \mathbf{v}_j \cdot \mathbf{n})\right] d\mathscr{S} \quad (13a)$$

or, with equation (5b), $\mathbf{v}_{\mathscr{S}} = \mathbf{v}$ and the divergence theorems,

$$\left\{\begin{matrix}\text{Net rate of increase for}\\ \text{hypothetical reversible system}\end{matrix}\right\}$$

$$= \int_{\mathscr{V}} \{ - \nabla \cdot p\mathbf{v} - \nabla \cdot (\boldsymbol{\tau} \cdot \mathbf{v}) + p_0 \nabla \cdot \mathbf{v} - \nabla \cdot \boldsymbol{\epsilon} + T_0 \nabla \cdot (\boldsymbol{\epsilon}/T) - \Sigma (\nabla \cdot (\bar{B}_j \rho_j \mathbf{v}_j - \bar{B}_{0j} \nabla \cdot \rho_j \mathbf{v}_j)\} d\mathscr{V} \quad (13b)$$

Since the system boundary moves with the local mass-average velocity [Appendix, equation (A.3)],

$$\left\{\begin{matrix}\text{Actual rate of increase}\\ \text{of available energy}\end{matrix}\right\} = \hat{\boldsymbol{a}} = \int_{\mathscr{V}} \rho \frac{D\hat{\boldsymbol{a}}}{Dt}\, d\mathscr{V} \quad (14)$$

By definition

$$\left\{\begin{matrix}\text{Rate of loss of}\\ \text{available energy in } \mathscr{V}\end{matrix}\right\} \equiv \dot{\mathscr{I}} = \int_{\mathscr{V}} \rho \dot{i}\, d\mathscr{V} \quad (15)$$

upon substituting equations (13), (14) and (15) into equation (12)

$$\dot{\mathscr{I}} = \dot{Q} + \int_{\mathscr{S}} (T_0/T) (\boldsymbol{\epsilon} \cdot \mathbf{n})\, d\mathscr{S} - W + p_0 \dot{\mathscr{V}} - \Sigma \int_{\mathscr{S}} \left[(B_j - B_{0j}) (\rho_j \mathbf{v}_j \cdot \mathbf{n})\right] d\mathscr{S} - \hat{\boldsymbol{a}} \quad (16a)$$

$$\dot{\mathscr{I}} = \int_{\mathscr{V}} \rho \dot{i}\, d\mathscr{V} = \int_{\mathscr{V}} \Big[- \nabla \cdot \boldsymbol{\epsilon} + T_0 \nabla \cdot (\boldsymbol{\epsilon}/T) - \nabla \cdot p\mathbf{v} - \nabla \cdot (\boldsymbol{\tau} \cdot \mathbf{v}) + p_0 \nabla \cdot \mathbf{v} - \Sigma (\nabla \cdot (\bar{B}_j \rho_j \mathbf{v}_j - \bar{B}_{0j} \nabla \cdot \rho_j \mathbf{v}_j) - \rho \frac{D\hat{\boldsymbol{a}}}{Dt} \Big] d\mathscr{V} \quad (16b)$$

Then, letting the size of this arbitrary system approach zero about the point (x, y, z),

$$\rho \dot{i}\ (x, y, z, t) = - \nabla \cdot p\mathbf{v} - \nabla \cdot (\boldsymbol{\tau} \cdot \mathbf{v}) + p_0 \nabla \cdot \mathbf{v} - \nabla \cdot \boldsymbol{\epsilon} + T_0 \nabla \cdot (\boldsymbol{\epsilon}/T) - \Sigma \left[\nabla \cdot (\bar{B}_j \rho_j \mathbf{v}_j - \bar{B}_{0j} \nabla \cdot \rho_j \mathbf{v}_j) - \rho \frac{D\hat{\boldsymbol{a}}}{Dt} \right. \quad (17a)$$

Equation (17a) is a *differential available energy balance – the equation of change of available energy.* The significance of each term in the equation is indicated in the foregoing analysis. Equation (17a) can be put into a form which is more readily applied to open systems by rewriting the Stokes

derivative term, $\rho\,(D\,\hat{a}/D\theta)$, according to equation (A.2) of the Appendix; thus,

$$\rho\dot{i} = -\nabla\cdot p\boldsymbol{v} - \nabla\cdot(\boldsymbol{\tau}\cdot\boldsymbol{v}) + p_0\,\nabla\cdot\boldsymbol{v} - \nabla\cdot\boldsymbol{\epsilon} + T_0\,\nabla\cdot(\boldsymbol{\epsilon}/T) - \Sigma\,(\nabla\cdot\overline{B_j}\,\rho_j\,\boldsymbol{v}_j - B_{0j}\,\nabla\cdot\rho_j\,\boldsymbol{v}_j) - \frac{\partial\,(\rho\,\hat{a})}{\partial t} - \nabla\cdot\rho\boldsymbol{v}\,\hat{a} \quad (17b)$$

6. The Macroscopic Available Energy Balance

Consider a system with boundary $\mathscr{S}$ moving at the velocity $\boldsymbol{v}_{\mathscr{S}}$ (which is not necessarily equal to $\boldsymbol{v}$). Upon integrating equation (17b) and applying the divergence theorems

$$\dot{\mathscr{I}} = \dot{Q} + \int_{\mathscr{S}} (T_0/T)\,(\boldsymbol{\epsilon}\cdot\boldsymbol{n})\,d\mathscr{S} - \int_{\mathscr{S}} [(p-p_0)\,\boldsymbol{v} + (\boldsymbol{\tau}\cdot\boldsymbol{v})]\cdot\boldsymbol{n}\,d\mathscr{S} - \Sigma\int_{\mathscr{S}} (B_j - \overline{B_{0j}})\,(\rho_j\,\boldsymbol{v}_j\cdot\boldsymbol{n})\,d\mathscr{S} - \int_{\mathscr{V}} \frac{\partial\,(\rho\,\hat{a})}{\partial t}\,d\mathscr{V} - \int_{\mathscr{S}} (\rho\,\hat{a}\,\boldsymbol{v}\cdot\boldsymbol{n})\,d\mathscr{S} \quad (c)$$

Now, by adding and subtracting the quantity

$$\left\{\int_{\mathscr{S}} \rho\,\hat{a}\,(\boldsymbol{v}_{\mathscr{S}}\cdot\boldsymbol{n})\,d\mathscr{S} + \int_{\mathscr{S}} [(p-p_0)\,\boldsymbol{v}_{\mathscr{S}} + (\boldsymbol{\tau}\cdot\boldsymbol{v}_{\mathscr{S}})]\cdot\boldsymbol{n}\,d\mathscr{S}\right\},$$

utilizing equation (5b) and the three-dimensional Leibniz theorem, and rearranging, the *macroscopic available energy balance* is obtained:

$$\dot{\mathscr{I}} = \underbrace{\dot{Q} + \int_{\mathscr{S}} (T_0/T)\,(\boldsymbol{\epsilon}\cdot\boldsymbol{n})\,d\mathscr{S}}_{(i)} \underbrace{- W + p_0\dot{\mathscr{V}}}_{(ii)} \underbrace{- \int_{\mathscr{S}} [\rho\,\hat{a}_f\,(\boldsymbol{v}-\boldsymbol{v}_{\mathscr{S}})\cdot\boldsymbol{n}]\,d\mathscr{S}}_{(iii)} \underbrace{- \Sigma\int_{\mathscr{S}} (\overline{B_j} - \overline{B_{0j}})\,(\rho_j\,\boldsymbol{v}_j\cdot\boldsymbol{n})\,d\mathscr{S}}_{(iv)} \underbrace{- \hat{a}}_{(v)} \quad (18)$$

where, by definition,

$$\hat{a}_f = \hat{a} + \left(\frac{p}{\rho}\right) - \left(\frac{p_0}{\rho}\right) + \frac{\boldsymbol{\tau}\cdot(\boldsymbol{v}-\boldsymbol{v}_{\mathscr{S}})\cdot\boldsymbol{n}}{\rho\,(\boldsymbol{v}-\boldsymbol{v}_{\mathscr{S}})\cdot\boldsymbol{n}} = \hat{H} - T_0\,\hat{S} + \hat{K} + \hat{\Phi} + \frac{\boldsymbol{\tau}\cdot(\boldsymbol{v}-\boldsymbol{v}_{\mathscr{S}})\cdot\boldsymbol{n}}{\rho\,(\boldsymbol{v}-\boldsymbol{v}_{\mathscr{S}})\cdot\boldsymbol{n}} - (\hat{H}_0 - T_0\,\hat{S}_0) \quad (19)$$

Inspection of equation (18) for the reversible case ($\dot{\mathscr{I}} \equiv 0$) reveals that $\hat{a}_f$ is the increase of available energy as a result of bulk mass flow across the boundary of the system – *the availability of flow energy* – per unit mass.

The macroscopic available energy balance of equation (18) complements the macroscopic mass, momentum, energy and Bernoulli (mechanical energy) balances of Bird [2]*. Reiterating, physical significance can be laid to each group of terms in equation (18). The rate of available energy loss within the system equals the net available energy added to the system due to transfers across the system boundary of (i) heat, (ii) work, (iii) bulk mass flow and (iv) diffusion at the boundary, less (v) the actual rate of available energy increase within the system. Solutions to this equation, of course, depend upon the process and therefore present problems of varying complexity. For most practical problems various parts of the equation are negligible and simplified forms can be obtained. For a closed system, equation (18) (or equation 16a) becomes

$$\dot{\mathscr{I}} = \dot{Q} + \int_{\mathscr{S}} (T_0/T)\,(\boldsymbol{\epsilon}\cdot\boldsymbol{n})\,d\mathscr{S} - W + p_0\dot{\mathscr{V}} - \hat{a}\Big]_{\text{closed system}} \quad (20)$$

Integrating with respect to time

$$\Delta\mathscr{I} = \mathscr{I}(t+\Delta t) - \mathscr{I}(t) = \Delta Q + \int_t^{t+\Delta t}\int_{\mathscr{S}} (T_0/T)\,(\boldsymbol{\epsilon}\cdot\boldsymbol{n})\,d\mathscr{S}\,dt - \Delta W_u - \Delta a\Big]_{\text{closed system}} \quad (21)$$

For a steady-flow system with one flow stream and no diffusion, and such that the thermodynamic properties are constant across the

*The engineering Bernoulli balance, which was presented in a restricted form in Ref. [2], is generalized in Ref [7].

VOL. 16 1962

entrance and exit, equation (18) yields (upon dividing by the mass flow rate J)

$$\hat{\mathscr{I}} = \hat{Q} + (1/J)\int_{\mathscr{S}} (T_0/T)(\boldsymbol{\epsilon}\cdot\boldsymbol{n})\,d\mathscr{S} - \hat{W} - (\hat{a}_{f,\,\text{exit}} - \hat{a}_{f,\,\text{ent.}})\Big]_{\text{steady flow}} \quad (22)$$

in which $\hat{\mathscr{I}}$ is the loss of available energy within the system per unit of mass flow. For more than one flow stream

$$\hat{\mathscr{I}} = \hat{Q} + \int_{\mathscr{S}} (T_0/T)(\boldsymbol{\epsilon}\cdot\boldsymbol{n})\,d\mathscr{S} - \hat{W} + \Sigma J\,\hat{a}_f\Big]_{\text{steady flow multi-stream}} \quad (23)$$

The summation is over the flow boundaries of the system; J is the *net* mass flow *into* the system and $\hat{a}_f$ is the specific availability of flow energy, at the given flow boundary (the shear component of $\hat{a}_f$ is usually neglected).

7. Available-energy Loss, Entropy Production and Friction

The concepts of *loss of available energy*, *entropy production* and *friction* are obviously related – each reflects the Second Law of Thermodynamics. However, an accounting of available energy evaluates the actual loss of a process, and allows a rational efficiency to be defined for *any* process. Of course, evaluation of the entropy production yields information about the irreversibility of the system. But the difficulty of ascribing physical significance to entropy makes it hard to see what the actual loss from irreversibility is. It is possible, though, to relate the loss of available energy and the entropy production. For the general system of equation (18) the energy balance required by the First Law of Thermodynamics yields [2, 6]

$$\hat{Q} - \hat{W} - \int_{\mathscr{S}} \rho\,\hat{E}_f\,[(\boldsymbol{v} - \boldsymbol{v}_{\mathscr{S}})\cdot\boldsymbol{n}]\,d\mathscr{S} - \Sigma\int_{\mathscr{S}} H_j(\rho_j\,\boldsymbol{v}_j\cdot\boldsymbol{n})\,d\mathscr{S} - \hat{U} - \hat{K} - \hat{\Phi} = 0 \quad (24)$$

where $\hat{E}_f$ is the specific *flow energy*, given by

$$\hat{E}_f = \hat{H} + \frac{\boldsymbol{\tau}\cdot(\boldsymbol{v} - \boldsymbol{v}_{\mathscr{S}})\cdot\boldsymbol{n}}{\rho\,(\boldsymbol{v} - \boldsymbol{v}_{\mathscr{S}})\cdot\boldsymbol{n}} + \hat{K} + \hat{\Phi} \quad (25)$$

Upon substituting equation (24) into (18), then with equations (19), (25) and (1),

$$\begin{aligned}\hat{\mathscr{I}} &= \int_{\mathscr{S}} (T_0/T)(\boldsymbol{\epsilon}\cdot\boldsymbol{n})\,d\mathscr{S} + p_0\hat{v} \\ &\quad - \int_{\mathscr{S}} \rho\,(\hat{a}_f - \hat{E}_f)\,[(\boldsymbol{v} - \boldsymbol{v}_{\mathscr{S}})\cdot\boldsymbol{n}]\,d\mathscr{S} \\ &\quad - \Sigma\int_{\mathscr{S}} (B_j - H_j - B_{0j})(\rho_j\,\boldsymbol{v}_j\cdot\boldsymbol{n})\,d\mathscr{S} \\ &\quad - \hat{\boldsymbol{a}} + \hat{U} + \hat{K} + \hat{\Phi} \\ \hat{\mathscr{I}} &= \int_{\mathscr{S}} (T_0/T)(\boldsymbol{\epsilon}\cdot\boldsymbol{n})\,d\mathscr{S} + p_0\hat{v} \\ &\quad + T_0\int_{\mathscr{S}} \rho\,\hat{S}\,[(\boldsymbol{v} - \boldsymbol{v}_{\mathscr{S}})\cdot\boldsymbol{n}]\,d\mathscr{S} \\ &\quad + \int_{\mathscr{S}} \rho\,(\hat{H}_0 - T_0\,\hat{S}_0)\,[(\boldsymbol{v} - \boldsymbol{v}_{\mathscr{S}})\cdot\boldsymbol{n}]\,d\mathscr{S} \\ &\quad + T_0\,\Sigma\int_{\mathscr{S}} S_j\,\rho_j\,\boldsymbol{v}_j\cdot\boldsymbol{n}\,d\mathscr{S} \\ &\quad + \Sigma\int_{\mathscr{S}} B_{0j}\,\rho_j\,\boldsymbol{v}_j\cdot\boldsymbol{n}\,d\mathscr{S} - p_0\hat{v} \\ &\quad + T_0\,\hat{S} + (\hat{H}_0 - T_0\,\hat{S}_0) \end{aligned} \quad (f)$$

With equation (3)

$$\begin{aligned}\hat{B}_0 = \hat{H}_0 - T_0\,\hat{S}_0 &= -\Sigma\int_{\mathscr{S}} H_{0j}(-T_0\,S_{0j})\,\rho_j\,(\boldsymbol{u}_j - \boldsymbol{v}_{\mathscr{S}})\cdot\boldsymbol{n}\,d\mathscr{S} \\ &= -\Sigma\int_{\mathscr{S}} \rho_j\,(H_{0j} - T_0\,S_{0j})\,(\boldsymbol{v} - \boldsymbol{v}_{\mathscr{S}})\cdot\boldsymbol{n}\,d\mathscr{S} \\ &\quad - \Sigma\int_{\mathscr{S}} (H_{0j} - T_0\,S_{0j})\,(\rho_j\,\boldsymbol{v}_j\cdot\boldsymbol{n})\,d\mathscr{S}\end{aligned}$$

But it is a general characteristic of partial specific quantities [4] that $\Sigma\,\rho_j\,\bar{A}_j = \rho\,A$; hence

$$\hat{H}_0 - T_0\,\hat{S}_0 = -\int_{\mathscr{S}} \rho(\hat{H}_0 - T_0\,\hat{S}_0)(\boldsymbol{v} - \boldsymbol{v}_{\mathscr{S}})\cdot\boldsymbol{n}\,d\mathscr{S} - \Sigma\int_{\mathscr{S}} (H_{0j} - T_0\,S_{0j})\,(\rho_j\,\boldsymbol{v}_j\cdot\boldsymbol{n})\,d\mathscr{S} \quad (g)$$

Substituting equation (g) into (f)

$$\dot{\mathscr{I}} = T_0\Big[\dot{S} + \int_{\mathscr{S}} (1/T)\,(\boldsymbol{\epsilon}\cdot\boldsymbol{n})\,d\mathscr{S} + \int_{\mathscr{S}} \rho\,\hat{S}\big[(\boldsymbol{v}-\boldsymbol{v}_{\mathscr{S}})\cdot\boldsymbol{n}\big]\,d\mathscr{S} + \Sigma\int_{\mathscr{S}} \rho_j \hat{S}_j\,\boldsymbol{v}_j\cdot\boldsymbol{n}\,d\mathscr{S}\Big] \quad (26)$$

This is the general macroscopic equation relating the loss of available energy to the entropy production. Thus, the loss rate equals the entropy production (the net entropy increase of the system $\dot{S}$ minus the net entropy flow into the system accompanying heat and mass flow) multiplied by the temperature of the surroundings, T_0.

Equation (26) can be reduced in the same manner as equation (18) for the closed system and particular steady-flow systems. These simplified forms, along with equations (21) and (22) can be found in the texts of Smith and Van Ness [8] Keenan [3], and Obert [9], with examples which illustrate their utility. Obert [10, 9] applies the First Law to non-steady problems; with the equations presented here an availability accounting may be made on such problems. For the isolated (or closed adiabatic) system

$$\dot{\mathscr{I}} = -\dot{\mathscr{A}} = T_0\,\dot{S}\big]_{\text{isolated system}} \quad (27)$$

Thus, for a reversible process $\dot{\mathscr{I}} = 0$, and for an irreversible process $\dot{\mathscr{I}} > 0$.

It is also of interest to obtain differential expressions relating the local loss of available energy and the local entropy production. Apply equation (26) to any system whose boundary travels with the local mass-average velocity; then, with equation (A.3) (Appendix), with the divergence theorem and letting the size of the arbitrary system approach zero about the point (x, y, z)

$$\rho\dot{i}\,(x,y,z,t) = T_0\Big[\rho\frac{D\hat{S}}{Dt} + \nabla\cdot\Big(\frac{\boldsymbol{\epsilon}}{T}\Big) + \Sigma(\nabla\cdot\rho_j\hat{S}_j\,\boldsymbol{v}_j)\Big] \quad (28)$$

Then, with equation (A.2)

$$\rho\dot{i} = T_0\Big[\frac{\partial(\rho\,\hat{S})}{\partial t} + \nabla\cdot\rho\,\hat{S}\,\boldsymbol{v} + \Sigma\,\nabla\cdot\rho_j\hat{S}_j\,\boldsymbol{v}_j + \nabla\cdot\Big(\frac{\boldsymbol{\epsilon}}{T}\Big)\Big] \quad (29)$$

Hirschfelder *et al.* [6] shows that the quantity in brackets in equations (28) and (29) is equal to the local volume rate of entropy production at (x, y, z) and t. Thus equation (28) or (29) shows that $\rho\dot{i}$, the volume loss rate of available energy, equals T_0 times the local entropy production per unit volume and unit time:

$$\rho\dot{i} = T_0\,g \quad (30)$$

This latter quantity, g, can be analysed into the contributions from each cause of irreversibility [6]. On the other hand, without the derivation leading to equations (28) and (29), it is not obvious that the available energy loss is equal to the product of entropy production and the dead-state temperature.

The friction of a process is equal to the difference between the work of a reversible process which traverses the same series of states as the real process, and the work of the actual process [7, 9]. It can be proved [7] that the local volume rate of friction is equal to the product of the entropy production and the *local* temperature:

$$\rho f = Tg \quad (31)$$

Equations (30) and (31) show that the friction, a *degradation*, is not identical to the available energy loss; the portion $f\big[1-(T_0/T)\big]$ is available (hence friction is often termed a "heating effect"). So, if $T > T_0$, the frictional degradation is not a complete loss of available energy; part could be regained as work. This point is illustrated by the following example: Consider the process of piping hot water from a large reservoir at 650 °R to an elevation of 10 ft. Let $p_0 = p_1 = p_2 = 14{\cdot}7$ p.s.i.a., $T_1 = T_2 = 650$ °R, $T_0 = 540$ °R, $v_2 = 10$ ft/sec, $\hat{W} = -23{\cdot}1$ ft lb_f/lb_m. From the energy equation the heat removed is

$$-\hat{Q} = -\hat{W} - \Delta\hat{K} - \Delta\hat{\Phi} = 12\text{ ft lb}_f/\text{lb}_m.$$

The entropy production in this isothermal steady system is equal to the net entropy flow from the system:

$$-\hat{Q}/T + \Delta\hat{S} = -\hat{Q}/T = 0{\cdot}0185\,\text{ft-lb}_f/(\text{lb}_m)(^\circ\text{R}).$$

The viscous friction can be evaluated [7] with the engineering Bernoulli equation presented by Bird [2. 5]:

$$\hat{E}_v = -\Delta \hat{K} - \Delta \hat{\Phi} - \hat{W} = 12 \text{ ft lb}_f/\text{lb}_m.$$

The available energy loss can be calculated with equation (26):

$$\hat{\mathscr{J}}_v = \hat{\mathscr{J}} = -T_0 [\hat{Q}/T] = 10 \text{ ft lb}_f/\text{lb}_m.$$

The difference between $\hat{E}_v$ and $\hat{\mathscr{J}}_v$ is equal to the useful work obtainable if the heat given off at $T = 650$ °R were reversibly taken to T_0 through a Carnot cycle. As a second example one could consider the same physical problem, but for adiabatic rather than isothermal flow; in this case the exit temperature would be greater than 650 °R, and the quantity $(\hat{E}_v - \hat{\mathscr{J}}_v)$ equals the useful work obtainable if the fluid at the exit state were reversibly brought to the thermostatic state [9] at p_1 and T_1, while its kinetic and potential energies are maintained equal to those at the exit.

Some authors have called the quantity E_v "the mechanical energy 'lost' by conversion to thermal energy (i.e.; energy degradation by viscous dissipation)." They also refer to E_v as "the *unrecoverable* loss in mechanical energy." These statements might perplex the student because *it is* possible to recover mechanical energy, of maximum amount $(\hat{E}_v - \hat{\mathscr{J}}_v)$ (and note the consequences when $T < T_0$).

Of course, in the actual sequence of processes advantage might not be taken of the availability $(\hat{E}_v - \hat{\mathscr{J}}_v)$. In this case the friction of the system is equal to the loss of available energy *within* the system plus that lost *outside* the system by not utilizing $(\hat{E}_v - \hat{\mathscr{J}}_v)$.

Paraphrasing the words of OBERT [9]: The true test of how efficient a system is operating is to examine how close reversibility is approached; efficiencies based on the First Law give no indication of this. "A better gauge of efficiency (one which indicates the approach to reversibility) is to measure the ratio of the available energy changes which occur . . . because of a . . . . . process." Thus, a criterion of performance (quite independent of First Law efficiencies) is called the *effectiveness** and defined

$$\mathscr{E} \equiv \frac{|\text{increase in available energy}|}{|\text{decrease in available energy}|} \tag{32}$$

The effectiveness is useful for any process. In the above example of the isothermal hot water pumping system

$$\mathscr{E} = \frac{-\hat{Q}(T_0/T) + \Delta \hat{a}_f}{|\hat{W}|}.$$

For the adiabatic system

$$\mathscr{E} = \Delta \hat{a}_f/|\hat{W}| = (|\hat{W}| - \hat{\mathscr{J}}_v)/|\hat{W}|.$$

For a heat exchanger WEBER and YORK [1] proposed the effectiveness

$$\mathscr{E} = \frac{J\ \Delta \hat{a}_f]_{\text{heated stream}}}{J\ \Delta \hat{a}_f]_{\text{heating stream}}}$$

Thus, even though friction, entropy production and loss of available energy are all valid measures of the imperfection of a process, it appears that available energy has advantages in certain respects:

(i) The friction does not account for the "reheat" effect. It does not give the system credit for the availability of the thermal energy obtained by degradation of the more valuable forms of energy; also, even if advantage is not taken of the "reheat" the friction does not properly locate the actual loss.

(ii) The entropy production does properly locate irreversibilities, but it is difficult to ascribe physical significance to the entropy.

(iii) The concept of available energy allows a rational efficiency, applicable to all processes, to be defined. It is for these reasons that an available energy balance (equation 18) is advocated to complement the macroscopic balances of BIRD.

Acknowledgement—The help and suggestions of Professor EDWARD F. OBERT are gratefully acknowledged. During the greater part of this work financial support was given by the General Electric Foundation, although it was completed under a National Science Foundation fellowship.

APPENDIX

The Stokes derivative of the function $\hat{A} = \hat{A}(x, y, z, t)$ is defined

$$\frac{D\hat{A}}{Dt} = \frac{\partial \hat{A}}{\partial t}\bigg)_{x,y,z} + \mathbf{v} \cdot \nabla \hat{A} \tag{A.1}$$

*Name suggested by KEENAN.

This is the derivative of the function

$$\tilde{A}(t) = \tilde{A}(x(t), y(t), z(t), t)$$

for the case when $x(t)$, $y(t)$, and $z(t)$ are the location of an observer travelling with the local mass-average velocity.

With the equation of continuity $\partial\rho/\partial t + \nabla \cdot \rho\boldsymbol{v} = 0$

$$\rho \frac{D\tilde{A}}{Dt} = \rho \frac{\partial \tilde{A}}{\partial t} + \tilde{A} \frac{\partial \rho}{\partial t} + \tilde{A} \nabla \cdot \rho\boldsymbol{v} + \rho\boldsymbol{v} \cdot \nabla \tilde{A} =$$

$$= \frac{\partial (\rho \tilde{A})}{\partial t} + \nabla \cdot \rho \tilde{A} v \qquad \text{(A.2)}$$

Integrating equation (A.2) over the volume of a system whose boundary moves with $\boldsymbol{v}_{\mathscr{S}} = \boldsymbol{v}$, then applying the divergence theorem and the three-dimensional Leibnitz theorem

$$\int_{\mathscr{V}} \rho \frac{D\tilde{A}}{Dt} d\mathscr{V} = \int_{\mathscr{V}} \frac{\partial (\rho \tilde{A})}{\partial t} d\mathscr{V} + \int_{\mathscr{S}} \rho \tilde{A}\, \boldsymbol{v} \cdot \boldsymbol{n}\, d\mathscr{S} =$$

$$= \frac{d}{dt} \int \rho \tilde{A}\, d\mathscr{V} \Big]_{\boldsymbol{v}_{\mathscr{S}} = \boldsymbol{v}} \qquad \text{(A.3)}$$

Notation

$\boldsymbol{a}(t)$ = available energy within system at time t

$\hat{\boldsymbol{a}}(x, y, z, t)$ = specific available energy at the point (x, y, z) and time t

$a_f(x, y, z, t)$ = specific availability of flow energy

$a_w(t)$ = availability of work transferred across system boundary from time zero to t

$a_Q(t)$ = availability of heat transferred across system boundary from time zero to t

$\boldsymbol{a}_d(x, y, z, t)$ = availability of diffusional energy flux (x, y, z) and t

$\boldsymbol{a}_\epsilon(x, y, z, t)$ = availability of heat flux at (x, y, z) and t

$B(t) = H - T_0 S$

$\hat{B}(x, y, z, t) = \hat{H} - T_0 \hat{S}$

$E(t) = U + K + \Phi$ = total energy contained in system at time t

$\hat{E}(x, y, z, t) = \hat{U} + \hat{K} + \hat{\Phi}$

$\hat{E}_f(x, y, z, t)$ = specific flow energy at the point (x, y, z) at time t

$E_v(t)$ = viscous friction within system from time zero

$\hat{E}_v$ = viscous friction rate per unit mass flow through steady system

$\boldsymbol{e}_d(x, y, z, t)$ = diffusional energy flux at (x, y, z, t)

$\mathscr{E}$ = effectiveness

$\hat{\boldsymbol{F}}_j(x, y, z, t)$ = body force on jth consitituent

$\mathscr{F}(t)$ = total friction within system from time zero

$f(x, y, z, t)$ = local friction rate (per unit mass)

$g(x, y, z, t)$ = local rate of entropy production per unit volume and unit time

$H(t)$ = enthalpy contained in system

$\hat{H}(x, y, z, t)$ = specific enthalpy

$\mathscr{I}(t)$ = loss of available energy within system from time zero

$\hat{\mathscr{I}}_v$ = viscous loss of available energy rate per unit of mass flow through a steady system

$\dot{\mathfrak{i}}(x, y, z, t)$ = local rate of available energy loss (per unit mass)

J = mass flow rate for steady system

$K(t)$ = kinetic energy contained in system

$\hat{K}(x, y, z, t)$ = specific kinetic energy

$M(t)$ = total mass contained in system

$\boldsymbol{n}$ = unit vector normal to surface of system (pointing outward)

$p(x, y, z, t)$ = pressure

$Q(t)$ = heat transferred across system boundary from time zero

$S(t)$ = entropy contained in system

$\hat{S}(x, y, z, t)$ = specific entropy

$\boldsymbol{s}_d(x, y, z, t)$ = diffusional entropy flux

$\mathscr{S}$ = surface of system

$T(x, y, z, t)$ = temperature

t = time

$U(t)$ = internal energy contained in system

$\hat{U}(x, y, z, t)$ = specific internal energy

$\boldsymbol{u}_j(x, y, z, t)$ = velocity of j-th constituent

$\boldsymbol{v}(x, y, z, t)$ = Mass-average velocity $= (1/\rho)\, \Sigma \rho_j \boldsymbol{u}_j$

$\boldsymbol{v}_j(x, y, z, t)$ = diffusion velocity $= \boldsymbol{u}_j - \boldsymbol{v}$

$\boldsymbol{v}_{\mathscr{S}}(x, y, z, t)$ = velocity of system boundary (surface)

$\mathscr{V}(t)$ = volume of system

$W(t)$ = work transferred across system boundary from time zero

$\dot{W}$ = work rate per unit mass flow through steady system

$W_p(t)$ = work done by pressure forces

$W_u(t)$ = useful work

$W_v(t)$ = work done by shear stresses

x, y, z = fixed space co-ordinates

$\epsilon(x, y, z, t)$ = thermal energy flux

$\Lambda(t)$ = general quantity contained in system

$\tilde{\Lambda}(x, y, z, t)$ = general quantity at (x, y, z, t)

$\rho(x, y, z, t)$ = density $= \Sigma \rho_j$

$\rho_j(x, y, z, t)$ = density of j-th constituent

$\boldsymbol{\tau}(x, y, z, t)$ = shear stress tensor

$\Phi(t)$ = potential energy contained in system

$\hat{\Phi}(x, y, z, t)$ = specific potential energy

Subscripts

j = value for j-th constituent

0 = value at dead state

d = quantity associated with diffusion

rev = reversible system

Marks above symbols

$\overline{\quad}$ = partial specific quantity

$\cdot$ = derivative with respect to time

VOL. 16 1962

References

[1] Weber H. C. and York R. *Trans. Amer. Inst. Chem. Engrs.* 1938 **34** 569.

[2] Bird R. B. *Chem. Engng. Sci.* 1957 **6** 123.

[3] Keenan J. H. *Thermodynamics* p. 290 John Wiley, New York 1941.

[4] Dodge B. F. *Chemical Engineering Thermodynamics.* pp. 75, 105. McGraw-Hill, New York 1944.

[5] Bird R. B., Stewart W. E. and Lightfoot E. N. *Transport Phenomena* pp. 405–6. John Wiley, New York 1960.

[6] Hirschfelder J. O., Curtiss C. F. and Bird R. B. *Molecular Theory of Gases and Liquids*, Section 11.1. John Wiley, New York 1954.

[7] Gaggioli R. A. *Chem. Engng. Sci.* 1961 **13** 167.

[8] Smith J. M. and Van Ness H. C. *Introduction to Chemical Engineering Thermodynamics.* Chap. 11. McGraw-Hill, New York 1959.

[9] Obert E. F. *Concepts of Thermodynamics* pp. 439–440, 27–28, 406–409. McGraw-Hill, New York 1960.

[10] Obert E. F. *Thermodynamics.* pp. 302–307. McGraw-Hill, New York 1948.

VOL
16
196

Chemical Engineering Science, 1961, Vol. 16, pp. 97 to 104. Pergamon Press Ltd., London. Printed in Great Britain.

Approximations to residence time distributions in mixing systems and some applications thereof

R. M. DeBaun and S. Katz
American Cyanamid Company, New York, U.S.A.

(*Received* 29 *December* 1960)

Abstract—Residence time distributions for a class of mixing systems are approximated in terms of the probability distributions of the x^2 statistics. The x^2 approximation is used to solve certain problems of transient analysis, and of the smoothing of random inlet concentration fluctuations. Some of these results are related to various design criteria.

Résumé—Les distributions de temps de séjour pour certains systèmes mélangeurs suivent approximativement la loi statistique du x^2. L'approximation du x^2 est utilisée pour résoudre certains problèmes d'analyse transitoire et de l'aténuation des fluctuations aléatoires de concentrations à l'entrée. Certains de ces résultats sont très voisins de critères employés dans des problèmes variés.

Zusammenfassung—Die Verweilzeitverteilung für eine Klasse von Mischsystemen werden angenähert ausgedrückt durch Wahrscheinlichkeitsverteilungen der x^2-Statistik. Die x^2-Wahrscheinlichkeit wird benutzt, um gewisse Probleme der Übergangsanalyse zu lösen und um Schwankungen der Zulaufkonzentration auszugleichen. Einige dieser Ergebnisse werden mit Kriterien der Auslegung in Beziehung gesetzt.

1. Introduction

Residence time distributions for more or less complicated mixing systems are the subject of continuing study, both experimental and theoretical [1–5]. They are, of course, widely used, although on somewhat equivocal grounds [6], for analysing the behaviour of reactor systems. This apart, however, they have an unambiguous place in studying the time dependent performance of mixing systems. Indeed, the differential residence time distribution is just the response of the system to an infinitely sharp spike of tracer of unit intensity (a Dirac delta function [7]) in the inlet stream.

The use of the residence time distribution in investigations of the strictly transient behaviour of a mixing system is well known. Thus the engineer in studying a purge cycle can determine the rate of approach of the system to a new steady state from the cumulative distribution of residence times. In investigating the reaction of the system to a momentary disturbance in one of its inputs he can describe the spreading-out in time of this momentary disturbance in terms of the differential distribution of residence times.

The use of residence time distributions in working out the behaviour of various systems from the kinetic point of view has also been exemplified [8].

Perhaps not so familiar is the use of the residence time distribution in a solution of design problems which involve the smoothing characteristics of mixing tanks. Here the designer, by anticipating the statistical structure of the inlet disturbance to be smoothed, can proceed directly to a knowledge of the statistics of the outlet stream in terms of the residence time distribution of the mixing system.

The present paper aims at presenting unified engineering methods of solution to both these broad classes of problems, based on a standard approximation to the residence time distribution of quite general mixing systems. This standard distribution is that of x^2 which is extensively tabulated. Section II below describes the x^2 distribution, in the form in which it will be used here. Section III gives the mathematical form of the residence time distribution for perfect mixers and for a one-dimensional diffusive system. Section IV shows how the distribution of residence times in cascades of the simple mixers considered in Section III may be approximated

by x^2. Section V shows how an empirical distribution such as might be obtained from a tracer experiment may be approximated by a x^2 distribution. Section VI discusses questions of transient analysis of mixing systems in terms of the x^2 distribution, and presents design criteria for analysing the response to a sharp momentary disturbance (delta function) and to a step disturbance. Section VII gives an approximate solution in terms of the x^2 distribution to the problem of smoothing random concentration fluctuations where the inlet disturbance is taken to be a Markov process.

II. The x^2 Distribution

The random variable ${x_f}^2$ (f degrees of freedom) is defined as the sum of the squares of f independent Gaussian random variables, each with zero mean and unit variance. We shall be concerned here with multiples of x^2, which we take in the form $\frac{1}{2}\,\theta\,{x_{2n}}^2$. In what follows, $\frac{1}{2}\,\theta\,{x_{2n}}^2$ will be interpreted as the residence time in a cascade of n stirred vessels, each of nominal residence time θ. This random variable has the probability density

$$K(t) = \frac{(t/\theta)^{n-1}\exp(-t/\theta)}{(n-1)!\,\theta}, \quad t > 0 \qquad (1)$$

i.e.

$$\text{Prob.}\left\{t < \frac{\theta}{2}\,{x_{2n}}^2 < t + dt\right\} = K(t), \quad t > 0$$

Since $K(t)$ is a probability distribution its integral over-all is unity

$$\int_0^\infty K(t)\,dt = 1$$

The mean and variance of $\frac{1}{2}\,\theta\,{x_{2n}}^2$ may be computed directly from its distribution

$$\text{mean} = \int_0^\infty t\,K(t)\,dt = n\theta \qquad (2)$$

$$\text{variance} = \int_0^\infty (t - n\theta)^2\,K(t)\,dt = n\theta^2 \qquad (3)$$

as well as its (complex) moment generating function (Fourier transformation)

$$L(\omega) = \int_0^\infty \exp(-i\omega t)\,K(t)\,dt = \frac{1}{(1 + i\,\theta\omega)^n} \qquad (4)$$

The probability density $K(t)$ can, of course, be readily calculated with the help of standard tables of the elementary functions. Its indefinite integral, the cumulative distribution function, is tabulated in most statistical texts. Perhaps the most extensive tables may be found in [9] which tabulates

$$Q(x^2/\nu) = \frac{2^{-\nu/2}}{(\nu/2 - 1)!}\int_{x^2}^\infty \exp(-x/2)\,x(\nu/2 - 1)\,dx \qquad (5)$$

and in [10] which tabulates

$$I(u, p) = \frac{1}{p!}\int_0^{u\sqrt{(p+1)}} \exp(-v)\,v^p\,dv \qquad (6)$$

In terms of these quantities

$$\int_x^\infty K(t)\,dt = Q\frac{(2x/\theta)}{2n} \qquad (7)$$

$$= 1 - I\left(\frac{x}{\theta\sqrt{n}}, n - 1\right)$$

$$= 1 - \int_0^x K(t)\,dt$$

These relations may be found helpful in using the cited tables.

III. Residence Time Distributions for Cascades of Simple Mixers

In preparation for assembling the residence time distribution of a cascade we begin by recapitulating the development of the residence time distribution for a single perfect mixer and for a one-dimensional diffuser.

Suppose a perfectly stirred vessel of volume V ft³ is continuously fed and depleted by a stream of Q ft³/sec. At time $t = 0$ (sec) imagine we charge the inlet stream with a sharp pulse of tracer of unit intensity [a Dirac delta function $\delta(t)$]. Then $K(t)$, the tracer concentration as a function

of time in the vessel and in the effluent, is determined by the differential material balance

$$V\frac{dK}{dt} = Q\left[\delta(t) - K\right];\quad K\Big|_{t=0} = 0$$

The effluent concentration $K(t)$ is just the residence time distribution in the mixer. Its (complex) moment generating function may be determined by applying transformation methods to the differential equation above, and is found to be in the form (4) with $n = 1$, where $\theta = V/Q$ is the nominal residence time. The residence time is accordingly distributed just as $\frac{1}{2}\theta x^2_2$, which is to say that it has the familiar exponential form $1/\theta \exp(-t/\theta)$ corresponding to (1) with $n = 1$. The mean residence time is just the nominal residence time θ, and the variance of the residence times is θ^2.

Consider now a one-dimensional (longitudinal) diffusive system, with longitudinal co-ordinate x (ft) measured from $x = 0$ at the inlet to $x = H$ at the outlet. Let the vessel have cross-sectional area A ft^2. Let the process gas (assumed incompressible) be fed at Q ft^3/sec, so that it has superficial velocity $V = Q/A$ ft/sec. Let the diffusivity of the system be D ft^2/sec. At time $t = 0$ (sec), charge the inlet stream with a delta function of tracer. Then $c(x, t)$, the tracer concentration in the vessel, is determined by the differential material balance.

$$A\frac{\partial c}{\partial t} = DA\frac{\partial^2 c}{\partial x^2} - Q\frac{\delta c}{\partial x} \qquad 0 < x < H \qquad (8)$$

$$c\Big|_{t=0} = 0$$

with the appropriate boundary conditions (9) specifying continuity at the outlet and no diffusion outside the system.

$$Q\,\delta(t) = Qc - DA\frac{\partial c}{\partial x}, \quad x = 0 \qquad (9)$$

$$\frac{\partial c}{\partial x} = 0, \qquad x = H$$

The effluent concentration, $C(L, t)$, i.e. $K(t)$, is just the residence time distribution in the system. The complex moment generating function $L(\omega)$ of the distribution $K(t)$ may as before be determined by applying transformation methods to the differential equations above and is found to be

$$(L\omega) = \frac{\exp(P/2)}{\cosh R(\omega) + (\frac{1}{2}P + i\theta)(\sinh R(\omega)/R(\omega))} \qquad (10)$$

where

$$R(\omega) = \sqrt{\left[\left(\frac{P}{2}\right)^2 + iP\theta\,\omega\right]} \qquad (11)$$

with $\theta = H/V$, the nominal residence time, and $P = HV/D$, a modified Peclet number. By expanding the moment generating function in powers of ω, one may show that the distribution has mean θ, variance $S\theta^2$ where S is given by (12).

$$S = \frac{\exp(-P) - (1 - P)}{P^2/2} \qquad (12)$$

The quantity S in (12) decreases steadily from $S = 1$ for $P = 0$ (perfect mixing) to $S = 0$ for infinite P (plug flow). Although the residence time in the diffuser is not distributed like a multiple of x^2, it does reduce to $\frac{1}{2}\theta x^2_2$ in the limiting case $P = 0$. And it will appear in what follows that it may in general be approximated by $\frac{1}{2}S\theta x^2_{2/S}$, which may be interpreted as the residence time in a cascade of $1/S$ perfect mixers each of mean residence time $S\theta$.

It is clear from the arrangement of the material balances in the two simple mixers foregoing, that if a number of these mixers are assembled in a cascade, each feeding the next, the moment generating function for the residence time distribution of the cascade will be the product of the moment generating functions for the residence time distributions of the individual stages. That is, if the individual residence time distributions are

$$K_1(t), \quad K_2(t), \quad K_3(t)$$

with the moment generating functions

$$L_1(\omega), \quad L_2(\omega), \quad L_3(\omega)$$

then the moment generating function for the cascade will be

$$L(\omega) = L_1(\omega) \times L_2(\omega) \times L_3(\omega)$$

and the distribution function for the cascade will be

$$K(t) = K_1(t)^* K_2(t)^* K_3(t)^*$$

where the symbol * denotes the convolution product;

$$K_1(t)^* K_2(t) = \int_0^t K(x) K_2(t-x)\,dx, \text{ etc.}; t > 0$$

These expressions for the residence time distribution in a cascade take a particularly simple form in the case of n perfect mixers each of the same nominal residence time θ. In this case, the residence time in the cascade is just $\frac{1}{2}\theta x_{2n}^2$ with the distribution (1). It should be noted that cascades of mixers of different residence times no longer have residence times distributed exactly like multiples of x^2.

The convolution relation given here is the mathematical expression of the fact, which is clear on physical grounds, that in computing the residence time distribution of a cascade, the residence times of the individual stages add like independent random variables. The most important consequence of this from our present point of view is that in combining into a summary distribution the residence time distributions in a cascade, not only do the means of the residence time distributions of the individual stages add, but also their variances. Thus, in a cascade of one-dimensional diffusers, with stage means $\theta_1, \theta_2, \ldots$ and stage variances $S_1\theta_1^2$, $S_2\theta_2^2$, it follows that the cascade mean is $\theta_1 + \theta_2 + \ldots$ and the cascade variance is $S_1\theta_1^2 + S_2\theta_2^2 + \ldots$. It is clear that some or all of the stages can be taken to be perfect mixers rather than diffusers by taking the corresponding S parameters equal to unity.

IV. Approximation of Analytical Distributions by Multiples of x^2

What we propose here is to approximate a cascade residence time distribution by the distribution of $\frac{1}{2}\theta x_{2n}^2$, chosing θ and n to make the mean and variance of the two distributions agree. Since the mean of $\frac{1}{2}\theta x_{2n}^2$ is $n\theta$ and its variance is $n\theta^2$ (2, 3) this agreement requires taking

$$\theta = \frac{S_1\theta_1^2 + S_2\theta_2 + \ldots}{\theta_1 + \theta_2 + \ldots} = \frac{\text{cascade variance}}{\text{cascade mean}} \qquad (13)$$

$$n = \frac{(\theta_1 + \theta_2 + \ldots)^2}{S_1\theta_1^2 + S_2\theta_2^2 + \ldots} = \frac{(\text{cascade mean})^2}{\text{cascade variance}} \qquad (14)$$

This kind of approximation is very familiar in mathematical statistics, and is continually used in a variety of contexts (cf., for example [11]).

Physically, we may think of the approximation to the distribution of the cascade residence time by $\frac{1}{2}\theta x_{2n}^2$ as the replacing of the cascade by an approximately equivalent cascade of n perfect mixers, each of nominal residence time θ (n need not be integral). As far as perfect mixers go ($S_1 = S_2 = \ldots = 1$), the approximation will be very good as long as there are only slight disparities among the several stage residence times, and again very good if there are great disparities due to a number of small stages in the cascade with a number of approximately equal much larger stages. Some intuitive idea as to how good the approximation is likely to be in general can be gained by consideration of intermediate cases like the following.

Consider the system of mixers with the following nominal residence times: $\theta_1 = 1{\cdot}7202$, $\theta_2 = 9{\cdot}5183$, $\theta_3 = 0{\cdot}8333$, $\theta_4 = 0{\cdot}1667$. The exact residence time distribution of the system may be computed following Section III, as the convolution of the familiar exponential distributions for the individual stages, and turns out to be

$$K(t) = \sum_{i=1}^{4} \alpha_i \exp(-\beta_i t); \quad t > 0 \qquad (15)$$

with coefficients and powers as in Table 1.

Table 1. Parameters of an exact residence time distribution

i	α_i	β_i
1	− 0·2754	0·5813
2	0·1431	0·1051
3	0·1352	1·2000
4	− 0·0029	6·0000

VOL. 16 1962

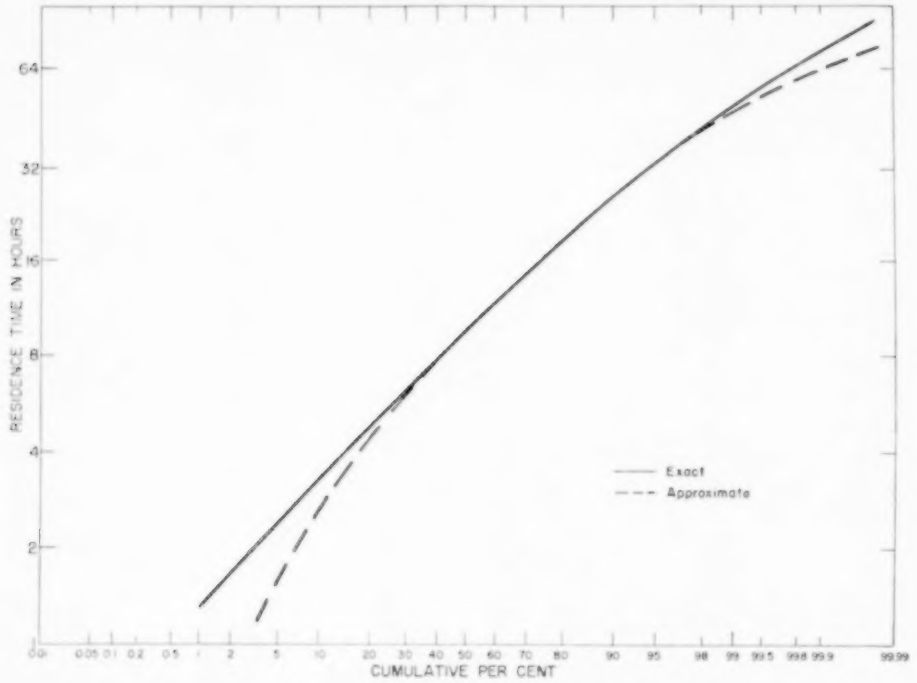

FIG. 1. Comparison of exact residence time distribution with the approximation using x^2.

Substitution in (13, 14) gives (15) approximately by $3{\cdot}85\ x^2_{3{\cdot}18}$. That is, we may loosely say that our system corresponds to 1·59 perfect mixers with residence times of 7·70 hr each. In Fig. 1 we compare the two cumulative distributions by plotting them on logarithmic probability paper.

V. Approximation of an Empirical Residence Time Distribution by the x^2 Distribution

Fig. 2 shows an experimental observation of a residence time distribution. The points were obtained by observing the recovery on the output side of a system of "spikes" of tracer dropped into the input side of the system.

Also in the Fig. are shown the percentiles of x^2 distribution for three and four degrees of freedom. (The x^2 distributions have been divided through by the numbers of degrees of freedom in order to facilitate the graphical comparison). As can be seen, x^2 with three degrees of freedom (a multiplicative constant aside) will give an excellent fit to the observed cumulative distribution.

A more systematic approximation scheme would be to estimate the mean μ and variance σ^2 of the observed sample distribution by some appropriate numerical or graphical method, and then to take the n and θ of (1) as

$$\theta = \sigma^2/\mu$$
$$n = \mu^2/\sigma^2 \qquad (16)$$

so as to satisfy the relations (2) and (3).

IV. Transient Analysis

If we consider a mixing system whose residence time distribution we approximate by that of $\frac{1}{2}\theta\ x^2_{2n}$, then as time progresses inlet concentration $c\,(t)$ is related to outlet concentration $c'\,(t)$ by

$$c'\,(t) = \int_0^\infty K\,(x)\,c\,(t-x)\,dx \qquad (17)$$

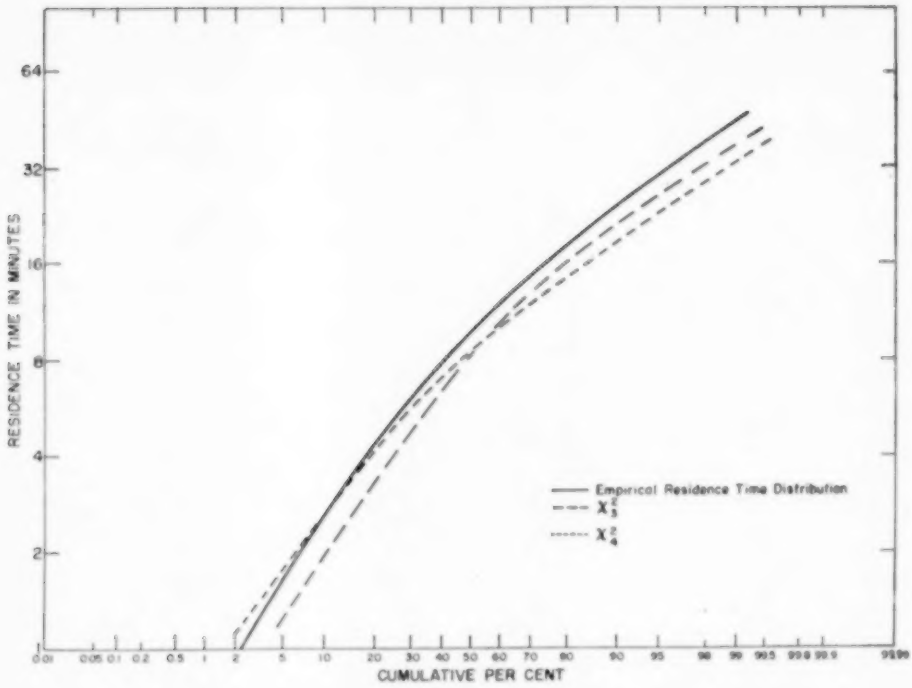

FIG. 2. Comparison of an experimentally determined residence time distribution with members of the x^2_n family of distributions.

where $K(x)$ is given by (1). Since $\int_0^\infty K(x)\,dx = 1$, a steady value of c will lead as it should to the same steady value of c', so that the c and c' in (17) can just as well be taken to denote the departure of the inlet and outlet concentrations from their steady states.

If the input disturbance is a sharp "spike," the output, which is exactly the differential residence time distribution, illustrates the spreading-out and dissipation in time of a momentary disturbance in the input. In this case,

$$c(t) = c_0\,\delta(t)$$

$$c'(t) = c_0\,K(t) \tag{18}$$

Or, if the input suddenly changes to a new level, the output, which is exactly the cumulative residence time distribution, illustrates the approach to a new steady state. In this case,

$$\begin{aligned} c(t) = c'(t) &= 0 \quad ; t < 0 \\ c(t) &= c_0 \quad ; t > 0 \\ c'(t) &= c_0 \int_0^t K(x)\,dx; \quad t > 0 \end{aligned} \tag{19}$$

As noted earlier, any particular case of (18) can readily be computed from standard tables of the elementary functions, and of (19) from the tables [9, 10] by way of the relations (7). Typical curves of this kind appear in Figs. 2 and 3 of [5], and are accordingly not reproduced here.

VII. Smoothing of Random Concentration Fluctuations

This section is given over to the development of working approximations to the exact expressions of (7) for the smoothing of random concentration fluctuations on passage through mixing systems.

Consider a mixing system whose residence time distribution has mean μ and variance σ^2, such as might be made up, following Section VI, of a number of stages with

$$\left.\begin{aligned}&\text{stage means} = \theta_1,\ \theta_2,\ \dots\\&\text{stage variances} = S_1\theta^2{}_1,\ S_2\theta^2{}_2,\ \dots\end{aligned}\right\} \quad (20)$$

so that

$$\left.\begin{aligned}\mu &= \theta_1 + \theta_2 + \dots\\ \sigma^2 &= S_1\theta_1{}^2 + S_2\theta^2{}_2 + \dots\end{aligned}\right\} \quad (21)$$

Suppose it fed with a stream whose concentration fluctuation $c(t)$ describes a stationary noise in time. Then the outlet fluctuation $c'(t)$ is also stationary, and if $K(t)$ is the residence time distribution of the system, $c'(t)$ is given in terms of $c(t)$ by (17). As in Section VI, we may take $c(t)$ and $c'(t)$ to represent departures from operating steady state levels.

We characterize the noisy inlet fluctuation $c(t)$ by its covariance function $\rho_c(\tau)$, alternatively by its power spectrum, $S_c(\omega)$,

$$S_c(\omega) = \tfrac{1}{2}\pi\int_{-\infty}^{\infty}\rho_c(\tau)\exp(i\omega t)\,dt$$

and ask how its spectrum has been altered (and its variance reduced) by passage through the mixing system. The answer is that the outlet spectrum $S_{c'}(\omega)$ is

$$S_{c'}(\omega) = S_c(\omega)\left|L(\omega)\right|^2 \quad (22)$$

and that the outlet variance $\sigma^2{}_{c'}$ is

$$\sigma^2{}_{c'} = \int_{-\infty}^{\infty} S_c(\omega)\left|L(\omega)\right|^2 d\omega \quad (23)$$

where $L(\omega)$ is the moment generating function (in the sense of Section II) of the residence time distribution $K(t)$. This moment generating function is just the transfer function (strictly, frequency response function) of the mixing system. (The absolute values in (22) and (23) must be taken in the sense of complex arithmetic).

In order to develop an approximate working solution to the smoothing problem we take the inlet concentration fluctuation $c(t)$ in the frequently encountered form of a Markov process, with covariance function

$$\rho_c(\tau) = \sigma^2{}_c\exp(-|\tau|/h) \quad (24)$$

and spectrum

$$S_c(\omega) = \frac{h\sigma^2{}_c}{\pi}\,\frac{1}{1+h^2\omega^2} \quad (25)$$

In (24) and (25) h is the characteristic time constant of the inlet concentration fluctuation, and $\sigma^2{}_c$ is its variance.

Now, taking $n = 1$ in (4) shows that the $L(\omega)$ corresponding to a single mixer has

$$\left|L(\omega)\right|^2 = \frac{1}{1+\theta^2\omega^2}$$

from which it appears, following (22), that the spectral shape (25) can be thought of as arising in the outlet of a stirred tank of mean residence time h fed with a " white " concentration fluctuation having the (flat) spectrum $h\sigma^2{}_c/\pi$. Thus, the mixing system (20) fed with the Markov process (24 and 25) is equivalent to a mixing system with

$$\begin{aligned}&\text{stage means} = h,\ \theta_1,\ \theta_2,\ \dots\\&\text{stage variances} = h^2,\ S_1\theta^2{}_1,\ S_2\theta^2{}_2,\ \dots\end{aligned} \quad (26)$$

fed with a concentration fluctuation having the flat spectrum

$$S_c(\omega) = \frac{h\sigma^2{}_c}{\pi} \quad (27)$$

Following (21), the mixing system (26) has

$$\begin{aligned}\text{cascade mean} &= h + \mu = h + \theta_1 + \theta_2 + \dots\\ \text{cascade variance} &= h^2 + \sigma^2 = h^2 + S_1\theta^2{}_1\\ &\quad + S_2\theta^2{}_2 + \dots\end{aligned} \quad (28)$$

Following (13) and (14) we approximate the residence time of the mixing system (26) by $\frac{1}{2}\theta\,x^2{}_{2n}$, where, from (28),

$$\begin{aligned}\theta &= \frac{h^2+\sigma^2}{h+\mu} = \frac{h^2 + S_1\theta^2{}_1 + S_2\theta^2{}_2 + \dots}{h+\theta_1+\theta_2+\dots}\\ n &= \frac{(h+\mu)^2}{h^2+\sigma^2} = \frac{(h+\theta_1+\theta_2+\dots)^2}{h^2+S_1\theta^2{}_1+S_2\theta^2{}_2+\dots}\end{aligned} \quad (29)$$

The variance of the outlet concentration fluctuation c' can then be computed from (23) with the S_c of (27) and the L of (4):

$$\sigma^2_{c'} = \frac{h\sigma^2_c}{\pi} \int_{-\infty}^{\infty} \frac{1}{(1 + \theta^2\,\omega^2)^n}\, d\omega \qquad (30)$$

The integral in (30) can be evaluated to give

$$\frac{\sigma^2_{c'}}{\sigma^2_c} = \frac{h}{\theta}\,\frac{(2n-2)!}{2^{2n-2}\{(n-1)!\}^2} \qquad (31)$$

The formula (31) is the desired approximate expression for the reduction in the variance of a concentration fluctuation with covariance function (24) on passage through the mixing system (20). The quantities n and θ are given by (29). Should n not be an integer the factorials required can be found tabulated in [12]. The range of validity of the approximate expression (31) is in general that of the χ^2 approximation discussed in Section IV. If the cascade (20) is made up of perfect mixers ($S_1 = S_2 = \ldots = 1$) the approximation will be very good as long as there are only slight disparities among the quantities

$$h,\ \theta_1,\ \theta_2\ \ldots \qquad (32)$$

and again very good if there are a few approximately equal large values among the quantities (32) which dominate the rest. The general validity of (31) must of course rest on detailed case by case examination, but we have found it to give surprisingly good results in a number of practical contexts.

VOL. 16 1962

References

[1] Danckwerts P. V. *Chem. Engng. Sci.* 1953 **2** 1.
[2] Danckwerts P. V., Jenkins J. W. and Place G. *Chem. Engng. Sci.* 1954 **3** 26.
[3] Klinkenberg A. and Sjenitzer F. *Chem. Engng. Sci.* 1958 **5** 258.
[4] Kramers H. and Alberda G. *Chem. Engng. Sci.* 1953 **2** 173.
[5] McMullin R. B. and Weber M. *Trans. Amer. Inst. Chem. Engng.* 1935 **31** 409.
[6] Danckwerts P. V., in *Chemical Reaction Engineering*, p. 93, Pergamon Press, London, 1957.
[7] Friedman B. *Principles and Techniques of Applied Mathematics* p. 134. John Wiley, New York 1956.
[8] Singer E., Todd D. B. and Guinn V. P. *Industr. Engng. Chem.* 1957 **49** 11.
[9] Pearson E. S. and Hartley H. O. *Biometrika Tables for Statisticans.* Vol. 1, p. 122, Cambridge University Press 1956.
[10] Pearson K. *Tables of the Incomplete Gamma Function* Cambridge University Press, 1951 Reissue.
[11] Box G. E. P. *Ann. Math. Statist.* 1954 **25** 290.
[12] Jahnke E. and Emde F. *Tables of Functions with Formulae and Curves.* p. 9, Dover Publications 1945.

nem cal Engineering Science, 1961, Vol. 16, pp. 105 to 112 Pergamon Press Ltd., London. Printed in Great Britain.

Reaction kinetics in fluidized beds

L. Massimilla* and H. F. Johnstone

University of Illinois, Urbana, Illinois, U.S.A.

(*Received* 27 *September* 1960; *in revised form* 16 *January* 1961)

Abstract—The purpose of this study is the clarification and extension of information on the kinetics of reactions in fluidized beds and in baffled fluidized beds, especially the oxidation of ammonia in the presence of a catalyst. The column used was 4·5 in. diameter and 43 in. high. The catalyst was manganous–bismuth oxide on alumina spheres of 100–325 mesh. The quantity of catalyst used ranged from 2 kg to 6 kg. The gas rates ranged from 0·17 ft^3/min to 2 ft^3/min (SCFM).

The conflicting results obtained in previous experiments have been partially explained and they now appear to be in substantial agreement with the theories proposed by previous investigators.

The results obtained when using baffled beds show that the baffles improve the conversion from 10 per cent to 40 per cent over that obtained in non-baffled fluidized reactors.

Résumé—Le but de cette étude est d'étendre et de rendre plus claires, les informations sur la cinétique de réactions en lits fluidisés avec ou sans chicanes, et en particulier l'oxydation de l'ammoniac en présence d'un catalyseur. La colonne utilisée avait un diamètre de 4,5 pouces, et 43 pouces de hauteur. Le catalyseur était un oxyde de manganèse et de bismuth sur des sphères d'alumine sélectionnées par les tamis 100–325 mailles. La quantité de catalyseur était de l'ordre de 2 à 6 kg. Les vitesses de gaz s'échelonnaient de 0,17 ft^3/min à 2 ft^3/min.

Les résultats aberrants obtenus dans les expériences précédentes ont été partiellement expliqués et ils sont maintenant en assez bon accord avec les théories proposées par les expérimentateurs précédents.

Les résultats obtenus lorsque l'on utilisait des lits avec chicanes montrent que celles-ci améliorent la conversion de 10 à 40% par rapport à celle obtenue dans des réacteurs fluidisés sans chicane.

Zusammenfassung—Der Zweck dieser Arbeit ist die Klärung und Ausweitung der Kenntnisse über die Kinetik von Reaktionen in Wirbelschichten mit und ohne Einbauten, besonders über die katalytische Oxydation von Ammoniak. Die benutzte Säule hatte einen Durchmesser von 4,5 in. und eine Höhe von 43 in. Der Katalysator bestand aus Mangan-Wismut-Oxyd auf Aluminium-Oxyd-Kugeln (Maschenweite 100–325). Die Katalysatormenge betrug zwischen 2 und 6 kg. Die durchgesetzten Gasmengen lagen zwischen 0,17 und 2 ft^3/min (SCFM).

Die widersprechenden Ergebnisse aus früheren Versuchen konnten zum Teil erklärt werden und erscheinen nun in Übereinstimmung mit den Theorien früherer Autoren. Die in Wirbelschichten mit Einbauten erhaltenen Ergebnisse zeigen, dass die Einbauten den Umsatz von 10 bis 40% steigern gegenüber dem Umsatz ohne Einbauten.

Introduction

One of the methods of carrying out reactions between a gas and a solid is by use of a fluidized bed. The over-all reaction rate between a gas and a fluidized bed of solid particles depends in part on how thorough the contact is between the gas and the solid particles. Thus, if there are non-uniformities in the gas distribution in the form of bubbles and channels the reaction rate would be expected to be decreased. Toomey and Johnstone [1] have suggested that a fluidized bed be regarded as composed of two distinct phases, a continuous phase and a discontinuous phase. The continuous phase consists of uniformly

*Present address: Institute of Industrial Chemistry, University of Naples, Naples, Italy.

dispersed particles together with the gas supporting them. The discontinuous phase consists entirely of the gas bubbles. They propose that the discontinuous phase begins to form at gas rates slightly higher than the minimum gas rate required for fluidization. This model implies that the contact between the gas and the solid particles is not as good in a fluidized bed as it is in a fixed bed, but the possibilities of some reaction taking place in the discontinuous phase and transfer of gas at the phase boundaries are not excluded.

In addition to the ineffective distribution of gas in a fluidized bed Gilliland and Mason [2, 3] and Danckwerts *et al.* [4] point out that back-mixing of the gas stream may decrease the efficiency of a fluidized bed when the reaction order is greater than zero. The data of Shen [5] and Shen and Johnstone [6] on the rate of catalytic decomposition of nitrous oxide in a fluid catalyst bed, of Mathis and Watson [7] on the catalytic dealkylation of cumene and of Glass [8] and Glass *et al.* [9] on the catalytic hydrogenation of ethylene support this conclusion.

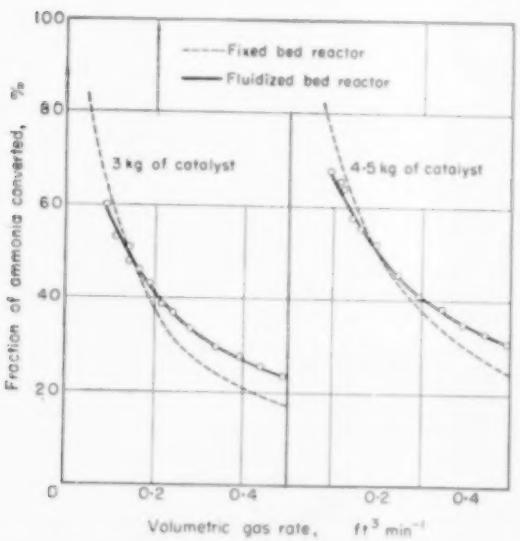

Fig. 1. Data on oxidation of ammonia in fixed and fluidized bed reactors by Shen [5] and Batchelor [10]. Experimental conditions: Catalyst: 165–200 mesh manganous–bismuth–alumina catalyst prepared as mentioned in the Experimental Section. Temperature: 250°C. Feed: 10 per cent ammonia – 90 per cent oxygen (by volume).

However, a discrepancy arises when one compares the data on low temperature oxidation of ammonia with oxygen in fixed and fluidized beds of catalyst obtained by Shen [5], Batchelor [10] and Johnstone *et al.* [11] using the same reactor.

In Fig. 1 some of the conversion data obtained by these authors on fluidized beds are shown as a function of the volumetric gas rate. Curves are also shown for the fractional conversion vs. flow rate calculated by extrapolating results of other experiments carried out by the same authors on fixed beds using upward flow of the gas at velocities lower than the minimum fluidization velocity. If such extrapolations are valid it appears that above a certain flow rate the conversion of ammonia in a fluidized bed is higher than that obtained in a fixed bed reactor. This situation, if it actually exists, is contrary to what one would expect if the ideas stated above are correct.

Further consideration suggests the reasons why such behaviour might be expected:

(1) The reaction mechanism might be changed to a diffusion-controlled step because of the increased velocity of the gas past the particles.

(2) The movement of the particles in the fluidized bed might increase the effectiveness of the particles surface for the reaction.

(3) Channelling occurred at the low upward velocity used in the fixed bed and this might lower the apparent reaction rate thus shifting the conversion curves downward.

(4) The catalyst might have had a different activity.

If the first of these reasons were true the two-phase fluidization concept of Toomey and Johnstone, in which the velocity of the gas in the dense phase where the reaction takes place remains constant and equal to that at incipient fluidization regardless of the total gas flow through the bed, would be disproved.

It was to improve the understanding of this matter of ammonia oxidation in fixed and fluidized beds that the present experiments were conducted. The experiments repeated, to an extent, some of the earlier experiments, but downward flow of the gas was used in the fixed bed to prevent channelling. Also, in order to

obtain a more definite trend of the curves for conversion vs. flow rate the measurements in fluidized beds were extended to a range of gas velocities three or four times greater than that used previously.

In addition, other experiments were conducted using screen baffles in the fluidized bed. In such a bed one can conduct a reaction under conditions which are between those of a fixed bed and a fluidized bed.

Since a baffled bed reactor has the advantages of good contact between gas and solid, which is characteristic of a fixed bed reactor, and of high heat transfer rates and low pressure drop, characteristic of a fluidized bed reactor, the study is appropriate.

VOL. 16 1962

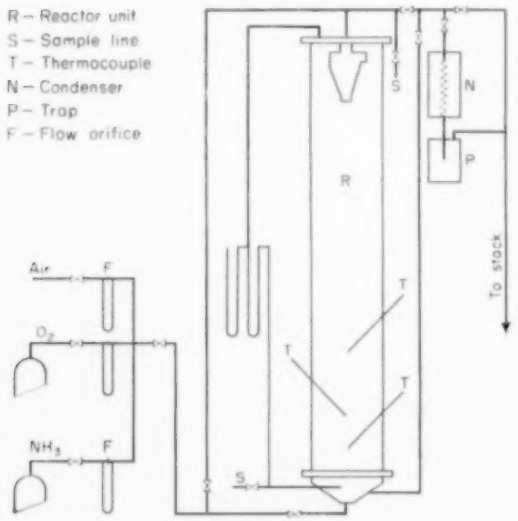

Fig. 2. Flow diagram of experimental equipment.

Experimental Section

Apparatus

A flow diagram of the experimental equipment is shown in Fig. 2. The equipment consists essentially of a heated reactor, supply tanks for air, oxygen and ammonia, equipment for measuring the flow rates of these gases, devices for sampling the gas entering or leaving the reactor and thermocouples for measuring the temperature of the catalyst bed. The arrangement of the valves was such that either upflow or downflow of the inlet gases was possible.

The reactor, which was 4½ in. i.d. and 43 in. high, was made of stainless steel. The lower flange was connected to an inlet section and a stainless steel porous plate, placed between the reactor and the inlet section, was used to support the bed and disperse the gas uniformly. The upper flange supported the cyclone separator used to remove the catalyst particles from the gas stream. The catalyst collected in the cyclone was returned to the reactor at the end of each series of runs.

The reactor was heated electrically by four chromel resistance ribbons wound on Alundum insulation around the reactor. The temperatures of the bottom and upper sections were controlled manually with Variacs and the temperature of the section immediately above the porous plate was regulated by an automatic controller.

The sample lines for the exit gas were also heated electrically to prevent condensation of water. The temperatures in the fluidized beds were measured by three iron–constantan thermocouples in stainless steel wells located in the axis of the column.

The internal structure of the reactor was modified for the experiments using a baffled bed. The baffles used consisted of a stack of stainless steel screen with 0·14 in. openings made of 0·035 in. wire. The screens fitted closely inside the column. They were separated by four stainless steel spacers ⅜ in. long. Four threaded ⅛ in. stainless steel rods were passed through the screens and the spacers and bolted to hold the stack of screens together. Seven iron–constantan thermocouples were attached to the screens in order to detect axial and radial temperature gradients in the fluidized beds during the experiments. The wires of the thermocouples were insulated with fibre-glass cloth and passed through steel tubings at the top of the reactor.

Catalyst

The catalyst was made by impregnating 20 kg of a (100–325 mesh) Alcoa alumina catalyst used for fluid cracking with 5 l. of solution containing 2,000 g. manganous nitrate and 700 g. bismuth

nitrate. It was dried for 5 days in a vacuum oven and roasted in an electric furnace for 48 hr at 375°C.

The catalyst was used without screening after impregnation. The geometric mean diameter of the particles was 105 μ and the density 2·06 g/cm³. The apparent density of the catalyst was 1·08 g/cm³.

The activity of the catalyst remained constant for several hundred hours.

Procedure

A weighed quantity of the catalyst, between 2 and 6 kg, was placed in the reactor through the top. The ratios L/D of the depth of the packed bed to the diameter of the column used for the three series of runs were 1·7 (2 kg of catalyst) to 3·4 (4 kg of catalyst) and 5·1 (6 kg of catalyst). The catalyst was fluidized with air while the reactor was being heated. When the reaction temperature, 250°C, was reached the oxygen–ammonia gas stream was substituted for the air. In all of the runs the inlet composition of the gas was approximately 10 per cent ammonia and 90 per cent oxygen. The absolute pressure at the top of the reactor was maintained at 840 mm Hg.

Simultaneous samples of the gas were drawn at the bottom and the top of the column through U-tubes containing magnesium perchlorate. The rate of sampling was about 0·01 ft³/min. The volumes of the gas samples were measured by wet-test meters after adsorption of ammonia and water vapour. The amount of ammonia adsorbed was found by dissolving the adsorbent and titrating the solution with standard acid.

The experimental procedure was essentially the same for both the fluidized bed and fixed bed experiments, the only difference being that in fixed bed experiments the reactor was operated down flow. After each run with fixed bed, the gas stream was passed upward through the bed to eliminate any temperature gradient formed by fluidization of the catalyst.

There was some difficulty in maintaining a constant and uniform temperature in the fixed bed for the entire period of the experiments, even when 2 kg of the catalyst were used. For this reason it was not possible to operate at flow rates higher than 0·33 ft³/min* with the fixed beds. At this flow rate uniformity of temperature within $\pm$ 5°C could be maintained. In the fluidized beds control of the temperature was easily maintained at all flow rates and for any amount of catalyst used.

Results

The data for fixed beds of 2 kg of catalyst have been interpreted on the basis of the conclusion of Johnstone *et al.* that, for the oxygen–ammonia ratio used, the oxidation of ammonia follows a pseudo-first order reaction for which the equation is

$$\ln (1 - \alpha) = - K \tau \qquad (1)$$

where α is the fraction of the ammonia oxidized, τ is the reciprocal space velocity expressed as volume of catalyst particles per unit of volumetric gas flow rate and K is a constant. Under the experimental condition used, in a range of gas flow rate from 0·17 ft³/min to 0·33 ft³/min, the average value of K was equal to 5·15 min^{-1} (deviations $\pm$ 0·2 min^{-1}).

Extrapolation of the results by means of equation (1) to higher flow rates and to beds of 4 and 6 kg of catalyst is shown by the broken lines in Figs. 3, 4 and 5. These Figs. also show the results obtained with fluidized beds of 2, 4 and 6 kg of catalyst.

In Figs. 3, 4 and 5 the curves for the fixed beds and fluidized beds do not intersect as in Fig. 1. This proves that the unusual results shown in Fig. 1, which are mentioned in the Introduction, must be attributed either to channelling in the fixed bed when using upward flow or to different activity of the catalyst used for the two sets of experiments.

The data of Figs. 3, 4 and 5 show that the oxidation of ammonia in fixed and fluidized beds of the catalyst used follows the same general trend reported for other reactions by other investigators. In a fixed-bed reactor the conversion is higher than in a fluidized-bed reactor under the same experimental conditions. Figs. 4

*Here and throughout the paper the volumetric gas rates are expressed as standard ft³/min (SCFM).

VOL 16 196

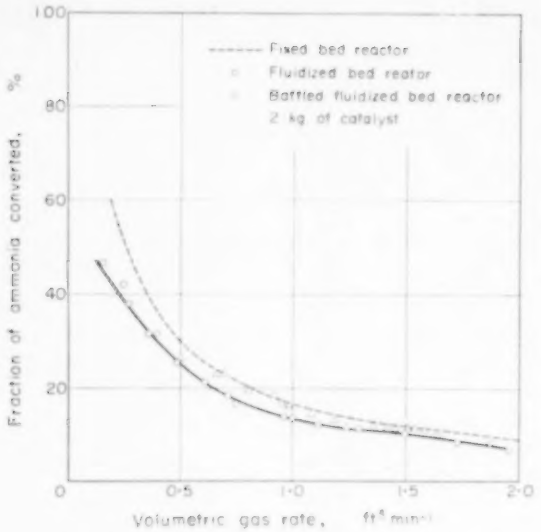
Fixed bed reactor
Fluidized bed reactor
Baffled fluidized bed reactor
2 kg of catalyst
Fraction of ammonia converted, %
Volumetric gas rate, ft³ min⁻¹

Fig. 3. Experiments with 2 kg of catalyst.

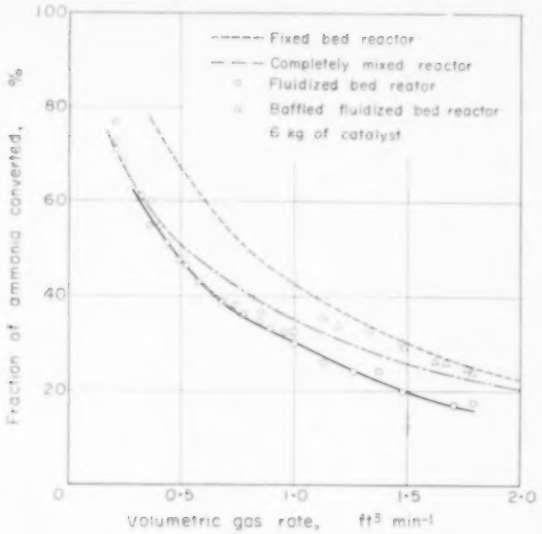

Fig. 5. Experiments with 6 kg of catalyst.

and 5 show also the importance of the by-passing of the gas in determining the conversion in fluidized operations. In fact, the conversions in fluidized-bed reactors are even lower than conversions calculated for corresponding fixed-bed reactors under the hypothetical assumption that the gas phase is completely mixed.

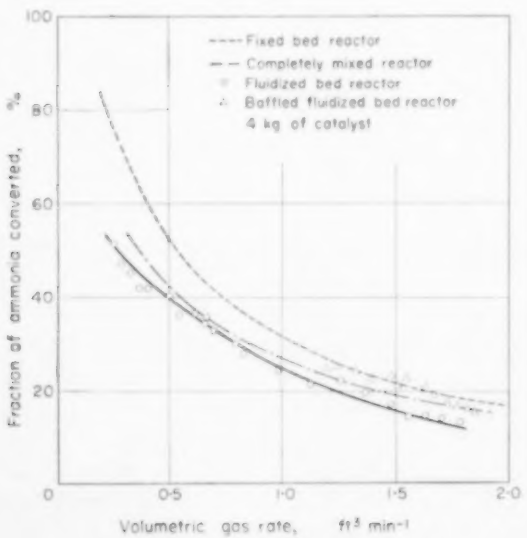

Fig. 4. Experiments with 4 kg of catalyst.

The curves in Figs. 4, 5 and 6 indicate the effect of the L/D ratio on the efficiency of fluidized bed reactors. The higher this ratio is the larger is the minimum difference between the conversion in fixed- and fluidized-bed reactors.

The change in the magnitude of the relative spread between the two conversions $(\alpha_{fl} - \alpha_{fl}/\alpha_{fl})$ as the flow rate increases may be interpreted on the basis of the results of previous studies on the behaviour of fluidized beds [12–16].

At the lower flow rates there is a more compact solid shell around the bubbles. Besides, channels are formed in the bed, through which gas flows preferentially. In these conditions there are, of course, low rates of gas transfer between the continuous and discontinuous phases and, thus, the value of $(\alpha_{fl} - \alpha_{fl})/\alpha_{fl}$ is high.

When the flow rate is increased, the more active, turbulent intermixing between the continuous and discontinuous phases brings the conversion in the fluidized bed closer to that for the fixed bed. Thus, the value of $(\alpha_{fl} - \alpha_{fl}/\alpha_{fl})$ may be reduced. It appears in Figs. 3 and 4 for experiments using ratios L/D equal to 1·7 and 3·4.

As the gas velocity is increased still further the effect of the by-passing of the gas becomes do-

minant again. The by-passing of a larger volume of gas compensates for any further improvement of the homogeneity of the bed. Thus, the value of $(x_0 - x_0)/x_0$ remains nearly constant or increases slightly, as shown in Figs. 3 and 4.

The maximum in the conversion of fluidized reactors as the gas flow rate increases appears to agree qualitatively with the data of Mathis and Watson [7] on the catalytic dealkylation of cumene and with the data of Shuster and Kisliak [17] on the uniformity of fluidized beds.

The practical interest in the optimum gas velocity for a fluidized reactor is evident since it defines the condition at which the bed should be operated in order to give conversion nearest that of a comparable fixed bed.

Although under more general considerations the optimum velocity, as defined, may not be the best for carrying out a given reaction, nevertheless it helps to overcome the main disadvantage of the fluidized beds compared to fixed beds, i.e. the non-homogeneity of the solid–gas system.

Unfortunately, kinetic data obtained in laboratory experiments are not always applicable for the design of industrial reactors. The effect of fluidization of solid on each reaction should be investigated and the condition of the fluidized bed related to the properties of the solid and the fluid and the operating variables such as gas flow rate, the L/D ratio and the diameter of the column. The data of Mathis and Watson and the present results on oxidation of ammonia show that the optimum gas flow rate may be less well defined as the L/D ratio increases and the spread between the conversion curves for fixed and fluidized bed increases as L/D increases. Mathis and Watson also found that the spread increases with the size of the reactor.

The effect of the L/D ratio on the efficiency of fluidized reactors can be studied by considering the effect of the gas rate on the mass transfer between the continuous and the discontinuous phases. Shen and Johnstone [6] showed that, for a first-order reaction, assuming that mixing within each phase is negligible, the mass transfer coefficient between the continuous and the discontinuous phases can be calculated from two simultaneous first-order linear differential equations obtained from a material balance in each phase:

$$\frac{dC_d}{dZ} = -\frac{t_d K_d}{L}(C_d - C_c)$$

$$\frac{dC_c}{dZ} = \frac{V_d}{V_c}\frac{t_d}{L} K_d (C_d - C_c) - \frac{t_c K C_c}{L}$$

where K_d is the transfer coefficient expressed as moles per unit time, per unit volume of bed per unit concentration difference between the two phases. Calculated values of mass transfer coefficients K_d are shown in Fig. 6. For 4 kg of catalyst the coefficient passes through a maximum at a flow of about 0·7 ft³/min; for 2 kg of catalyst the coefficient increases up to a flow rate of 1·3 ft³/min and then levels off; and for 6 kg of catalyst it decreases beyond 0·25 ft³/min.

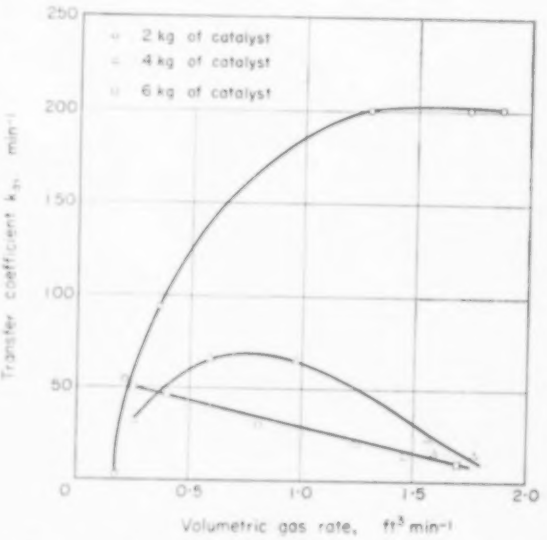

Fig. 6 Effects of volumetric gas rate on transfer coefficients K_d.

Fluidized Reactor with Screens

Previous work carried out by Massimilla *et al.* [18] has shown that the homogeneity of a fluidized solid–gas system is improved by the presence of screen grids. The effect of this kind of baffle on the friction factor, density distribution and mixing of the solid were observed. They pointed out that fluidized beds with screen grids

VOL. 16 1962

are comparable to fixed beds, as far as the uniformity of distribution of the solid is concerned, over an important range of flow rates. They also showed that when the grids are properly designed the pressure drop in a baffled solid–gas system increases only slightly with the flow rates. Further studies have shown that, beyond a certain gas velocity, the rate of heat transfer at the wall of the container and in the solid phase of a baffled fluidized bed is as high as it is in fluidized beds without screens. Moreover, recent studies [19, 20] have demonstrated that screen baffles improve horizontal mass and heat transfer in fluidized beds minimizing the effect of the by-passing of the discontinuous phase through the bed. They also noticed that back-mixing of the gas in fluidized bed is reduced by the use of grids [20], similarly to the effect of other types of baffles [21].

Before testing the effect of the screen baffles on the oxidation of ammonia at low temperature preliminary experiments were carried out at room temperature in a Lucite column to find the most effective type of grid which gave the best homogeneity of the bed.

The screens alone caused no oxidation of ammonia when tested with 10 per cent ammonia and 90 per cent oxygen, at 250°C.

As expected, it was not possible to maintain uniform temperature in the beds with screens over the whole range of the gas velocities used in the experiments with unbaffled beds. Only above 0·7 ft³/min for a bed of 2 kg and above 1·0 ft³/min for beds 4 and 6 kg of catalyst the temperatures were fairly uniform. The conversion data for these ranges are shown in Figs. 3, 4 and 5. For each ratio of L/D there is a flow rate above which the conversion approaches that in the fixed bed. It is not likely that the baffles break up the stream of bubbles rising in the bed at lower flow rates. Experiments, however, could not be carried out in this range because of variations in the temperature of the bed.

The results obtained with the screens agree qualitatively with the conclusions of Glass [8] on the effect of obstructions in fluidized beds. This author found that the presence of 6-mesh stainless steel screens appreciably increased the rate of conversion in a 2 in. i.d. reactor. He also found that the presence of baffles made the temperature control more difficult in the range of flow rates used, which was higher than that used in the present work. Possibly the larger reactor made the temperature in the ammonia oxidation more uniform.

The agreement between the results with fixed-bed and baffled fluidized-bed reactors for beds of 2 and 4 kg of catalyst does not indicate that the mechanism of the catalysed reaction is the same in both reactors. It is probable that the agreement is the result of the combination of two opposing factors acting in baffled fluidized beds, with some residual by-passing even in the presence of the grids and increased effectiveness of the particle surfaces for the chemical reaction because of the motion of the catalyst.

The exact effect of the screens on the over-all kinetics of a reaction cannot be generalized from results of experiments on one catalyst, since the nature of the reaction between the gas and the fluidized particles, the heat of reaction, the effect of the interfacial velocity and the size of the reactor all affect the conversion rate.

Conclusions

The low temperature oxidation of ammonia in fluidized beds of manganese–bismuth–alumina catalyst is consistent with the theories suggested by previous investigators for interpreting reaction kinetics in fluidized beds.

The difference in the conversion in fluidized and fixed bed reactors depends on the flow rate. It is noticeable at low flow rates because of the channelling and the high stability of the bubbles in poorly fluidized beds. An optimum velocity for conversion in fluidized beds has been found.

Screen baffles used to improve the homogeneity of fluidized solid–gas systems are most effective at the higher flow rates.

It was not possible to carry out isothermal conversion at low flow rates on baffled beds because of the poor circulation of the solid and the high exothermicity of the reaction. At low flow rates stirring the bed may be more useful for improving the conversion in a fluidized catalytic reactor.

Acknowledgement—This investigation was carried out with the aid of funds supplied by the Italian Rotary Club in the form of a travel and a subsistence grant to Dr. Massimilla.

The authors acknowledge with gratitude the aid of K. A. Benson in the experimental work.

Notation

C = concentration	moles/ft^3
D = diameter of the reactor	ft
K = reaction rate constant	min^{-1}
K_d = mass transfer coefficient	min^{-1}
L = depth of catalyst bed	ft
t = detention time	hr
V = volumetric gas velocity	ft^3/min
Z = length co-ordinate	ft
α = fraction conversion	dimensionless
τ = reciprocal space velocity	min

Subscripts

c = continuous phase
d = discontinuous phase
fi = fixed bed
fl = fluidized bed

References

[1] Toomey R. D. and Johnstone H. F. *Chem. Engng. Progr.* 1952 **48** 220.
[2] Gilliland E. R. and Mason E. A. *Indust. Engng. Chem.* 1949 **41** 1191.
[3] Gilliland E. R. and Mason E. A. *Indust. Engng. Chem.* 1952 **44** 218.
[4] Danckwerts P. V., Jenkins J. W. and Place G. *Chem. Engng. Sci.* 1954 **3** 26.
[5] Shen C. Y. Ph.D. Thesis, University of Illinois 1954.
[6] Shen C. Y. and Johnstone H. F. *Amer. Inst. Chem. Engrs. J.* 1955 **3** 349.
[7] Mathis J. F. and Watson C. C. *Amer. Inst. Chem. Engrs. J.* 1956 **2** 518.
[8] Glass W. B., Sc. D. Thesis, Massachusetts Institute of Technology 1956.
[9] Glass W. B., Lewis W. K. and Gilliland E. R. *Ann. Meeting, Amer. Inst. Chem. Engrs., Chicago, Illinois* 1957.
[10] Batchelor J. D., Ph.D. Thesis, University of Illinois 1952.
[11] Johnstone H. F., Batchelor J. D. and Shen C. Y. *Amer. Inst. Chem. Engrs. J.* 1955 **1** 318.
[12] Leva M., Grummer M., Weintraub M. and Pollachik M. *Chem. Engng. Prog.* 1948 **44** 619.
[13] Yasui G. and Johanson L. N. *Amer. Inst. Chem. Engrs. J.* 1958 **4** 445.
[14] Davidson J. F., Paul R. C., Smith M. J. S. and Duxbury H. A. *Inst. Chem. Engrs.* 1959 **37** 323.
[15] Massimilla L. and Westwater J. W. *Amer. Inst. Chem. Engrs. J.* 1960 **6** 134.
[16] Baumgarten P. K. and Pigford R. L. *Amer. Inst. Chem. Engrs. J.* 1960 **6** 115.
[17] Shuster W. W. and Kisliak P. *Chem. Engng. Progr.* 1952 **48** 455.
[18] Leva M. *Fluidization* pp. 98, 105, 200, 278, 281. McGraw-Hill, New York 1959.
[19] Cabella A., Di Poggio E. and Massimilla L. *Il Calore* 1958 **29** 167.
[20] Bracale S., Cabella A. and Massimilla L. *Chim. e Industr.* 1958 **40** 621.
[21] Overcashier R. H., Todd D. B. and Olney R. B. *Amer. Inst. Chem. Engrs.* 1959 **5** 54.

Chemical Engineering Science, 1961, Vol. 16, pp. 113 to 119. Pergamon Press Ltd., London. Printed in Great Britain.

The use of Stereoscopic Photography for the measurement of Velocities in Liquids

R. M. Nedderman

Department of Chemical Engineering, Pembroke Street, Cambridge

(*First received* 28 *January* 1961; *in revised form* 6 *February* 1961)

Abstract—A method of measuring all three components of the velocity of particles suspended in a fluid is described. The method has been developed to give an accuracy of ± 0·001 cm for the measurement of distance and ± 1 per cent for the measurement of velocity. There is no fundamental reason why these should not be bettered.

Résumé—L'auteur expose une méthode de mesure des trois composantes de la vitesse de particules en suspension dans un fluide. La méthode a été développée avec une exactitude de ± 0,001 cm pour la mesure des distances et ± 1% pour la mesure des vitesses. Cette méthode semble pouvoir être améliorée.

Zusammenfassung—Eine Methode zur Messung aller drei Geschwindigkeitskomponenten von Teilchen, die in einem strömenden Medium suspendiert sind, wird beschrieben. Die entwickelte Methode hat eine Genauigkeit von ∓ 0,001 cm für die Entfernungsmessung und von ∓ 1% für die Geschwindigkeitsmessung. Der weiteren Verbesserung dieser Methode steht grundsätzlich nichts entgegen.

Introduction

This paper is a shortened version of part of a thesis [1] submitted to the University of Cambridge. Further details can be found from that work.

In the course of work on thin (ca. 1 mm) films of liquid flowing down vertical surfaces it became necessary to develop a new method of measuring velocity profiles. Films are very sensitive to disturbances and are broken up by any stationary measuring device such as a Pitot tube. It was clear therefore that some form of flow visualization (the observation of small particles moving with the fluid) would have to be used.

Flow visualization has been used before, by Townend and Fage [2], Preston and Fage [3] and by Clayton [4]. None of the above was able to measure more than two components of velocity, or to measure velocities in more than one plane at any time. Of the three methods Clayton's is the most suitable for use on films but this suffers from the disadvantage of a highly non-linear calibration curve, particularly near the wall, and confusion due to multiple reflections in the gas–liquid interface.

It was therefore decided that a new approach was necessary and it seemed likely that stereoscopic photography would be a useful method. All three co-ordinates of position can be found from a stereoscopic pair of photographs and hence all three components of velocity. This method is an advance on those mentioned above in that the velocities are obtained throughout a volume. It is also an improvement on Clayton's method in that the calibration curve is nearly linear and is most nearly linear near the wall, making it particularly suitable for very thin films.

Though the method was developed for use in films it is by no means limited to this application. It can be used for all fluid systems capable of being photographed and can also be used for finding the spacial distribution of particles. The theory of the method, and such practical precautions as were found to be necessary, are given here in the hope that they will be of use to others wanting to use this method.

This method does not differ in principle from that of Miller [5], but he was concerned with distances of the order of a thousand times those with which this paper deals.

Apparatus

The method was developed for use on a 1 in. diameter vertical tube. It was found that the photographs had to be accurately in focus and that the striations in commercial extruded perspex tubes caused too much distortion. Consequently the tube was broken at the section to be examined and a 3 in. long 1 in. internal diameter highly polished perspex cell was inserted. The outside of the cell was a 1½ in. square for convenience in lighting. A grid of lines 0·1 in. apart and less than 0·001 in. deep was scribed on the cell wall to provide a zero for readings of depth.

The best results were obtained when the camera axes were co-planar with the cell axis. This arrangement also gave a more linear calibration curve than that in which the camera axes were in a plane perpendicular to the cell axis. The two cameras, Contax II cameras, fitted with f.3·5, 50 mm Tessar lenses and 12 cm of extension tube, were mounted in a vertical plane with their axes converging at 40°. This angle was not critical and was determined mainly by the shape of the cameras. The arrangement of the cameras and the cell is shown in Fig. 1.

In order to get a simple calibration it is necessary to have the magnification of both cameras the same. Consequently the normal method of focussing, whereby the distance between the lens and the photographic plate is varied, could not be used. The cameras were therefore focussed by moving them bodily. This was made possible by mounting them on Hogarth two-way sliding vice tables with screw feed calibrated to 0·001 in. The cameras were fitted with plate backs so that ground glass screens could be used for focussing.

The best results were obtained when spherical particles were used, as asymmetric particles appeared brighter on one photograph than on the other, leading to confusion. Air bubbles, glass beads and dispersions of oil were tried. Air bubbles were found to give the best photographs and could be made sufficiently small to have negligible drift velocity. (A 0·001 in. diameter bubble rises through water at about 0·003 in/sec). Air bubbles were therefore used as in Clayton's work [4].

To preserve symmetry the bubbles had to be lit horizontally. When a bubble is lit from behind, the lens effect produces an image some distance behind the centre. Thus with back lighting corrections have to be made to readings of depth. With side lighting the image is displaced to one side. The bubbles were therefore lit from both sides, the average position of the two images giving the position of the centre of the bubble. The bubble diameter can be calculated from the distances between the two images thus enabling oversized bubbles to be detected. It was to facilitate the side lighting that the outside of the cell was made square.

The bubbles were lit with a flashing light so that they appeared on the photograph as rows of dots. The velocities were found by measuring the distance between two successive dots. It is difficult to synchronize two flashing lights so only one light was used, the beam being split in two, and directed on to the right paths by a series of mirrors. These can be seen in Fig. 1. The flashing light was made, as in Clayton's work, by intercepting the beam from a suitable light source by a spinning perspex disk with sections of the perimeter blacked out. The inner portion of the disk was painted with a symmetrical pattern so that it could be timed stroboscopically against the mains frequency. A photographic flash bulb was usually used as the light source. With this about eight interruptions could be obtained. An advantage of a flash bulb over a steady light was that the camera shutters need not be synchronized. They could be left open and the exposure regulated by the strength of the flash bulb.

The photographs were analysed in a Zeiss stereoscope originally designed for use in aerial surveying. It consisted essentially of two travelling microscopes coupled together so that as well as being able to measure distances in the normal manner it could measure the difference in the lengths of the two images of the same object.

The photographs were put in the stereoscope and viewed each with one eye. They were then moved so that the two images of a particular point were both under the crosswires of their respective eyepieces. Both photographs were

VOL.
16
1962

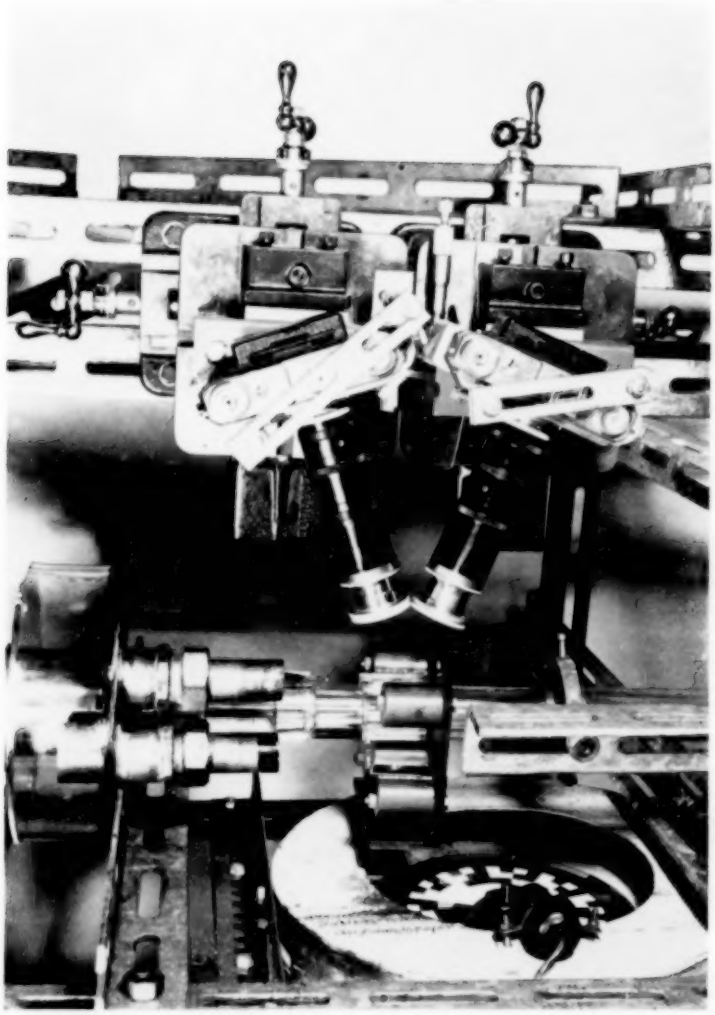

FIG. 1.

VOL
16
196

VOL. 16 1962

then moved the same distance by a calibrated screw until another point was behind the crosswires of the left-hand eyepiece. The right-hand photograph was then moved by another calibrated screw until the corresponding image was behind the left-hand crosswires. This second movement was the difference in length of the images.

When very accurately focussed photographs were obtained a visually stereoscopic effect was produced. Altering the distance between the two photographs moved the stereoscopic image vertically with respect to the crosswires. By adjusting points of the image to the same height as the crosswires the differences in lengths could be obtained to much greater accuracy than by the straightforward method described above.

Theoretical Calibration

(a) *Normal method*

This theory is worked out for the case when the optical axes of the cameras intersect at some point on the inside wall of the cell (the optical axis being defined as the path of a ray of light passing through the centre of the lens and the centre of the photographic plate). This point R (see Fig. 2) is taken as the origin of co-ordinates, with the x axis parallel to the cell axis and the y axis perpendicular to the cell wall. In this analysis only points in the plane of the cameras ($z = 0$) are considered.

The lengths of the images of the line PR, where P is the point (x, y) are calculated.

Let L be the distance of the lens from the cell
E be the distance of the lens from the photographic plate
Δ be the thickness of the cell wall
μ_1 be the refractive index of the cell wall
μ_2 be the refractive index of the liquid in the cell
α, β, γ, α^+, β^+, γ^+ be angles defined by Fig. 2
$\delta\alpha$ be $\alpha - \alpha^+$, $\delta\beta$ be $\beta - \beta^+$, $\delta\gamma$ be $\gamma - \gamma^+$.

The length of the extension tube prevents $\delta\alpha$ being greater than 0·05 rad. so it is assumed throughout that

$$\delta\alpha = \sin \delta\alpha = \tan \delta\alpha$$

The laws of optics give:

$$\begin{aligned} \sin \alpha &= \mu_1 \sin \beta = \mu_2 \sin \gamma \\ \sin \alpha^+ &= \mu_1 \sin \beta^+ = \mu_2 \sin \gamma^+ \end{aligned} \qquad (1)$$

and the geometry of Fig. 2 gives

$$L \tan \alpha + \Delta \tan \beta = L \tan \alpha^+ + \Delta \tan \beta^+ + x + y \tan \gamma^+ \qquad (2)$$

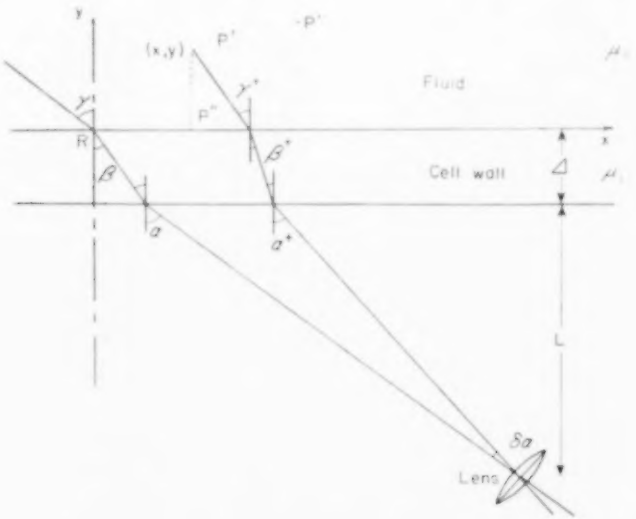

Fig. 2.

Expanding (1) and (2) by Taylor's theorem and solving for $\delta\alpha$ we get

$$\delta\alpha = Ax + Ay\tan\gamma + \\ + (AB\tan\gamma - m_2\sec^2\gamma)\,Ax\,Ay + \frac{AB}{2}(Ax)^2 + \\ + \left(\frac{AB}{2}\tan^2\gamma - m_2\sec^2\gamma\tan\gamma\right)(Ay)^2 + \ldots \quad (3)$$

where $$A^{-1} = L\sec^2\alpha + \Delta\, m_1\sec^2\beta \quad (4)$$

$$B = 2L\sec^2\alpha\tan\alpha + \Delta\,(3m_1^2 - 1)\sec^2\beta\tan\beta \quad (5)$$

m_1 and m_2 being defined by

$$\tan\alpha = \frac{1}{m_1}\tan\beta = \frac{1}{m_2}\tan\gamma \quad (6)$$

In practice (Ax) and (Ay) are less than 0·02 so equation (3) will converge rapidly.

The length D_R of the image of PR on the right-hand plate will be given by $D_R = E\,\delta\alpha$.

The length D_L of the image of PR on the left-hand plate can be obtained by a similar analysis, the only difference being that in equation (3) the signs of all terms except those involving odd powers of x are reversed.

The stereoscope measures the mean length of the images R_x and the difference in their lengths R_y. Clearly:

$$R_x = E\,Ax + E\,(AB\tan\gamma - \\ - m_2\sec^2\gamma)\,Ax\,Ay + \ldots \quad (7)$$

$$R_y = 2E\tan\gamma\,Ay + AEB\,(Ax)^2 + \\ + E\,(AB\tan^2\gamma \\ - 2\,m_2\sec^2\gamma\tan\gamma)\,(Ay)^2 + \ldots \quad (8)$$

Equation (7) cannot contain even powers of x and equation (8) cannot contain odd powers of x, therefore these equations are correct to one higher power of x than appears at first sight.

Putting in the dimensions of the apparatus, i.e.

$$E = 170\text{ mm}, \quad L = 60\text{ mm}, \quad \Delta = 6\text{ mm}, \\ \alpha = 20^\circ, \quad \mu_1 = 1{\cdot}5, \quad \mu_2 = 1{\cdot}33$$

we have in millimetres

$$R_y = 1{\cdot}20\,y + 0{\cdot}0218\,x^2 - 0{\cdot}0129\,y^2 + \ldots \quad (9)$$

$$R_x = 2{\cdot}36\,x - 0{\cdot}0119\,xy + \ldots \quad (10)$$

Since the depth of focus of the cameras put an upper limit of y at about 1 mm and x at 3 mm, it was assumed that

$$R_y = 1{\cdot}20\,y + 0{\cdot}0218\,x^2 \quad (11)$$

$$R_x = 2{\cdot}36\,x \quad (12)$$

would be correct to an accuracy of 1 per cent.

Except at the edges of the film the x^2 term in equation (11) can be neglected. The equations are then linear and distances such as PP' can be measured without reference to the origin. At the edges of the film the x^2 correction must be applied unless it can be eliminated by difference. This is possible if P lies directly behind one of the circumferential grid lines. If P'' is the point on the grid line directly beneath P then the distance PP'' measured on the stereoscope can be converted to y without the x^2 correction. When P is not directly behind a grid line the position of the origin must be determined. This is possible by observing the longitudinal grid lines, which being lines of $y = 0$ appear to be parabolas. x equals zero at the apices of the parabolas.

Measurements in the z direction were of minor interest in the problems for which this method was used so no theoretical calibration was made. It was found experimentally that

$$R_z = 2{\cdot}36\,z = EAz.$$

(b) "*Moving in*" *technique*

For points remote from the wall a different technique must be used. The above method is still applicable but as the wall grid will be out of focus there is no zero from which to take readings. This is overcome by the following technique:

The cameras were focussed on the wall grid and a photograph was taken. Both cameras were then moved in a certain distance until they were focussed on the area under investigation. Another photograph was taken on the same plate. The net result of this was that the grid appeared to be in the middle of the fluid. Measurements were taken from this false grid in the normal manner. The distance between the false grid and the cell wall was a function of the camera movement only and could be calculated in the following way. See Fig. 3.

The apparent movement of the grid, t, equals

VOL 16 196

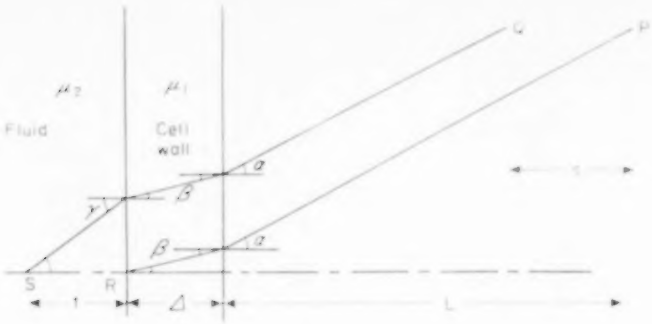

FIG. 3.

the movement of the intersection of the camera axes. With the camera lens at P the optical axes intersect at R, on the cell wall. The cameras were moved a distance, s, bringing the right-hand lens to Q and the intersection of the optical axes to S. Clearly:

$$t \tan \gamma + \Delta \tan \beta + (L - s) \tan \alpha = \Delta \tan \beta + L \tan \alpha$$

$$\text{i.e.} \quad t \tan \gamma = s \tan \alpha$$

$$\text{i.e.} \quad m_2 t = s. \qquad (13)$$

It might be thought that this method depends on the accuracy with which the optical axes originally intersected on the grid. This is not so provided equation (11) holds equally well for small distances at R and at S. The movement of the cameras, not their position, is the important factor in this method

Experimental Calibration

The effective distance from the lens to the cell could not be measured with sufficient accuracy to make the theoretical calibration reliable. The apparatus was therefore calibrated empirically. To do this it was necessary to have a series of points at known distances from the wall throughout the working range. It was found that lines

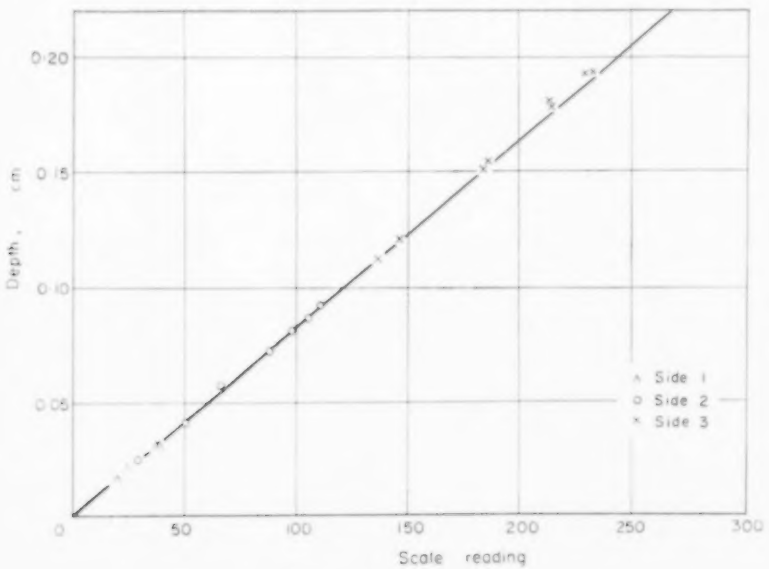

FIG. 4. Calibration curve.

scribed on a piece of perspex gave the best results.

A perspex rod of the same diameter as the tube (to 0·001 of an inch) had four flats cut into one end. These had maximum depths of $\frac{1}{64}$, $\frac{1}{32}$, $\frac{1}{16}$ and $\frac{1}{8}$ in. Lines at approximately $\frac{1}{20}$ in. spacing were scribed on the flats parallel to an perpendicular to the axis of the rod, forming a square grid. These grid were measured to 0·0001 in. by a travelling microscope. The depth of each line below the tube wall could then be calculated.

As many readings as there were grid lines could be taken. These are plotted against the known depths in Fig. 4. It can be seen that the relationship is sensibly linear up to 2 mm from the wall. The slope of the line agrees with the theoretical to within the accuracy of the measurement of the distance from cell to lens, which was about 10 per cent. The calibration constants for the x and z direction could also be found from the photographs, these too lay within the limits of the theoretical values.

It was found possible to read R_y consistently to 0·001 cm and R_x and R_z to 0·002 cm. Therefore with the calibration constants of the order of 1 and 2 respectively the accuracy is equal for all three directions and is about $\pm$ 0·001 cm.

A similar method was used to calibrate the moving-in technique. The results are plotted in Fig. 5. It is seen that the results cannot be distinguished from theory.

Conclusion

A method of stereoscopic photography has been developed for measuring the positions of moving bubbles at known intervals of time, thus giving a velocity profile. Distances can be measured to within 0·001 cm over a range of 0·1 cm. The method can be extended to greater depths, thus making it applicable to any flow systems, though a theoretical calibration would be difficult if the photographs had to be taken through highly curved surfaces. The method has been calibrated theoretically for cylindrical tubes and it was found that the calibration curve was nearly linear. This was confirmed by experiment.

The method is slow and it takes several minutes to obtain one reading from the photographs. This makes it rather unsuitable for fluctuating flow when a large number of readings are needed to give a reasonable average. There are however many situations in which this is the only method that will give any results and its development was therefore considered worthwhile.

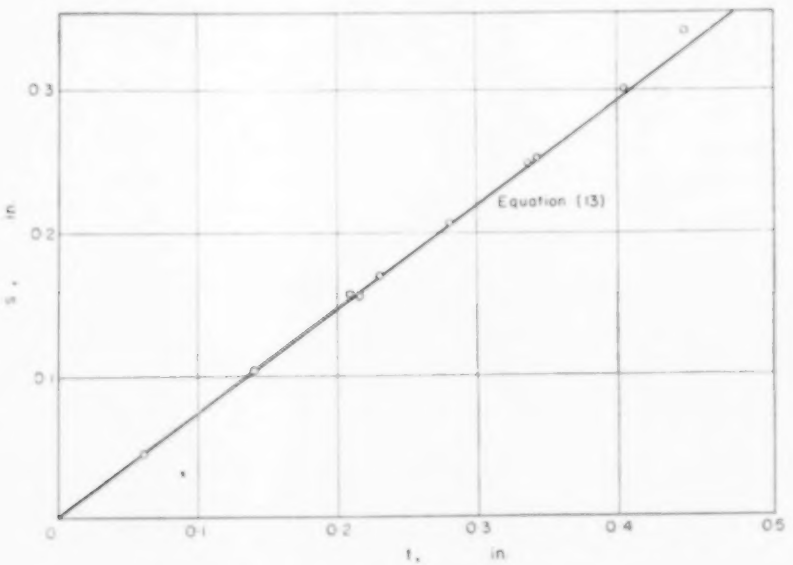

Fig. 5. 'Moving-in' technique calibration curve.

Acknowledgements—I wish to thank my supervisor, Professor T. R. C. Fox, for suggesting this method and for much help and guidance throughout the work. I would also like to thank the workshop staff of the Department of Chemical Engineering, University of Cambridge, for help in setting up the apparatus and the Esso Petroleum Company for financial assistance.

Notations

A = defined by equation (4)
B = defined by equation (5)
D_L = length of image on left-hand plate
D_R = length of image on right-hand plate
E = distance of lens from photographic plate
L = distance of lens from cell
R_x, R_y, R_z = readings obtained from stereoscope
m_1, m_2 = defined by equation (6)
s = movement of cameras
t = apparent movement of grid
x, y, z = co-ordinates of position
Δ = thickness of cell wall
α, α^+, β, β^+, γ, γ^+, $\delta\alpha$ = angles defined in Fig. 2
μ_1 = refractive index of cell wall
μ_2 = refractive index of liquid

References

[1] Nedderman R. M. Ph.D. Thesis, Cambridge 1960.
[2] Townend H. C. H. and Fage A. *Proc. Roy. Soc.* 1932 **A 135** 656.
[3] Preston J. H. and Fage A. *Proc. Roy. Soc.* 1941 **A 178** 202.
[4] Clayton C. G. A. Ph.D. Thesis, Cambridge 1959.
[5] Miller J. E. *Geophys. Res. Pap.*, 1952 **19** 294.

VOL. 16 1962

Chemical Engineering Science, 1961, Vol. 16, pp. 120 to 126. Pergamon Press Ltd., London. Printed in Great Britain.

The Measurement of Velocities in the Wall Region of Turbulent Liquid Pipe Flow

R. M. Nedderman
Department of Chemical Engineering, Pembroke Street, Cambridge

First received 28 *January*, 1961 ; *in revised form* 6 *February* 1961)

Abstract—Stereoscopic photography has been used to measure the velocities in the wall region of turbulent liquid pipe flow. Measurements were made on water in a 1 in. diameter tube at Reynolds Numbers of 12,000 and 19,000. The mean velocities are in substantial agreement with those found in air by other people. The instantaneous velocities show that even in the so-called laminar sub-layer, the velocity is by no means steady.

Résumé—Les vitesses d'écoulement turbulent de liquide dans un tube ont été mesurées en utilisant la photographie stéréoscopique. Les mesures ont été faites avec l'eau dans un tube de 1 pouce pour des nombres de Reynolds 12,000 et 19,000. Les vitesses moyennes sont en très bon accord avec celles trouvées dans l'air par d'autres auteurs. Les vitesses instantanées montrent que même dans la prétendue sous couche laminaire, la vitesse n'est pas du tout constante.

Zusammenfassung—Die stereoskopische Photographie wurde benutzt, um die Geschwindigkeit einer Flüssigkeit in der Wandzone eines Rohres bei turbulenter Strömung zu messen. Die Messungen wurden mit Wasser in einem Rohr von 1 in. Durchmesser bei Reynoldszahlen von 12,000 und 19,000 durchgeführt. Die mittleren Geschwindigkeiten sind in grundsätzlicher Übereinstimmung mit denen, die andere Autoren mit Luft fanden. Die momentanen Geschwindigkeiten zeigen, dass selbst in der sogenannten laminaren Unterschicht die Geschwindigkeit unstetig ist.

Introduction

This paper is an abridgement of part of a Ph.D. Thesis [1] submitted to the University of Cambridge. Further details can be found in that work.

Chemical engineers are often concerned with the velocities very close to a solid boundary in turbulent liquid flow. Such velocities, and particularly the fluctuations in these velocities, must be known for the theoretical predictions of rates of heat transfer or dissolution.

These velocities have never been measured for y^+ less than 15 and it is usual to assume that they can be deduced from the known behaviour of air. In particular it is often assumed that von Karman's [2] dimensionless velocity profile

$$u^+ = y^+, \quad y^+ < 5 \tag{1}$$

$$u^+ = -3{\cdot}05 + 5 \ln y^+ \qquad 5 < y^+ < 30 \tag{2}$$

$$u^+ = 5{\cdot}5 + 2{\cdot}5 \ln y^+ \qquad 30 < y^+ \tag{3}$$

holds. This is not satisfactory for several reasons but has given rise to the classification of the wall layer into three regions: laminar sub-layer, buffer layer and turbulent core respectively.

The apparatus was constructed for the measurement of the velocities in thin films of liquid, but it was thought to be of interest to make a few measurements on the wall region of turbulent flow in a pipe running full. Only two series of results were obtained, at Reynolds numbers of 12,000 and 19,000. The measurements were made at values of y^+ down to about 1 and since few results are available in the region it was thought worthwhile publishing these measurements.

Previous Work

The velocity profile not too close to the tube wall has been worked out, using different assumptions, by Prandtl [3], von Karman [4], Hinze [5] and Millikan [6] as:

$$u^+ = A + B \ln y^+$$

where A and B are constants to be determined experimentally and u^+ and y^+ are the velocity and distance from the wall made non-dimensional

with the wall shear stress τ_0, density ρ and viscosity μ thus:

$$u^+ = u\sqrt{\frac{\tau_0}{\rho}}$$

$$y^+ = y\frac{\sqrt{\tau_0\,\rho}}{\mu}.$$

This has been confirmed by NIKURADSE [7] and many others [8, 9] for both liquids and gases. The values of A and B vary between authors but $A = 5{\cdot}5$ and $B = 2{\cdot}5$ are often accepted. This equation holds only for those regions in which the eddy viscosity is much larger than the molecular viscosity, i.e. for $y^+ > 30$.

The eddy viscosity decreases near the wall, and very close to the wall (say $y^+ < 5$) it becomes negligible compared to the molecular viscosity. ELROD [10] calculates that $\rho\epsilon/\mu \propto (y^+)^4$ for y^+ very small (ϵ is the eddy viscosity). TOWNSEND [11] disputes this, giving the exponent as 3. In either case ϵ become very small and hence the velocity profile becomes asymptotic to $u^+ = y^+$, the equation for laminar flow. This equation does not hold for the whole of the range $y^+ < 30$ and it is the bridging of the gap between the two equations which has caused much of the speculation about this subject.

At least nine semi-theoretical profiles have been proposed, [9, 12–19] for the region $y^+ < 30$. All are very complicated and some cannot be expressed in closed form. There is little difference in the numerical values calculated from these equations.

Three empirical formulae have been proposed:

(1) That of VON KARMAN [2], mentioned above.

(2) That of DUNN [20] and later SCHLINGER *et al.* [21].

$$u^+ = \frac{1}{0{\cdot}0695}\tanh 0{\cdot}0695\,y^+ \qquad (4)$$

which is not a good fit with the most reliable experimental results, and

(3) That of SLEICHER [22]

$$u^+ = \frac{1}{0{\cdot}091}\tan^{-1} 0{\cdot}091\,y^+ \qquad (5)$$

This last is as good a fit with experiment as any other profile and is at the same time mathematically the simplest. Unfortunately since it implies that $\rho\epsilon/\mu \propto y^{+2}$ it does not fulfil either ELROD's [10] or TOWNSEND's [11] criterion.

Two theories about the nature of the flow close to the wall are noteworthy. Firstly, EINSTEIN and LI [19] postulate a laminar layer which grows with time until it becomes unstable and breaks away, after which the cycle restarts. It can be shown from this theory that the least velocity of any section is given by

$$u^+ = \tfrac{1}{2}\,y^+. \qquad (6)$$

Secondly, KLINE and RUNSTADLER [23] maintain that there are regions of laminar flow, called "islands of hesitation," separated by regions containing turbulent vortices.

Measurements in the region $y^+ < 30$ have been made by LAUFER [8], REICHARDT [9], DEISSLER [15], SLEICHER [22] and SHIGEMITSU [24], all using air. Their results are too scattered to distinguish easily between the theoretical profiles but they are all close to SLEICHER's empirical profile. There are no measurements for liquids.

APPARATUS

The measurements were made by the stereoscopic photography of minute air bubbles, less than 1/1000 of an inch in diameter, moving with the liquid. The details of this technique are given elsewhere [1, 25]. The measurements were made in a 3 in. long, 1 in. diameter cell which was fitted in the middle of a vertical 10 ft, 1 in. diameter extruded perspex tube. Great care was taken to make the junction between the tube and the cell as smooth as possible. The cell was scribed internally with lines to act as a zero for readings and was then polished until it felt smooth. It was then assumed that the scratches were small enough not to affect the flow.

The tube was held on an angle iron frame firmly bolted to the laboratory wall and vibration was minimized by having all the moving parts mounted on a separate frame resting on rubber blocks.

A 15 in. × 15 in. × 30 in. galvanized iron tank

was used as a sump. From this the water was pumped to a constant head tank of the same size fitted with perforated zinc sheets to prevent swirl. The perspex tube was fitted directly into the bottom of the tank and led to a bank of rotameters and then back to the sump. No effort was made to smooth the junction between the tube and the tank as Deissler [15] found that the steady state was reached sooner in these circumstances. He gives 45 diameters as a sufficient entry length. These measurements were made at 60 diameters.

The air bubbles were formed by bleeding a small amount of air from an aspirator bottle into the pump. During the residence in the head tank the large bubbles rose to the surface and only the very small ones went down the tube.

Experimental Work

Runs were made at Reynolds numbers of 1200, 12,000 and 19,000. The first was laminar and was made merely to get an estimate of the scatter of the method. The other two were turbulent. The results are shown in Figs. 1, 2 and 3.

Though it was possible to measure the flow rates and temperatures with sufficient accuracy it was not possible to control them to that accuracy. Consequently the results for any one run were taken at various Reynolds numbers (e.g. 18,500–19,500 for Run 3). As the results, in their dimensionless form, should be insensitive to Reynolds number this should be of no consequence.

The flow rates were measured by rotameters which were calibrated frequently by timing the water into a measuring cylinder or a tank resting on a 10 cwt balance. The temperature was measured to 0·1°C at the top and bottom of the tube. There was found to be no difference in these temperatures. The viscosity of the water was measured at 25°C by an Ostwaldt viscometer. The result was the same as that quoted by Perry [26] so his values of viscosity were taken at other temperatures.

It was not possible to measure the skin friction directly. The small pressure drop due to this would have been masked by the unknown change in density due to the air bubbles. The results were therefore made non-dimensional by the shear-stress calculated from Moody's [27] data. Moody claims an accuracy of $\pm$ 5 per cent which places an upper limit on the accuracy of these experiments.

The method of measurement gives the velocities of individual bubbles. These can be considered as instantaneous velocities of elements of the fluid, because the bubbles are so small as to have negligible drift velocity. Since the flow is turbulent a range of velocities will be found at any section. To find the mean velocity the instantaneous readings were arranged in order of increasing y^+ and divided into groups of 20. The mean distance, y^+, and the root mean square velocity $\tilde{u}^+$ were found and plotted in Fig. 4. The root mean square was thought to be the more relevant mean for the velocity as the results would then be in line with those obtained with Pitot tubes or other devices that give root mean square velocities directly. In Run 3 the v (normal) and w (circumferential) components of velocity were also measured. A distinction is made in Fig. 3 between those bubbles moving with appreciable velocity to or from the wall, showing a general correlation between u high and v negative, i.e. a bubble moving towards the wall has a greater longitudinal velocity than one moving away from it.

Discussion

Fig. 1 shows that the results for the laminar flow lie on a smooth curve. The entry length of 60 diameters is less than the generally accepted [26] value for flow at a Reynolds number of 1,200 so a slight deviation from the theoretical parabola was expected and was in fact found. The smoothness of the curve makes it clear that the scatter in Fig. 2 and 3 is due to turbulence and not experimental error.

It is clear from Fig. 4 that 20 points are insufficient to give a reliable average. Many more points would be needed but this was impracticable due to the slowness of the method of measuring the velocities. The number was however sufficient to determine the order of magnitude of the mean velocity which was all that was expected of the method.

VOL. 16 1962

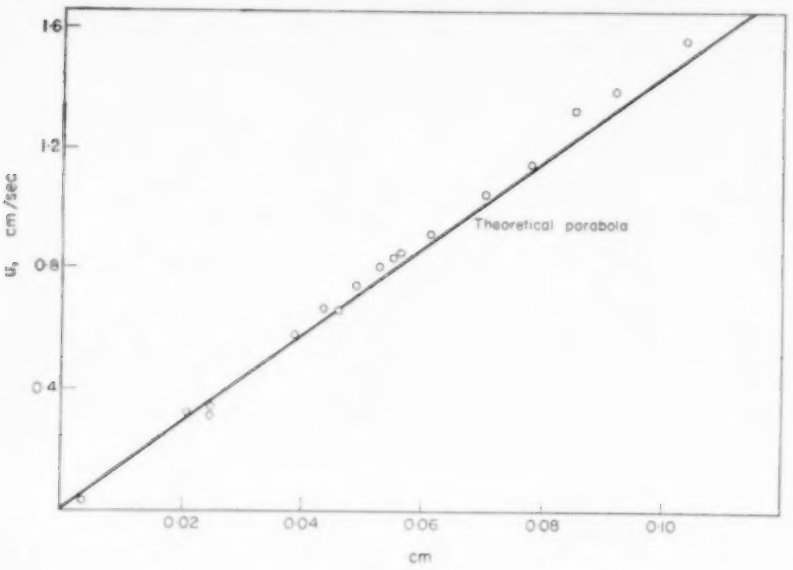

FIG. 1. Velocity profile Re = 1200

Fig. 4 shows that there is a difference in the mean dimensionless velocities of the two runs which is beyond the scatter of either. This is just within the uncertainty of MOODY's expression for the pressure-drop, but this explanation seems unlikely. The effect could be caused by the velocity profile being a function of Reynolds number. At low Re's this is so, the profile

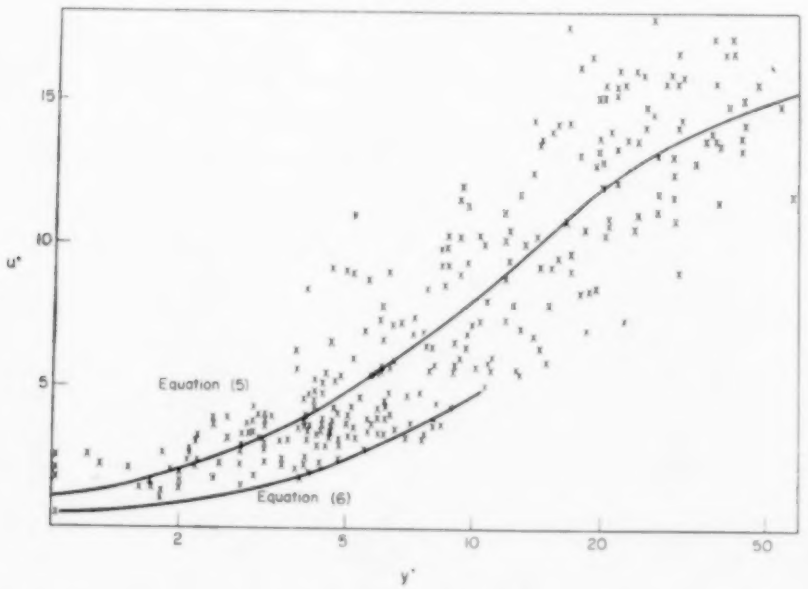

FIG. 2. Instantaneous velocities Re = 12,000.

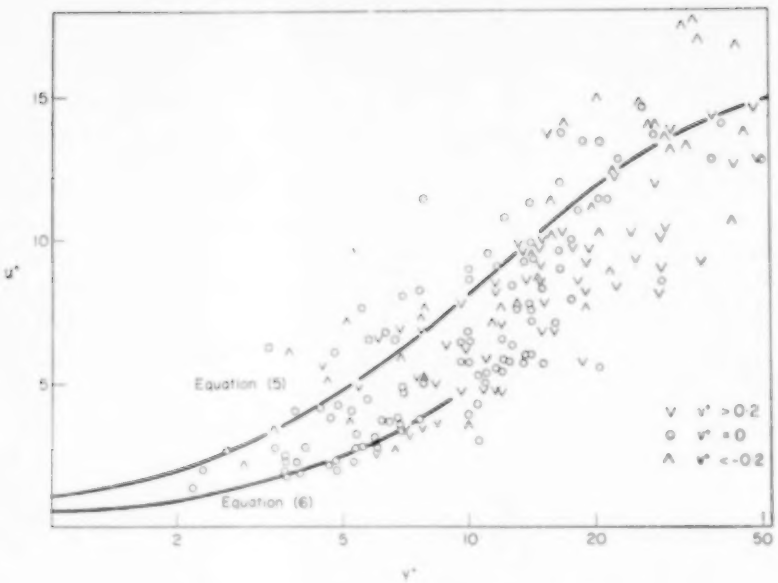

FIG. 3. Instantaneous velocities Re = 19,000.

becoming independent of Reynolds number assymptotically at high Reynolds numbers. However, it is the results at the lower Reynolds number (Run 2) which are in the best agreement with SLEICHER's profile for high Reynolds numbers, suggesting that both the Reynolds numbers were high enough to give the limiting profile. It seems therefore that, unless there is

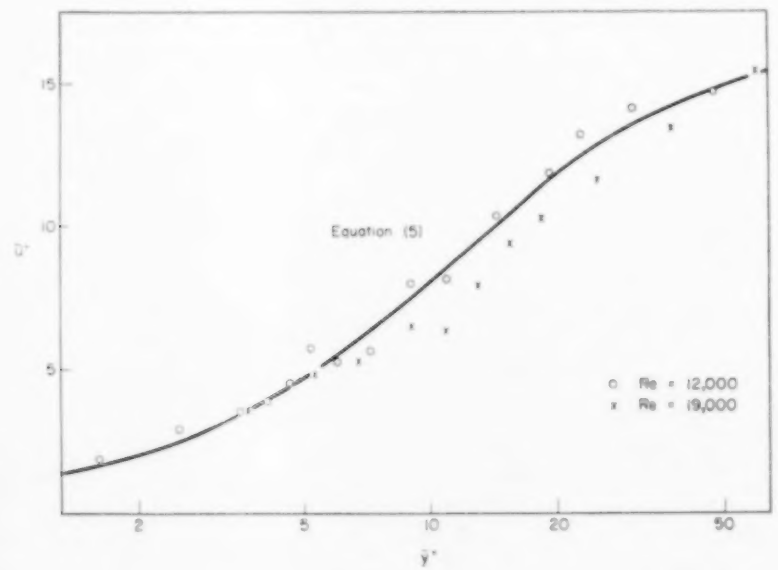

FIG. 4. Mean velocities.

an error in the estimation of the wall shear stress, there must be a systematic but unidentified error in one or both of the runs but probably in Run 3. Great as this error seems it is only 50 per cent higher than the scatter in the best results for air and is less than the scatter in some previous results.

Figs. 2 and 3 show the instantaneous velocities. These form a wedge around equation (5) as expected. There are velocity fluctuations below $y^+ = 3$ showing that the flow here is not steady, though the mean velocities (Fig. 4) lie close to the laminar profile of $u^+ = y^+$, showing that the eddy viscosity is small. It can also be seen from Fig. 2 that EINSTEIN and LI's prediction of the least velocity at any section is quite accurate. The agreement is not so good in Fig. 3 but this is consistent with the general lowness of the results for that run.

VOL. 16 1962

It can be seen from Fig. 2 that there is a shortage of low velocities in the region $y^+ < 3$. This causes the mean velocities to lie above $u^+ = y^+$, implying a negative eddy viscosity – an impossible situation. It is well known that in shear flow there is a repulsion of particles from the wall, causing a gradient in the particle concentration. This is discussed by SAFFMAN [28] though he is unable to explain the effect. In a region where a gradient in particle concentration exists eddies moving towards the wall are much more likely to contain a bubble than those moving away. Hence any flow visualization technique is biased towards bubbles moving in the direction of the wall, and hence towards high velocities.

The field of view of the cameras was approximately 5 mm × 5 mm × 1 mm and so several bubbles were found on each pair of photographs. It was found that these velocities were not correlated with each other, that is to say, on no pair were all the velocities either high or low, showing that the eddies were smaller than the field of view. It is not clear from the work of EINSTEIN and LI over what area their growing layer exists but the implication is that it is large. This is contradicted by the above result. On a few occasions two bubbles were found, one directly behind the other, in which the one further from the wall had the lower velocity. This situation cannot occur on the EINSTEIN–LI model. Similar criticisms can be applied to the KLINE–RUSTADLER theory; the experiments showing that if islands of hesitation exist they are less than 1 mm high or 5 mm across. The results seem to be best explained by the concept of small random eddies.

CONCLUSION

The velocities in turbulent liquid pipe flow were measured in the region $1 < y^+ < 30$. It was found that the velocities, in their non-dimensional form, could not be distinguished from velocities measured in air by other people. It is concluded that SLEICHER's profile is the best correlation of the results.

All previous measurements on the wall region have been made using hot-wire anemometers. Stereoscopic photography is a more fundamental method and this work provides a useful independent check on the validity of hot-wire anemometry in this region.

Acknowledgements—I wish to thank my supervisor, Professor T. R. C. FOX, for suggesting this problem and for much help and guidance throughout the work. I would also like to thank the workshop staff of the Chemical Engineering Department, Cambridge, for help in setting up the apparatus, and the Esso Petroleum Company for financial assistance.

NOTATIONS

A = experimental constant
B = experimental constant
u = velocity in downstream direction
v = velocity normal to tube wall
w = circumferential velocity
y = distance normally from tube wall
ϵ = eddy viscosity
μ = absolute viscosity
ρ = density
τ_0 = wall shear stress

Superscripts

$+$ = dimensionless form
$-$ = arithmetic mean
$\sim$ = root mean square

References

[1] Nedderman R. M. Ph.D. Thesis, Cambridge 1960.
[2] von Karman T. *Trans. Amer. Soc. Mech. Engng.* 1939 **61** 705.
[3] Prandtl L. *Z. angew. Math.* 1925 **5** 136.
[4] von Karman T. *Proc. 3rd Int. Congr. App. Mech Stockholm* 1930 p. 85
[5] Hinze J. O. *Turbulence* New York 1959.
[6] Millikan C. B. *Proc. 5th Int. Congr. App. Mech. Cambridge, Mass.* 1938 p. 386.
[7] Nikuradse J. *Z. Ver. dtsch. Ing.* 1933 361.
[8] Laufer J. N.A.C.A. T.R.1174 1954.
[9] Reichardt H. *Z. angew. Math.* 1925 **5** 136.
[10] Elrod H. G. *J. Aero. Sci.* 1957 **24** 468.
[11] Townsend A. A. Private Communications.
[12] Hama F. R. *J. Aeronaut. Sci.* 1950 **20** 648.
[13] Squire H. B. *Phil. Mag.* (7) 1948 **39** 1.
[14] Rotta, J. *Ing. Arch.* 1950 **18** 277.
[15] Deissler R. G. N.A.C.A. T.N.2138 1950.
[16] Deissler R. G. N.A.C.A. T.N.3145 1954.
[17] Miles J. W. *J. Aeronaut. Sci.* 1957 **24** 704.
[18] van Driest E. R. *Heat Trans. and Fluid Mech. Inst. Los Angeles* XII 1955.
[19] Einstein H. A. and Li H. *Heat Trans. and Fluid Mech. Inst. Los Angeles* XIII 1955.
[20] Dunn L. G. *3rd Anglo-Amer. Aero. Conf. Brighton* 1951.
[21] Schlinger W. G., Berry V. J., Mason J. L. and Sage B. H. *Industr. Engng. Chem.* 1958 **45** 663.
[22] Sleicher C. A. *Trans. Amer. Soc. Mech. Engng.* 1958 **80** 693.
[23] Kline S. J. and Runstadler P. W. *J. Appl. Mech.* 1959 **26** 166.
[24] Shigemitsu R. *J. Phys. Soc. Japan* 1957 **12** 183.
[25] Nedderman R. M. (in press).
[26] Perry J. H. *Chemical Engineers Handbook* New York 1950.
[27] Moody L. F. *Trans. Amer. Soc. Mech. Engng.* 1944 **66** 671.
[28] Saffman P. G. Ph.D. Thesis, Cambridge 1957.

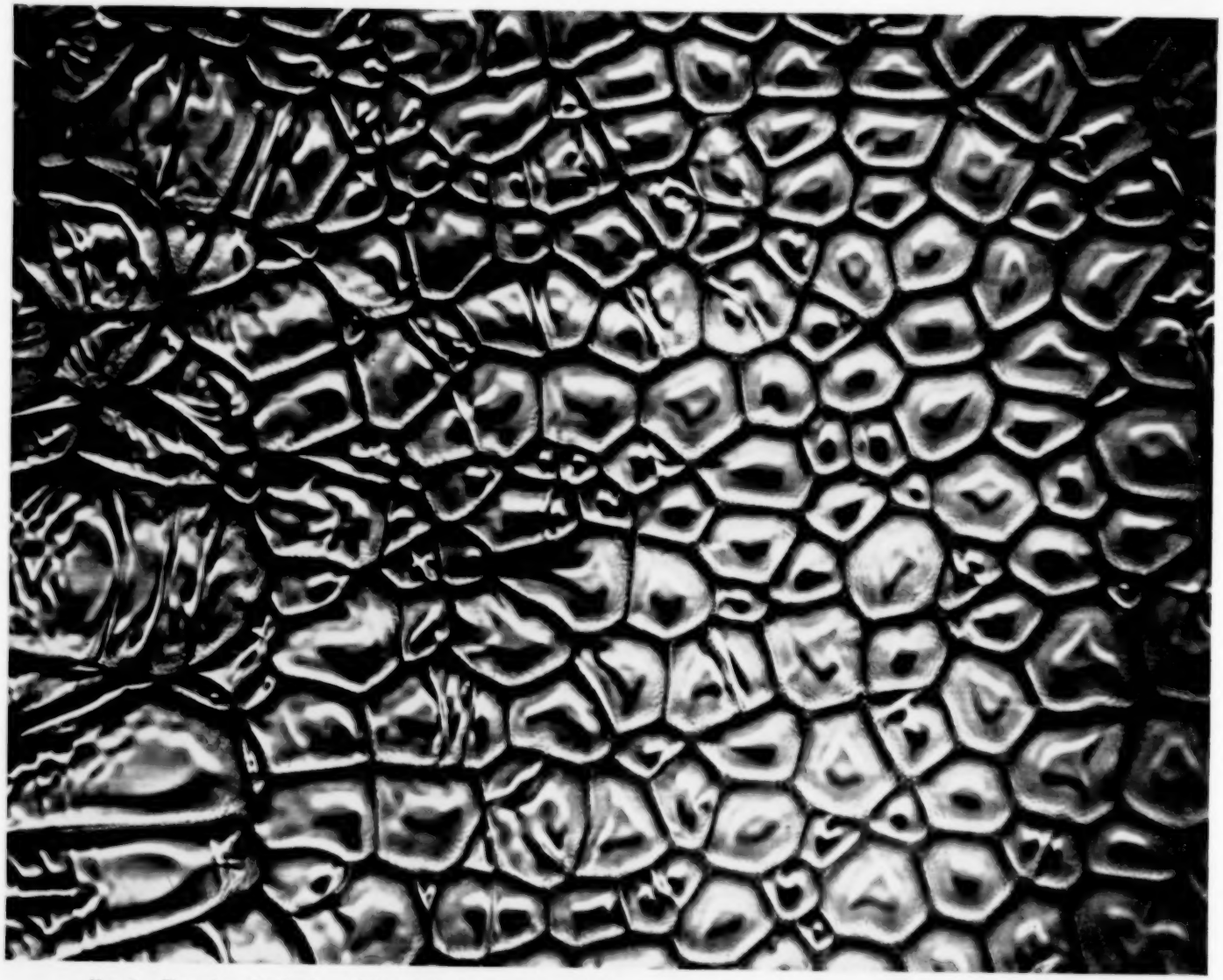

FIG. 1. Top view of a horizontal liquid–liquid interface exhibiting an organized cellular pattern accompanying mass transfer. Upper phase: ethyl acetate; lower phase: 10 per cent acetic acid in ethylene glycol. Schlieren photograph taken 13 min after forming the interface. Field of view is 1·4 cm × 1·1 cm.

VOL
16
196

FIG. 2. Elongated stripes at 16 hr. Test conditions and magnification are the same as in Fig. 1.

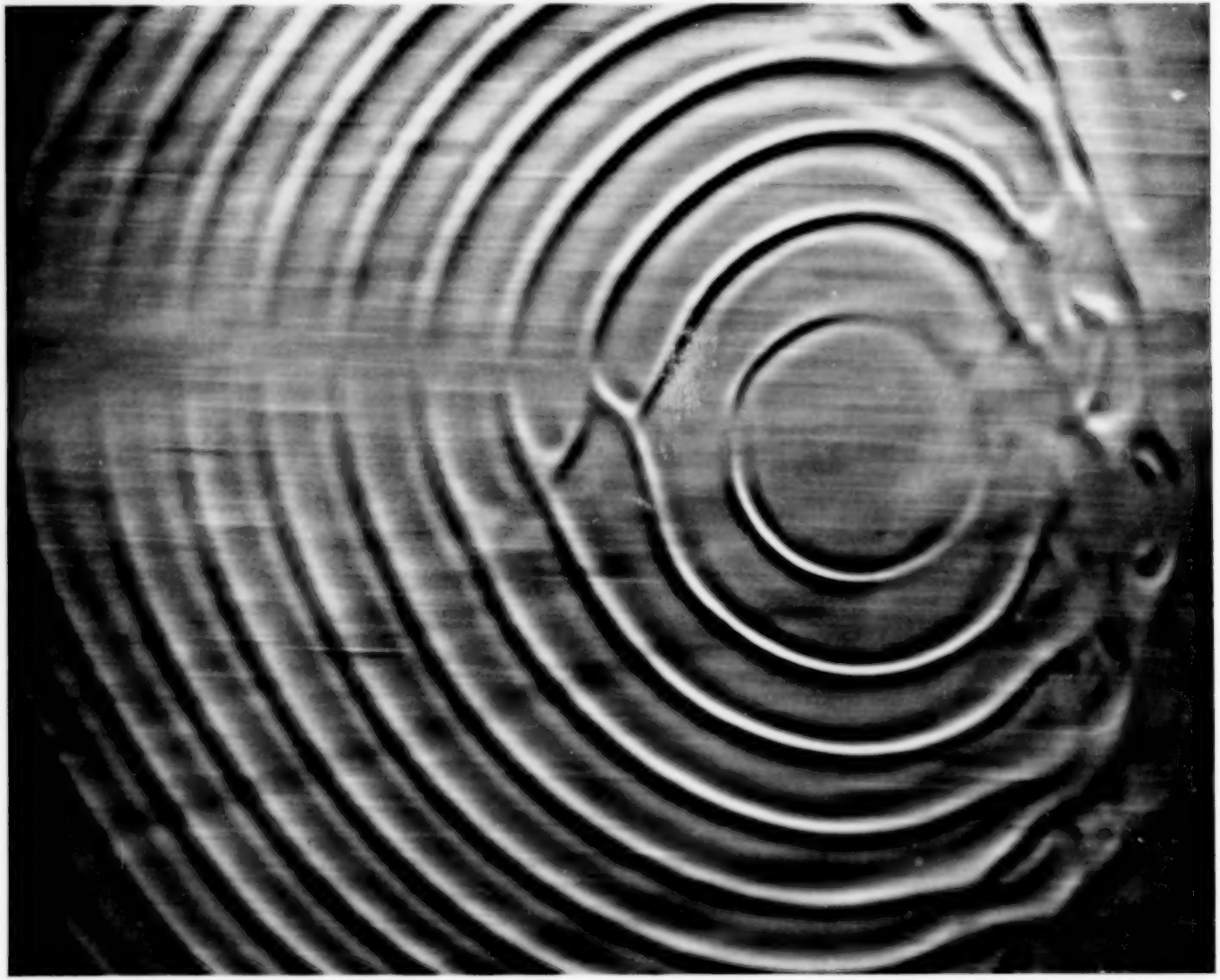

FIG. 3. Slow, concentric ripples are the last stage of organized interfacial activity. The interface is the same as in Fig. 2, 54 hr. after its formation.

VOL. 16
1962

Chemical Engineering Science, 1961, Vol. 16, p. 127. Pergamon Press Ltd., London. Printed in Great Britain

Shorter Communications

Natural convection cells accompanying liquid-liquid extraction

(*Received* 9 *June* 1961)

THE TRADITIONAL description of mass transfer in liquid–liquid extraction uses a two-film model. Although the two-film theory is adequate for prediction of transfer rates in many ternary systems, a number of exceptions have been documented [1]. The latter systems exhibited abnormally high rates that could not be explained on the basis of pure molecular diffusion. It was found later that the high rates were caused by interfacial turbulence – spontaneous agitation of the interface between two unequilibrated liquid phases.

Theoretical treatment of the phenomenon was lacking until recently when STERNLING and SCRIVEN formulated their theory of organized interfacial motion in a flat interface. Their imaginative paper [2] received wide attention, and the Colburn Award of the American Institute of Chemical Engineers was granted to these authors as a result.

STERNLING and SCRIVEN predict that spontaneous interfacial flows can occur organized in a cellular pattern. The basic unit of flow is a roll cell within which liquid is circulating. The roll cells are presumed to be analogous to BÉNARD cells for heat transfer which are exhibited by an unconfined, horizontal, thin layer of pure liquid heated from below. BÉNARD proved the existence of heat transfer cellular convection by still photography [3].

Interfacial turbulence has been observed by a large number of investigators. In all cases but one the phenomenon was found to be a disorganized and chaotic process. Recently LINDE [4] photographed the interface of the system isoamyl alcohol-sodium cetyl sulphate-water in profile and was able to record a single roll cell with a wave length of about 17 mm.

The object of the experimental work described herein is to investigate the existence and characteristics of cellular motion during mass transfer.

In the present study interfacial activity is recorded by motion picture and still photography using the Schlieren technique. The cameras are aimed straight down viewing a flat 65 × 85 mm interface between two liquid phases at room temperature. The lower phase, 15 mm thick, consists of a solution of acetic acid in ethylene glycol. Ethyl acetate forms the 17 mm thick upper phase. The ternary system used here is of Type I. It is not subjected to any form of forced convection during the tests.

The Sternling–Scriven theory predicts that this system should exhibit roll cells. Fig. 1 proves the existence of a network of polygonal cells on the interface itself. An analysis of the schlieren motion pictures indicates that, in the heavy phase, liquid rises in the centre of these polygonal cells, reaches the interface, and flows radially outward to sink down at the cell boundaries.

Polygonal cells are found to be either stationary, occupying a fixed position, or propagating across the interface. Both types increase their size with time, in accordance with theory. Average cell size ranges from 0·04 to 0·14 cm. These sizes are within 50 per cent of the predicted roll cell wave lengths.

As time passes the cells not only increase their size but also change to elongated stripes which appear in clusters as shown in Fig. 2. After a long time this pattern evolves into slow-moving, widely spaced concentric ripples (Fig. 3). These become fainter and fainter and finally disappear as the system approaches equilibrium. Interfacial activity has been observed to last as long as 72 hr.

Patterns similar to Figs. 1 and 2 were observed by BÉNARD for heat transfer. The ripples in Fig. 3 however are unexpected either from the Sternling-Scriven theory or from previous observations.

Experimental work in this study is continuing and will be reported in due time.

E.I. du Pont de Nemours and Company
New Johnsonville, Tennessee

Department of Chemistry and Chemical Engineering
University of Illinois ALUF ORELL
Urbana, Illinois. J. W. WESTWATER

REFERENCES

[1] LEWIS J. B. *Chem. Engng. Sci.* 1954 **3** 260.

[2] STERNLING C. V. and SCRIVEN L. E. *A.I.Ch.E. Journal* 1959 **5** 514.

[3] BÉNARD H. *Rev. gen. Sci. pur. appl.* 1900 **11** 1261, 1309.

[4] LINDE H. *Fette, Seifen, Anstrichmittel* 1958 **60** 826.

Chemical Engineering Science, 1961, Vol. 16, pp. 128 to 134. Pergamon Press Ltd., London. Printed in Great Britain.

Letters to the Editors

Heat transfer coefficients at the entry to the heating section

(*Received* 3 *February* 1961)

In a recent investigation [1] of heat transfer to aqueous suspensions of spherical particles both when fluidized and during hydraulic transport the possibility was considered of calculating the heat transfer coefficients from the temperature gradient in the pipe wall immediately upstream from the heating section. Heat is transferred by conduction along the tube-wall away from the heating section, and, in the steady state, the longitudinal temperature gradient will be a function principally of the heat transfer coefficient to the fluid or suspension and the thermal conductivity of the wall material.

The following derivation applies in the steady state, and takes into account the effect of the rise in temperature of the fluid and the effect of fluid back-mixing.

The fluid is assumed to flow from $y = \infty$ towards the heat source, and the mean fluid and the wall temperatures θ_f and θ_w, respectively, are assumed to be equal to each other at $y = \infty$, where they are arbitrarily assigned the value of zero. Hence θ_f and θ_w are, respectively, the rise in the mean temperature of the fluid and the temperature of the wall from infinity to y. The temperature θ_f of the fluid at y is taken to be the conventional bulk mean, i.e., the temperature if the fluid at y were perfectly mixed. The average temperature of the element of fluid shown in Fig. 1 will change because of heat transfer from the walls and because of the conduction of heat axially through the fluid. The change may be expressed in differential form by

$$\frac{\pi D_i^2}{4} C \rho u \frac{d\theta_f}{dy} = \frac{\pi D_i^2 k_f}{4} \frac{d^2\theta_f}{dy^2} + \pi D_i h (\theta_w - \theta_f). \quad (1)$$

The amount of heat flowing into the wall segment bounding the element must equal the amount of heat flowing out plus the heat transferred to the fluid and hence

$$\frac{k\pi (D_0^2 - D_i^2)}{4} \frac{d^2\theta_w}{dy^2} = + \pi D_i (\theta_w - \theta_f). \quad (2)$$

Equations (1) and (2) may be combined by differentiation of (2) and simplified to yield

$$\frac{k_f kb \left[1 + (b/D_i)\right]}{C \rho u h} \frac{d^4\theta_w}{dy^4} - \frac{kb}{h} \left[1 + (b/D_i)\right] \frac{d^3\theta_w}{dy^3} - \left\{ \frac{k_f}{C \rho u} - \frac{4kb \left[1 + (b/D_i)\right]}{C \rho u D_i} \right\} \frac{d^2\theta_w}{dy^2} + \frac{d\theta_w}{dy} = 0. \quad (3)$$

The exact solution of this equation to determine h is possible, but is extremely tedious without the aid of a computer.

However, if $\theta_f \ll \theta_w$, equation (2) may be solved directly, and, provided the wall thickness is small compared with the pipe diameter, may be written

$$\frac{d^2\theta_w}{dy^2} - \frac{h}{kb} \theta_w = 0. \quad (4)$$

By applying the boundary conditions $d\theta_w/dy = 0$ at $y = \infty$ and $\theta_w = \theta_{wi}$ at $y = 0$, the solution in terms of θ_w is found to be

$$\theta_w = \theta_{wi} \exp\left[-\sqrt{(h/kb)}\, y\right] \quad (5)$$

where h is assumed to be constant. If the effect of axial back-mixing is small, the heat transferred to the fluid from ∞ to y will be equal to the heat flow down the pipe-wall at y, and hence θ_f, the mean fluid temperature, may be determined:

$$q_w = k \pi D_i b \sqrt{\left(\frac{h}{kb}\right)} \theta_w = \pi D_i \sqrt{(hkb)}\, \theta_w \quad (6)$$

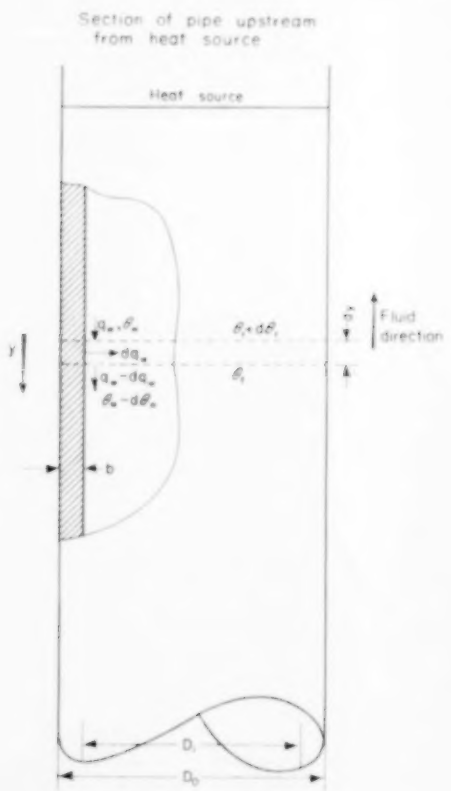

Fig. 1.

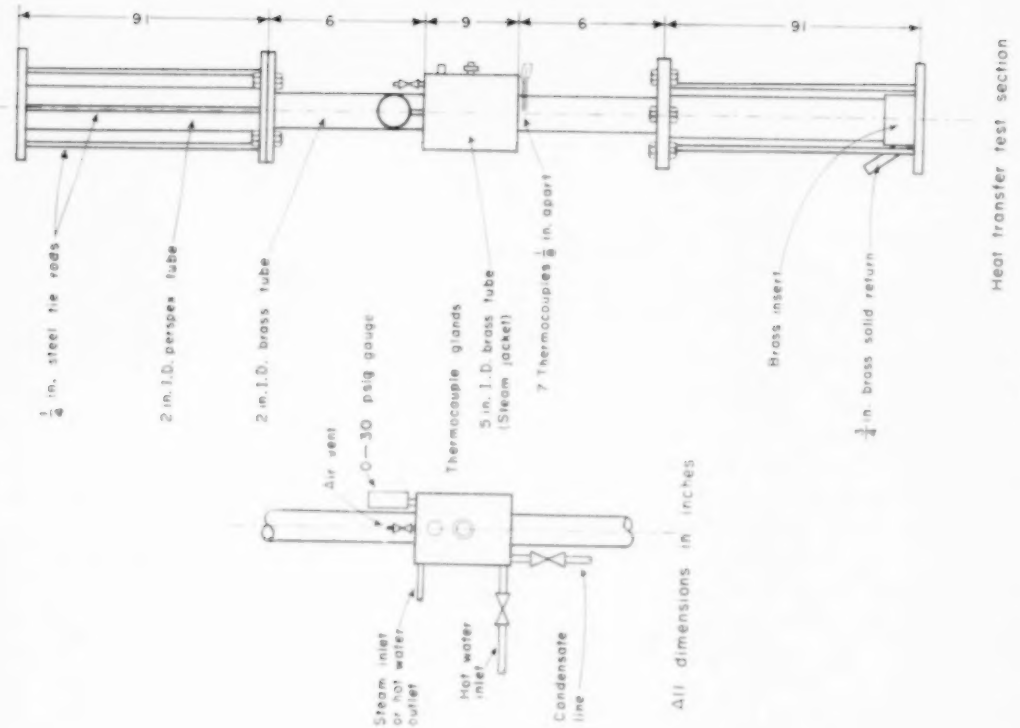

Fig. 2.

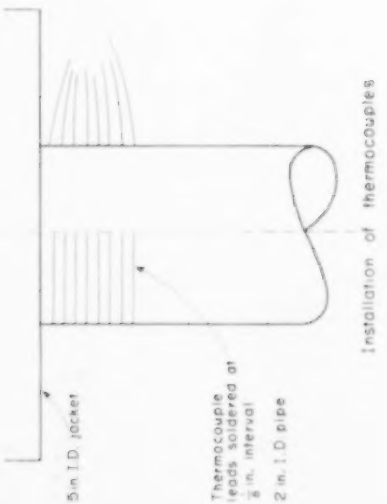

Installation of thermocouples

Fig. 3.

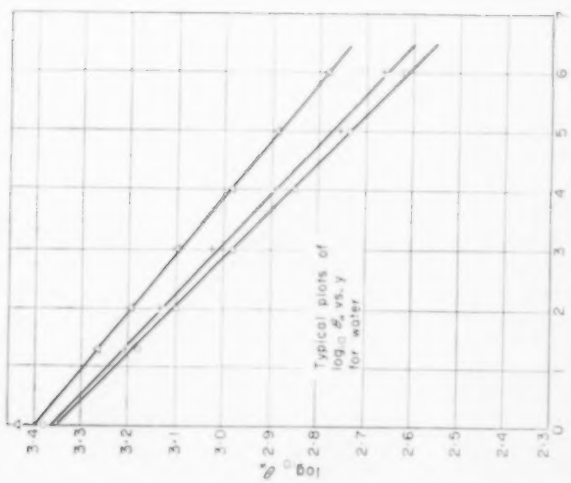

Fig. 4.

and $$\theta_f = \frac{4\sqrt{(h\,k\,b)}}{C\,\rho\,u\,D_i}\,\theta_w. \qquad (7)$$

In the practical case of the turbulent flow of liquids $C\,\rho\,uD_i$ is usually very large relative to $4\sqrt{(hkb)}$ and hence θ_f is very small with respect to θ_w. Although θ_w is theoretically equal to θ_f only at infinity, in practice it will be indistinguishable from θ_f at only a few pipe-diameters below the heating section, and the pipe need not be very long for equation (5) to be valid.

The apparatus shown in Fig. 2 was constructed to check heat transfer coefficients calculated by means of equation (5) against those obtained by conventional methods. The heat-transfer section of this apparatus consists of a 2 in. i.d. brass tube fitted with a 5 in. i.d. brass steam-jacket. The wall temperature θ_w was measured by means of seven copper–constantan thermocouples mounted at $\frac{1}{8}$ in. intervals below the jacket. The leads were wound around the circumference of the pipe as shown in Fig. 3 in order to minimize the effects of conduction.

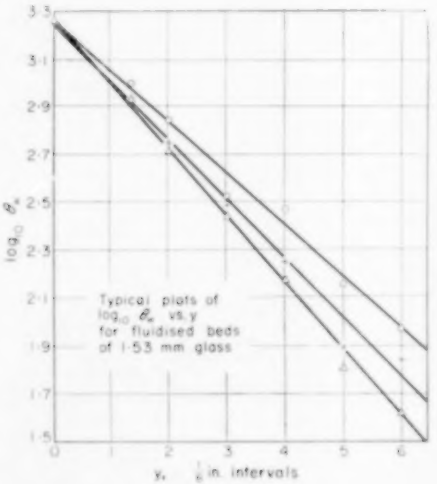

Fig. 5.

Experimental measurements were made of the wall temperature θ_w for a series of runs at different velocities both with water alone and with a system of 1·53 mm glass spheres fluidized in water. The heat transfer coefficient was determined from the slopes of plots of $\log_{10}\theta_w$ against y, which should be linear for constant h according to equation (5). The slope of the curves will be equal to $-(1/2{\cdot}303)\sqrt{(h/bk)}$, from which h may be computed. Typical plots of $\log_{10}\theta_w$ against y are given in Fig. 4 for water, and in Fig. 5 for the fluidized system. It is seen that the plots are linear, indicating that over the short distance considered ($\frac{1}{8}$ in.) h is constant. A logarithmic plot of the heat transfer coefficient h against velocity u is given in Fig. 6 for water (Curve A). It is seen

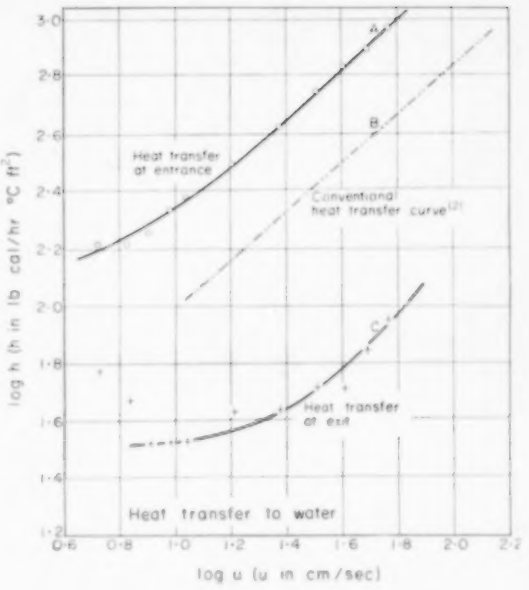

Fig. 6.

that the slope of the curve is 0·8, as expected, but that the actual values of the heat transfer coefficient are about double those obtained by conventional means [2] and predicted by equation (8) (Cufve B).

$$\frac{hD_i}{k_f} = 0{\cdot}023\left(\frac{D_i u\,\rho}{\mu}\right)^{0{\cdot}8}\left(\frac{C\,\mu}{k_f}\right)^{0{\cdot}4} \qquad (8)$$

Also plotted in Fig. 6 (see curve C) are some values of the heat transfer coefficient which were calculated using equation (5), but where the thermocouples were located downstream from the heating section. In this case, if both the heat in the wall and the fluid are now considered to be flowing from 0 to ∞, i.e. if the axis is reversed, and if $\theta_w = \theta_f = 0$ at infinity, equation (2) will still be valid, as will the solution given by equation (5) because once again $\theta_f < \theta_w$. These values are more scattered, but the average values are much *less* than those obtained by conventional means.

Very similar results were obtained from the measurements with fluidized beds, where the coefficients obtained at the entry to the heating section were found to be more than twice as great as those obtained by the conventional method (Fig. 7).

These phenomena are readily explained, since, at the entry to the heating section, the thermal boundary layer has not reached an equilibrium thickness, and hence the heat transfer coefficient in that region is greater than that under conditions of fully developed flow. At the exit to the heating section, on the other hand, the thermal boundary layer is already formed, and the heat transfer coefficients measured are much less than the average in

the heating section because the presence of the hot laminar sub-layer prevents the temperature decay in the wall.

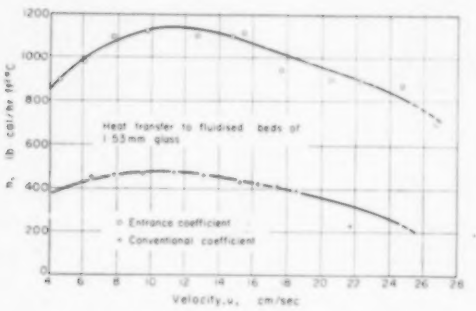

FIG. 7.

These results show how local values of the heat transfer coefficient can differ from the average values, and illustrate the approximate nature of the model based on the bulk mean temperature difference $(\theta_w - \theta_f)$.

Equation (6) may be used to determine when a correction for end-effect error should be included in the conventional method for determining heat transfer coefficients. Usually q_w will be very small compared with the total heat input, but under certain conditions (e.g. where b and D_i are large and θ_w high and where the heating section s very short), q_w may be significant compared with the total heat input and a correction should be made.

Acknowledgments—The author is indebted to Professor D. M. NEWITT, in whose laboratories this work was carried out, to Mr. Th. W. WILLEMSE, Delft, for his valuable suggestions, and especially to Professor J. F. RICHARDSON, Swansea, for his constant supervision, help and encouragement. Thanks are also due to the National Research Council of Canada for a Special Overseas Scholarship which was held during the course of the work.

NOTATION

b	= wall thickness	L
C	= heat capacity of fluid	$HM^{-1}\theta^{-1}$
D_i	= Internal diameter of pipe	L
D_0	= External diameter of pipe	L
h	= heat transfer coefficient	$HL^{-2}T^{-1}\theta^{-1}$
k	= Thermal conductivity of wall material	$LH^{-1}T^{-1}\theta^{-1}$
k_f	= Longitudinal conductivity of fluid	$HL^{-1}T^{-1}\theta^{-1}$
q_w	= Rate of heat flow down tube-wall	HT^{-1}
u	= Velocity of fluid in the y direction	LT^{-1}
y	= distance from heat source	L
θ_f	= fluid temperature, = 0 at $y = \infty$	θ
θ_w	= wall temperature, = 0 at $y = \infty$	θ
ρ	= density of fluid	ML^{-3}
μ	= viscosity of fluid	$ML^{-1}T^{-1}$

Department of Chemical Engineering,
Imperial College, London, S.W.7.

J. W. SMITH*

*Present address: *Department of Chemical Engineering,*
University of British Columbia, Vancouver 8, B.C., Canada.

REFERENCES

[1] RICHARDSON J. F. and SMITH J. W., *Trans. Inst. Chem. Engrs.* 1961. To be published.
[2] MCADAMS W. H., *Heat Transmission* (3rd Ed.) p. 228. McGraw–Hill, New York 1954.

A note on boundary conditions for flow reactors

(*Received* 22 *May* 1961)

THE PROPER boundary conditions to use for flow reactors with diffusion has received much discussion in recent years. DANCKWERTS [2] discussed the case of no diffusion in the sections leading into and out of the chemical reactor, with a first-order reaction occurring. The boundary condition at the reactor entrance was taken to be (see Fig. 1),

$$c_0 = c_1(O^-) = c(O^+) - \frac{D}{u}\frac{dc(O^+)}{dz} \qquad (1)$$

This was obtained by a mass balance, and yields a discontinuity in the concentration at this point. Since there is no diffusion in the entrance section, the concentration is constant throughout the section, and equation (1) can be written as,

$$c_1(-\infty) = c_0 = c(O^+) - \frac{D}{u}\frac{dc(O^+)}{dz} \qquad (2)$$

where $c_1(-\infty)$ is the concentration at some point upstream of the reactor entrance. The boundary condition at the outlet was taken to be

$$\frac{dc(L^-)}{dz} = 0 \qquad (3)$$

This was obtained from a mass balance by intuitive reasoning.

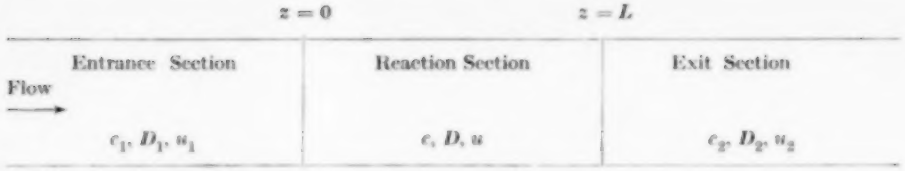

FIG. 1.

PEARSON [6] later showed that the boundary conditions used by Danckwerts for this case are the proper ones by re-solving the problem with a diffusion coefficient that varied continuously throughout the entrance, reaction, and exit sections. This coefficient was chosen such that in the limit it approached the discontinuous one used by Danckwerts. Pearson then showed that the continuous solution approached the solution of Danckwerts in the limit, thereby justifying Danckwerts' boundary conditions. ARIS and AMUNDSON [1] also deduced equation (1) from probability considerations.

WEHNER and WILHELM [7] considered the more general problem of arbitrary values of diffusion coefficients in each section. This situation is more logical from a physical point of view since diffusion effects are never completely absent in any part of a real system. By solving three simultaneous differential equations for the entrance, reaction, and exit sections with a first-order chemical reaction occurring, they obtained analytical solutions for each section. From these solutions, the following conclusions were obtained:

1. at the entrance boundary, the total flux is always given by equation (2) for any (finite) values of the diffusion coefficients. Note that with diffusion in the entrance section, $c_1(-\infty) \neq c_1(O^-)$, so that equation (1) is not true for $D_1 \neq O$.

2. At the exit boundary, equation (3) is true, again for any (finite) values of the diffusion coefficients. The solution for the reaction section is independent of the conditions in the inlet and outlet sections and thus the differential equation for the reaction section can be solved by itself with equations (2) and (3) to give the same result as would be obtained from the simultaneous solution of the differential equations for all three sections.

All of the preceding work was done for only first-order chemical reactions, since complete analytical solutions cannot be obtained for other cases because of the non-linearity of the differential equations. The numerical solution of the three simultaneous differential equations for a non-linear reaction would be tedious, and so authors dealing with these non-linear cases have assumed that the conclusions obtained by Danckwerts or Pearson, or by Wehner and Wilhelm were true in general [3, 4, 5].

We shall now show that the conclusions reached by Wehner and Wilhelm are true for any order of reaction. The equations to be solved are,

$$\frac{D_1}{u_1}\frac{d^2c_1}{dz^2} - \frac{dc_1}{dz} = O \qquad z < O \tag{4}$$

$$\frac{D}{u}\frac{d^2c}{dz^2} - \frac{dc}{dz} = f(c) \qquad O < z < L \tag{5}$$

$$\frac{D_2}{u_2}\frac{d^2c_2}{dz^2} - \frac{dc_2}{dz} = O \qquad z > L \tag{6}$$

with the general boundary conditions,

$$c_1(-\infty) = c_0 \tag{7}$$

$$c_1(O^-) = c(O^+) \tag{8}$$

$$c_1(O^-) - \frac{D_1}{u_1}\frac{dc_1(O^-)}{dz} = c(O^+) - \frac{D}{u}\frac{dc(O^+)}{dz} \tag{9}$$

$$c(L^-) = c_2(L^+) \tag{10}$$

$$c(L^-) - \frac{D}{u}\frac{dc(L^-)}{dz} = c_2(L^+) - \frac{D_2}{u_2}\frac{dc_2(L^+)}{dz} \tag{11}$$

$$c_2(+\infty) = \text{finite} \tag{12}$$

As stated previously, a complete analytical solution to this system of equations is not possible because of the non-linearity of equation (5). However, the solutions to equations (4) and (6) can easily be found,

$$c_1 = A_1 + A_2 e^{u_1 z/D_1} \tag{13}$$

$$c_2 = A_3 + A_4 e^{u_2 z/D_2} \tag{14}$$

In order to satisfy the boundary conditions (7) and (12)

$$A_1 = c_0$$

$$A_4 = 0$$

Thus

$$c_1 = c_0 + A_2 e^{u_1 z/D_1} \tag{15}$$

$$c_2 = A_3 \tag{16}$$

The remaining constants, A_2 and A_3, would be found from equations (8) to (11) in conjunction with the solution of equation (5). However, these constants need not be known in order to arrive at our conclusions.

From equation (15),

$$c_1(O^-) = c_0 + A_2 \tag{17}$$

$$\frac{dc_1(O^-)}{dz} = \frac{u_1}{D_1} A_2 \tag{18}$$

Substituting equations (17) and (18) into equation (9) gives,

$$c_0 = c(O^+) - \frac{D}{u}\frac{dc(O^+)}{dz} \tag{19}$$

Thus equation (2) is true for any finite value of the diffusion coefficients for any order of reaction. From equation (16),

$$\frac{dc_2}{dz} = 0$$

$$= \frac{dc_2(L^+)}{dz} \tag{20}$$

Substituting equations (20) and (10) into equation (11) gives,

$$\frac{dc(L^-)}{dz} = 0 \tag{21}$$

which is the same as equation (3).

Equations (19) and (21) show that the conclusions reached by Wehner and Wilhelm for first order reactions are also true for reactions of any order, and the assumptions used by [3, 4, 5] were correct. The advantage of using equations (19) and (21) rather than equations (7) to (12), which are true in general, is that the differential equation for the reaction section may be solved independently of those for the entrance and exit sections. Thus, rather than three simultaneous differential equations, only one must be solved, which is much easier.

Kenneth B. Bischoff
Department of Chemical Engineering
The University of Texas
Austin 12, *Texas.*

(Work done while National Science Foundation Postdoctoral Fellow at the University of Gent, Belgium).

Notation

A = integration constant
c = reactant concentration
D = diffusion coefficient
f = rate function for chemical reaction
L = length of reactor
u = velocity
z = axial coordinate

Subscripts:
0 refers to initial concentration of reactant
1 refers to entrance section
2 refers to exit section

References

[1] Aris R. and Amundson N. R. *Amer. Inst. Chem. Engrs. J.* 1957 **3** 280.
[2] Danckwerts, P. V. *Chem. Engng. Sci.* 1953 **2** 1.
[3] De Maria F., Longfield J. E. and Butler G. *Indust. Engng. Chem.* 1961 **53** 259.
[4] Fan L. and Bailie R. C. *Chem. Engng. Sci.* 1960 **13** 63.
[5] Levenspiel O. and Bischoff K. B. *Industr. Engng. Chem.* 1959 **51** 1431.
[6] Pearson J. R. A. *Chem. Engng. Sci.* 1959 **10** 281
[7] Wehner J. F. and Wilhelm R. H. *Chem. Engng. Sci.* 1956 **6** 89.

Unsteady state heat transfer in stationary packed beds

(*Received* 15 *June* 1961)

In an earlier paper under the above title in this Journal [1] we presented two sets of exact solutions to the given heat transfer problem – equations (11*a*, *b*) and (12*a*, *b*) in that paper – which analytically were perfectly equivalent. As we have learnt that in actual practice eq. (11 *a*, *b*) have distinct advantages over eq. (12 *a*, *b*), we should like to comment on our previous article as follows.

Comparison of eq. (11 *a*, *b*) and (12 *a*, *b*) shows that eq. (11 *a*, *b*) contain the arbitrary temperature distribution functions θ_1 and θ_2 as such, together with the second derivatives of the function F; eq. (12 *a*, *b*) contain the first derivatives of the arbitrary functions θ_1 and θ_2, together with the first derivatives of F.

In actual practice eq. (11 *a*, *b*) is likely to work more accurately than eq. (12 *a*, *b*), since the (empirical) functions θ_1 and θ_2 need not be differentiated.

Furthermore, the second derivatives of F, which occur in eq. (11 *a*, *b*) can be reduced to the following simple formulae:

$$\frac{\delta^2 F}{\delta Y\, \delta Z} = e^{-Y-Z} I_0(2\sqrt{YZ}) \tag{1}$$

$$\frac{\delta^2 F}{\delta Y^2} = -e^{-Y-Z}\frac{Z}{\sqrt{YZ}} I_1(2\sqrt{YZ}) \tag{2}$$

$$\frac{\delta^2 F}{\delta Z^2} = -e^{-Y-Z}\frac{Y}{\sqrt{YZ}} I_1(2\sqrt{YZ}) \qquad (3)$$

Eq. (1) follows directly from the former eq. (13). Eq. (2) and (3) follow from this eq. (1) and the derivatives with respect to Y and Z of the former eq. (7).

These three formulae* are more convenient than the first derivatives of F which occur in eq. (12 *a*, *b*). Whilst the former eq. (17 *a*, *b*) and (18 *a*, *b*) give these first derivatives with sufficient accuracy, they cannot be employed for Y and Z under 2. As the integrals in eq. (12 *a*, *b*) also extend over these low values of Y and Z, ONSAGER's more involved approximation of the derivatives or the exact power series for F has to be used as well. This complicates the application of eq. (12 *a*, *b*).

It must be concluded that, in view of the above eq. (1), (2) and (3), the solutions represented earlier by eq. (11 *a*, *b*) for the practice of numerical computation are more accurate and more convenient than eq. (12 *a*, *b*).

The modified Bessel functions $I_0(u)$ and $I_1(u)$ have been tabulated for $0 < u < 10$, e.g. by JAHNKE and EMDE (2). For higher values of the variable, which will often be of interest in these heat transfer problems, the following well-known series expansions are useful:

$$I_0(u) = \frac{e^u}{\sqrt{2\ u}}\left(1 + \frac{1}{8u} + \frac{9}{128\,u^2} + \frac{75}{1024\,u^3} + \ldots\right) \qquad (4)$$

$$I_1(u) = \frac{e^u}{\sqrt{2\,\pi\,u}}\left(1 - \frac{3}{8u} - \frac{15}{128\,u^2} - \frac{105}{1024\,u^3} - \ldots\right) \qquad (5)$$

For the present practical purposes these series may be truncated after the second term. Substitution in the above equations gives the following approximate formulae for the cases where $\sqrt{YZ} > 5$:

$$\frac{\delta^2 F}{\delta Y\,\delta Z} = K\left(1 + \frac{0{\cdot}065}{\sqrt{YZ}}\right) \qquad (6)$$

$$\frac{\delta^2 F}{\delta Y^2} = -K\sqrt{\frac{Z}{Y}}\left(1 - \frac{0{\cdot}190}{\sqrt{YZ}}\right) \qquad (7)$$

$$\frac{\delta^2 F}{\delta Z^2} = -K\sqrt{\frac{Y}{Z}}\left(1 - \frac{0{\cdot}190}{\sqrt{YZ}}\right) \qquad (8)$$

in which $K(Y, Z) = 0{\cdot}2821\, e^{-(\sqrt{Y}-\sqrt{Z})^2}(YZ)^{-1/4}$ (9)

The coefficients 0·065 and 0·190 contain small corrections for the terms ignored. This increases the accuracy of the formulae for relatively low values of $\sqrt{YZ}$. For $\sqrt{YZ} > 5$ they are less than 0·1 per cent in error.

Acknowledgement—A suggestion by Prof. H. BLISS of Yale University that it would be useful to study the possibility of using second derivatives of F, calculated from eq. (17 *a*, *b*) or (18 *a*, *b*), in eq. (11 *a*, *b*), which led us to this work, is gratefully acknowledged.

Bataafse Internationale Petroleum Maatschappij N.V.
(Royal Dutch/Shell Group) A. KLINKENBERG
The Hague, Holland. A. HARMENS

*The following limits are also of practical interest:

$$\lim_{Y=0}\frac{\delta^2 F}{\delta Y\,\delta Z} = e^{-Z} \qquad \lim_{Z=0}\frac{\delta^2 F}{\delta Y\,\delta Z} = e^{-Y}$$

$$\lim_{Y=0}\frac{\delta^2 F}{\delta Y^2} = -Ze^{-Z} \qquad \lim_{Z=0}\frac{\delta^2 F}{\delta Z^2} = -Ye^{-Y}$$

REFERENCES

[1] KLINKENBERG A. and HARMENS A. *Chem. Eng. Sci.* 1960 **11** 260.

[2] JAHNKE E. and EMDE F. *Tables of functions with formulae and curves*, 4th ed., Dover Publications, New York, 1945, p. 226.

VOL. 16 196

Chemical Engineering Science, 1961, Vol. 16, pp. 135 to 138. Pergamon Press Ltd., London. Printed in Great Britain.

Book Reviews

C. R. Buxton and H. S. Jackson: Translation from Russian for Scientists. Blackie, Glasgow 1960, 299 pp., 30s.

The value of Russian to scientists has become increasingly evident during recent years and two useful small textbooks, Maximilian Fourman's *Science Russian Course* and Dennis Ward's *Russian for Scientists*, have been published to satisfy some of the needs of technical specialists. The former consist of a short introduction to Russian grammar followed by a series of extracts relating to various fields of scientific study, while the latter provides a more detailed background to the language with exercises for the would-be translator. Both books, which are relatively cheap, include vocabularies and may therefore be used without a dictionary.

C. R. Buxton's and H. S. Jacksons' *Translation from Russian for Scientists* is a more ambitious work. Its scope is more comprehensive than that of either of the two above-mentioned books because, although entirely original, it represents an excellent combination of both and hence justifies its higher cost.

The authors have divided the book into five Sections. Section A – a little less than a third of the volume – is devoted to grammar and supplies the reader with a clear explanation of all grammatical difficulties which he is likely to encounter. It might perhaps have been helpful to beginners if this Section were printed with stress-marks on the emphasized syllables, at least in the pages allotted to Reading Practice (pp. 7–16), as this could be of great assistance to those who hope eventually to be able to pronounce as well as read Russian. In other respects this Section is admirably devised and pp. 73–89 on Word Formation, the intricacies of prefixes and suffixes etc. should be particularly valuable to scientist readers. Sections B and C provide illustrations of the lessons already taught. The former contains a graded series of Sentences for Translation (both ways) with notes and individual vocabularies incorporating cross-references to explanations listed in Section A ; in the latter the authors have prepared seventeen Annotated Texts, the first five of which are so printed as to afford the reader the maximum guidance in translation. The two final Sections contain short excerpts covering a wide variety of scientific topics, the English titles of which are given in the Contents. Section D includes ninety-two passages relating to the field of Physics and Electrical Engineering ; Section E includes a further seventy-six relating to that of Chemistry and Chemical Engineering. There are two pages of useful abbreviations, a full vocabulary and an index.

The book is well produced and has very few misprints.

P. S. Squire

Radioactive Wastes—Their Treatment and Disposal. Edited J. C. Collins. E. and F. Spon, London 1960. xxi + 239 pp. 55s.

The rapid developments which have taken place in the last two decades in the field of atomic energy, whether in the operation of nuclear reactors and the associated irradiated fuel chemical separation plants, or in the widespread use of radioactive isotopes in industry, research laboratories and in hospitals, have lead to difficulties in disposing of increasingly large quantities of radioactive waste. This may be gaseous, liquid or solid and each presents special problems and may lead to dangers to present and future generations. This book which explains the problems and describes the methods which are at present in use for radioactive waste disposal, is intended for civil, municipal and chemical engineers, factory inspectors, medical officers of health, industrial chemists and biologists who are concerned with disposal of our domestic and industrial wastes. It is particularly appropriate at a time when legislation to deal with all aspects of the handling of radioactive materials is under consideration.

Mr. J. C. Collins, Lecturer in Civil Engineering at Manchester University, is the General Editor of the book which contains ten chapters each written by experts in their particular subject. The first four chapters deal very adequately with necessary background information. Thus the first chapter describes the nature of radioactivity, decay processes and units. This is followed by a survey of the sources of radioactive wastes, a very good chapter on radiological hazards and a description of the various methods available for the assay of radioactivity. The rest of the book is devoted to methods of disposal ; liquids, solids and gases are covered separately. Special mention should be made of the chapter dealing with the present and proposed legislation concerning users of radioactive materials.

The treatment is mainly descriptive and is such that it is very suitable for the professional persons for whom it is intended. The chemical engineer who is new to the subject will find it useful for background information but, if he wishes to consider radioactive effluent plant design, it will be necessary to go to the extensive literature which is now available and to which reference is made at the end of chapters.

It seems a pity that so little mention is made of laboratory wastes. Many municipal engineers, factory inspectors and even medical officers of health are becoming faced with the problems involved in disposing of relatively small activities of a variety of radioactive materials. Whilst there is no complete solution to this problem at present,

it would have been useful to give guidance as to the amounts of solid radioactive waste which can be disposed of in a local authority tip or the amount of liquid radioactive waste which can be discharged to a sewer.

The glossary of terms, symbols and abbreviations, more extensive in this book than is usual, are most valuable but it does seem unfortunate to continue the use of the symbols RaF for Po^{210} or Polonium-210, ThX for Ra^{224} or Radium-224 etc. in a book published in 1960.

This is an excellent book, even though rather expensive at 55s., and is strongly recommended to the class of readers for whom it is intended.

G. R. Hall

S. H. Bransom: **Applied Thermodynamics**, D van Nostrand Company, London 1960. pp. vii + 230. 30s.

G. Hargreaves: **Elementary Chemical Thermodynamics**, Butterworths, London 1961. pp. viii + 120. 10s. 6d.

These two paper-backed issues continue the admirable trend of issuing books for students in a form suitable to their pockets. Courses are now so crowded with lectures, seminars, calculations classes and the like, not to mention practical work, that any move which will encourage the opposite tendency is to be welcomed. Some years ago a man went to a university to 'read' for a degree, today he seems to go to a university to 'study' chemistry or to 'do' chemical engineering. Undoubtedly one of the causes of this change of attitude has been a dearth of suitable books at the right prices, especially at the growing points of science and technology. This has encouraged the multiplication of lectures to 'cover the syllabus' and the degradation of their function from the critical and evocative to the merely didactic. Given suitable books, however, the reversal of this trend becomes possible, and would be welcomed by students and teachers alike. In principle therefore, any good book at the low price level of the two under consideration may expect a welcome and may hope for a recommendation as a book for students to buy and read.

Dr. Bransom's book is unusual, a definite departure from the beaten track of textbooks on Thermodynamics for Physicists, Thermodynamics for Chemists, Thermodynamics for Engineers. The ground it covers is essentially that required for students of Chemical Engineering at second or third year university standard, but it could with profit be read by any whose studies bring them into touch with applied thermodynamics. The method of the book is eclectic rather than exhaustive, but the inclusion of references both to original papers and to books should stimulate the necessary wider reading. The chapter on Equilibria seems inadequate: phase and reaction equilibria together merit more than the rather brief treatment, ten pages, here given, in which reaction in solution, in particular, receives the barest mention. It is disappointing, too, that the reader of this chapter is not directed to Denbigh's excellent "Principles of Chemical Equilibrium" (although this book is referred to elsewhere).

The final chapter is most stimulating. In it the theme of Distillation is used to illustrate and draw together many of the principles of the earlier chapters. Here, too, some of the defects of the chapter on Equilibria, at least as regards vapour-liquid equilibria, are made good. Altogether, an able book which can be recommended for acquisition by students of thermodynamics.

Mr. Hargreaves' book is rather slighter. "It is intended for Higher National Certificate and B.Sc. students who are starting thermodynamics for the first time." It consists of very brief statements of the first and second laws of thermodynamics conceived of as postulates from which the rest follows. It is interesting, and praiseworthy, that in these statements it is not found necessary to 'limp eccentrically round half-completed cycles.' However, perhaps from their very brevity, these statements are on occasion misleading. Thus the derivation (pp. 73–74) of the equation $dU = TdS - PdV$ leaves an impression that it is only applicable to constant pressure reversible processes. After these statements of fundamentals the book continues with applications, treating Change of State, the Law of Mass Action, and the Effect of Temperature on Equilibrium, with worked examples by way of illustration. Some of the presentation is untidy; for example in the derivation (pp. 79–80) of the Clausius–Clapeyron equation, it is confusing to use the words state, phase, and species as synonymous.

This book can be recommended with reservations. As a convenient summary in the hands of a good first-year student of chemistry attending good lectures, it could be very useful, but the discussion of critical points is not full enough for it to be safely put into the hands of someone studying alone or with only intermittent supervision.

H. P. Hutchinson

G. Tine: **Gas Sampling and Chemical Analysis in Combustion Processes**, Pergamon Press, London 1961. xv + 94 pp., 42s.

It is made clear in the preface that this book, No. 47 in the AGARD series, is a review of experimental technique as applied to combustion phenomena of interest in aeronautics. Professor Tine, of the University of Naples, studied his subject during recent visits to about thirty laboratories in Britain, France, Germany and the United States.

The major part of the book, fifty-three pages, is devoted to sampling, and possible errors are divided into two groups according to whether they originate outside or inside the sampling probe. The first kind of error occurs if the probe interferes with the combustion process, or if the nature of the flow outside the probe prevents the collection of a representative sample. The second kind of error occurs

VOL 16 196

if the composition of the sample alters after it has entered the probe, and may be avoided or minimised by quenching by means of forced convection cooling, expansion, dilution, or a combination of these methods. An outline of relevant theory is given, but in general the author concludes that at present this is of limited assistance in estimating sampling errors, because the practical situations are so complex and many of the factors are not accurately known. He suggests some practical methods of testing sampling systems; one method involves preparing a uniform suspension by pouring a known quantity of particles through a sieve into still air, and this seems rather optimistic.

The remaining thirty pages are devoted to a short review of gas analysis, especially physical methods. Jet engines produce rather dilute exhaust gases, and several pages are devoted to the analysis of such mixtures.

VOL. 16 1962

Of the 127 references, two are dated 1959 and the rest are earlier. There is no author index, and the subject index contains only 57 entries and is of limited value.

So short a book could not cover the whole field of gas sampling and analysis, but there are omissions even in the limited field considered. For example, the thermal conductivity method is stated to be suitable only for binary mixtures, without mention of an ingenious extension to ternary mixtures by Minter and Burdy in 1951. Nevertheless, the importance, and the difficulty, of ensuring that samples are representative make this systematic survey gas sampling useful and stimulating.

M. J. G. Wilson

Proceedings of the Fourth Conference on Carbon, University of Buffalo, 1959. Pergamon Press, London, 1960. xii + 778 pp. £7. 10s.

This volume contains, in English, all but five of the papers submitted to the Fourth Conference on Carbon, co-sponsored by the American Carbon Committee and the University of Buffalo, and held at the latter university, 15–19 June, 1959. It is the third volume of a series, the previous books having covered the first three carbon conferences. These biennial meetings on carbon in the U.S.A. seem to have become firmly established as a forum for physicists, chemists and technologists interested in carbon, its production and its applications. The American Carbon Committee is composed of members who represent university, government and industrial laboratories studying such diverse forms of carbon as diamond, natural graphite, electrode carbons and graphites, carbon black and activated carbons.

The Committee attempts to ensure that these conferences are truly international in character. Out of a total of eighty papers, over half were from the U.S.A., fourteen were from Great Britain, seven were from France and six from Japan.

The papers are grouped into five sessions, the first one being mainly concerned with the surface properties of activated carbons, charcoal and carbon blacks, but papers on oxidation are also included. The reactions between carbon and gases such as oxygen, carbon dioxide and steam over a wide range of temperatures and pressures, are of great importance to technology. The information given may throw light on problems of combustion, the behaviour of graphite in gas-cooled nuclear reactors, gas-manufacturing technology and the smelting of ores. Some of the techniques used by authors in this section are particularly fascinating. Hennig, for example, has studied a number of the chemical reactions of graphite by making kinetic studies on single crystals and by simultaneous electron microscope studies. It has been observed that graphite crystals irradiated by neutrons react more rapidly with oxygen than unirradiated crystals. This was attributed to oxygen attack at vacancies and vacancy clusters.

The second group of papers, on electron properties, is mainly of interest to the solid state physicist, but the third group contains information of interest to those concerned with carbonization processes. Basic investigations into the chemical and physical changes occurrig during then coking of industrial materials such as coal, tar and pitch are always handicapped by the fact that the starting materials are enormously complex and ill-defined. In an attempt to overcome this difficulty it is becoming common practice to study the carbonization of pure chemicals or single polymers. Studies have been carried out on the formation of carbon from polyvinylidene chloride, from benzene, from acetylene and even from certain vat dyes.

The next session was concerned with mechanical and thermal properties. Chemical engineers and others using graphite as a material of construction are probably aware of the fact that industry produces many different grades. Although it may seem to be a relatively easy matter to break a few samples of graphite in order to determine its strength, an interpretation of the mechanical behaviour of carbons and graphites is difficult in view of their complex structure. Relatively little is known about the way in which the coke grains or the crystallites are bonded together. Davidson and Losty rightly point out that the nature of the voids between the crystallites has not yet been thoroughly studied. Graphite as a porous medium should present a fascinating challenge to students of fluid flow since it is such a versatile material. It is lamentable that no detailed study of the permeability to fluids of graphites and carbons has yet been reported.

The fifth and final part of this volume is headed "Carbon Technology, Friction and Wear." This section is lacking in information concerning the preparation and manufacturing processes of carbons and graphites, thus reflecting the blanket of secrecy which exists over commercial operations.

In fact, the session seems to be unduly weighted with papers on friction and the behaviour of carbon brushes. However, the Armour Research Foundation describe some work in which the conventional pitch binder used in graphite production was replaced by synthetic resins in an

attempt to obtain superior physical properties in the final artefact. A paper from Harwell referred to the experimental programme of its Chemical Engineering Division, which has the object of making practical variations in manufacturing conditions, observing the effects of these on technical properties and where possible, correlating the latter with the basic structural parameters. Results derived from pore structure variations only are described.

It is very regrettable that the discussions which took place at the Fourth Conference on Carbon are not recorded. Carbon technologists, apart from the few who attended the conference in person, must rely entirely on their own critical faculty when they study the so-called Proceedings of the Conference. It is also sad that there should be a lapse of sixteen months between the conference and the publication of the papers, particularly so when it is realised that there is only a lapse of twenty-four months between succeeding conferences. One reason for this delay may perhaps be in the fact that the papers do not have to be written *before* the conferences are held.

This up-to-date survey of carbon technology will be valuable to physical chemists, solid state physicists and all types of research worker in every branch of the carbon industries. However, it is unlikely to interest chemical engineers, unless they are either directly engaged with carbon production processes or are greatly concerned with the use of graphite as a material of construction. In the latter connexion, it is noteworthy that the applications of graphite are extending rapidly, particularly concerning the use of speciality materials where high temperatures are encountered, such as in nuclear reactors, heat exchangers and space rockets.

F. Roberts.

VOL
16
196

SELECTION OF CURRENT PAPERS OF INTEREST TO CHEMICAL ENGINEERS

R. J. Newcombe and R. Woods: High speed cinematographic investigations at the dropping mercury electrode. *Trans. Faraday Soc.* 1961 **57** 130–134.

A. E. Nielsen: Diffusion-controlled growth of a moving sphere. The kinetics of crystal growth in potassium perchlorate precipitation. *J. Phys. Chem.* 1961 **65** 46–49.

A. G. Ogston: On the variation of the sedimentation rate of spherical particles with concentration. *J. Phys. Chem.* 1961 **65** 51–53.

R. J. Bearman and V. S. Vaidhyanathan: Composition dependence of the thermal conductivity of regular solutions. *J. Chem. Phys.* 1961 **34** 264–265.

R. H. Margarvey and R. L. Bishop: The wake of a moving drop. *Nature, Lond.* 1960 **188** 735–736.

P. N. Rowe and P. F. Wace: Gas-flow patterns in fluidized beds. *Nature, Lond.* 1960 **188** 737–738.

N. G. Maroudas and H. Sawistowski: Surface renewal and interphase mass transfer. *Nature, Lond.* 1960 **188** 1186.

S. Nagata: Mass transfer in liquid–solid agitation systems. *Kagaku Kogaku* 1960 **24** 618–626.

S. Nagata and I. Yamaguchi: Mass transfer and chemical reaction in liquid–solid agitation systems. *Kagaku Kogaku* 1960 **24** 726–735.

S. Nagata, I. Yamaguchi and M. Harada: Mass transfer and chemical reaction in liquid–liquid agitation systems. Agitation effects on the internal mixing of droplets. *Kagaku Kogaku* 1960 **24** 742–748.

R. Koch: Some modern methods for increasing the mass transfer in absorption processes. *Przem. Chem.* 1960 **39** 265–269. (In Polish).

I. V. Robu: Mass transfer between a mobile and a stationary phase—II. Mechanism of successive differential extraction. *Lucranile. inst. petrol. si graz Bucuresti* 1959 **5** 109–123.

I. V. Robu: Mass transfer between a mobile and a stationary phase—III. Differential absorption. *Lucranile. inst. petrol. si graz Bucuresti* 1959 **5** 125–129.

R. Darmois: A study of some packed distillation columns. *Rev. Inst. franc. Petrole* 1960 **15** 1708. (In French).

K. Nishikawa: Nucleate boiling under reduced pressure. *Mem. Fac. Engng., Kyushu* 1960 **19** 63–71.

A. Vignes: Mass transfer between two fluid phases—I. Rate of passage of a constituent across the interface of two phases. *J. Chim. Phys.* 1960 **57** 980. II. Diffusional rate of transfer of one constituent between two semi-infinite phases. *Ibid.* 1960 **57** 991. III. Influence of surface-active agents on the transfer rate. *Ibid.* 1960 **57** 999. (In French).

B. V. Derjaguin and S. S. Dukhin: Theory of flotation of small and medium size particles. *Bull. Inst. Min. Metall.* 1961 **70** 221–246.

LIST OF JOURNALS REVIEWED REGULARLY

The principle by which these journals are selected is that they are likely to contain occasional articles of interest to chemical engineers, but that they are not journals which often are available to or read by chemical engineers.

Proceedings of the Royal Society: Series A
Philosophical Transactions of the Royal Society
Philosophical Magazine
Transactions of the Faraday Society
Nature (London)
Quarterly Journal of Mechanics and Applied Mathematics
Journal of Fluid Mechanics
Journal of Applied Physics
British Journal of Applied Physics
Proceedings of the Physical Society of London

VOL.
16
1962

Quarterly of Applied Mathematics
Journal of Mathematics and Physics
Americal Journal of Physics
Quarterly Reviews
Journal of Physical Chemistry
Journal of Chemical Physics
Applied Scientific Research (Series A)
Transactions of the American Institute of Mechanical Engineers, including:
- Journal of Engineering for Power (Series A)
- Journal of Engineering for Industry (Series B)
- Journal of Heat Transfer (Series C)
- Journal of Basic Engineering (Series D)
- Journal of Applied Mechanics (Series E)

Transactions of the Institute of Mechanical Engineers (London)
Journal of the Institute of Petroleum
Journal of the Royal Aeronautical Society
Journal of Meteorology
Quarterly Journal of the Royal Meteorological Society
Journal of Scientific Instruments
Journal of the Electrochemical Society
Journal of Applied Chemistry
Bulletin of the Institute of Mining and Metallurgy
Also, various Continental, Chinese, Japanese and other journals occasionally.

SELECTION OF CURRENT SOVIET PAPERS OF INTEREST TO CHEMICAL ENGINEERS*

VOL. 16 1962

YA. G. GOROSHCHENKO, A. G. BABKIN, V. G. MAYOROV and S. A. FEDYUSHKINA: Continuous process for the separation of niobium and tantalum by extration with *cyclo*hexanone. *Zh. prikl. Khim.* 1961 **34** 43–49.

K. I. LOPATIN: Purification of water gas by solutions of ethanolamine. *Zh. prikl. Khim.* 1961 **34** 66–70.

M. M. DUBININ and E. D. ZABELINA: Adsorption properties and microporous structure of industrial active charcoals. *Zh. prikl. Khim.* 1961 **34** 113–120.

N. A. GOLDBERG and V. I. KUCHERYAVY: On modelling of chemisorption processes. *Zh. prikl. Khim.* 1961 **34** 151–156.

E. RUCKENSTEIN: On the problem of mixing during bubbling of vapour through liquid on plates in a rectification column. *Zh. prikl. Khim.* 1961 **34** 157–161.

V. V. KAFAROV and V. S. MURAVYEV: Mass transfer in packed columns at inversion of phases. *Zh. prikl. Khim.* 1961 **34** 214–218.

L. I. KAZARNOVSKAYA, N. M. DYKHNO and E. V. VAGIN: Recovery of methane from mixtures with inert gases. *Khim. Prom.* 1961 (1) 29–32.

I. P. MUKHLENOV, D. G. TRABER, M. F. MIKHALEV and YA. M. SHMEKKER: Oxidation of sulphur dioxide using a suspended catalyst bed. *Khim. Prom.* 1961 (1) 42–46.

N. I. GELPERIN and V. B. KVASHA: Maintenance of optimum temperature conditions in chemical reactors. *Khim. Prom.* 1961 (1) 51–56.

V. M. OLEVSKI and V. P. RUCHINSKI: Application of film columns with parallel-sheet packing for separation by rectification of the products of oxidation of *cyclo*hexane. *Khim. Prom.* 1961 (1) 57–62.

V. S. KOMAROV and N. F. ERMOLENKO: Dependence of selectivity of adsorption on the nature of binary mixtures. *Zh. Fiz. Khim.* 1961 **35** 9–14.

P. M. NASSONOV: Adsorption isotherm and sorption and desorption kinetics of gases on heterogeneous surfaces. *Zh. Fiz. Khim.* 1961 **35** 118–128.

P. P. PUGACHEVICH: Apparatus for surface tension measurement by the method of maximum gas-bubble pressure. *Zh. Fiz. Khim.* 1961 **35** 212–213.

A. K. MANOBYAN: Graphico-analytical method for calculation of piping between the heater and the rectification column. *Khim. Tekh. Topl. Masel.* 1961 **6** (1) 48–51.

M. I. FRIDLAND, I. M. RAZUMOV and A. I. SKOBLO: On calculation of entrainment of particles by gas in fluidized bed equipment. *Khim. Tekh. Topl. Masel.* 1961 **6** (2) 36–38.

N. I. GELPERIN and V. B. KVASHA: Determination and maintenance of optimum temperature range in chemical reactors. *Khim. Tekh. Topl. Masel.* 1961 **6** (2) 39–45.

A. S. LYSHEVSKI: Fields of concentration of an atomized liquid in an axially symmetrical stream. *Inzh. Fiz. Zh.* 1961 **4** (2) 27–32.

Y. A. MIKHAILOV: Heat and mass transfer on pressure reduction. *Inzh. Fiz. Zh.* 1961 **4** (2) 33–43. Transfer phenomena in drying by pressure reduction.

A. I. MOCHALIN: Heating of a finite cylinder by an instantaneous point source of heat. *Inzh. Fiz. Zh.* 1961 **4** (2) 44–51.

G. D. RABINOVICH: Non-stationary heat transfer in a counterflow recuperative apparatus. *Inzh. Fiz. Zh.* 1961 **4** (2) 58–62.

P. N. FEDOSEYEV and A. E. ELETSKI: Thermal drying of wheat with low moisture gradients in the grain. *Inzh. Fiz. Zh.* 1961 **4** (2) 63–69.

*To assist readers, translations of any article appearing in the above list can be obtained at a reasonable charge. All orders should be addressed to the Administrative Secretary of the Pergamon Institute at either Headington Hill Hall, Oxford or 122 East 55th Street, New York 22, whichever is more convenient.

G. T. Sergeyev: Heat and mass transfer during evaporation of liquid in forced gas flow. *Inzh. Fiz. Zh.* 1961 **4** (2) 77–81.

S. S. Zabrodski: Hydraulic resistance of a bed during pseudo-fluidization in a conical apparatus. *Inzh. Fiz. Zh.* 1961 **4** (2) 92–94.

B. I. Fedorov and Z. P. Shulman: Application of permeable porous ceramics to the experimental study of the phenomena of mass transfer. *Inzh. Fiz. Zh.* 1961 **4** (2) 99–102.

G. E. Morozov: Experimental determination of the effective coefficient of heat conduction and diffusion for bodies possessing channel-type porosity by the electrical analogue method. *Inzh. Fiz. Zh.* 1961 **4** (2) 103–105.

A. N. Devoino: Present state of knowledge on heat transfer in rarefield gases. *Inzh. Fiz. Zh.* 1961 **4** (2) 119–130.

V. I. Yudovich: Unsteady two-dimensional motion of an ideal incompressible fluid. *Dokl. Akad. Nauk SSSR.* 1961 **136** 564–567.

V. I. Ilichev: Occurrence of cavities in turbulent boundary layers and wake currents. *Dokl. Akad. Nauk SSSR.* 1961 **136** 1047–1050.

M. A. Goldshtik, A. K. Leontyev and I. I. Palevyev: Aerodynamics of a vortex chamber. *Teploenergetika.* 1961 **8** (2) 40–45.

V. V. Talakvadze: Theory and design of centrifugal nozzles. *Teploenergetika.* 1961 **8** (2) 45–49.

V. N. Adryanov: Effects of dissipation in radiant heat transfer. *Teploenergetika.* 1961 **8** (2) 63–66.

L. A. Vulis, A. M. Gurvich and V. G. Klinger: Modelling of radiant heat exchange in furnaces by means of light. *Teploenergetika.* 1961 **8** (2) 67–71.

A. A. Zhukauskas and A. A. Shlanchyauskas: Heat transfer and flow resistance of bundles of staggered pipes in transverse flow of liquid. *Teploenergetika.* 1961 **8** (2) 72–75.